AD_____

Award Number: DAMD17-98-1-8614

TITLE: Mechanisms of Virus-Induced Neural Cell Death

PRINCIPAL INVESTIGATOR: Kenneth L. Tyler, M.D.

CONTRACTING ORGANIZATION: University of Colorado Health Sciences Center
Denver, Colorado 80262

REPORT DATE: September 2003

TYPE OF REPORT: Annual

PREPARED FOR: U.S. Army Medical Research and Materiel Command
Fort Detrick, Maryland 21702-5012

DISTRIBUTION STATEMENT: Approved for Public Release;
Distribution Unlimited

REPORT DOCUMENTATION PAGE

Form Approved
OMB No. 074-0188

1. AGENCY USE ONLY (Leave blank)	2. REPORT DATE	3. REPORT TYPE AND DATES COVERED
	September 2003	Annual (15 Aug 2002 - 14 Aug 2003)

4. TITLE AND SUBTITLE
Mechanisms of Virus-Induced Neural Cell Death

5. FUNDING NUMBERS
DAMD17-98-1-8614

6. AUTHOR(S)
Kenneth L. Tyler, M.D.

7. PERFORMING ORGANIZATION NAME(S) AND ADDRESS(ES)
University of Colorado Health Sciences Center
Denver, Colorado 80262

E-Mail: ken.tyler@uchsc.edu

8. PERFORMING ORGANIZATION REPORT NUMBER

9. SPONSORING / MONITORING AGENCY NAME(S) AND ADDRESS(ES)
U.S. Army Medical Research and Materiel Command
Fort Detrick, Maryland 21702-5012

10. SPONSORING / MONITORING AGENCY REPORT NUMBER

11. SUPPLEMENTARY NOTES
Original contains color plates: All DTIC reproductions will be in black and white.

12a. DISTRIBUTION / AVAILABILITY STATEMENT
Approved for Public Release; Distribution Unlimited

12b. DISTRIBUTION CODE

13. ABSTRACT (Maximum 200 Words)

We are using experimental infection with reoviruses to study how viruses induce cell death (apoptosis), and the significance of apoptosis in the pathogenesis of viral infection. We have developed one of the best-characterized experimental models for investigating and manipulating viral cell death pathways. We have shown that apoptosis is a major mechanism of reovirus-induced cell death in murine models of key human viral infections including myocarditis and encephalitis. We have shown that apoptosis is a major mechanism of reovirus-induced cell death in murine models of key human viral infections including myocarditis and encephalitis. We have shown that inhibiting apoptosis can reduce the degree of virus-induced histological injury in target organs and prolong the survival of infected animals. In virus-infected cells, apoptosis is initiated by activation of death receptors, and that its full expression requires augmentation by mitochondrial pro-apoptotic factors including Smac/Diablo. We have identified the pro-apoptotic Bcl-2 family protein Bid, as a key intermediary between death receptor and mitochondrial apoptotic pathways, and are currently investigated the role of other Bcl-2 family proteins including Bid and Bax. We have also shown that reovirus infection induces a two phase regulation of the nuclear transcription factor NF-κB, with initial activation followed by subsequent inhibition and are currently utilizing oligonucleotide microarrays to study virus-induced alterations in gene expression and the transcription factors that regulate this process.

14. SUBJECT TERMS
Apoptosis, Caspases, Reovirus, Encephalitis, Neurons, NF-κB, JNK

15. NUMBER OF PAGES
143

16. PRICE CODE

17. SECURITY CLASSIFICATION OF REPORT	18. SECURITY CLASSIFICATION OF THIS PAGE	19. SECURITY CLASSIFICATION OF ABSTRACT	20. LIMITATION OF ABSTRACT
Unclassified	Unclassified	Unclassified	Unlimited

Table of Contents

INTRODUCTION (Subject, Purpose, Scope of the Research)

The signs and symptoms of viral infection result from the capacity of viruses to damage or kill cells in different organs. Two distinct patterns of cell death, necrosis and apoptosis can be distinguished based on a variety of biochemical and morphological criteria. Apoptotic cell death is characterized by diminution in cell size, membrane blebbing, and compaction, margination and fragmentation of nuclear DNA. We have recently shown, in work supported by this grant, that apoptosis is a key mechanism by which viruses injure the central nervous system in a variety of important human infections including herpes simplex encephalitis, cytomegalovirus encephalitis, and progressive multifocal leukoencephalopathy (see reportable outcomes #6,7).

Most apoptotic processes are triggered by the activation of caspases, a family of cellular cysteinyl proteases that can be hierarchically ordered into initiator and effector enzymes. Following proteolytic activation by initiator caspases, effector caspases act on a variety of cellular substrates to induce the morphological changes characteristic of apoptosis. Individual initiator caspases are associated with different cellular organelles involved in specific cell death pathways. In the extrinsic pathway, apoptosis is mediated by the binding of apoptosis inducing ligands such as TRAIL, TNF, or FasL to their cognate cell surface "death receptors". This binding leads to formation of a death-inducing signal complex (DISC) that activates caspase 8, the death-receptor associated initiator caspase. Death signals initiated at the mitochondrion result in the release of a variety of pro-apoptotic factors including cytochrome *c,* Smac/DIABLO (Second mitochondrial activator of caspases), and AIF (apoptosis inducing factor). Although the actions of mitochondrial pro-apoptotic factors are diverse, two important pathways include apoptosome-mediated activation of the initiator caspase 9 triggered by cytosolic release of cytochrome *c,* and augmentation of caspase activity by the inhibition of cellular inhibitor of apoptosis proteins (IAPs) mediated by their binding to Smac/DIABLO. The subject and purpose of this research project is to study the mechanisms by

which viruses induce apoptotic cell death in cell culture and animal models of virus-infection, and in human CNS tissues.

PROGRESS REPORT

This is the fifth annual progress report on this research project. Twelve papers have been published in the 7/1/2002-2003 reporting period (see Reportable Outcomes). Reprints of all published papers have been included as an appendix. Research funded by this grant has been presented at national and international scientific meetings including the 22nd Annual Meetings of the American Society for Virology, and the 5th meeting of the International Society for Neurovirology (see Reportable Outcomes). In accordance with the technical reporting requirements for this grant, we have substituted journal publications for detailed descriptions of specific aspects of the research. However, to facilitate review of this report, we have also briefly summarized the key research findings in these papers in the text. Reference numbers in text refer to papers listed in Reportable Outcomes. Accomplishments are reviewed below and keyed to the specific aims/statement of work (SOW) as outlined in the original research application and subsequent expansions.

Original SOW 1: Is apoptosis a general feature of human viral encephalitis?

Papers describing work conducted under this part of the SOW have been published in ***Archives of Neurology*** (ref. 6) and ***Journal of Infectious Diseases*** (ref.7). We initially selected herpes simplex virus (HSV) and cytomegalovirus (CMV) encephalitis (7) to study, as HSV encephalitis represents the most common cause of severe sporadic focal encephalitis in the U.S., and CMV encephalitis is the most common congenital neurological infection in humans. Specimens from ten immunocompetent patients with HSV encephalitis and three immunocompetent infants

with congenital CMV encephalitis were examined for viral antigen distribution, pathology, and evidence of apoptosis as indicated by positive staining for the activated form of caspase 3, or terminal dUTP nick end labeling (TUNEL). We found evidence of apoptosis in 6/7 brain specimens from patients who had died of acute HSV encephalitis, and in 0/3 samples from patients who had died of other causes following a remote history of HSV encephalitis. We also found apoptosis in a child who had died of acute CMV infection but not in patients who had a remote history of infection. In order to determine if apoptosis was occurring in infected cells, sections from HSV-infected brains were double-labeled for viral antigen and activated caspase 3 (apoptosis marker). Apoptotic cells were found to include both infected (antigen positive)

neurons and glial, as well as uninfected cells in close proximity to infected cells ("bystander apoptosis"). In the case of CMV infection the majority of apoptotic cells were neurons that contained viral antigen. Comparing HSV and CMV infection it appeared that bystander apoptosis was more significant in HSV infection, and only rarely seen in CMV infection. There was no correlation between the degree of inflammatory response in tissue specimens, as identified by CD3+ cells, and apoptosis. We subsequently expanded our studies to examine apoptosis in brain tissue from patients with progressive multifocal leukoencephalopathy (PML)(6). PML has become one of the most important opportunistic viral CNS infections, due largely to its prevalence in patients with AIDS. We found that apoptosis occurred almost exclusively in JC virus-infected oligodendrocytes at the periphery of demyelinating lesions in PML. Apoptosis was not detected in the 'bizarre' astrocytes that are characteristic of PML, nor in neurons. This result is consistent with the fact that JCV infection in astrocytes is abortive (non-productive) and that the virus fails to infect neurons. These studies (6,7) represent the first demonstration that apoptosis occurs in the CNS in these key human viral encephalitides, and the first demonstration that apoptosis is an important mechanism of CNS injury in viral infections other than HIV.

As part of our studies characterizing apoptosis in human CNS viral infections, we have performed extensive analysis of brain material and CSF specimens of patients with acute viral encephalitis. Our experience obtaining and characterizing this material lead to additional publications in the ***Annals of Neurology*** (8) describing the use of quantitative PCR to characterize Epstein-Barr virus infections of the CNS, and in ***Journal of Clinical Virology*** (12) describing the use of PCR in the diagnosis of herpesvirus infections of the CNS. We measured EBV DNA by quantitative PCR and EBV mRNA by RT-PCR in 28 patients with EBV-associated CNS infections. We found that patients with EBV-associated CNS lymphomas (n=14) had high EBV DNA copy numbers but relatively modest CSF cell counts. By contrast patients with EBV encephalitis (n=10) had both high EBV DNA copy number and a prominent CSF pleocytosis. Lytic cycle EBV mRNA, a marker of EBV replication, was found in both patients with EBV-associated CNS lymphoma and acute encephalitis.

Expanded SOW Aim 1.1: Cellular apoptotic pathways activated in human viral apoptosis.

As noted above, we have shown that activated caspase 3 can be detected in areas of apoptosis in brain tissues from patients with CMV and HSV encephalitis, and correlated theses results with detection of apoptosis by TUNEL and the presence of inflammatory cells (using CD3 as a marker) (6,7).

Expanded SOW Aim 1.2: Examine apoptotic pathways and the effects of inhibiting apoptosis in a murine encephalitis model.

In previously reported work supported by this grant we have shown that apoptosis occurs in both the CNS and heart in murine models of reovirus-induced apoptosis. These studies formed the basis for this expansion of the original SOW. In a paper published in the ***Journal of Neurovirology*** (9) we have now extended our studies of CNS apoptosis to show that we can detect activated caspase

3 in apoptotic cells in the murine CNS, and have used co-labeling to correlate infected (antigen positive) and apoptotic cells, and to identify the predominant apoptotic cell type as neurons (9). We have also shown that caspase 3 is infected in the brains of reovirus-infected mice (9). We have now performed experiments testing the capacity of two pan-caspase inhibitors (ZVAD-fmk and OPH) and of minocycline to inhibit apoptosis and protect mice against lethal intracerebral challenge with reovirus. Studies are also currently underway in caspase 3 knockout mice (courtesy of Richard Flavell, Yale University). Preliminary studies indicate that all these caspase inhibitors decrease the number of apoptotic cells in the CNS, reduce the extent of histopathological injury, and prolong survival after viral challenge. A manuscript describing these results is in preparation, and aspects of this work were recently presented at the 5th Meeting of the International Society of Neurovirology (see Reportable Outcomes).

Expanded SOW Aim 1.3: Examine changes in gene expression in a murine model of CNS encephalitis in which apoptotic injury is critical to pathogenesis. In work supported by this grant, we have used large-scale oligonucleotide arrays (Affymetrix GeneChips) to examine changes in the expression of mRNAs for cell cycle regulatory genes following reovirus-infected HEK cells. In an effort to set the stage for in vivo studies, we examined reovirus-induced changes in genes involved in regulation of apoptosis and DNA damage and repair in infected cells in culture. During the current reporting period we published a paper in the ***Journal of Virology*** describing reovirus-induced alterations in expression of apoptosis and DNA repair genes (1). For these studies cells were infected with the apoptosis-inducing reovirus type 3 Abney (T3A) strain and with a non-apoptosis inducing reovirus strain (reovirus type 1 Lang, T1L). Gene expression was analyzed using Affymetrix U95A chips containing features representing >12,000 human genes. We found that expression of 24 genes involved in regulation of apoptosis was significantly altered ($\geq$ 2-fold), with 22 being up-regulated and two down-regulated, in T3A compared to mock infected cells. Of this set

of 22 genes only 5 were also differentially expressed in T1L infected as compared to mock-infected cells. The involved genes included ten genes involved in mitochondrial apoptotic signaling, three in ER stress signaling, four in death receptor signaling, four apoptotic proteases, and three other genes. In addition to inducing many genes involved in regulation of apoptosis, these studies also indicated that viral infection altered expression of 14 genes involved in repair of DNA damage, thirteen of which were down regulated by the apoptosis inducing T3A strain. Infection with the non-apoptosis inducing T1L strain did not alter expression of any DNA repair genes.

In an effort to validate the oligonucleotide array data, levels of expression of selected genes was also analyzed by RT-PCR. We found an excellent correlation between microarray and PCR data for the twelve genes tested. Finally, we also investigated expression of protein in infected mice of SMN (survival motor neuron), the protein product of a gene whose expression was shown to be up regulated in both genechip and RT-PCR studies. We found that, as would be predicted by the mRNA expression studies, that levels of SMN were significantly up-regulated in reovirus infected mice by day 7-8 post-infection compared to uninfected controls and infected mice early following infection (days 3-5).

Original SOW 2.0: Is the ceramide/sphingomyelin pathway involved in reovirus-induced apoptosis? This aim was previously revised and expanded based on work accomplished to more broadly identify cellular pathways involved in reovirus-induced apoptosis.

Expanded SOW 2.1, 2.2, & 2.3: Identify cellular pathways leading to the activation of NF-□B and JNK/c-JUN in reovirus-infected cells, and the genes regulated by these transcription factors.

We have previously shown in work supported by this grant that reovirus infection is associated with the activation of NF-κB and that infection also leads to the selective activation of mitogen activated protein kinase pathways including both the ERK and JNK pathways. In a paper

published during the current reporting period in the ***Journal of Biological Chemistry*** (4), we have now shown that after initially activating NF-κB, reovirus infection subsequently induces an inhibition of NF-κB activation. During this second phase, reovirus infection can also be shown to block NF-κB activation induced by both TNF and etoposide. The canonical pathway for NF-κB activation involves the phosphorylation, ubiquitination, and subsequent degradation of IκB, the cytosolic inhibitor of NF-κB. Reovirus-induced inhibition of NF-κB activation requires viral replication, and involves virus-induced inhibition of IκB degradation through as yet unidentified mechanisms. We have hypothesized that the initial phase of reovirus-induced early NF–κB activation is required for the expression of pro-apoptotic NF-κB dependent genes and the subsequent inhibition prevents later expression of anti-apoptotic NF-κB dependent genes.

In a paper published during the current reporting period in the ***EMBO Journal*** (2) we have extended our previously characterization of the role of MEKK1, a MAPK kinase kinase (MAP3K) upstream of JNK in apoptosis-related processes. We have previously shown, in work supported by this grant, that reovirus infection is associated with MEKK1 activation, and that inhibition of this activation dramatically inhibits reovirus-induced JNK activation. In this paper, we now show that MEKK1 is required for activation of calpain, a cysteine protease that we have previously shown, in work also supported by this grant, is activated following reovirus infection in cell culture and in vivo. We have also shown that inhibition of calpain activation results in inhibition of reovirus-induced apoptosis both in cultured cells, and in a murine model of reovirus-induced myocarditis in vivo.

In collaboration with Dr. Gary Johnson (Chair, Department of Pharmacology, University of North Carolina, previously at the UCHSC Department of Pharmacology) and Dr. Imran Shah in the Bioinformatics Group of the Gene Expression Core Facility at UCHSC, we have identified patterns of transcriptional regulation that provide an explanation for the specific sets of genes activated

following reovirus infection. A manuscript describing these results is in preparation. We initiated these studies by (a) identifying all genes up-regulated following reovirus infection in HEK cells (done, see prior reports and current report reference 1), (b) using GenBank (www.ncbi.nlm.nih.gov) and other sources to obtain ~1000 kb of nucleotide sequence upstream of the initial start codon of these reovirus-regulated genes (done), (c) using TRANSFAC (http://transfac.gbf.de/TRANSFAC) a transcription factor database, and TRANSPATH (http://193.175.244.148/) a signal transduction pathway database and other databases containing information about promoter binding sequences to identify the pattern and order of transcription factor binding sites in genes up-regulated following reovirus infection compared to non-altered control genes (in progress). We have found that there are several unique clusters of transcription factor binding regions ("modules") in genes whose expression is altered in reovirus infected cells, as compared to genes whose expression is not altered in infected cells, and to genes randomly represented on the test chips. These results are consistent with a model in which reovirus infection induces the expression of a specific limited set of transcription factors, and that this set in turn induces the expression of a limited number of host cell genes containing appropriate modules of binding sites for these transcription factors. Based on this analysis we have also predicted that reovirus infection might be associated with activation of the transcription factor SREBP, a prediction we have now confirmed in infected cells.

Expanded SOW 2.4: Identify the role of the mitochondrion in reovirus-induced apoptosis. In two papers published during the current reporting period in the ***Journal of Virology*** (10) and ***Cell Death and Differentiation*** (11) we have shown that reovirus infection in HEK cells is associated with release of the mitochondrial pro-apoptotic factors cytochrome *c* and Smac/DIABLO, but not of AIF. Cytochrome *c* forms part of the apoptosome involved in activation of the mitochondrial-related initiator caspase, caspase 9. We have also shown that caspase 9 is activated following reovirus infection (11). Reovirus infection is also associated with the release of

Smac/DIABLO (10). This protein facilitates apoptosis by binding to cellular inhibitor of apoptosis (IAP) proteins that act to inhibit caspase activation. Binding of Smac/DIABLO to IAPs prevents their inhibition of caspase activity, thereby augmenting apoptosis. We have shown that, consistent with the release of Smac/DIABLO, reovirus infection is associated with a selective down-regulation of specific cellular IAPs including XIAP, cIAP1, and survivin (10). We have also shown, using cells expressing a dominant negative form of caspase 9, that is likely Smac/DIABLO release rather than caspase 9 activation, that plays the critical role in augmenting reovirus-induced apoptosis.

Expanded SOW 2.5: Identify the mechanism by which reovirus infection sensitizes cells to killing by TRAIL. We have previously shown in work supported by this grant that reovirus-induced apoptosis in non-neuronal cells involves the apoptosis-inducing ligand TRAIL and its associated death receptors, DR4 and DR5 (see 3). Reovirus-induced killing of a wide variety of human cervical, breast, and lung cancer derived cell lines is also due to apoptosis and mediated by TRAIL. Reovirus infection and TRAIL act synergistically to induce apoptosis, and reovirus infection sensitizes cells to killing by TRAIL. As part of the studies of reovirus-induced NF-κB regulation (4) (see above), we have shown that the ability of reovirus to inhibit NF-κB activation is required for their capacity to sensitize cells to TRAIL killing.

Original SOW 3.0: Is reovirus apoptosis associated with aberrant regulation of cell cycle progression and does this dysregulation occur in post-mitotic neurons?

We have previously shown in work supported by this grant that reovirus infection is associated with dysregulation of cell cycle, and the induction of G2/M cell cycle arrest. We have shown that infection is associated with inhibition of the G2/M checkpoint kinase $p34^{cdc2}$, and that this in turn may result from up-regulation of $p34^{cdc2}$ kinases including chk1 and wee1, and inhibition of the activity of the $p34^{cdc2}$ phosphatase, CDC25C (3). We have used oligonucleotide microarrays to identify the set of genes involved in cell cycle regulation whose expression is either up- or down-

regulated following reovirus infection (see Expanded SOW 1.3). The studies supported by this grant have now made reovirus-induced cell G2/M arrest one of the best characterized models of virus-induced cell cycle perturbation.

Expanded SOW 3.1: Evaluate apoptotic pathways in both primary and continuous neuronal cell lines.

We have examined apoptotic pathways activated following reovirus infection in both mouse neuroblastoma (NB41A3) and primary cortical neuronal cultures. A paper describing this work has been published during the reporting period in the ***Journal of Neurovirology*** (9). Apoptotic pathways activated following reovirus infection in primary neuronal cultures are similar, but not identical, to those in non-neuronal cells (see ref. 3 for review). In both neurons and non-neuronal cultures apoptosis involves cell surface death receptors. However, in neurons, in contrast to HEK cells, we have evidence that both TNF and FasL in addition to TRAIL may play a role in apoptosis (9). In all cell types examined to date, infection is followed by caspase 8 activation which can be detected using antibodies specific for the activated form of caspase 8 (9). In HEK cells, mitochondrial pro-apoptotic factors play a critical role in augmenting death-receptor initiated apoptosis (see ref. 3, 10,11). By contrast, in neurons release of mitochondrial cytochrome *c* into the cytoplasm occurs only at low levels at late times following infection (9). Consistent with this result, caspase 9 activation occurs at only low levels, and peptide inhibitors with relative specificity for caspase 9 (Ac-LEHD-CHO) are less effective then caspase 8 (Ac-IETD-CHO), caspase 3 (Ac-DEVD-CHO), or pan-caspase inhibitors (Ac-ZVAD-CHO) in blocking reovirus-induced neuronal apoptosis.

Expanded SOW 3.2: Identify the role of reovirus σ1s protein in reovirus-induced cell cycle dysregulation.

We have recently shown that the reovirus σ1s protein contains a classical nuclear localization signal (NLS). We have created a plasmid that allows for expression of σ1s coupled both to green

fluorescent protein (GFP) and to the protein pyruvate kinase (PK). Because its size exceeds the limits for passive diffusion into the nucleus, the transfected fusion protein GFP-PK does not enter the nucleus unless it is actively transported. We have shown that coupling the σ1s protein to this construct (σ1s-GFP-PK) allows for nuclear transport, establishing that σ1s contains a functional NLS. We have subsequently generated a construct in which the putative σ1s NLS, encompassing a highly arginine and lysine (KR) rich set of amino acids at positions #14-21, has been deleted. The resulting construct $\sigma 1s_{\Delta NLS}$-GF-PK) is no longer transported to the nucleus. This indicates that region of σ1s between AAs 14-21 is necessary for the nuclear localization of σ1s. A paper describing these results is in preparation, and aspects of this research have been presented at the annual meeting of the American Society of Virology (see Reportable Outcomes).

KEY RESEARCH ACCOMPLISHMENTS:

SOW 1

*Apoptosis is an important feature of CNS injury in human CNS viral infections caused by herpes simplex virus, cytomegalovirus, and JC virus (progressive multifocal leukoencephalopathy, PML).

*Apoptosis in human CNS viral infections is associated with activation of caspase 3 and can occur in both virally infected neurons and in cells in proximity to infected cells ("bystander apoptosis").

*Bystander apoptosis occurs with greater frequency in HSV compared to CMV encephalitis.

* Both human Epstein-Barr virus encephalitis and primary CNS lymphoma are associated with the presence in CSF of large copy numbers of EBV DNA and with detectable lytic cycle mRNAs consistent with active viral replication.

* Inhibition of caspase activation by pancaspase inhibitors can inhibit apoptosis, reduce the extent and severity of CNS histopathological injury and prolong survival in a murine model of reovirus encephalitis.

*Reovirus infection is associated with altered expression of genes involved in apoptosis and DNA repair. Down-regulation of DNA repair genes may contribute to reovirus-induced apoptosis.

SOW 2

*Reovirus infection is associated with two distinct phases of NF-κB regulation including an early activation phase followed by later inhibition of both virus-induced and stimulus induced (TNF, etoposide) NF-κB activation.

*MEKK1 is required for calpain-dependent proteolysis.

*Virus-induced alterations in gene expression are dependent upon the presence in regulated genes of ordered sets of transcription factor binding sites (modules and super-modules) that occur with significantly greater frequency in genes up-regulated during viral infection compared to genes whose expression remains unaltered.

*Reovirus-induced apoptosis in non-neuronal cells is initiated by death-receptor activation, but requires augmentation by mitochondrial apoptotic pathways for its full expression.

*Mitochondrial pro-apoptotic factors released following reovirus infection in epithelial and human cancer cell lines include both cytochrome *c* and Smac/DIABLO but not apoptosis inducing factor (AIF).

*Activation of mitochondrial apoptotic pathways is associated with the subsequent down-regulation of cellular IAPs including XIAP, cIAP1.

SOW 3

*Reovirus induced apoptosis in primary neuronal cultures involves pathways that are similar to but not identical with those identified in non-neuronal cells including initiation through death receptors and the requirement for augmentation via mitochondrial events including the release of Smac.

*Reovirus protein σ1s contains a classic nuclear localization signal (NLS), and can mediate the nuclear import of fusion proteins.

REPORTABLE OUTCOMES

Publications (Copies included in the appendix).

1: DeBiasi RL, Clarke P, Meintzer S, Jotte R, Kleinschmidt-Demasters BK, Johnson GL, Tyler KL. Reovirus-induced alteration in expression of apoptosis and DNA repair genes with potential roles in viral pathogenesis.
J Virol. 2003 Aug;77(16):8934-47. PMID: 12885910

2: Cuevas BD, Abell AN, Witowsky JA, Yujiri T, Johnson NL, Kesavan K, Ware M, Jones PL, Weed SA, DeBiasi RL, Oka Y, Tyler KL, Johnson GL. MEKK1 regulates calpain-dependent proteolysis of focal adhesion proteins for rear-end detachment of migrating fibroblasts.
EMBO J. 2003 Jul 1;22(13):3346-55. PMID: 12839996

3: Clarke P, Tyler KL.
Reovirus-induced apoptosis.
Apoptosis. 2003 Mar;8(2):141-50. PMID: 12766474

4: Clarke P, Meintzer SM, Moffitt LA, Tyler KL. Two distinct phases of virus-induced nuclear factor kappa B regulation enhance tumor necrosis factor-related apoptosis-inducing ligand-mediated apoptosis in virus-infected cells.
J Biol Chem. 2003 May 16;278(20):18092-100. PMID: 12637521

5: Mann MA, Tyler KL, Knipe DM, Fields BN. Type 3 reovirus neuroinvasion after intramuscular inoculation: viral genetic determinants of lethality and spinal cord infection.
Virology. 2002 Nov 25;303(2):213-21. PMID: 12490384

6: Richardson-Burns SM, Kleinschmidt-DeMasters BK, DeBiasi RL, Tyler KL. Progressive multifocal leukoencephalopathy and apoptosis of infected oligodendrocytes in the central nervous system of patients with and without AIDS.
Arch Neurol. 2002 Dec;59(12):1930-6. PMID: 12470182

7: DeBiasi RL, Kleinschmidt-DeMasters BK, Richardson-Burns S, Tyler KL. Central nervous system apoptosis in human herpes simplex virus and cytomegalovirus encephalitis.
J Infect Dis. 2002 Dec 1;186(11):1547-57. PMID: 12447729

8: Weinberg A, Li S, Palmer M, Tyler KL. Quantitative CSF PCR in Epstein-Barr virus infections of the central nervous system.
Ann Neurol. 2002 Nov;52(5):543-8. PMID: 12402250

9: Richardson-Burns SM, Kominsky DJ, Tyler KL. Reovirus-induced neuronal apoptosis is mediated by caspase 3 and is associated with the activation of death receptors.
J Neurovirol. 2002 Oct;8(5):365-80. PMID: 12402163

10: Kominsky DJ, Bickel RJ, Tyler KL. Reovirus-induced apoptosis requires mitochondrial release of Smac/DIABLO and involves reduction of cellular inhibitor of apoptosis protein levels.

J Virol. 2002 Nov;76(22):11414-24. PMID: 12388702

11: Kominsky DJ, Bickel RJ, Tyler KL. Reovirus-induced apoptosis requires both death receptor- and mitochondrial-mediated caspase-dependent pathways of cell death.

Cell Death Differ. 2002 Sep;9(9):926-33. PMID: 12181743

12: DeBiasi RL, Kleinschmidt-DeMasters BK, Weinberg A, Tyler KL.

Use of PCR for the diagnosis of herpesvirus infections of the central nervous system.

J Clin Virol. 2002 Jul;25 Suppl 1:S5-11. PMID: 12091076

Presentations at National or International meetings.

Richardson-Burns S, **Tyler KL**. W13-5. Bcl-2 family proteins Bid and Bim play a key role in regulating the reovirus-induced mitochondrial pathway of apoptosis in primary neuronal cultures. 22nd Annual Meeting of the American Society for Virology. University of California, Davis July 12-16, 2003.

Clarke P, Meintzer SM, **Tyler KL**. W13-8. Two distinct phases of virus-induced NF-kappaB-regulation enhance Trail-induced apoptosis in infected cells. 22nd Annual Meeting of the American Society for Virology. University of California, Davis July 12-16, 2003.

Hoyt C, Poggioli GJ, **Tyler KL**. W42-10. Reovirus nonstructural protein sigma 1 small is a novel nucleocytoplasmic shuttling protein. 22nd Annual Meeting of the American Society for Virology. University of California, Davis July 12-16, 2003.

Richardson-Burns S, **Tyler KL**. I.131. Identification and manipulation of neuronal apoptotic signaling pathways in reovirus-infected neuronal cell cultures and in a murine model of viral encephalitis. 5th International Symposium on Neurovirology, Baltimore, September 2-6, 2003. (J Neurovirol 9(suppl 3). 30-31, 2003).

Selected Additional Invited Presentations of Research Results (Kenneth L. Tyler, M.D.)

2002- Neurology/Neurosurgery Grand Rounds, Washington University, St. Louis, MO.

2002- Seminar Speaker, Department of Pathology & Laboratory medicine. Texas A&M School of Medicine, College Station, TX.

2003- Seminar Speaker, Department of Microbiology & Molecular genetics, Harvard Medical School, Boston, MA.

2003- C. Miller Fisher Rounds and Neuroscience Seminar, Departments of Neurology Brigham & Women's Hospital and Massachusetts general Hospital, Boston, MA.

2003- Seminar Speaker, Departement de Virologie, Institut Pasteur, Paris, France

CONCLUSIONS

Due in significant part to support provided by this grant, reoviruses have become one of the best understood models of virus-induced apoptosis. Viral genes and proteins involved in induction of apoptosis have been identified. The caspase activation pathways involved in apoptosis have been defined in both neuronal and non-neuronal cells, as has the role of specific mitochondrial pro-apoptotic factors. The capacity of the virus to activate specific MAPK cascades and their associated transcription factors has been characterized, and studies are currently underway to establish the entire network of genes that are up-regulated following viral infection. The importance of apoptosis in a variety of in vivo models of infection including encephalitis and myocarditis has been

established, and studies are currently underway to determine whether key apoptotic pathways identified in vitro are also active in vivo. Targeted interventions that modulate apoptosis and enhance cell survival in vitro are being tested for efficacy as novel anti-viral strategies in vivo. The importance of apoptosis as a mechanism of CNS injury has also been established in a variety of key human viral infections, providing added significance to its study in both cell culture and experimental models of infection.

JOURNAL OF VIROLOGY, Aug. 2003, p. 8934–8947 Vol. 77, No. 16
0022-538X/03/$08.00+0 DOI: 10.1128/JVI.77.16.8934–8947.2003

Reovirus-Induced Alteration in Expression of Apoptosis and DNA Repair Genes with Potential Roles in Viral Pathogenesis

Roberta L. DeBiasi,[1,2,3] Penny Clarke,[2] Suzanne Meintzer,[2] Robert Jotte,[4,5] B. K. Kleinschmidt-Demasters,[2,6] Gary L. Johnson,[5,7] and Kenneth L. Tyler[2,3,8,9,10]*

Departments of Pediatrics,[1] Neurology,[2] Hematology and Oncology,[4] Pharmacology,[5] Pathology,[6] Medicine,[8] Microbiology,[9] and Immunology[10] and Program in Molecular Signal Transduction,[7] University of Colorado Health Sciences Center, and Denver Veterans Affairs Medical Center,[3] Denver, Colorado 80220

Received 14 January 2003/Accepted 19 May 2003

Reoviruses are a leading model for understanding cellular mechanisms of virus-induced apoptosis. Reoviruses induce apoptosis in multiple cell lines in vitro, and apoptosis plays a key role in virus-induced tissue injury of the heart and brain in vivo. The activation of transcription factors NF-κB and c-Jun are key events in reovirus-induced apoptosis, indicating that new gene expression is critical to this process. We used high-density oligonucleotide microarrays to analyze cellular transcriptional alterations in HEK293 cells after infection with reovirus strain T3A (i.e., apoptosis inducing) compared to infection with reovirus strain T1L (i.e., minimally apoptosis inducing) and uninfected cells. These strains also differ dramatically in their potential to induce apoptotic injury in hearts of infected mice in vivo—T3A is myocarditic, whereas T1L is not. Using high-throughput microarray analysis of over 12,000 genes, we identified differential expression of a defined subset of genes involved in apoptosis and DNA repair after reovirus infection. This provides the first comparative analysis of altered gene expression after infection with viruses of differing apoptotic phenotypes and provides insight into pathogenic mechanisms of virus-induced disease.

The mechanisms by which viruses cause cytopathic effects in infected host cells are complex and only partially defined. Apoptosis is a direct mechanism of cellular injury and death, which can occur in the course of normal tissue development or as a pathological response to a variety of noxious stimuli. Mammalian reoviruses have served as useful models for studies of the viral and cellular mechanisms that are operative in host cell damage and death (14, 57, 80, 81). Reoviruses induce apoptosis in a multiple cell lines in vitro and in murine models of encephalitis and myocarditis in vivo (18, 58, 68). Prototype strains serotype 3 Abney (T3A) and serotype 3 Dearing (T3D) induce apoptosis more efficiently than strain serotype 1 Lang (T1L). Differences in the capacity of reoviruses to induce apoptosis map to the viral S1 gene, which encodes the viral attachment protein σ1 (15, 69, 82).

The signaling pathways by which reoviruses induce apoptosis in target cells are complex. Involvement of death receptor- and mitochondrion-mediated pathways of apoptosis as well as cysteine protease activation have been demonstrated (11, 43). Binding of tumor necrosis factor (TNF)-related apoptosis-inducing ligand (TRAIL) to its cell surface death receptors—DR4 and DR5—plays a central role in reovirus-induced apoptosis in HEK293 cells and in several cancer cell lines (11, 12), and other death-inducing ligands such as FasL are equally important in neurons (68). Activation of death receptor-related apoptotic pathways results in a coordinated pattern of caspase activation (43, 44, 68). Mitochondrial apoptotic pathways act to augment death receptor-initiated apoptosis, and apoptosis can be inhibited by stable overexpression of Bcl-2 (43, 44, 69). Blockade of cysteine protease activity using selective caspase inhibitors in vitro (11, 43) and calpain inhibitors in vivo (18) results in decreased apoptosis in target cells and tissues.

Reovirus infection results in activation of cellular transcription factors, including NF-κB (16) and c-Jun (13), and this activation plays a critical role in apoptosis. In the case of c-Jun, there is an excellent correlation between the capacity of viral strains to activate the JNK/c-Jun pathway and their ability to induce apoptosis (13). Inhibition of the activation of NF-κB by stable expression of the NF-κB inhibitor IκB, whether by the use of proteosome inhibitors or by targeted disruption of the genes encoding the p65 or p55 subunits of NF-κB, results in inhibition of reovirus-induced apoptosis (16). The close correlation between transcription factor activation and reovirus-induced apoptosis strongly suggests that new gene expression is critical for this process; therefore, we investigated the cellular response to reovirus infection at the transcriptional level. This was achieved by comparing transcriptional alterations after infection with a reovirus strain that efficiently induces apoptosis (i.e., T3A) with alterations after infection with a strain that induces minimal apoptosis (i.e., T1L). These strains also differ in their potential for inducing apoptotic myocardial injury in a murine model of viral myocarditis; T3A infection causes myocarditis and apoptotic myocardial injury, whereas T1L does not.

Using high-throughput screening of over 12,000 genes by using high-density oligonucleotide microarrays, we have identified transcriptional alterations in a defined subset of genes. When grouped into functional categories, a significant propor-

* Corresponding author. Mailing address: Department of Neurology (B-182), University of Colorado Health Sciences Center, 4200 East 9th Ave., Denver, CO 80262. Phone: (303) 393-4684. Fax: (303) 393-4686. E-mail: Ken.Tyler@uchsc.edu.

tion of altered transcripts include genes involved in apoptosis and DNA repair, and it is this subset that forms the focus of this paper. The findings described herein are the first large-scale description of virus-induced alterations in apoptotic signaling at the transcriptional level, including kinetics of these changes after infection with strains that differ in apoptosis-inducing phenotype. These findings lend important insight into specific mechanisms of viral pathogenesis, since apoptosis has previously been demonstrated to be a critical mechanism for reovirus-induced damage in vitro and in vivo.

MATERIALS AND METHODS

Cells, virus, and infection. Human embryonic kidney 293 (HEK293) cells (ATCC CRL 1573) were plated in T75 flasks at a density of 5×10^6 cells per flask in a volume of 12 ml of Dulbecco's modified Eagle's medium supplemented with 10% heat-inactivated fetal bovine serum, 2 mM L-glutamine (Gibco-BRL), 1 mM sodium pyruvate (Gibco-BRL), and 100 U of streptomycin (Gibco-BRL) per ml. Monolayers were infected 24 h after plating, when cells were 60 to 70% confluent. Reovirus strains T3Abney (T3A) and T1Lang (T1L) (P2 stock) were used to infect monolayers at a multiplicity of infection (MOI) of 100 PFU per cell. A high MOI was used to ensure that all susceptible cells were infected and because pilot studies in our laboratory indicated that high-multiplicity infection enhanced the reproducibility of gene expression studies. Virus was adsorbed for 1 h at 37°C in a volume of 2 ml, during which time flasks were rocked every 15 min. Following adsorption, flasks were incubated at 37°C after the addition of 10 ml of fresh medium. T3A-infected cells were harvested at 6, 12, and 24 h after viral infection. T1L-infected cells were harvested at 24 h postinfection. For control infections, HEK293 monolayers were inoculated with a cell lysate suspension, which was prepared identically to viral stocks but which lacked infectious virus.

Cell harvests and RNA extraction. Cells were harvested by gently pipetting adherent and nonadherent cells from the flasks into 50-ml centrifuge tubes. After centrifugation (DuPont Sorvall 6000) at 1,200 rpm for 5 min, cell pellets were resuspended in phosphate-buffered saline (PBS) and transferred to Eppendorf tubes for total RNA extraction (RNeasy Mini Total RNA isolation kit; QIAGEN). Total RNA was extracted from each flask independently, resulting in duplicate RNA samples for each infection condition at 6, 12 (mock, T3A), and 24 (mock, T3A and T1L) h postinfection. A total of 16 RNA samples were prepared, and the yield and purity of extracted RNA were determined by spectrophotometry.

Target preparation. Biotinylated cRNA targets were prepared from a 10-μg aliquot of each total RNA sample by following Affymetrix instructions and protocols. Briefly, total RNA was reverse transcribed to double-stranded cDNA (Superscript Choice; Gibco-BRL) by using high-pressure liquid chromatography-purified T7-$(dT)_{24}$ oligomer for first-strand cDNA synthesis. Second-strand synthesis was performed by using T4 DNA polymerase, and double-stranded cDNA was isolated by using phenol-chloroform extraction with phase-lock gels. Isolated cDNA was in vitro transcribed and labeled (by using biotin-UTP and biotin-CTP) to produce biotin-labeled cRNA (BioArray High-Yield RNA transcript labeling kit; ENZO). Labeled cRNA was isolated by using RNeasy Mini Kit spin columns (QIAGEN). Yield and purity were quantified by using spectrophotometry. Labeled cRNAs were fragmented in 100 mM potassium acetate, 30 mM magnesium acetate, and 30 mM Tris-acetate (pH 8.1) for 35 min at 94°C to produce labeled cRNA fragments of 60- to 300-bp length. For hybridization, cRNA target integrity was analyzed with Affymetrix control (Test 2) arrays to assess degradation and hybridization performance prior to hybridization to Affymetrix Human U95A high-density oligonucleotide microarrays. The U95A microarray contains cDNA oligomer that is complementary to 12,000 human genes with known function (no expressed sequence tags), which currently represents the most comprehensive coverage of the human genome represented on a single microarray. Each of the 16 prepared target cRNAs was independently hybridized to a U95A array. Eukaryotic hybridization controls bioB, bioC, bioD, and cre were also included in the hybridization cocktail. Hybridization was carried out for 16 h at 45°C with rotation at 60 rpm. Microarrays were washed and stained with streptavidin-phycoerythrin conjugate by using the Affymetrix GeneChip Fluidics Station 400, following standard Affymetrix protocols. Staining intensity was antibody amplified by using a biotinylated antistreptavidin antibody at a concentration of 3 μg per ml which was followed by a second streptavidin-phycoerythrin conjugate stain, and hybridization intensity was analyzed by scanning at 570 nM. All hybridization and scanning steps were performed at the University of Colorado Health Sciences Center Cancer Center Microarray Core Facility.

Data analysis. Each gene on the U95A array was represented by a group of 20 different 25-base cDNA oligomers that were complementary to a cRNA target transcript (i.e., perfect-match probes). As a hybridization specificity control, each perfect match oligomer was accompanied by an oligomer differing from the perfect match sequence by a single base pair substitution (i.e., mismatch probes). The combination of perfect-match and -mismatch cDNA oligomers for each gene is termed a probe set. Affymetrix-defined mathematical analyses (metrics) were performed to assess specific versus nonspecific hybridization of experimental cRNA targets to each probe set. Data files were analyzed by using GeneChip Microarray Suite software (version 4.0).

Initially, hybridization of cRNA targets derived from each of the 16 experimental samples was analyzed independently. By using Affymetrix-defined absolute mathematical algorithms describing perfect-match and -mismatch hybridization, each gene was defined as absent or present and was assigned a raw numerical value. Next, comparisons were made between virus-infected and mock-infected chips at each of the three time points postinfection. Raw numerical values were scaled to allow comparison between arrays. Genes considered absent (excess of mismatch hybridization or no hybridization) were not excluded from analysis, since genes changing from present to absent, absent to present, or present to present (but which increased in magnitude) were all important subsets of transcriptional alteration following viral infection compared to mock infection. By using Affymetrix-defined comparison mathematical algorithms, differential hybridization (between chips) to each cDNA probe was analyzed and designated as not changed, increased, marginally increased, decreased, or marginally decreased, and a change in expression (n-fold) was calculated. Finally, a four-way comparison of both virus-infected replicates to both mock-infected replicates at a given time point was assessed, and the mean change (n-fold) was calculated and reported along with standard error of the mean.

A gene was considered upregulated following virus infection if it was present in both virus-infected samples and if its expression increased by greater than or equal to twofold in each virus-infected sample compared to both mock-infected samples. Conversely, a gene was considered downregulated if it was present in both mock-infected samples and if its expression was decreased by greater than or equal to twofold in each virus-infected sample compared to both mock-infected samples. Genes whose expression changed by less than twofold were not considered up- or downregulated. Similarly, in order to ensure the reproducibility of the data presented, genes whose expression differed from mock-infected samples in only one of the two paired viral chips were not considered up- or downregulated.

To assess the reproducibility of hybridization results, the degree of variability in transcriptional expression among mock- and virus-infected replicate conditions was analyzed. For 99.6% of represented genes, expression was unchanged between mock-mock or virus-virus replicates. Transcriptional differences were noted in an average of 0.4% ± 0.1% of the total pool of transcripts between replicate conditions, but the genes involved represent a distinct population from the genes found to be up- or downregulated compared to virus-infected to mock-infected cells. The degree of variability in transcriptional expression as a function of time was also assessed by comparing differences in gene expression between mock infections following 6, 12, and 24 h of culture. A small proportion of transcripts were altered in response to duration of cell culture alone (1.2% ± 0.2% of the total pool). These genes were excluded from subsequent analysis.

RT-PCR. Reverse transcriptase PCR (RT-PCR) was utilized to confirm changes in expression of selected genes as identified by analysis of oligonucleotide microarrays. For RT-PCR, RNA was extracted from infected and control HEK293 cells by using infection and extraction procedures identical to those described above. RNA was converted to cDNA by using the SuperScript preamplification system (Gibco-BRL) with the supplied oligo $d(T)_{12-18}$ primer. Reverse transcription was performed at 42°C for 1 h. Semiquantitative PCR was performed by using primers generated for human DR4 (forward, 5′-CTG AGC AAC GCA GAC TCG CTG TCC AC-3′; reverse, 5′-TCC AAG GAC ACG GCA GAG CCT GTG CCA T-3′), human DR5 (forward, 5′-GCC TCA TGG ACA ATG AGA TAA AGG TGG CT-3′; reverse, 5′-CCA AAT CTC AAA GTA CGC ACA AAC GG-3′), human DCR1 (forward, 5′-GAA GAA TTT GGT GCC AAT GCC ACT G-3′; reverse, 5′-CTC TTG GAC TTG GCT GGG AGA TGT G-3′), GADD 34 (U83981) (forward, 5′-ACA CGG AGG AGG AGG AAG AT-3′; reverse, 5′-ACA GAG GAG GAA GGC AAG GT-3′), Bcl-10 (AJ006288) (forward, 5′-TCC ACA CTT CTC AGG TTG CTT-3′; reverse, 5′-AAT GGG GAA GAA GGA GAG GA-3′), caspase 3 (forward, 5′-GGT TCA TCC AGT CGC TTT GT-3′; reverse, 5′-AAC CAC CAA CCA ACC ATT C-3′; 207-bp product), Par-4 (forward, 5′-CTG AA CAT TTG CAT CCC TGT-3′; reverse, 5′ATG AAG CAG GGC AGA AAG AG-3′; 239-bp

product), SMN (U80017) (forward, 5′-CCA GAG CGA TGA TGA CA-3′; reverse, 5′-TGG GTA AAT GCA ACC GTC TT-3′; 246-bp product), DNA polymerase α (L24559) (forward, 5′-TGC TTG ACC TGA TTG CTG TC-3′; reverse, 5′-ATG ACG GGA CAA AGA CAA GG-3′; 197-bp product), ParpL (AF057160) (forward, 5′-CGC AAG GTC CAG AGA GAA AC-3′; reverse, 5′-TCC CAG GTT CAC TTC TTT GG-3′; 244-bp product), SRP40 (U30826) (forward, 5′-AGA CGA AAT GCT CCA CCT GT-3′; reverse, 5′-CGA GAC CTG CTT CTT GAC CT-3′; 281-bp product), XP-C p125 (D21089) (forward, 5′-AGA GCA GGC GAA GAC AAG AG-3′; reverse, 5′-GAT GGA CAG GCC AAT AGC AT-3′; 199-bp product), and β-actin (forward, 5′-GAA ACT ACC TTC AAC TTC AAC TCC ATC-3′; reverse, 5′-CGA GGC CAG GAT GGA GCC GCC-3′ (24). PCRs were performed by using serial dilutions of each cDNA (1:5, 1:10, and 1:20) to estimate the linear range for each primer pair by interpretation of band intensity. To avoid saturation of the PCR and maximize the ability to detect relative quantitative differences between experimental samples, the highest-input cDNA dilution that produced visible PCR products was utilized for comparisons of transcript abundance, and PCR cycles were limited to 25. RT-PCR for actin was performed in parallel with each PCR of interest for each experimental sample (as a control to ensure equal input load of cDNA in each reaction). PCR cycle conditions were 94°C for 30 seconds, 55°C for 30 seconds, and 72°C for 1 min for 25 cycles. PCR products were resolved on a 2% agarose–ethidium bromide gel run at 100 V for 1 h. Products were visualized by UV illumination with Fluor-S (Bio-Rad) software imaging. Each reaction was performed at least twice in independent experiments to confirm reproducibility.

Animal infections and immunohistochemistry. Reovirus strain 8B is an efficiently myocarditic reovirus that has been previously characterized (74) and has been shown to induce apoptotic myocardial injury in neonatal mice (18). Two-day-old Swiss-Webster (Taconic) mice were intramuscularly inoculated with 1,000 PFU of 8B reovirus (20-μl volume) in the left hind limb. Mock-infected mice received gel saline vehicle inoculation (20-μl volume; 137 mM NaCl, 0.2 mM $CaCl_2$, 0.8 mM $MgCl_2$, 19 mM H_3BO_3, 0.1 mM $Na_2B_4O_7$, 0.3% gelatin). At 1 to 7 days postinfection, mice were sacrificed and hearts were immediately immersed in 10% buffered formalin solution. After mounting as transverse sections, hearts were embedded in paraffin and sectioned to 6-μm thickness. For quantification of the degree of myocardial injury, hematoxylin- and eosin-stained midcardiac sections (at least two per heart) were examined at ×125 magnification by light microscopy and evaluated for histologic evidence of myocarditis.

Immunohistochemical analysis of survivin (SMN) expression was carried out on identical sections to assess expression over the 7 days following reovirus infection. SMN antiserum was produced in New Zealand White rabbits by immunization with the amino terminus of the surviving amino peptide sequence (PTLPPAWQPFLKDHRI) linked to keyhole limpet hemocyanin by the method of Ambrosisni. Immunoglobulins from the rabbit before immunization were purified by affinity chromatography with protein A (Pierce, Rockford, Ill.). Western blot analysis against total protein extract from HeLa cells showed reactivity with a single band of protein of approximately 16.5 kDa—consistent with the expected molecular mass. Western blotting with preimmune serum showed no immunoreactivity. Slides were deparaffinized through xylene and rehydrated through a graded alcohol series. Endogenous peroxidase was blocked with 3% hydrogen peroxide for 15 min. Antigen retrieval was performed with a 0.1 M citrate buffer for 10 min at 120°C. Primary antibody was diluted to 1.8 ng/μl in PBS (pH 7.4) with 1% bovine serum albumin applied to sections and incubated in a humidity chamber overnight at 4°C. Following three washes in PBS for 5 min each, incubation in secondary antibody labeled with polymer-linked horseradish peroxidase (Envision +; Dako, Carpinteria, Calif.) was carried out for 30 min at room temperature in a humidity chamber. Following three washes in PBS, sections were developed with 3′-diaminobenzidine (Dako) and counterstained with hematoxylin. Negative controls were performed by substitution with the preimmune immunoglobulin from the same rabbit. Positive control consisted of a colon carcinoma section that has been extensively studied in our laboratory and which shows strong staining that is consistently reproducible in this tissue.

RESULTS

Global analysis of gene expression following reovirus infection. At 6, 12, and 24 h postinfection, transcriptional expression of each of 12,000 genes present on the HU95A microarray was compared for each pair of T3A (strongly apoptosis inducing [APO+]) virus-infected and mock-infected arrays. Similar analysis was carried out at 24 h postinfection for each pair of T1L (weakly apoptosis-inducing [APO−]) virus-infected and mock-infected arrays. The subset of genes that were transcriptionally altered following T3A (APO+) infection compared to mock infection was determined. This subset of genes was also compared to those genes that were differentially expressed following T1L (APO−) infection compared to mock infection. At 6 h post-T3A (APO+) infection, expression of 18 genes (0.2% of the total genes present on the array) was altered (all with increased expression) by twofold or greater in T3A (APO+)-infected cells compared to mock-infected cells. By 12 h post-T3A (APO+) infection, expression of 86 genes (0.7%) was altered (29 genes with increased expression and 57 genes with decreased expression) in virus-infected compared to mock-infected cells. By 24 h post-T3A (APO+) infection, expression of 309 genes (2.6%) was altered (215 with increased expression and 94 with decreased expression) in virus-infected compared to mock-infected cells. In contrast, at 24 h post-T1L (APO−) infection, expression of only 59 genes (0.4%) was altered (45 with increased expression and 14 with decreased expression) in virus-infected compared to mock-infected cells. A complete listing of all genes with twofold or greater changes in expression following T3A and T1L infection is available online at http://www.uchsc.edu/sm/neuro/tylerlab/personnel/completelisting.pdf. When categorized into functionally related families, a large number of differentially expressed genes following T3A (APO+) infection were noted to encode proteins involved in apoptosis (Table 1) and DNA repair (Table 2). These genes were not differentially expressed following T1L (APO−) infection [with the exception of five genes in common between T3A (APO+) and T1L (APO−)], indicating that these changes in gene expression likely correlate with differences in virus-induced pathogenicity rather than resulting from nonspecific cellular responses to viral infection.

Reovirus-induced alteration in expression of genes involved in apoptosis. Expression of 24 genes related to the regulation of apoptosis was altered in T3A (APO+) reovirus-infected cells. These genes encode proteins that participate in apoptotic signaling involving death receptors, endoplasmic reticulum (ER) stress, mitochondrial signaling, and cysteine proteases (Table 1). For 22 of these 24 genes, significant alteration (>2-fold) in expression was not apparent until 24 h postinfection. Only five of these genes were also differentially expressed following T1L (APO−) infection.

Altered expression of genes involved in death receptor signaling pathways. We have previously shown that members of the TNF receptor superfamily of cell surface death receptors, including DR4, DR5, and their apoptosis-inducing ligand, TRAIL, play a critical role in reovirus-induced apoptosis (11, 12). We wished to determine whether alterations in expression levels of genes encoding these proteins were altered following reoviral infection. Using oligonucleotide microarrays, we did not detect significant changes in gene expression of TRAIL or the death receptors DR5, decoy receptor 1 (DcR-1), or DcR-2 at 6, 12, and 24 h postinfection in reovirus-infected cells compared to mock-infected controls (Table 3). DR4 was not represented on the U95A microarray. Expression of genes encoding other important members of the TNF receptor superfamily and their ligands was also unchanged in reovirus-infected cells including Fas, Fas ligand, TNF-α, TNF-β, and TNF receptor and TNF receptor-related protein (Table 3).

We performed additional analysis of death receptor-related

TABLE 1. Reovirus-induced alteration in expression of genes encoding proteins known to regulate apoptotic signaling

Gene	GenBank accession no.[a]	Change in expression (*n*-fold)[b] at the indicated time (h) after infection with:			
		T3A			T1L
		6	12	24	24
Mitochondrial signaling					
Pim-2 proto-oncogene homologue	U77735			−2.2 ± 0.1	
MCL1	L08246			2.0 ± 0.0	2.2 ± 0.0
BAC 15E1-cytochrome *C* oxidase polypeptide	AL021546			2.1 ± 0.0	
Par-4	U63809			2.1 ± 0.0	
HSP-70 (heat shock protein 70 testis variant)	D85730			2.2 ± 0.1	
BNIP-1 (BCL-2 interacting protein)	U15172			2.3 ± 0.2	
SMN/Btfp44/NAIP (survival motor neuron/neuronal apoptosis inhibitor protein)	U80017			2.5 ± 0.1	
DRAK-2	AB011421			2.8 ± 0.2	
SIP-1	AF027150			3.0 ± 0.2	
DP5	D83699			5.5 ± 1.1	
ER stress-induced signaling					
ORP150	U65785			−2.4 ± 0.2	
GADD 34	U83981	6.8 ± 0.2		3.7 ± 0.2	2.9 ± 0.2
GADD 45	M60974		3.3 ± 0.2	4.9 ± 0.1	4.4 ± 0.1
Death receptor signaling					
Bcl-10	AJ006288			5.6 ± 1.1	
PML-2	M79463			3.4 ± 0.3	
Ceramide glucosyltransferase	D50840			4.0 ± 1.2	
Sp100	M60618			6.5 ± 0.3	
				5.8 ± 0.6	
Proteases					
Calpain (calcium-activated neutral protease)	X04366			−2.6 ± 0.1	
Beta-4 adducin	U43959			−2.1 ± 0.1	
Caspase 7 (lice-2 beta cysteine protease)	U67319			2.6 ± 0.2	
Caspase 3 (CPP32)	U13737			3.2 ± 0.2	2.8 ± 0.1
Undefined					
Frizzled related protein	AF056087			−2.5 ± 0.1	−3.3 ± 0.5
TCBP (T cluster binding protein)	D64015			3.3 ± 0.2	
Cug-BP/hNAb50 RNA binding protein	U63289			6.6 ± 1.1	

[a] GenBank accession number corresponds to sequence from which the Affymetrix U95A probe set was designed.
[b] Data are means ± standard errors of the means.

gene expression, including DR4, DR5, DcR-1, and DcR-2 following T3A (APO+) infection by RT-PCR (Fig. 1). DR4 expression was increased at 12 and 24 h post-T3A infection compared to mock infection. In contrast, expression of DR5 was unchanged following T3A infection, thus confirming results obtained from microarray analysis. DcR-1 transcripts were not detectable in either mock- or T3A-infected cells. DcR-2 expression appeared to be decreased at 24 h post-T3A infection compared to mock-infected cells in this RT-PCR analysis. However, consistent with the microarray results, this decrease was not seen in RNase protection assays (data not shown).

Microarray analysis also revealed differential expression of four genes that encode proteins that may be involved in modulation of death receptor-associated signaling cascades in T3A (APO+)-infected cells at 24 h postinfection: PML-2, ceramide glucosyltransferase, Bcl-10, and Sp100 were increased 3.4 ± 0.3-, 4.0 ± 1.2-, 5.6 ± 1.1-, and 6.1 ± 0.5-fold, respectively. We used RT-PCR to confirm the upregulated expression of BCL-10 at 24 h post-T3A (APO+) infection (Fig. 1). Taken together, these results suggest that, with the exception of DR4

TABLE 2. Reovirus-induced alteration in expression of genes encoding proteins known to be involved in DNA repair

Gene	GenBank accession no.[a]	Change in expression (*n*-fold)[b] at the indicated time (h) after infection with:			
		T3A			T1L
		6	12	24	24
DNA ligase 1	M36067			−8.2 ± 1.1	
PARPL	AF057160			−6.3 ± 0.7	
XP-C repair complementing protein (p125)	D21089			−3.4 ± 0.1	
DNA polymerase gamma	U60325		−1.9 ± 0.1	−2.9 ± 0.1	
ERCC5	L20046		−2.7 ± 0.1		
DNA polymerase alpha	L24559			−2.5 ± 0.2	
HLP (helicase-like protein)	U09877		−2.4 ± 0.1		
GTBP	U28946		−2.0 ± 0.1	−2.1 ± 0.0	
DDB2 (p48 subunit)	U18300			−2.0 ± 0.0	
RAD 54 homologue	X97795			−2.0 ± 0.1	
Mi2 autoantigen	X86691		−1.3 ± 0.1	−2.0 ± 0.1	
MMS2	AF049140			2.1 ± 0.0	
Rad-51-interacting protein	AF006259			2.6 ± 0.2	
Rec-1	AF084513			2.4 ± 0.4	

[a] GenBank accession number corresponds to sequence from which the Affymetrix U95A probe set was designed.
[b] Data are means ± standard errors of the means.

TABLE 3. Genes encoding proteins known to be involved in apoptotic signaling which were not differentially expressed following reovirus T3A or T1L infection

Gene	GenBank accession no.[a]
Death receptor signaling	
TRAIL	U37518
DR5 (TRAIL-R2)	AF014794
Decoy receptor 1 (TRAIL-R3)	AF014794
Decoy receptor 2	AF029761
TNF	M16441
TNF-α	X02910
TNF-β	D12614
TNF receptor	M58286
TNF receptor 2-related protein	L04270
Fas (Apo-1/CD95)	X83490, X83492, Z70519, X82279, X63717
Fas ligand (FasL)	U11821, D38122
Mitochondrial signaling	
Bcl-2	M13994, M14745[b], M13995[b]
BAX alpha	L22473
BAX beta	L22474
BAX gamma	L22475[b]
BAX delta	U19599
Proteases	
Caspase 2 (Ich-1)	U13021,[b] U13022[b]
Caspase 9 (Mch-6)	U60521[b]
Caspase 4 (ICErel-II)	U28014
Caspase 5 (ICErel-III)	U28015
Caspase 6 (Mch2)-isoform alpha	U20536
Caspase 8 (MACH-alpha 1, MACH-beta 1, MACH-beta 2)	X98172, X98176, X98175
Caspase 10 (Mch4)	U60519

[a] GenBank accession number corresponds to sequence from which the Affymetrix U95A probe set was designed. Multiple accession numbers are noted for multiple representations of a particular gene (unique probe sets) on the U95A microarray.

[b] Indicates multiple representations of a particular gene derived from the same GenBank sequence.

and DcR-2, changes in death receptor and ligand gene expression are unlikely to play a critical role in reovirus-induced apoptosis. However, transcriptional alterations in genes encoding proteins that modulate death receptor signaling may play a role in reovirus-induced apoptosis.

Altered expression of genes involved in mitochondrial signaling pathways. Mitochondrial pathways play an important role in reovirus-induced apoptosis in HEK293 cells (43, 44). Following reovirus infection, both cytochrome *c* and Smac/DIABLO are released from mitochondria and trigger the activation of caspase 9 as well as the degradation of inhibitors of apoptosis (43, 44). Reovirus-induced apoptosis in MDCK and HEK293 cells is inhibited by stable overexpression of Bcl-2 (43, 44, 69), which is consistent with a significant role for the mitochondrial apoptosis pathway during reovirus infection.

Among genes whose expression was altered in T3A (APO+)-infected cells were 10 genes encoding proteins involved in mitochondrial signaling. This group included genes encoding a number of proteins known to interact with Bcl-2, including SMN, whose expression was increased 2.5 ± 0.1-fold, and SMN-interacting protein 1 (SIP-1), whose expression was increased 3.0 ± 0.2-fold. Expression of genes encoding several other Bcl-2-interacting proteins included the Bcl-2 family member MCL-1, prostate apoptosis response 4 (Par-4), DAP kinase-related apoptosis-inducing protein kinase 2 (DRAK-2), neuronal death protein 5 (DP-5), and Bcl-2-interacting protein 1 (BNIP-1), each of which were upregulated two- to sixfold following T3A (APO+) infection (Table 1). With the exception of MCL-1, expression of these genes was unaltered following T1L (APO−) infection. Bcl-2 itself was not differentially expressed in virus-infected cells, nor was the proapoptotic Bcl-2 family member BAX (Table 3).

We used RT-PCR to confirm changes in the expression of selected genes involved in mitochondrial signaling and interaction with Bcl-2 (Fig. 2). We found that the expression of SMN was increased at 24 h post-T3A (APO+) infection but not at earlier time points. Expression of Par-4 was increased at 12 and 24 h post-T3A (APO+) infection, thus confirming results obtained with oligonucleotide arrays.

These results add to previous data demonstrating that Bcl-2 plays an important regulatory role in reovirus-induced apoptosis by revealing a complex interplay of Bcl-2 regulatory factors at the transcriptional level in T3A (APO+)-infected cells.

Altered expression of genes involved in ER stress pathways. In addition to death receptor and mitochondrial pathways of apoptosis, stress signals originating in the Golgi apparatus and ER can also trigger apoptosis (79, 86). Viral proteins are potent inducers of ER stress responses (7, 22, 64). Three genes

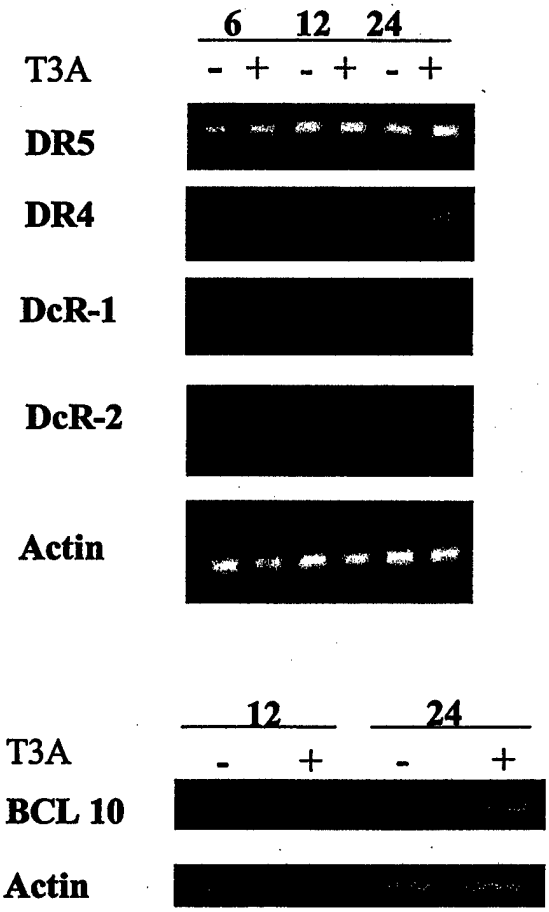

FIG. 1. Expression of genes related to death receptor-mediated apoptotic signaling is altered following reovirus T3A infection. HEK293 cells were either mock (−) or T3A (+) infected at an MOI of 100 PFU per cell. mRNA was collected at 6, 12, and 24 h postinfection and analyzed by semiquantitative RT-PCR for expression of selected transcripts encoding proteins involved in death receptor-mediated apoptotic signaling.

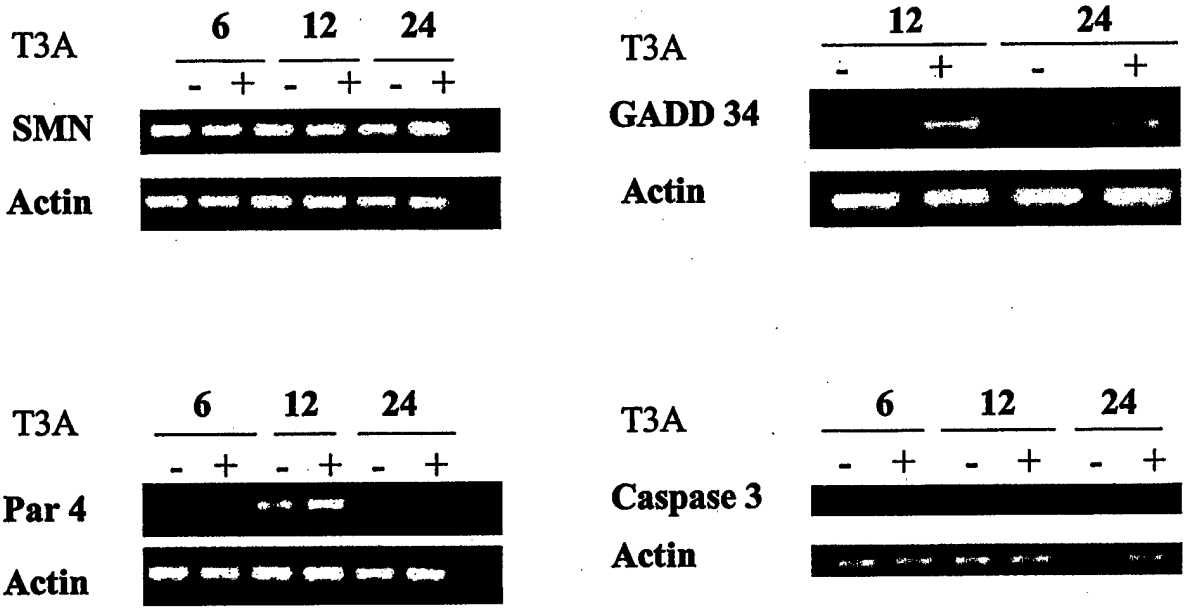

FIG. 2. Expression of genes related to mitochondrion-, ER stress-, and protease-mediated apoptotic signaling is altered following reovirus T3A infection. HEK293 cells were either mock (−) or T3A (+) infected at an MOI of 100 PFU per cell. mRNA was collected at 6, 12, and 24 h postinfection and analyzed by semiquantitative RT-PCR for expression of selected transcripts encoding proteins involved in mitochondrial (SMN and Par-4) and ER stress (GADD 34)-mediated apoptotic signaling as well as for caspase 3, a cysteine protease involved in apoptosis.

encoding proteins that are potentially involved in ER stress-related responses were differentially expressed following both T3A (APO+) and T1L (APO−) infection (Table 1). Two of these genes encode growth arrest and DNA damage (GADD)-inducible proteins GADD 34 and GADD 45. Alterations in the expression of these genes were among the earliest changes in gene expression detected in T3A (APO+)-infected cells. The increased expression of GADD 45 following reovirus infection has been discussed previously in terms of its role in reovirus-induced cell cycle regulation (65). Expression of GADD 34 was increased 6.8 ± 0.2-fold as early as 6 h post-T3A (APO+) infection. This was the largest increase in expression found for any apoptosis-related gene at any time following infection. Expression remained increased at 24 h postinfection, although the magnitude of the increase declined (3.7 ± 0.2-fold). Expression of GADD 34 and GADD 45 was also upregulated at 24 h post-T1L (APO−) infection—by 2.9 ± 0.2-fold and 4.4 + 0.1-fold, respectively. In order to confirm the increased expression of GADD 34 detected by using oligonucleotide arrays, we performed RT-PCR on reovirus-infected HEK293 cells by using GADD 34-specific primers. GADD 34 transcripts were increased at 12 and 24 h post-T3A (APO+) infection compared to mock infection (Fig. 2), thus confirming microarray results. In addition to transcriptional upregulation of genes encoding GADD proteins, transcripts for ORP150—an ER resident protein involved in the misfolded protein rescue response—were downregulated by 2.4 ± 0.2-fold following T3A (APO+)—not T1L (APO−)—infection.

These results suggest that ER stress-induced apoptotic signaling may play a role in reovirus infection. However, the fact that altered expression in GADD genes occurred following both T1L (APO−) and T3A (APO+) infection (although at lower levels in T1L [APO−] infection) suggests that these pathways may play a less-critical role in determining virus-induced apoptotic injury and rather are activated as a nonspecific cellular response to reoviral infection.

Altered expression of genes encoding cysteine proteases. Initiation of apoptosis through death receptor, mitochondrial, or ER and Golgi pathways results in the activation of specific initiator caspases. These caspases in turn activate additional caspases, culminating in the activation of effector caspases. Effector caspases, exemplified by caspases 3 and 7, act on substrates, including laminins and the caspase-activated DNase responsible for inducing the morphological features of apoptosis in target cells (28). Caspases 3, 8, and 9 are activated in reovirus-infected cells, and inhibition of caspase activation inhibits apoptosis (43).

Expression of genes encoding the effector caspases 3 and 7 were increased at 24 h following T3A (APO+) reovirus infection but not at earlier time points, consistent with their role as downstream effector caspases that are activated at the terminus of caspase cascades. Caspase 7 expression was increased 2.6 ± 0.2-fold, and that of caspase 3 was increased 3.2 ± 0.2-fold (Table 1). Caspase 3 expression was also increased at 24 h post-T1L (APO−) infection at lower levels (2.8 + 0.1-fold). Expression of genes encoding other caspases was not significantly altered following reovirus infection, including that of caspases 2, 4, 5, 6, 8, 9, and 10 (Table 3). Caspases 11, 12, 13, and 14 were not represented on the U95A microarray.

Because of the importance and central role of caspase 3 as a common effector in death receptor, mitochondrial, and ER and Golgi apoptotic signaling pathways, we wished to confirm the increased expression of this gene by using RT-PCR. Caspase 3 expression was increased over expression levels in mock-infected cells at 24 h post-T3A (APO+) infection (Fig. 2), thus confirming results obtained via oligonucleotide microarrays. Although not detected by microarray analysis, caspase 3 expression was noted to be decreased at 12 h post-T3A

(APO+) infection, preceding the increase seen at 24 h postinfection.

These results suggest that although caspase activity is clearly modulated at the protein level following reovirus infection, transcriptional upregulation of genes encoding effector caspases may also play a role in effecting reovirus-induced apoptotic injury. The fact that caspase 3 transcripts were noted to initially decrease at 12 h postinfection and then increase at 24 h postinfection indicates that transcriptional regulation is likely a complex and dynamic process that is tightly linked to rapid changes in caspase protein levels and states within infected cells.

Reovirus-induced alteration in expression of genes related to DNA repair. DNA damage is one of the basic stimuli that induces apoptosis. Cells have evolved complex mechanisms for sensing both single-strand and double-strand DNA breaks and initiating their repair (67). Expression of 14 genes encoding multiple classes of DNA repair enzymes was altered in T3A (APO+)-infected cells (Table 2). For 9 of these 14 genes, significant alteration (>2-fold) in expression was not apparent until 24 h postinfection, and 11 of these 14 alterations represented downregulation of expression. Transcription of DNA repair genes was not altered following T1L (APO−) infection. This global transcriptional downregulation of multiple classes of DNA repair enzymes following T3A (APO+) infection, which ranged from two- to eightfold, has not previously been appreciated.

Among downregulated DNA repair enzymes, expression of poly(ADP-ribosyl)-transferase (PARPL) was decreased 6.3 ± 0.7-fold, XP-C repair complementing protein 125 was decreased 3.4 ± 0.1-fold, and DNA polymerase α was decreased 2.5 ± 0.2-fold compared to expression levels in mock- or T1L-infected cells. We used RT-PCR to confirm transcriptional alterations following T3A (APO+) infection compared to mock and T1L (APO−) infection in these three DNA-repair enzymes (Fig. 3). Transcripts for XP-C and DNA polymerase α were decreased at 12 and 24 h post-T3A (APO+) infection, and PARPL was downregulated at 24 h post-T3A (APO+) infection, thus confirming the decreases in expression detected by microarray analysis. In contrast, in T1L (APO−)-infected cells, transcripts for PARPL were unchanged, transcripts for XPC were only minimally decreased (much less so than the dramatic reductions seen in T3A [APO+]-infected cells), and transcripts for DNA polymerase α were increased.

These results suggest that, as well as directly stimulating proapoptotic signaling pathways, T3A (APO+) reovirus infection may also facilitate apoptosis by downregulating the host cell's transcription of genes encoding proteins that have the capacity to repair DNA damage.

Translation of microarray data into the in vivo model of reovirus-induced myocarditis. Although changes in mRNA levels do not necessarily represent changes in protein expression, we next investigated whether previously unrecognized changes in gene expression identified by microarray analysis of reovirus-infected cells in vitro could be directly translated into delineation of pathogenic mechanisms of reovirus-induced apoptosis in vivo. Specifically, we wished to determine if an observed alteration in gene expression would be predictive of changes in expression of the relevant protein in a model of reovirus-induced tissue injury characterized by apoptosis. To

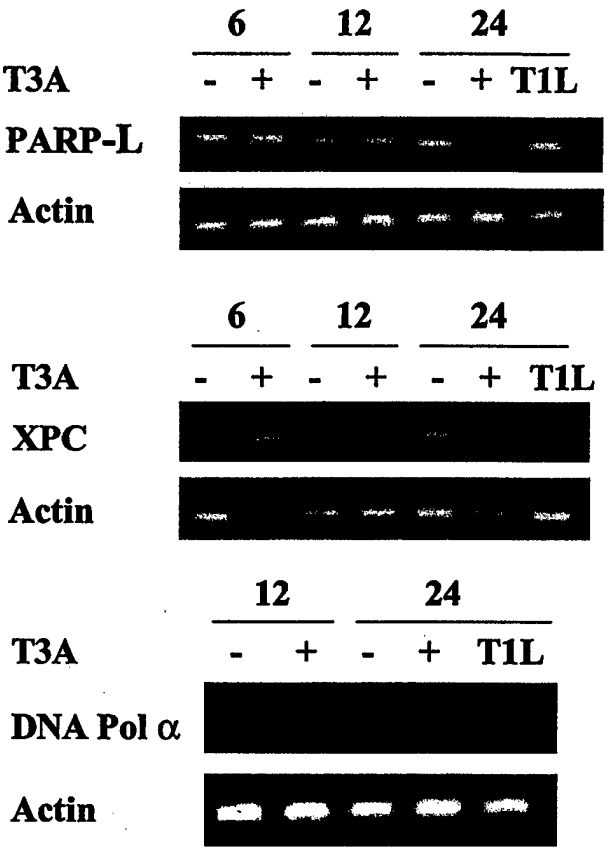

FIG. 3. Genes encoding DNA repair proteins are differentially expressed following reovirus infection. HEK293 cells were either mock (−) or T3A (+) infected at an MOI of 100 PFU per cell, and mRNA was collected at 6, 12, and 24 h postinfection. HEK293 cells were also infected with T1L at an MOI of 100 PFU per cell, with mRNA collected at 24 h postinfection. Samples were analyzed by semiquantitative RT-PCR for expression of selected transcripts encoding proteins important for DNA repair.

this end, we analyzed murine myocardial tissue following reovirus strain 8B infection, since 8B is efficiently myocarditic in neonatal mice (74), and we have previously shown that apoptosis is an important component of myocardial tissue injury following 8B infection (18).

Altered expression of genes encoding Bcl-2 regulatory proteins (which have an impact on mitochondrial apoptotic signaling) were among the most abundant changes detected by microarray analysis. We selected one of these Bcl-2 regulatory proteins, SMN, for analysis in vivo, since transcripts for SMN were noted to be selectively increased at 24 h following infection with the apoptosis-inducing strain in the microarray experiment, and this result was confirmed by RT-PCR. We therefore analyzed myocardial tissues from reovirus 8B-infected mice by immunohistochemistry on days 1 to 7 postinfection for expression of SMN in relation to histologic evidence of virus-induced apoptotic tissue damage. SMN was maximally expressed within myocardial lesions in temporal and spatial concordance with histologically detectable apoptotic myocardial injury on days 7 and 8 postinfection (Fig. 4). SMN was not detected in myocardial tissue without evidence of apoptotic myocardial injury on days 1, 3, and 5 postinfection, nor was

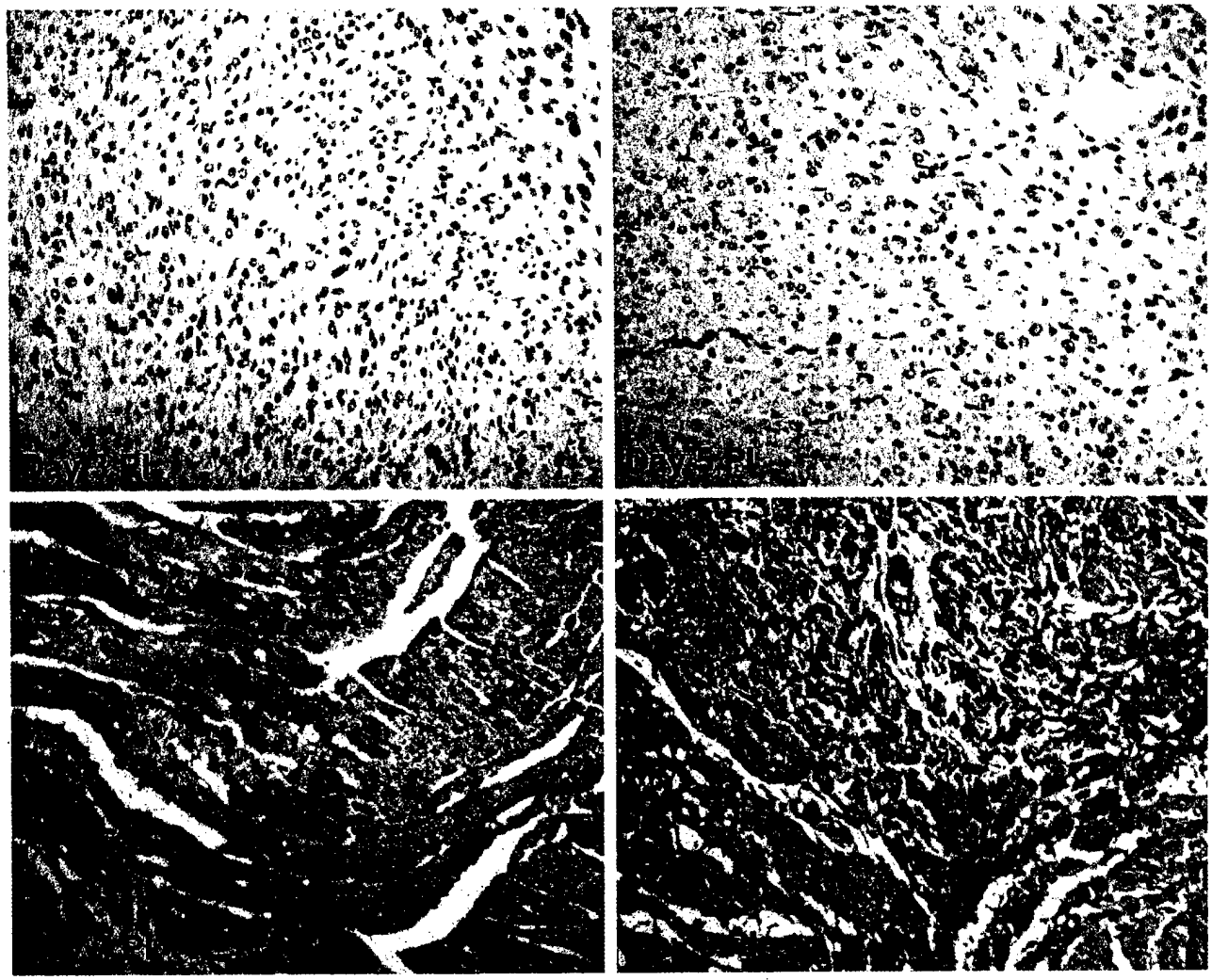

FIG. 4. SMN expression is increased in reovirus 8B-infected myocardial tissues, coincident with myocardial apoptotic injury. Neonatal Swiss-Webster mice were intramuscularly infected with 1,000 PFU of 8B virus. Myocardial tissues were analyzed on days 1 to 7 postinfection for histologic evidence of myocarditis as well as for expression of SMN by immunohistochemistry, since we have previously shown that apoptotic myocardial injury is detected at 7 days postinfection in this model. SMN protein was detected (brown stain) in infected myocardial tissue beginning on day 7 postinfection (at the time that histologic evidence of myocarditis was detected, within discrete myocardial lesions). Neither SMN nor evidence of myocardial injury was detected at earlier time points postinfection, as demonstrated on days 3 and 5 postinfection. Original magnification, ×40.

it detected in tissues from mock-infected animals. The significance of SMN upregulation within injured myocardial tissue is being investigated further. However, these results illustrate that microarray analysis of transcriptional changes following reovirus infection may provide a useful springboard toward the delineation of critical virus-induced pathogenic signaling pathways that are operative at the protein level.

DISCUSSION

Transcriptional changes related to apoptosis. Using high-throughput microarray analysis, we now demonstrate that reovirus infection is associated with differential expression of genes encoding proteins that participate in apoptotic signaling, including death receptor-, mitochondrion-, and ER stress-mediated pathways as well as DNA repair. These results represent the first large-scale description of virus-induced alterations in apoptotic signaling at the transcriptional level, including the kinetics of these changes following infection with viral strains that differ in apoptosis-inducing phenotype. The fact that the majority of these alterations occurred preferentially in T3A (APO+)- and not T1L (APO−)-infected cells suggests that interpretation of these alterations may provide important insight into critical mechanisms of reovirus-induced pathogenesis.

Microarray analysis has been increasingly utilized to investigate global transcriptional alterations following viral infection of many types, including human immunodeficiency virus (20, 83), herpesviruses (i.e., herpes simplex virus, varicella-zoster virus, Epstein-Barr virus, cytomegalovirus, and Kaposi's sarcoma-associated herpesvirus) (10, 29, 36, 39, 90, 93), rotavirus (17), Sindbis virus (38), hepatitis B (32) and C (5) viruses,

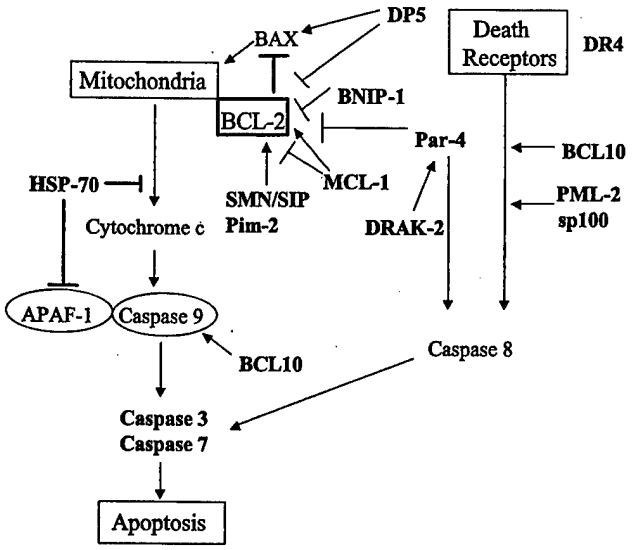

FIG. 5. Schematic of mitochondrion- and death receptor-related transcriptional alterations detected by microarray analysis following reovirus infection. Transcripts that were differentially expressed in HEK293 cells following reovirus infection compared to mock infection are indicated in boldface type. Please see Discussion for details of each indicated transcript.

measles virus (8), influenza virus (23), enterovirus (63), and papillomavirus (55). Although several groups have reported isolated alterations in transcription of genes related to apoptotic signaling following viral infection, none of these studies was specifically designed to understand the specific pathogenic mechanisms by which apoptosis-inducing viruses inflict damage on infected cells. In a comparison of two strains of Sindbis virus that differed in neurovirulence, differential transcriptional alteration of several genes related to mitochondrial apoptotic signaling was noted, including Bcl-2 family members *mcl-1*, *bfl-1*, and PBR (38). Transcriptional alteration of genes related to mitochondrial apoptotic signaling, including cytochrome *c* and inhibitors of apoptosis was also reported following rotavirus infection of caco-2 cells (17). Altered transcripts for several members of death receptor-mediated signaling pathways were reported following hepatitis C infection of hepatocytes (5), including TRAIL, TNF-R, and Fas. Likewise, TRAIL and Fas transcripts were altered in a study of papillomavirus infection of cervical keratinocytes (55). Altered transcripts for caspase 8 and TRAF4, known to be involved in death receptor signaling, have also been reported following varicella-zoster virus infection of skin fibroblasts (39). In addition to these alterations, several groups have noted transcriptional alteration in genes encoding serpins, which are known to inhibit caspases (17, 39). Transcripts for NF-κB and c-Jun—which have been linked to apoptotic signaling pathways—have also been altered following several types of viral infection.

Our study is the first that was specifically designed to dissect virus-induced alteration in apoptosis-related transcription and the first to report alteration in coordinated groups of genes with relevance to several major apoptotic signaling pathways, as well as being the first to mention global (or even isolated) downregulation of DNA repair gene transcripts following viral infection. The potential implications of identified transcriptional alterations are discussed in further detail below. Schematics that summarize the apoptosis-related transcriptional changes identified following reovirus infection are depicted in Fig. 5 (mitochondrial and death receptor signaling) and Fig. 6 (ER stress and death receptor signaling) for reference in this discussion.

Death receptor pathways. Members of the TNF receptor superfamily of cell surface death receptors—specifically DR4, DR5 and their apoptosis-inducing ligand, TRAIL—play a critical role in reovirus-induced apoptosis in HEK293 cells (11). We did not detect significant alteration in the expression of any TNF receptor superfamily members or their ligands by microarray analysis, but we did detect upregulation of transcripts for DR4 and downregulation of the decoy receptor DcR-2 by RT-PCR. This suggests, with the possible exception of DR4 and DcR-2, that reovirus activation of death receptor pathways does not involve changes in gene expression but rather occurs predominantly at the protein level. However, microarray analysis did detect alteration in the expression of genes encoding BCL-10, PML-2, and ceramide glucosyltransferase. The proteins encoded by these genes can modulate death receptor signaling, suggesting that reovirus-induced alterations in expression of these genes might influence death receptor signaling cascades.

Bcl-10 (derived from B-cell malt lymphomas) binds to TRAF2, a key accessory mediator of TNF-R signaling (78, 91). This binding can perturb TRAF-related activation of mitogen-activated protein kinases (MAPK), including JNK, and can induce the activation of the transcription factor NF-κB (25, 76, 78, 87, 91, 92). Bcl-10 contains a caspase activation and recruitment domain and can bind to procaspase-9, thereby promoting its autoproteolytic activation (45, 76, 92). Overexpression of Bcl-10 induces apoptosis in a variety of cells, including HEK293 cells (92), and it may provide a potential link between the capacity of reoviruses to activate JNK cascades, activate the transcription factor NF-κB, and induce apoptosis. PML-2 (encoded by the acute promyelocytic leukemia gene) has been

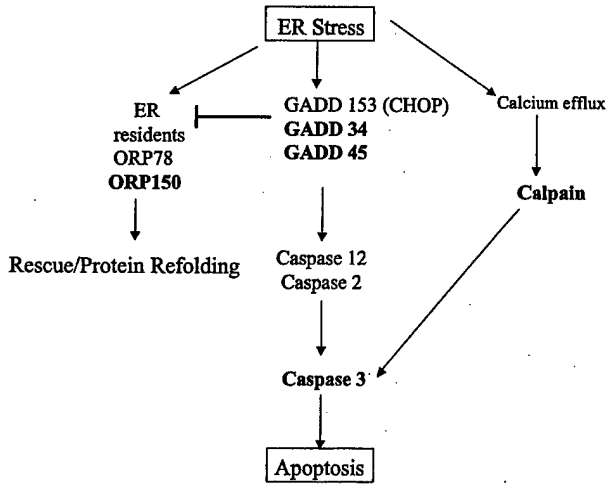

FIG. 6. Schematic of ER stress-related transcriptional alterations detected by microarray analysis following reovirus infection. Transcripts that were differentially expressed in HEK293 cells following reovirus infection compared to mock infection are indicated in boldface type. Please see Discussion for details of each indicated transcript.

shown to enhance activation of death receptor-mediated pathways involving Fas-Fas ligand and TNF and TNF-R (84, 85), suggesting the possibility that it could also potentiate signaling through DR4 and DR5. The mechanism of action of PML is unclear but appears to involve the activation of effector caspases, including caspase 3 (85). Ceramide has been implicated as an important signaling intermediary involved in both Fas-Fas ligand-mediated apoptosis and activation of MAPK cascades (27, 56, 62) Although expression of genes encoding ceramide synthesis were not altered in infected cells, the gene encoding ceramide glucosyltransferase was upregulated. This enzyme catalyzes the initial glycosylation step in glycosphingolipid synthesis to produce glucosylceramide, and its upregulation could potentially enhance ceramide signaling.

Bcl-2 and mitochondrial signaling pathways. Pro- and antiapoptotic members of the Bcl-2 family interact at the surface of the mitochondria, where complex homo- and heterodimeric interactions regulate release of proapoptotic molecules including cytochrome *c*, Smac/DIABLO, and apoptosis-inducing factor (28). Reovirus infection is associated with release of cytochrome *c* from the mitochondria into the cytoplasm and with activation of caspase 9 (43). Stable overexpression of the antiapoptotic molecule Bcl-2 inhibits reovirus-induced apoptosis in both MDCK (69) and HEK293 cells (43, 44). These results suggest that, in order to induce apoptosis, reovirus must overcome the antiapoptotic effects of Bcl-2 and related family members in order to activate mitochondrial apoptotic pathways.

Genes encoding several proteins that inhibit the activity of Bcl-2 and therefore facilitate apoptosis were found to be upregulated in reovirus-infected cells. These included Par-4, DRAK-2, DP5, and BNIP-1. Par-4 was initially identified in prostate tumor cells undergoing apoptosis but is widely expressed in human tissues (50). Although the exact mechanism of action of Par-4 is not known, it can facilitate apoptosis by suppression of Bcl-2 expression, inhibition of NF-κB activation, and activation of caspase 8 (2, 9, 21). DRAK-2 is a member of a novel family of nuclear serine-threonine kinases that can induce apoptosis (72). These kinases are known to associate with Par-4, and coexpression of Par-4 and the Zip kinase (42) (related to DRAK-2) enhances apoptosis (60). DP-5 (a death-promoting gene) contains a BH3 domain that allows it to interact with Bcl-2 family proteins. Overexpression of DP5 induces apoptosis in a variety of cells (33, 34). DP5 activation is linked with calcium release from ER stores, suggesting that DP-5 may play a role as a link between ER stress-induced and mitochondrial apoptotic pathways (33). BNIP-1 is a member of a novel BH3 domain-containing protein family that interacts with both Bcl-2 and Bcl-xL to inhibit their antiapoptotic actions, thereby enhancing apoptosis induction (49).

In addition to the upregulation of transcripts encoding Bcl-2-inhibitory proteins, downregulation of transcripts encoding proteins that promote Bcl-2 activity could contribute to promotion of apoptosis following reovirus infection. Pim 2 protooncogene homologue is a serine-threonine kinase that is highly expressed in a variety of tissues that may play an antiapoptotic role by enhancing Bcl-2 expression (3, 75). It is one of the few apoptosis regulatory genes that was downregulated following reovirus infection. Since the Pim 2 gene product enhances

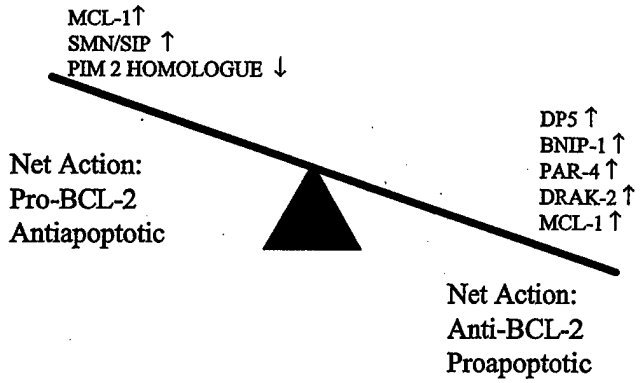

FIG. 7. Transcriptional regulation of Bcl-2 modulatory proteins is a central theme in reovirus-induced apoptosis. Expression of eight transcripts encoding proteins known to influence Bcl-2 activity was altered following reovirus infection. The predicted result of the observed transcriptional alterations would be net inhibition of Bcl-2, and thus promotion of apoptosis, in reovirus-infected cells. Please see Discussion for details of each indicated transcript.

Bcl-2 expression, its downregulation might reduce levels of Bcl-2 in infected cells and thereby enhance apoptosis.

In parallel with these transcriptional alterations with expected anti-Bcl-2 implications, alterations were also noted in expression of transcripts encoding proteins expected to promote the action of Bcl-2 and block apoptosis. Genes encoding two proteins that may act as positive modulators of Bcl-2—SMN and SIP—were found to be upregulated following reovirus infection. SMN interacts with Bcl-2 to enhance its antiapoptotic activity (35). SIP-1 interacts with SMN to form a heterodimeric complex (22a). Coexpression of SMN and Bcl-2 provides a synergistic protective effect against Bax-induced or Fas-mediated apoptosis (35, 73). Expression of the gene encoding the Bcl-2 family member MCL-1 was also upregulated following reovirus infection. MCL-1 may exert either pro- or antiapoptotic activity by modulation of the activity of Bcl-2 or by acting independently (6).

Taken together, these results suggest a model in which reovirus infection is associated with the altered expression of multiple modulators of Bcl-2 in infected host cells, with the balance tipped toward genes encoding proteins that would be predicted to inhibit Bcl-2 activity and thereby promote apoptosis (Fig. 7). Although changes in mRNA levels do not necessarily predict changes in protein expression, we demonstrated that at least one of these proteins, SMN, is altered in vivo in a biologically relevant model of reovirus infection, in close temporal and spatial association with evidence of virus-induced apoptotic myocardial tissue injury.

In addition to the modulatory struggle at the Bcl-2 level, alteration of a transcript encoding a protein with a separate role in mitochondrial apoptotic signaling was detected. HSP-70 homologue expression was increased following reovirus infection. HSP-70 is an antiapoptotic chaperone protein (52) that inhibits mitochondrial release of cytochrome *c* and blocks the recruitment of procaspase 9 to the apoptosome complex (4, 47, 71). Although the cellular actions of HSP-70 are predominantly antiapoptotic, the protein also plays a role during reovirus replication in facilitating the trimerization of the reovirus σ1 protein (46). Since this protein is a critical determinant of

reovirus apoptosis and reovirus-induced activation of specific MAPK signaling cascades (13), HSP-70 homologue may also facilitate apoptosis through its actions during virion assembly.

ER stress pathways. The accumulation of abnormal quantities of protein or of malfolded proteins in the Golgi apparatus or ER may trigger kinase cascades that result in the activation of caspase 12 (7, 53, 54). This initiator caspase triggers activation of effector caspases, such as caspase 3. One of the cellular markers of Golgi and ER stress is an increase in the quantities of specific GADD proteins such as GADD 135/CHOP (41, 94). Expression of genes encoding two of the five currently described members of the GADD family, GADD 34 and GADD 45, were increased following reoviral infection. These genes were the earliest ones found to be significantly upregulated following reovirus infection. The upregulation of ER stress apoptosis-inducing transcripts was complemented by downregulated expression of the gene for ORP 150, which encodes a protein involved in refolding malfolded protein transcripts within the ER (32a). In addition to a potential role for GADD 34 for ER stress-mediated pathways, GADD 34 induction parallels that of BAX in other models of apoptosis (30), thus suggesting a possible link to mitochondrion-regulated apoptosis signaling pathways, which are known to play an important role in reoviral infection. These results suggests that ER stress pathways may be activated as an early event following reoviral infection and that ER stress-induced apoptotic signaling may contribute to reovirus-induced apoptosis. However, the fact that altered gene expression occurred following both T1L (APO−) and T3A (APO+) infection [although at lower levels in T1L (APO−) infection] suggests the possibility that this pathway may play a less-critical role in determining virus-induced apoptotic injury and rather is activated as a nonspecific cellular response to reoviral infection.

Cysteine proteases. Death receptor, mitochondrial, and Golgi and ER pathways of apoptosis all initiate the activation of specific initiator caspases, which in turn trigger the activation of a limited set of downstream effector caspases, including caspase 3. Caspases 3, 8, and 9 are all activated during reovirus infection (43), and inhibition of this activation inhibits reovirus-induced apoptosis. Expression of the genes encoding caspases 3 and 7 were increased following reovirus infection. This suggests that, as well as inducing the activation of specific caspases at the posttranslational level, reovirus infection also results in upregulation of caspase gene expression that would be predicted to increase the levels of key effector caspases in infected cells.

We have previously shown that the cysteine protease calpain is also activated in reovirus-infected fibroblasts and myocardiocytes in vitro (19) and in the heart in vivo (18). This activation appears to be an extremely early event that can be detected as early as 30 min following infection of cells with purified virus. Inhibition of calpain activation inhibits apoptosis and reduces reovirus-induced cytopathic effects in vitro and prevents reovirus-induced apoptotic myocardial injury in vivo (18). The mechanism for the proapoptotic actions of calpains is not fully understood but may involve activation of and activation by several caspases (40, 51, 53, 66, 70, 88). Calpain can also facilitate activation of NF-κB by degrading its cytoplasmic inhibitor, IκB (1).

Surprisingly, rather than being upregulated, the expression of the gene encoding calpain was downregulated in reovirus-infected cells. This downregulation was apparent only at 24 h postinfection and could potentially represent a negative feedback response to calpain activation at the protein level: initial increases in calpain activity in infected cells could potentially be countered by downregulation of calpain expression at the transcriptional level at later time points.

Transcriptional changes related to DNA repair. Expression of transcripts encoding multiple classes of DNA repair enzymes was decreased following T3A (APO+)—but not T1L (APO−)—reovirus infection. Most DNA repair mechanisms involve a recognition step in which single- or double-stranded DNA breaks are identified, followed by the sequential action of helices that unwind damaged segments, nucleases that incise the damaged region, polymerase that resynthesizes DNA, and ligases that repair DNA strand breaks. Failure of any of these steps can result in accumulation of DNA damage and the subsequent induction of apoptosis (67).

DNA nucleotide mismatches or mutations are recognized by a mismatch-binding factor that consists of two distinct proteins—hMSH2 and G/T mismatch binding protein (GTBP)—both of which are required for mismatch-specific binding (61). The gene encoding GTBP was downregulated >2-fold at both 12 and 24 h post-T3A (APO+) infection. Downregulation of GTBP would be expected to impede recognition of single-strand DNA breaks or mutations that distort the structure of the DNA helix.

Once damage has been sensed, helicases unwind damaged DNA as a precursor to excision of the damaged segments. RAD54 homologue, Mi2 autoantigen, and helicase-like protein are three helicases (26) whose transcripts were downregulated following reovirus infection. Genes encoding two nucleotide excision repair enzymes, ERCC5 and XP-C repair-complementing protein p125, were both downregulated following T3A (APO+) reovirus infection. These enzymes are involved in repairing single-strand DNA breaks or in repairing nucleotide mutations that distort the structure of the DNA helix (67). Damaged DNA binding protein 2 (DDB2) may also play a role in nucleotide excision repair (95)—and like ERCC5 and XP-C repair-complementing protein p125, expression of genes encoding DDB2 was also downregulated in T3A (APO+)-infected cells.

Once damage is recognized, the helix is unwound, the damaged area is excised, and new DNA synthesis is required to replace the damaged nucleotides. At least nine DNA polymerases involved in various aspects of DNA replication and repair have been identified in eukaryotes (31). DNA polymerase α and DNA polymerase γ transcripts were both downregulated following T3A (APO+) reovirus infection. DNA polymerase α is primarily required for DNA replication but also interacts with and coordinates other DNA polymerases and cellular factors required for DNA repair. DNA polymerase γ is the sole polymerase required for mitochondrial replication and plays an important role in the efficient repair of mismatched DNA in vitro as well as in the repair of damaged DNA (31, 89).

Following DNA synthesis, the repaired segment must be religated with the rest of the helix. DNA ligases promote the rejoining of both double- and single-stranded DNA breaks (37, 77). Expression of the gene encoding DNA ligase 1 showed the most change in expression of any DNA repair-related gene

analyzed (downregulated 8.2 ± 1.1-fold at 24 h post-T3A infection). The second-largest change in gene expression following T3A reovirus infection was that of PARPL. PARPL attaches poly(ADP-ribose) chains to damaged DNA, a process termed ribosylation. Ribosylation is a key step during DNA repair and transcription that prevents binding of transcription factors to regions of damaged DNA (48). Thus, PARPL may serve as a molecular switch between transcription and repair of DNA to avoid expression of damaged genes (59).

The downregulation of genes encoding DNA damage and repair has not previously been appreciated as a consequence of reoviral infection. The fact this global downregulation occurred following T3A (APO+) and not T1L (APO−) reovirus infection suggests that, as well as directly stimulating proapoptotic signaling pathways, T3A reovirus infection may result in signaling pathways that facilitate apoptosis by hampering the capacity of the host cell to repair DNA damage.

Regulatory mechanisms involved in apoptosis, DNA repair, and cell cycle regulation are highly integrated and involve a number of overlapping and intersecting signaling pathways and proteins. Expression analysis performed by using high-density oligonucleotide arrays provides a unique opportunity to investigate the complex mechanisms responsible for pathogenic effects in reovirus-infected cells and tissues. Transcriptional analysis may not only be directly translatable into in vivo models of myocarditis and encephalitis, but more importantly, it may provide testable hypotheses that may not have been explored in the absence of a large-scale analysis of multiple concurrent signaling networks. Work is in progress to further investigate the models suggested in this report by manipulating genes with potentially central themes and observing effects on apoptosis and cell cycle arrest as well as effects on signaling cascades known to be operative in the reovirus model.

ACKNOWLEDGMENTS

We thank Samuel Pan for his contribution to RT-PCR validation of microarray data and Vicki VanPutten for technical assistance in analysis of microarray data.

REFERENCES

1. **Baghdiguian, S., M. Martin, I. Richard, F. Pons, C. Astier, N. Bourg, R. T. Hay, R. Chemaly, G. Halaby, J. Loiselet, L. V. Anderson, D. M. Lopez, M. Fardeau, P. Mangeat, J. S. Beckmann, and G. Lefranc.** 1999. Calpain 3 deficiency is associated with myonuclear apoptosis and profound perturbation of the IκB α/NF-κB pathway in limb-girdle muscular dystrophy type 2A. Nat. Med. **5**:503–511.
2. **Barradas, M., A. Monjas, M. T. Diaz-Meco, M. Serrano, and J. Moscat.** 1999. The downregulation of the pro-apoptotic protein Par-4 is critical for Ras-induced survival and tumor progression. EMBO J. **18**:6362–6369.
3. **Baytel, D., S. Shalom, I. Madgar, R. Weissenberg, and J. Don.** 1998. The human Pim-2 proto-oncogene and its testicular expression. Biochim. Biophys. Acta **1442**:274–285. (Erratum, **1444**:312–313, 1999.)
4. **Beere, H. M., B. B. Wolf, K. Cain, D. D. Mosser, A. Mahboubi, T. Kuwana, P. Tailor, R. I. Morimoto, G. M. Cohen, and D. R. Green.** 2000. Heat-shock protein 70 inhibits apoptosis by preventing recruitment of procaspase-9 to the Apaf-1 apoptosome. Nat. Cell Biol. **2**:469–475.
5. **Bigger, C. B., K. M. Brasky, and R. E. Lanford.** 2001. DNA microarray analysis of chimpanzee liver during acute resolving hepatitis C virus infection. J. Virol. **75**:7059–7066.
6. **Bingle, C. D., R. W. Craig, B. M. Swales, V. Singleton, P. Zhou, and M. K. Whyte.** 2000. Exon skipping in Mcl-1 results in a bcl-2 homology domain 3 only gene product that promotes cell death. J. Biol. Chem. **275**:22136–22146.
7. **Bitko, V., and S. Barik.** 2001. An endoplasmic reticulum-specific stress-activated caspase (caspase-12) is implicated in the apoptosis of A549 epithelial cells by respiratory syncytial virus. J. Cell Biochem. **80**:441–454.
8. **Bolt, G., K. Berg, and M. Blixenkrone-Moller.** 2002. Measles virus-induced modulation of host-cell gene expression. J. Gen. Virol. **83**:1157–1165.
9. **Camandola, S., and M. P. Mattson.** 2000. Pro-apoptotic action of PAR-4 involves inhibition of NF-κB activity and suppression of BCL-2 expression. J. Neurosci. Res. **61**:134–139.
10. **Carter, K. L., E. Cahir-McFarland, and E. Kieff.** 2002. Epstein-Barr virus-induced changes in B-lymphocyte gene expression. J. Virol. **76**:10427–10436.
11. **Clarke, P., S. M. Meintzer, S. Gibson, C. Widmann, T. P. Garrington, G. L. Johnson, and K. L. Tyler.** 2000. Reovirus-induced apoptosis is mediated by TRAIL. J. Virol. **74**:8135–8139.
12. **Clarke, P., S. M. Meintzer, A. C. Spalding, G. L. Johnson, and K. L. Tyler.** 2001. Caspase 8-dependent sensitization of cancer cells to TRAIL-induced apoptosis following reovirus-infection. Oncogene **20**:6910–6919.
13. **Clarke, P., S. M. Meintzer, C. Widmann, G. L. Johnson, and K. L. Tyler.** 2001. Reovirus infection activates JNK and the JNK-dependent transcription factor c-Jun. J. Virol. **75**:11275–11283.
14. **Clarke, P., and K. L. Tyler.** 2003. Reovirus-induced apoptosis: a minireview. Apoptosis **8**:141–150.
15. **Connolly, J. L., E. S. Barton, and T. S. Dermody.** 2001. Reovirus binding to cell surface sialic acid potentiates virus-induced apoptosis. J. Virol. **75**:4029–4039.
16. **Connolly, J. L., S. E. Rodgers, P. Clarke, D. W. Ballard, L. D. Kerr, K. L. Tyler, and T. S. Dermody.** 2000. Reovirus-induced apoptosis requires activation of transcription factor NF-κB. J. Virol. **74**:2981–2989.
17. **Cuadras, M. A., D. A. Feigelstock, S. An, and H. B. Greenberg.** 2002. Gene expression pattern in Caco-2 cells following rotavirus infection. J. Virol. **76**:4467–4482.
18. **DeBiasi, R. L., C. L. Edelstein, B. Sherry, and K. L. Tyler.** 2001. Calpain inhibition protects against virus-induced apoptotic myocardial injury. J. Virol. **75**:351–361.
19. **DeBiasi, R. L., M. K. Squier, B. Pike, M. Wynes, T. S. Dermody, J. J. Cohen, and K. L. Tyler.** 1999. Reovirus-induced apoptosis is preceded by increased cellular calpain activity and is blocked by calpain inhibitors. J. Virol. **73**:695–701.
20. **de la Fuente, C., F. Santiago, L. Deng, C. Eadie, I. Zilberman, K. Kehn, A. Maddukuri, S. Baylor, K. Wu, C. G. Lee, A. Pumfery, and F. Kashanchi.** 2002. Gene expression profile of HIV-1 Tat expressing cells: a close interplay between proliferative and differentiation signals. BMC Biochem. **3**:14.
21. **Diaz-Meco, M. T., M. J. Lallena, A. Monjas, S. Frutos, and J. Moscat.** 1999. Inactivation of the inhibitory κB protein kinase/nuclear factor κB pathway by Par-4 expression potentiates tumor necrosis factor α-induced apoptosis. J. Biol. Chem. **274**:19606–19612.
22. **Everett, H., and G. McFadden.** 1999. Apoptosis: an innate immune response to virus infection. Trends Microbiol. **7**:160–165.

22a. **Fischer, U., Q. Liu, and G. Dreyfuss.** 1997. The SMN-SIP1 complex has an essential role in spliceosomal snRNP biogenesis. Cell **90**:1023–1029.

23. **Geiss, G. K., M. C. An, R. E. Bumgarner, E. Hammersmark, D. Cunningham, and M. G. Katze.** 2001. Global impact of influenza virus on cellular pathways is mediated by both replication-dependent and -independent events. J. Virol. **75**:4321–4331.
24. **Griffith, T. S., S. R. Wiley, M. Z. Kubin, L. M. Sedger, C. R. Maliszewski, and N. A. Fanger.** 1999. Monocyte-mediated tumoricidal activity via the tumor necrosis factor-related cytokine, TRAIL. J. Exp. Med. **189**:1343–1354.
25. **Guiet, C., and P. Vito.** 2000. Caspase recruitment domain (CARD)-dependent cytoplasmic filaments mediate bcl10-induced NF-κB activation. J. Cell Biol. **148**:1131–1140.
26. **Hammermann, R., U. Warskulat, and D. Haussinger.** 1998. Anisoosmotic regulation of the Mi-2 autoantigen mRNA in H4IIE rat hepatoma cells and primary hepatocytes. FEBS Lett. **435**:21–24.
27. **Hannun, Y. A.** 1996. Functions of ceramide in coordinating cellular responses to stress. Science **274**:1855–1859.
28. **Hengartner, M. O.** 2000. The biochemistry of apoptosis. Nature **407**:770–776.
29. **Hobbs, W. E., and N. A. DeLuca.** 1999. Perturbation of cell cycle progression and cellular gene expression as a function of herpes simplex virus ICP0. J. Virol. **73**:8245–8255.
30. **Hollander, M. C., Q. Zhan, I. Bae, and A. J. Fornace, Jr.** 1997. Mammalian GADD34, an apoptosis- and DNA damage-inducible gene. J. Biol. Chem. **272**:13731–13737.
31. **Hubscher, U., H. P. Nasheuer, and J. E. Syvaoja.** 2000. Eukaryotic DNA polymerases, a growing family. Trends Biochem. Sci. **25**:143–147.
32. **Iizuka, N., M. Oka, H. Yamada-Okabe, N. Mori, T. Tamesa, T. Okada, N. Takemoto, A. Tangoku, K. Hamada, H. Nakayama, T. Miyamoto, S. Uchimura, and Y. Hamamoto.** 2002. Comparison of gene expression profiles between hepatitis B virus- and hepatitis C virus-infected hepatocellular carcinoma by oligonucleotide microarray data on the basis of a supervised learning method. Cancer Res. **62**:3939–3944.

32a. **Ikeda, J., S. Kaneda, K. Kuwabara, S. Ogawa, T. Kobayashi, M. Matsumoto, T. Yura, and H. Yunagi.** 1997. Cloning and expression of cDNA encoding the human 150 kDa oxygen-regulated protein, ORP150. Biochem. Biophys. Res. Commun. **230**:94–99.

33. **Imaizumi, K., T. Morihara, Y. Mori, T. Katayama, M. Tsuda, T. Furuyama, A. Wanaka, M. Takeda, and M. Tohyama.** 1999. The cell death-promoting gene DP5, which interacts with the BCL2 family, is induced during neuronal

apoptosis following exposure to amyloid beta protein. J. Biol. Chem. **274:** 7975–7981.
34. **Imaizumi, K., M. Tsuda, Y. Imai, A. Wanaka, T. Takagi, and M. Tohyama.** 1997. Molecular cloning of a novel polypeptide, DP5, induced during programmed neuronal death. J. Biol. Chem. **272:**18842–18848.
35. **Iwahashi, H., Y. Eguchi, N. Yasuhara, T. Hanafusa, Y. Matsuzawa, and Y. Tsujimoto.** 1997. Synergistic anti-apoptotic activity between Bcl-2 and SMN implicated in spinal muscular atrophy. Nature **390:**413–417.
36. **Jenner, R. G., M. M. Alba, C. Boshoff, and P. Kellam.** 2001. Kaposi's sarcoma-associated herpesvirus latent and lytic gene expression as revealed by DNA arrays. J. Virol. **75:**891–902.
37. **Johnson, A. P., and M. P. Fairman.** 1997. The identification and purification of a novel mammalian DNA ligase. Mutat. Res. **383:**205–212.
38. **Johnston, C., W. Jiang, T. Chu, and B. Levine.** 2001. Identification of genes involved in the host response to neurovirulent alphavirus infection. J. Virol. **75:**10431–10445.
39. **Jones, J. O., and A. M. Arvin.** 2003. Microarray analysis of host cell gene transcription in response to varicella-zoster virus infection of human T cells and fibroblasts in vitro and SCIDhu skin xenografts in vivo. J. Virol. **77:** 1268–1280.
40. **Kato, M., T. Nonaka, M. Maki, H. Kikuchi, and S. Imajoh-Ohmi.** 2000. Caspases cleave the amino-terminal calpain inhibitory unit of calpastatin during apoptosis in human Jurkat T cells. J. Biochem. (Tokyo) **127:**297–305.
41. **Kaufman, R. J.** 1999. Stress signaling from the lumen of the endoplasmic reticulum: coordination of gene transcriptional and translational controls. Genes Dev. **13:**1211–1233.
42. **Kogel, D., H. Bierbaum, U. Preuss, and K. H. Scheidtmann.** 1999. C-terminal truncation of Dlk/ZIP kinase leads to abrogation of nuclear transport and high apoptotic activity. Oncogene **18:**7212–7218.
43. **Kominsky, D. J., R. J. Bickel, and K. L. Tyler.** 2002. Reovirus-induced apoptosis requires both death receptor- and mitochondrial-mediated caspase-dependent pathways of cell death. Cell Death Differ. **9:**926–933.
44. **Kominsky, D. J., R. J. Bickel, and K. L. Tyler.** 2002. Reovirus-induced apoptosis requires mitochondrial release of Smac/DIABLO and involves reduction of cellular inhibitor of apoptosis protein levels. J. Virol. **76:**11414–11424.
45. **Koseki, T., N. Inohara, S. Chen, R. Carrio, J. Merino, M. O. Hottiger, G. J. Nabel, and G. Nunez.** 1999. CIPER, a novel NF κB-activating protein containing a caspase recruitment domain with homology to herpesvirus-2 protein E10. J. Biol. Chem. **274:**9955–9961.
46. **Leone, G., M. C. Coffey, R. Gilmore, R. Duncan, L. Maybaum, and P. W. Lee.** 1996. C-terminal trimerization, but not N-terminal trimerization, of the reovirus cell attachment protein is a posttranslational and Hsp70/ATP-dependent process. J. Biol. Chem. **271:**8466–8471.
47. **Li, C. Y., J. S. Lee, Y. G. Ko, J. I. Kim, and J. S. Seo.** 2000. Heat shock protein 70 inhibits apoptosis downstream of cytochrome c release and upstream of caspase 3 activation. J. Biol. Chem. **275:**25665–25671.
48. **Lindahl, T., and R. D. Wood.** 1999. Quality control by DNA repair. Science **286:**1897–1905.
49. **Low, B. C., Y. P. Lim, J. Lim, E. S. Wong, and G. R. Guy.** 1999. Tyrosine phosphorylation of the Bcl-2-associated protein BNIP-2 by fibroblast growth factor receptor-1 prevents its binding to Cdc42GAP and Cdc42. J. Biol. Chem. **274:**33123–33130.
50. **Mattson, M. P., W. Duan, S. L. Chan, and S. Camandola.** 1999. Par-4: an emerging pivotal player in neuronal apoptosis and neurodegenerative disorders. J. Mol. Neurosci. **13:**17–30.
51. **McGinnis, K. M., M. E. Gnegy, Y. H. Park, N. Mukerjee, and K. K. Wang.** 1999. Procaspase-3 and poly(ADP)ribose polymerase (PARP) are calpain substrates. Biochem. Biophys. Res. Commun. **263:**94–99.
52. **Mosser, D. D., A. W. Caron, L. Bourget, A. B. Meriin, M. Y. Sherman, R. I. Morimoto, and B. Massie.** 2000. The chaperone function of hsp70 is required for protection against stress-induced apoptosis. Mol. Cell. Biol. **20:**7146–7159.
53. **Nakagawa, T., and J. Yuan.** 2000. Cross-talk between two cysteine protease families—activation of caspase-12 by calpain in apoptosis. J. Cell Biol. **150:** 887–894.
54. **Nakagawa, T., H. Zhu, N. Morishima, E. Li, J. Xu, B. A. Yankner, and J. Yuan.** 2000. Caspase-12 mediates endoplasmic-reticulum-specific apoptosis and cytotoxicity by amyloid-β. Nature **403:**98–103.
55. **Nees, M., J. M. Geoghegan, T. Hyman, S. Frank, L. Miller, and C. D. Woodworth.** 2001. Papillomavirus type 16 oncogenes downregulate expression of interferon-responsive genes and upregulate proliferation-associated and NF-κB-responsive genes in cervical keratinocytes. J. Virol. **75:**4283–4296.
56. **Obeid, L. M., C. M. Linardic, L. A. Karolak, and Y. A. Hannun.** 1993. Programmed cell death induced by ceramide. Science **259:**1769–1771.
57. **Oberhaus, S. M., T. S. Dermody, and K. L. Tyler.** 1998. Apoptosis and the cytopathic effects of reovirus. Curr. Top. Microbiol. Immunol. **233**(Reovir.ii):23–49.
58. **Oberhaus, S. M., R. L. Smith, G. H. Clayton, T. S. Dermody, and K. L. Tyler.** 1997. Reovirus infection and tissue injury in the mouse central nervous system are associated with apoptosis. J. Virol. **71:**2100–2106.
59. **Oei, S. L., J. Griesenbeck, M. Schweiger, and M. Ziegler.** 1998. Regulation of RNA polymerase II-dependent transcription by poly(ADP-ribosyl)ation of transcription factors. J. Biol. Chem. **273:**31644–31647.
60. **Page, G., D. Kogel, V. Rangnekar, and K. H. Scheidtmann.** 1999. Interaction partners of Dlk/ZIP kinase: co-expression of Dlk/ZIP kinase and Par-4 results in cytoplasmic retention and apoptosis. Oncogene **18:**7265–7273.
61. **Palombo, F., P. Gallinari, I. Iaccarino, T. Lettieri, M. Hughes, A. D'Arrigo, O. Truong, J. J. Hsuan, and J. Jiricny.** 1995. GTBP, a 160-kilodalton protein essential for mismatch-binding activity in human cells. Science **268:**1912–1914.
62. **Perry, D. K.** 1999. Ceramide and apoptosis. Biochem. Soc. Trans. **27:**399–404.
63. **Pietiainen, V., P. Huttunen, and T. Hyypia.** 2000. Effects of echovirus 1 infection on cellular gene expression. Virology **276:**243–250.
64. **Ploegh, H. L.** 1998. Viral strategies of immune evasion. Science **280:**248–253.
65. **Poggioli, G. J., R. L. DeBiasi, R. Bickel, R. Jotte, A. Spalding, G. L. Johnson, and K. L. Tyler.** 2002. Reovirus-induced alterations in gene expression related to cell cycle regulation. J. Virol. **76:**2585–2594.
66. **Rami, A., R. Agarwal, G. Botez, and J. Winckler.** 2000. μ-Calpain activation, DNA fragmentation, and synergistic effects of caspase and calpain inhibitors in protecting hippocampal neurons from ischemic damage. Brain Res. **866:** 299–312.
67. **Rich, T., R. L. Allen, and A. H. Wyllie.** 2000. Defying death after DNA damage. Nature **407:**777–783.
68. **Richardson-Burns, S. M., D. J. Kominsky, and K. L. Tyler.** 2002. Reovirus-induced neuronal apoptosis is mediated by caspase 3 and is associated with the activation of death receptors. J. Neurovirol. **8:**365–380.
69. **Rodgers, S. E., E. S. Barton, S. M. Oberhaus, B. Pike, C. A. Gibson, K. L. Tyler, and T. S. Dermody.** 1997. Reovirus-induced apoptosis of MDCK cells is not linked to viral yield and is blocked by Bcl-2. J. Virol. **71:**2540–2546.
70. **Ruiz-Vela, A., D. B. Gonzalez, and A. Martinez.** 1999. Implication of calpain in caspase activation during B cell clonal deletion. EMBO J. **18:**4988–4998.
71. **Saleh, A., S. M. Srinivasula, L. Balkir, P. D. Robbins, and E. S. Alnemri.** 2000. Negative regulation of the Apaf-1 apoptosome by Hsp70. Nat. Cell Biol. **2:**476–483.
72. **Sanjo, H., T. Kawai, and S. Akira.** 1998. DRAKs, novel serine/threonine kinases related to death-associated protein kinase that trigger apoptosis. J. Biol. Chem. **273:**29066–29071.
73. **Sato, K., Y. Eguchi, T. S. Kodama, and Y. Tsujimoto.** 2000. Regions essential for the interaction between Bcl-2 and SMN, the spinal muscular atrophy disease gene product. Cell Death Differ. **7:**374–383.
74. **Sherry, B., F. J. Schoen, E. Wenske, and B. N. Fields.** 1989. Derivation and characterization of an efficiently myocarditic reovirus variant. J. Virol. **63:** 4840–4849.
75. **Shirogane, T., T. Fukada, J. M. Muller, D. T. Shima, M. Hibi, and T. Hirano.** 1999. Synergistic roles for Pim-1 and c-Myc in STAT3-mediated cell cycle progression and antiapoptosis. Immunity **11:**709–719.
76. **Srinivasula, S. M., M. Ahmad, J. H. Lin, J. L. Poyet, T. Fernandes-Alnemri, P. N. Tsichlis, and E. S. Alnemri.** 1999. CLAP, a novel caspase recruitment domain-containing protein in the tumor necrosis factor receptor pathway, regulates NF-κB activation and apoptosis. J. Biol. Chem. **274:**17946–17954.
77. **Teo, S. H., and S. P. Jackson.** 1997. Identification of *Saccharomyces cerevisiae* DNA ligase IV: involvement in DNA double-strand break repair. EMBO J. **16:**4788–4795.
78. **Thome, M., F. Martinon, K. Hofmann, V. Rubio, V. Steiner, P. Schneider, C. Mattmann, and J. Tschopp.** 1999. Equine herpesvirus-2 E10 gene product, but not its cellular homologue, activates NF-κB transcription factor and c-Jun N-terminal kinase. J. Biol. Chem. **274:**9962–9968.
79. **Tirasophon, W., K. Lee, B. Callaghan, A. Welihinda, and R. J. Kaufman.** 2000. The endoribonuclease activity of mammalian IRE1 autoregulates its mRNA and is required for the unfolded protein response. Genes Dev. **14:**2725–2736.
80. **Tyler, K. L.** 1998. Pathogenesis of reovirus infections of the central nervous system. Curr. Top. Microbiol. Immunol. **233** (Reovir.ii):93–124.
81. **Tyler, K. L., P. Clarke, R. L. DeBiasi, D. Kominsky, and G. J. Poggioli.** 2001. Reoviruses and the host cell. Trends Microbiol. **9:**560–564.
82. **Tyler, K. L., M. K. Squier, S. E. Rodgers, B. E. Schneider, S. M. Oberhaus, T. A. Grdina, J. J. Cohen, and T. S. Dermody.** 1995. Differences in the capacity of reovirus strains to induce apoptosis are determined by the viral attachment protein σ1. J. Virol. **69:**6972–6979.
83. **van't Wout, A. B., G. K. Lehrman, S. A. Mikheeva, G. C. O'Keeffe, M. G. Katze, R. E. Bumgarner, G. K. Geiss, and J. I. Mullins.** 2003. Cellular gene expression upon human immunodeficiency virus type 1 infection of $CD4^+$-T-cell lines. J. Virol. **77:**1392–1402.
84. **Wang, Z. G., L. Delva, M. Gaboli, R. Rivi, M. Giorgio, C. Cordon-Cardo, F. Grosveld, and P. P. Pandolfi.** 1998. Role of PML in cell growth and the retinoic acid pathway. Science **279:**1547–1551.
85. **Wang, Z. G., D. Ruggero, S. Ronchetti, S. Zhong, M. Gaboli, R. Rivi, and P. P. Pandolfi.** 1998. PML is essential for multiple apoptotic pathways. Nat. Genet. **20:**266–272.
86. **Welihinda, A. A., W. Tirasophon, and R. J. Kaufman.** 1999. The cellular

response to protein misfolding in the endoplasmic reticulum. Gene Expr. 7:293–300.

87. **Willis, T. G., D. M. Jadayel, M. Q. Du, H. Peng, A. R. Perry, M. Abdul-Rauf, H. Price, L. Karran, O. Majekodunmi, I. Wlodarska, L. Pan, T. Crook, R. Hamoudi, P. G. Isaacson, and M. J. Dyer.** 1999. Bcl10 is involved in t(1;14)(p22;q32) of MALT B cell lymphoma and mutated in multiple tumor types. Cell **96**:35–45.
88. **Wood, D. E., and E. W. Newcomb.** 1999. Caspase-dependent activation of calpain during drug-induced apoptosis. J. Biol. Chem. **274**:8309–8315.
89. **Wood, R. D., and M. K. Shivji.** 1997. Which DNA polymerases are used for DNA repair in eukaryotes? Carcinogenesis **18**:605–610.
90. **Yang, W. C., G. V. Devi-Rao, P. Ghazal, E. K. Wagner, and S. J. Triezenberg.** 2002. General and specific alterations in programming of global viral gene expression during infection by VP16 activation-deficient mutants of herpes simplex virus type 1. J. Virol. **76**:12758–12774.
91. **Yoneda, T., K. Imaizumi, M. Maeda, D. Yui, T. Manabe, T. Katayama, N. Sato, F. Gomi, T. Morihara, Y. Mori, K. Miyoshi, J. Hitomi, S. Ugawa, S. Yamada, M. Okabe, and M. Tohyama.** 2000. Regulatory mechanisms of TRAF2-mediated signal transduction by Bcl10, a MALT lymphoma-associated protein. J. Biol. Chem. **275**:11114–11120.
92. **Zhang, Q., R. Siebert, M. Yan, B. Hinzmann, X. Cui, L. Xue, K. M. Rakestraw, C. W. Naeve, G. Beckmann, D. D. Weisenburger, W. G. Sanger, H. Nowotny, M. Vesely, E. Callet-Bauchu, G. Salles, V. M. Dixit, A. Rosenthal, B. Schlegelberger, and S. W. Morris.** 1999. Inactivating mutations and overexpression of BCL10, a caspase recruitment domain-containing gene, in MALT lymphoma with t(1;14)(p22;q32). Nat. Genet. **22**:63–68.
93. **Zhu, H., J. P. Cong, G. Mamtora, T. Gingeras, and T. Shenk.** 1998. Cellular gene expression altered by human cytomegalovirus: global monitoring with oligonucleotide arrays. Proc. Natl. Acad. Sci. USA **95**:14470–14475.
94. **Zinszner, H., M. Kuroda, X. Wang, N. Batchvarova, R. T. Lightfoot, H. Remotti, J. L. Stevens, and D. Ron.** 1998. CHOP is implicated in programmed cell death in response to impaired function of the endoplasmic reticulum. Genes Dev. **12**:982–995.
95. **Zolezzi, F., and S. Linn.** 2000. Studies of the murine DDB1 and DDB2 genes. Gene **245**:151–159.

The EMBO Journal Vol. 22 No. 13 pp. 3346–3355, 2003

MEKK1 regulates calpain-dependent proteolysis of focal adhesion proteins for rear-end detachment of migrating fibroblasts

Bruce D.Cuevas[1,2], Amy N.Abell[1], James A.Witowsky[1], Toshiaki Yujiri[3], Nancy Lassignal Johnson[1], Kamala Kesavan[1], Marti Ware[1], Peter L.Jones[4,5], Scott A.Weed[5,6], Roberta L.DeBiasi[4,7,8], Yoshitomo Oka[3], Kenneth L.Tyler[7,8,9] and Gary L.Johnson[1,2,9]

Departments of [1]Pharmacology, [4]Pediatrics, [8]Neurology, [9]Medicine, [5]Cell & Structural Biology, [6]Craniofacial Biology, University of Colorado Health Sciences Center, Denver, CO 80262, [7]Denver Veterans Affairs Medical Center, Denver, CO 80220, USA and [3]Third Department of Internal Medicine, Yamaguchi University of Medicine, Yamaguchi, Japan

[2]Corresponding authors
e-mail: bruce.cuevas@uchsc.edu or glj@med.unc.edu

Herein, we define how MEKK1, a MAPK kinase kinase, regulates cell migration. MEKK1 is associated with actin fibers and focal adhesions, localizing MEKK1 to sites critical in the control of cell adhesion and migration. EGF-induced ERK1/2 activation and chemotaxis are inhibited in MEKK1–/– fibroblasts. MEKK1 deficiency causes loss of vinculin in focal adhesions of migrating cells, increased cell adhesion and impeded rear-end detachment. MEKK1 is required for activation of the cysteine protease calpain and cleavage of spectrin and talin, proteins linking focal adhesions to the cytoskeleton. Inhibition of ERK1/2 or calpain, but not of JNK, mimics MEKK1 deficiency. Therefore, MEKK1 regulates calpain-mediated substratum release of migrating fibroblasts.
Keywords: calpain/MEKK1/rear-end detachment

Introduction

Cell migration involves at least four basic components: extension of the leading edge, adherence to the substratum, release of adherence at the trailing edge and retraction of the trailing uropod. While adherence is necessary to exert force on a surface and produce forward movement, release of adherence at the uropod must occur for cell migration to continue. Control of adherence, and release thereof, is thus a critical regulatory function for migrating cells. Whereas extension and adherence have been studied extensively, few proteins have been characterized as regulators of the adhesion-release process during cell migration. Recently, the cysteine proteinase calpain has emerged as an important regulator of cell adhesion (Huttenlocher *et al.*, 1997; Bialkowska *et al.*, 2000). Originally referred to as Ca^{2+}-dependent neutral protease (Beckerle *et al.*, 1987), the calpain family includes two ubiquitously expressed isoforms, μ- and m-calpain (murine calpains 1 and 2, respectively) (Huang and Wang, 2001). Calpains have been suspected to regulate cell adhesion due to their ability to cleave several focal adhesion and cytoskeletal proteins (Pfaff *et al.*, 1999; Wang and Yuen, 1999). Further, calpain has been shown to be associated with cell adhesion complexes (Beckerle *et al.*, 1987), and calpain-deficient fibroblasts display inhibited migration (Arthur *et al.*, 2000; Dourdin *et al.*, 2001). Overexpression of the calpain inhibitor calpastatin also impairs cell detachment and migration (Potter *et al.*, 1998). Calpain has been proposed to regulate cell detachment through proteolytic cleavage of adhesion complex proteins in the trailing edge of migrating cells (Palecek *et al.*, 1998). An understanding of calpain regulation during migration has remained elusive. Recently, the MEK/ERK1/2 signaling pathway has been linked to calpain activation as the pharmacological MEK inhibitor PD98059 was shown to inhibit EGF-induced calpain activation (Glading *et al.*, 2000). Subsequent studies revealed that membrane-proximal ERK1/2 activity is required for EGF-induced m-calpain activation and cell migration (Glading *et al.*, 2001).

MEKK1 is a MAPK kinase kinase that is activated in response to changes in cell shape and the microtubule cytoskeleton (Yujiri *et al.*, 1999). Dual regulation of JNK and ERK1/2 pathways by low concentrations of growth factors like EGF and by microtubule-disrupting agents like nocodazole is mediated by MEKK1 (Yujiri *et al.*, 1998). Targeted gene disruption of MEKK1 demonstrated that it functionally regulates cell migration both *in vivo* and *in vitro* (Yujiri *et al.*, 2000). Our results reveal an association of MEKK1 with focal adhesions and actin fibers entering the focal adhesions. MEKK1 regulates the limited proteolysis of the focal adhesion proteins talin and spectrin. Characterization of MEKK1-null mouse embryo fibroblasts demonstrates that MEKK1 regulates the ERK1/2 pathway for control of calpain-catalyzed rear-end detachment.

Results

MEKK1 regulates cell adhesion

Comparison of wild-type and MEKK1–/– fibroblasts readily defines a function for MEKK1 in regulating cell adhesion and migration. We found that MEKK1–/– fibroblasts have a marked increase in adherence to the culture substratum relative to wild-type fibroblasts (Figure 1A). Using wild-type and MEKK1–/– cells that had been serum starved and then challenged with or without serum, the culture plates were inverted and centrifuged. The remaining attached cells were counted as a measure of adherence, with greater number of cells after centrifugation being indicative of increased adherence (Lotz *et al.*, 1989). This simple assay clearly demonstrates the increased adherence of MEKK1–/– cells relative to wild-type fibroblasts. Even though

MEKK1–/– cells show an increased adherence in the centrifugation assay, their rate of attachment on fibronectin or tissue culture plastic alone is similar to the rate of attachment of wild-type cells (Figure 1B). The increased adherence in the centrifugation assay, but similar attachment rate of MEKK1–/– compared with wild-type fibroblasts, suggested MEKK1 regulates release of cell adhesion. We used live cell microscopy to show that MEKK1–/– fibroblasts are, indeed, inhibited in random migration and rear-end detachment (see Supplementary data available at *The EMBO Journal* Online). Both wild-type and MEKK1–/– fibroblasts are capable of extending lamellipodia necessary for forward movement, and both cell types develop tails or uropods at the trailing edge as the cell moves in the direction of the leading edge. However, as wild-type fibroblasts have the ability to detach and retract their trailing edge, MEKK1–/– cell forward progress is impeded by an inability of the uropod to detach from the substrate, thereby giving the appearance that MEKK1–/– cells are tethered at their trailing end. Thus, the increased adherence of MEKK1–/– cells is, at least in part, a result of defective detachment from the substratum.

MEKK1 regulates directed cell migration

Inhibited movement of MEKK1–/– fibroblasts was readily demonstrated using both transwell migration and *in vitro* wound response assays. Chemotaxis toward serum is inhibited in MEKK1–/– compared with wild-type fibroblasts (Figure 2A), consistent with a defect in cell movement that would be observed with a loss of rear-end detachment. Further, when soluble fibronectin is used as a chemotactic agent, migration is reduced by 50% in MEKK1–/– versus wild-type cells (Figure 2B). Although EGF by itself is a weak chemotactic agent, EGF combined with fibronectin produces a synergistic effect relative to fibronectin alone to induce chemotaxis (Maheshwari *et al.*, 1999) (Figure 2B). This synergistic effect is completely absent in MEKK1-deficient cells, thus demonstrating that MEKK1 is required for the EGF/fibronectin-induced fibroblast migration.

When a confluent contact-inhibited fibroblast culture is 'wounded' using a razor swipe, the cells along the edge of the wound are contact inhibited on all sides save one, and will migrate into the wound opening. Wild-type fibroblasts will migrate into the wound space within 5 h after initiation of the wound (Figure 2C). In contrast, MEKK1–/– fibroblast migration into the open area of the wound is markedly inhibited. Indeed, the time required by MEKK1–/– fibroblasts to completely close a standardized wound (24.5 h) is significantly ($P < 0.05$) prolonged compared with the MEKK1+/+ cells (11 h) (Figure 2D). By 12 h post-wounding, some MEKK1–/– fibroblasts have migrated into the wound site but do not reach numbers or distances achieved by MEKK1+/+ fibroblasts. This indicates that MEKK1–/– fibroblasts are markedly defective, but not completely inhibited in directed migration. The loss of migration is a direct consequence of MEKK1 deficiency because MEKK1 add-back by transfection of MEKK1–/– cells restores migration into the wound (Figure 2C and D). It is possible that the migration defect of MEKK1–/– cells was due to the loss of expression of a secreted factor such as a cytokine, protease or extracellular

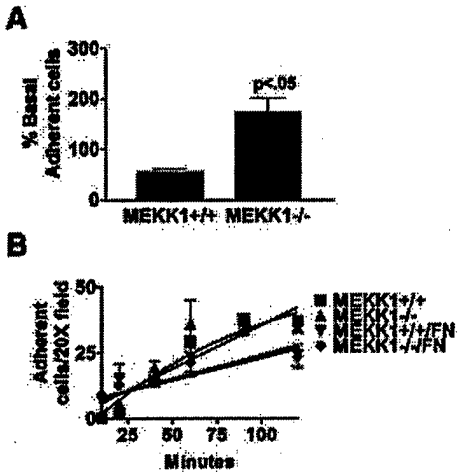

Fig. 1. MEKK1-deficient fibroblasts show increased adherence characteristic of a defect in rear-end detachment. (**A**) Wild-type or MEKK1–/– MEFs were serum starved for 8 h, then treated with media with or without 10% fetal bovine serum (FBS). The plates were then inverted and centrifuged at 2300 *g* for 5 min. Adherent cells remaining attached to the well surface were stained with Wright's stain and quantitated. Cell adherence is represented as the percent of the total serum-treated cells compared with the non-treated cells; 100% was taken as the number of wild-type cells in the dish before serum challenge, inversion and centrifugation. MEKK1–/– cells with serum challenge is >100% because more cells are retained after centrifugation than for the non-serum-stimulated wild-type cells, indicative of the increased adherence of MEKK1–/– cells. Results shown are the mean ± SEM of at least three independent experiments, and the statistical significance was determined by Student's *t*-test. (**B**) Fibroblasts were resuspended in complete media and allowed to attach to either untreated or fibronectin-coated tissue culture plates. Cells were monitored for 2 h and the number of attached cells determined by phase microscopy. A digital movie of migrating MEKK1+/+ and MEKK1–/– fibroblasts is available as Supplementary data.

matrix protein. To determine whether the migration defect in MEKK1–/– cells was due to loss of a secreted factor, MEKK1–/– and wild-type fibroblasts were co-cultured (Figure 2E) and their respective migration analyzed by the *in vitro* wound healing assay. MEKK1–/– and wild-type fibroblasts were stained with different vital fluorescent dyes so they could be readily distinguished when co-cultured. Strikingly, after 5 h post-wounding, wild-type but not MEKK1–/– fibroblasts have extensively moved into the wound space. Virtually no MEKK1–/– fibroblasts in co-culture with MEKK1+/+ fibroblasts have migrated into the wound space, demonstrating that co-culture with wild-type cells can not restore migration to MEKK1–/– fibroblasts. Thus, the migration defect of MEKK1–/– fibroblasts is not rescued by secreted factors from wild-type cells. This result strongly suggests that the defective migration of MEKK1–/– fibroblasts is not due to an inability to secrete a required protein.

Vinculin content in focal adhesions is diminished in migrating MEKK1–/– fibroblasts

The MEKK1–/– phenotype is characterized by increased adherence, defective rear-end detachment and inhibited migration, suggesting a defect in the regulation of focal adhesions. To address the consequence of MEKK1 deficiency in the regulation of focal adhesions of migrating cells, we used quantitative immunofluorescence analysis

to measure vinculin content in focal adhesions of migrating wild-type (Figure 3A) and MEKK1–/– (Figure 3C) fibroblasts. The experiment required a 12 h incubation after inflicting the razor swipe to allow migration of MEKK1–/– cells into the wound site, and a larger wound than that of Figure 2D. Analysis of 58 wild-type and 97 MEKK1–/– fibroblasts migrating into the scrape wound of confluent monolayers indicated 2.8-fold ($P < 0.0001$) less vinculin in focal adhesions of MEKK1–/– versus wild-type fibroblasts (Figure 3D). This result is consistent with the inability of migrating MEKK1–/– fibroblasts to properly organize the complex of proteins in focal adhesions. While vinculin may also be organized at cell-to-cell contacts, we have found that vinculin consistently co-localizes with the focal adhesion protein talin in mouse embryo fibroblasts (data not shown) and as such serves as a surrogate assay for focal adhesion formation. Further, as organized vinculin staining is indicative of focal adhesions, loss of vinculin staining indicates that the increased adherence of MEKK1-deficient cells is not due to an increased number or size of focal adhesions as has been observed in FAK–/– fibroblasts. This indicates that the change in adherence and focal adhesion composition resulting from MEKK1 deficiency is different from that observed with loss of FAK expression. Importantly, the add-back of MEKK1 expression restores vinculin content to focal adhesions in migrating fibroblasts (Figure 3B and D). Stationary MEKK1–/– and wild-type fibroblasts in confluent monolayers have similar vinculin staining (data not shown), consistent with MEKK1 signaling being important for regulation of the turnover of focal adhesions during migration and not in the ability to form focal adhesions. The partial restoration of vinculin to focal adhesions is likely due to the level of MEKK1 expressed in the add-back clone, which is only 20% of MEKK1 protein in wild-type fibroblasts. Stable expression of MEKK1 by add-back to MEKK1–/– cells is extremely difficult. This is predictably due to the regulation of MEKK1 expression during the cell cycle that is not mimicked by using other promoters or viral LTRs to express MEKK1, and the toxicity of MEKK1 overexpression (Yujiri *et al.*, 1999). Despite intensive effort, we have not been able to achieve stable add-back clones that express >20% of wild-type MEKK1 protein. Interestingly, our preliminary findings suggest that the level of talin and FAK, unlike vinculin, may be similar in MEKK1–/– and wild-type fibroblasts (data not shown). To determine whether MEKK1 does indeed differentially regulate protein composition in focal adhesions, it will be necessary to perform quantitative immunofluorescence analysis of several focal adhesion proteins in stationary and migrating wild-type, MEKK1–/– and add-back fibroblasts.

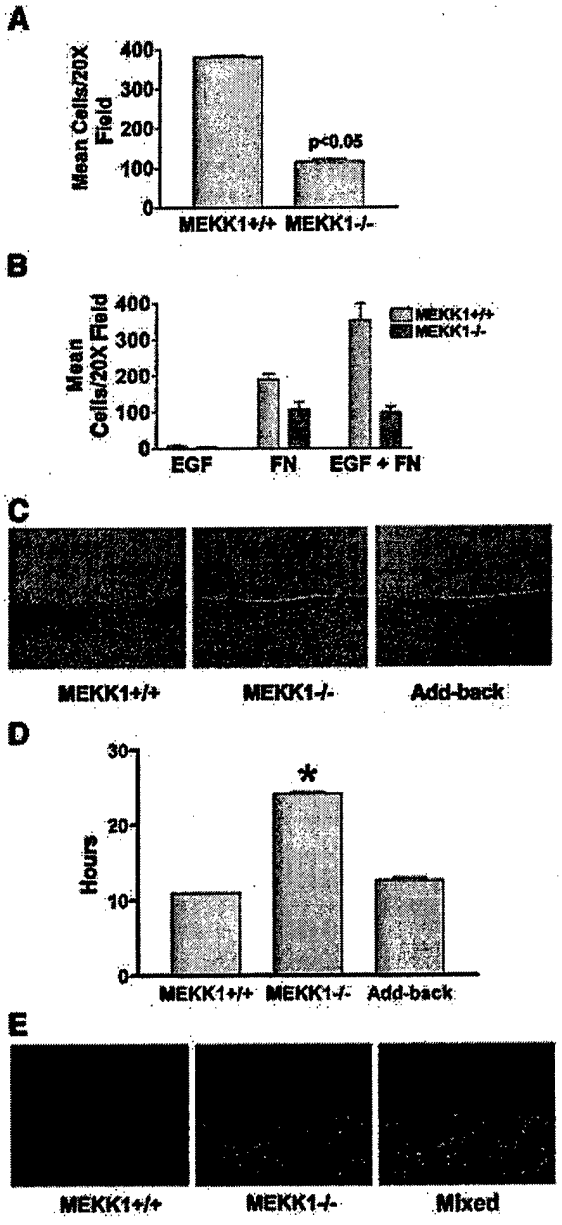

EGF stimulates the formation of MEKK1–FAK complexes

Figure 4A shows that when serum-starved fibroblasts are stimulated with EGF, MEKK1 is co-immunoprecipitated with FAK. Co-expression of MEKK1 and FAK in

Fig. 2. MEKK1 expression is necessary for fibroblast migration. (A) Fibroblasts were seeded into the upper chamber of a Transwell migration plate with 5% FBS in the lower chamber. Cells traversed after 5 h to the lower surface of the membrane were quantitated. The results shown are the mean ± SEM of at least three independent experiments. (B) Fibroblasts were treated as in (A) except that the bottom well of the Transwell contained either 1 nM EGF, 100 μg/ml fibronectin or the combination of EGF and fibronectin. (C and E) Wild-type or MEKK1–/– fibroblasts were seeded onto coverslips and allowed to grow overnight. In addition, MEKK1–/– fibroblasts stably transfected with full-length MEKK1 (Add-back) were analyzed. Each confluent culture was 'wounded' with a razor and observed over the course of 5 h for migration into the wound space (*in vitro* wound healing assay). (C) is a DIC image of migrating cells. (D) The time required for confluent fibroblasts in a tissue culture plate to close a standardized wound (200 μm) is represented by the graph. Results shown are the mean ± SEM of at least three independent experiments, and the statistical significance was determined by Student's *t*-test (*$P < 0.05$). (E) Cells were first stained with the fluorescent vital dyes PKH26 (red; MEKK1+/+) or PKH67 (green; MEKK1–/–) and then mixed in equal numbers before seeding onto coverslips, and treated as described above. The fluorescence image depicts the migration of MEKK1+/+ (wild type) and MEKK1–/– cells in co-culture. The data are representative samples from at least three independent experiments.

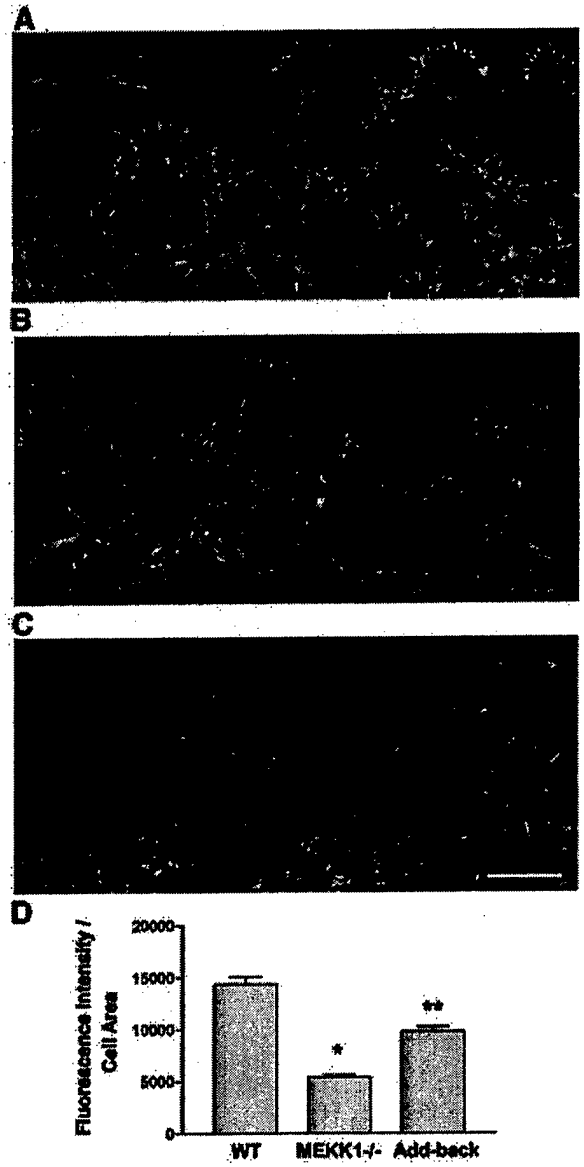

Fig. 3. Vinculin content in focal adhesions is diminished in migrating MEKK1–/– fibroblasts. A 0.4 μm deconvolved image section of the cell having the brightest focal adhesion staining was used for the measurement of integrated intensity of vinculin content for MEKK1+/+ (A), add-back (B) and MEKK1–/– (C) fibroblasts. The intensity of vinculin staining was measured per cell area of the section. The add-back clone stably expresses full-length MEKK1 and was derived from the MEKK1–/– fibroblasts. The bar graph in (D) shows the analysis from three experiments where 58 wild-type, 97 MEKK1–/– and 96 add-back cells were analyzed for integrated vinculin staining intensity per cell area. Vinculin content in the MEKK1–/– clone is diminished at a statistically significant level from wild-type MEKK1+/+ cells (*$P < 0.0001$) and add-back cells (**$P < 0.001$). Bar = 50 μm.

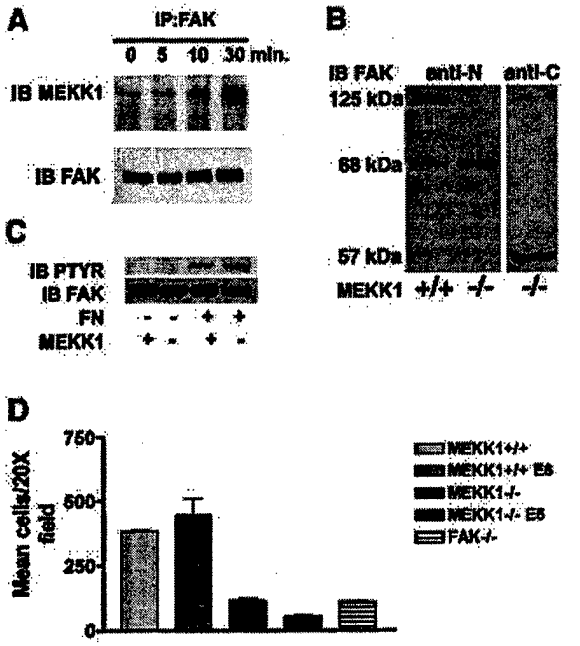

Fig. 4. MEKK1 and FAK form a complex in EGF-stimulated fibroblasts. (A) Wild-type mouse embryo fibroblasts were treated with 100 ng/ml EGF for the indicated times. After cell lysis, endogenous FAK was immunoprecipitated with anti-FAK antibody, and associated MEKK1 detected by MEKK1 immunoblotting. Total immunoprecipitated FAK was measured by anti-FAK immunoblotting using the same blots as that for MEKK1 analysis. (B) Wild-type (MEKK1+/+) and MEKK1–/– fibroblasts stably expressing papilloma virus E6/E7 proteins were immunoblotted for FAK protein expression using an antibody recognizing the N- or C-terminal domain of FAK. FAK is a 125 kDa protein with N- and C-terminal cleavage fragments of 68 and 57 kDa, respectively. (C) Serum-starved MEKK1+/+ or MEKK1–/– MEFs were allowed to adhere to fibronectin-coated bacterial plates for 30 min, and then lysed. Endogenous FAK was immunoprecipitated with anti-FAK antibodies, and the level of tyrosine-phosphorylated FAK determined by phosphotyrosine immunoblotting. The membrane was then stripped and total FAK was assessed by FAK immunoblotting. (D) MEKK1+/+ and MEKK1–/– fibroblasts ± E6/E7 protein expression were analyzed for migration in Transwell assays using 5% FBS as described for Figure 2A. *Inhibition of MEKK1–/– E6/E7 cell migration is statistically significant relative to FAK–/– cells ($P < 0.05$) and MEKK1–/– cells ($P < 0.001$).

HEK293 cells by transient transfection demonstrated that they could be reciprocally co-immunoprecipitated (Yujiri *et al.*, 2003). These findings demonstrate the interaction of MEKK1 with FAK-associated protein complexes and that endogenous MEKK1 recruitment into FAK complexes is regulated by a growth factor that stimulates both FAK and MEKK1 kinase activities (Fanger *et al.*, 1997). Thus, EGF induces the stable association of MEKK1 with FAK, altering the protein composition of focal adhesions.

Focal adhesion turnover, and therefore cell adhesion, is proposed to be modulated not only by signaling pathways involving protein phosphorylation, but by proteolysis of focal adhesion components as well. Interestingly, FAK and MEKK1 are regulated both by phosphorylation and proteolytic cleavage (Cooray *et al.*, 1996; Schlesinger *et al.*, 1998; Cary *et al.*, 2002). The discovery that MEKK1 becomes stably associated with FAK suggested that MEKK1 functions in focal adhesion signaling. The increased adherence and inhibition of migration resulting from MEKK1 deficiency also demonstrates that MEKK1 has an important role in the function of focal adhesions.

MEKK1 localizes with focal adhesions

Expression of EGFP–MEKK1 in MEKK1–/– MEFs demonstrates its association with focal adhesions and actin fibers entering the focal adhesions (Figure 5). The localization of EGFP–MEKK1 with focal adhesions is

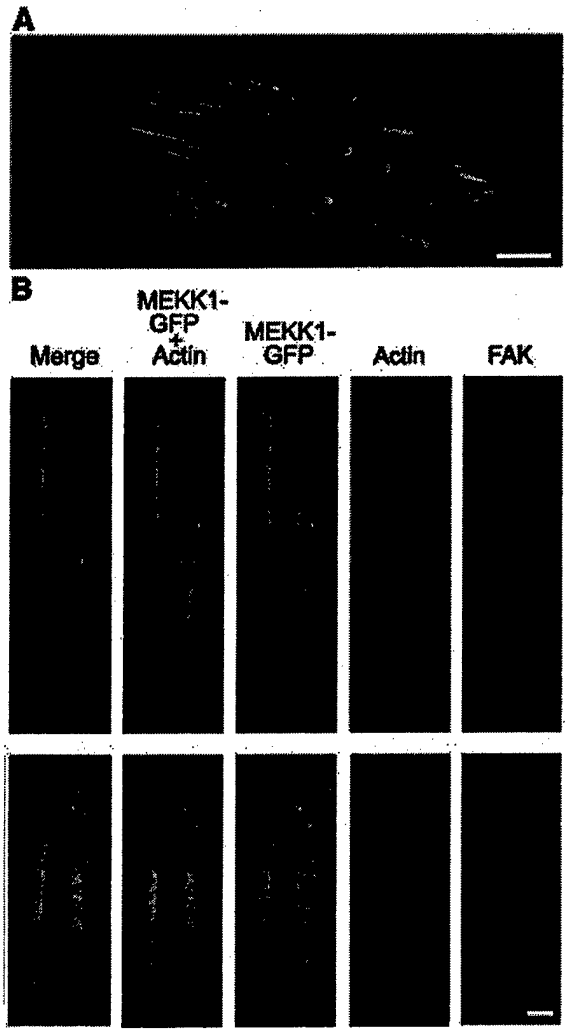

Fig. 5. MEKK1 localizes to focal adhesions. MEKK1–/– fibroblasts were transfected with EGFP–MEKK1, incubated in serum-free media for 12 h, then processed as described in Materials and methods and subjected to immunofluorescence analysis. **(A)** An MEKK1–/– MEF transfected with EGFP–MEKK1 and treated with anti-FAK antibodies (FAK displayed as red fluorescence). Bar = 10 μm. **(B)** Displayed are two representative examples of co-localization of EGFP–MEKK1 with endogenous FAK (purple) and actin (red). Bar = 1 μm.

consistent with its co-immunoprecipitation with FAK (Figure 4). We did not observe a measurable increase of EGFP–MEKK1 in focal adhesions of EGF-stimulated cells despite an increased stable association of MEKK1 in FAK immunoprecipitates. This suggests that the EGF stimulation of MEKK1–FAK co-immunoprecipitation may be related to increased stabilization of the complex, possibly due to phosphorylation-related responses, rather than a re-localization of MEKK1 to focal adhesions. It should also be noted that caspase-mediated cleavage of MEKK1 compelled us to use a mutant MEKK1 protein for these studies. The caspase-cleavage site residues had been mutated to alanines (Widmann *et al.*, 1998). The caspase-cleaved fragments do not appear to localize to focal adhesions. Cumulatively, the co-immunoprecipitation and immunofluorescence studies demonstrate that MEKK1 localizes, in part, to focal adhesions and actin filaments entering focal adhesions for the control of cell adherence.

E6/E7 papilloma virus proteins induce FAK proteolysis in MEKK1–/– fibroblasts

E6/E7 expression immortalizes primary fibroblasts by inducing the degradation of p53. We had used E6/E7 for immortalization of both wild-type and MEKK1–/– mouse embryo fibroblasts. We quickly realized that there was a significant difference in the phenotype of MEKK1–/– fibroblasts but not wild-type fibroblasts that had been immortalized with papillomavirus E6/E7 proteins versus immortalization by serial passage. In addition to stimulating p53 degradation, the E6 oncoprotein binds to the focal adhesion protein paxillin (Turner, 2000). One outcome of E6 expression is the disruption of paxillin association with vinculin and FAK (Tong *et al.*, 1997; Turner, 2000). Relative to primary MEKK1–/– fibroblasts, or MEKK1–/– fibroblasts immortalized by serial passage, MEKK1–/– fibroblasts expressing E6/E7 were extremely flat and highly adherent to the substratum, reminiscent of FAK–/– cells (Ilic *et al.*, 1995). In contrast, E6/E7-expressing wild-type fibroblasts were more rounded and less adherent to substratum. Figure 4B shows that E6/E7 expression in MEKK1–/– fibroblasts causes a near quantitative cleavage of FAK. This contrasts with E6/E7-expressing MEKK1+/+ fibroblasts where FAK remains intact. This result is consistent with MEKK1 being associated with FAK–paxillin–vinculin complexes and playing a protective role against E6/E7-induced FAK degradation. This suggests that EGF-induced MEKK1 association with focal adhesions alters the organization and interaction of focal adhesion proteins.

Functionally, MEKK1 protects FAK from E6/E7-mediated degradation, but MEKK1 expression is not required for fibronectin binding-induced stimulation of FAK tyrosine phosphorylation (Figure 4C). With MEKK1–/– fibroblasts immortalized by serial passage, fibronectin stimulation of FAK tyrosine phosphorylation is similar to that observed with MEKK1+/+ fibroblasts. This result indicates that FAK tyrosine phosphorylation is largely independent of the role MEKK1 plays in organization, signaling and proteolytic susceptibility of focal adhesion proteins.

E6/E7-induced FAK cleavage in MEKK1–/– fibroblasts causes a migration defect more severe than that observed with FAK–/– or MEKK1–/– fibroblasts not expressing the E6/E7 oncoproteins (Figure 4D). FAK–/– fibroblasts, like MEKK1–/– fibroblasts, exhibit a marked reduction in migration in transwell assays (Figure 4D). Unlike E6/E7 wild-type fibroblasts that readily migrate toward serum, E6/E7 MEKK1–/– fibroblasts display a migration defect more severe than either MEKK1–/– or FAK–/– fibroblasts that do not express the E6/E7 proteins (Figure 4D). Thus, MEKK1 is important in maintaining the integrity and protein composition of focal adhesion complexes and is functionally required for fibroblast migration. The combined loss of MEKK1 and FAK exacerbates the migration defect resulting from the loss of either kinase alone.

MEKK1 regulates calpain activation

Previous studies have suggested that the intracellular cysteine protease calpain is involved in the regulation of

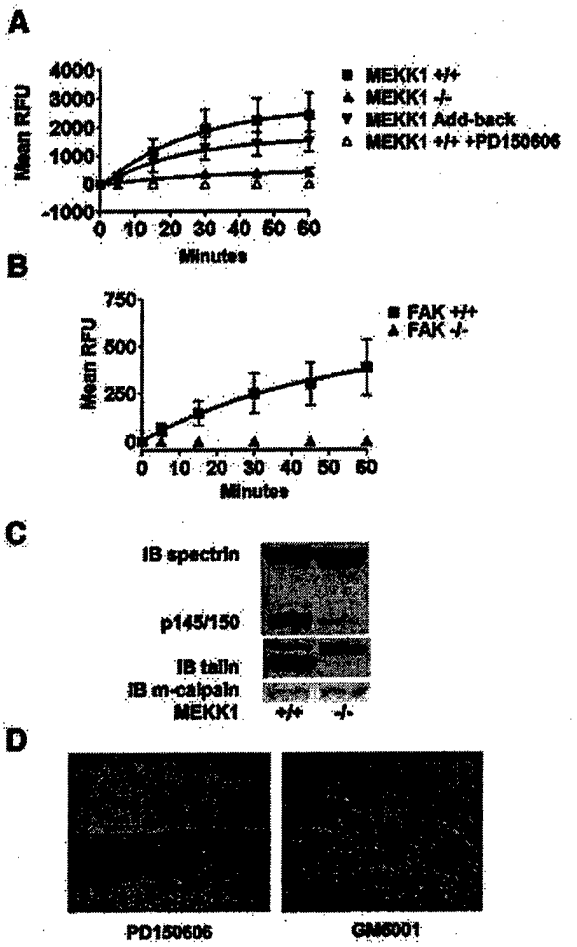

Fig. 6. MEKK1-deficient fibroblasts show reduced calpain activity, and calpain inhibition mimics MEKK1 deficiency. *In vivo* calpain activity was assessed in fibroblasts using the cell-permeable, fluorescent calpain substrate SLLVY-AMC (A and B) and by anti-spectrin or anti-talin immunoblotting (C). (A) MEKK1+/+ cells in the presence and absence of the calpain inhibitor PD150606 (50 μM), MEKK1–/– and MEKK1 add-back cells were used for measurement of calpain activity. (B) FAK+/+ and FAK–/– cells were used to measure calpain activity as in (A). (C) The anti-spectrin and anti-talin immunoblots were stripped and reprobed with anti-m-calpain antibodies to verify protein levels. The immunoblots are representative of at least three independent experiments. (D) Wild-type fibroblasts grown to confluency on coverslips were pre-treated for 1 h with 50 μM PD150606 (left panel) or 2 μM GM6001, a matrix metalloproteinase inhibitor (right panel), and then analyzed for migration using the *in vitro* wound healing assay following a razor swipe in the continuous presence of inhibitor. Results are representative of at least three independent experiments for each set of experiments in (A–D).

rear-end detachment of migrating cells (Huttenlocher *et al.*, 1997; Frame *et al.*, 2002; Glading *et al.*, 2002), the migration defect of MEKK1–/– fibroblasts. Using a cell-permeable fluorogenic calpain substrate, we discovered that MEKK1–/– cells have significantly less calpain proteinase activity than wild-type fibroblasts (Figure 6A). Similarly, in culture conditions identical to the *in vitro* wound assay, MEKK1–/– fibroblasts have significantly less calpain activity than wild-type fibroblasts. Cleavage of the fluorogenic substrate is blocked using a calpain-specific inhibitor, PD150606, which prevents Ca^{2+} binding to calpain and does not significantly inhibit either cathepsins or caspases (Wang *et al.*, 1996), confirming that the assay is specifically measuring calpain activity (Figure 6A). Just as add-back of MEKK1 protein by transfection of MEKK1–/– fibroblasts rescued adherence and migration, add-back of MEKK1 also restored calpain regulation (Figure 6A). Even though the add-back clone expresses MEKK1 protein at only 20% of the MEKK1 expression of wild-type fibroblasts, it is sufficient to at least partially restore calpain activation, and rescue both migration and adherence. As we had demonstrated that MEKK1 is associated with focal adhesions (Figures 4 and 5), we asked whether FAK was necessary for calpain activation. Since FAK-deficient fibroblasts have been found to have severe migration defects (Ilic *et al.*, 1995), we wanted to determine whether loss of FAK from the signaling complex affected calpain activity. Strikingly, calpain activity in serum-treated FAK-deficient fibroblasts was dramatically reduced compared with that of FAK-expressing cells (Figure 6B). Taken together, our data support the existence of a complex containing FAK and MEKK1 that is required for calpain control of cell adherence and migration.

$\alpha_2\beta_2$ spectrin (fodrin) is a structural protein linking the cytoskeleton to membranes and is a defined calpain substrate (Wang and Yuen, 1999; Wang, 2000). Calpain cleavage of spectrin produces a specific pattern of proteolytic peptide fragments of 145–150 kDa (Wang and Yuen, 1999; Wang, 2000) that are unique to calpain and are different in size from those generated by caspases (Wang and Yuen, 1999; Wang, 2000). We found that calpain-specific spectrin fragments generated in wild-type fibroblasts were nearly undetectable in MEKK1–/– fibroblasts (Figure 6C). This finding demonstrates the loss of cleavage of an endogenous calpain substrate in MEKK1–/– fibroblasts. Cleavage of another calpain substrate, talin, was similarly reduced in the MEKK1-deficient cells (Figure 6C). While calpain activity was diminished in MEKK1–/– fibroblasts, immunoblotting indicated that total calpain protein expression was similar in wild-type and MEKK1–/– fibroblasts (Figure 6C). This result is consistent with the existence of a MEKK1-dependent signaling complex that regulates calpain activity but not calpain expression. Together, the loss of both spectrin and talin cleavage, coupled with reduced hydrolysis of the fluorogenic calpain-specific substrate, clearly demonstrates a loss of calpain activation in MEKK1–/– cells. Importantly, PD150606, the calpain-specific inhibitor, blocks the migration of wild-type fibroblasts in the *in vitro* wound assay (Figure 6D). However, GM6001, an inhibitor of metalloproteinases that function to remodel the extracellular matrix, did not inhibit fibroblast migration into the wound space, thereby demonstrating the specific requirement of calpain inhibition for disrupted migration in this assay. The findings demonstrate that the MEKK1-dependent regulation of calpain activity is required for cell migration.

MEKK1 regulates ERK1/2 activity

The MEK inhibitor PD98059 blocks ERK1/2 activation, inhibits calpain activation and cell motility (Glading *et al.*, 2000). However, as PD98059 may influence Ca^{2+} influx independently of MEK activity (Pereira *et al.*, 2002), and

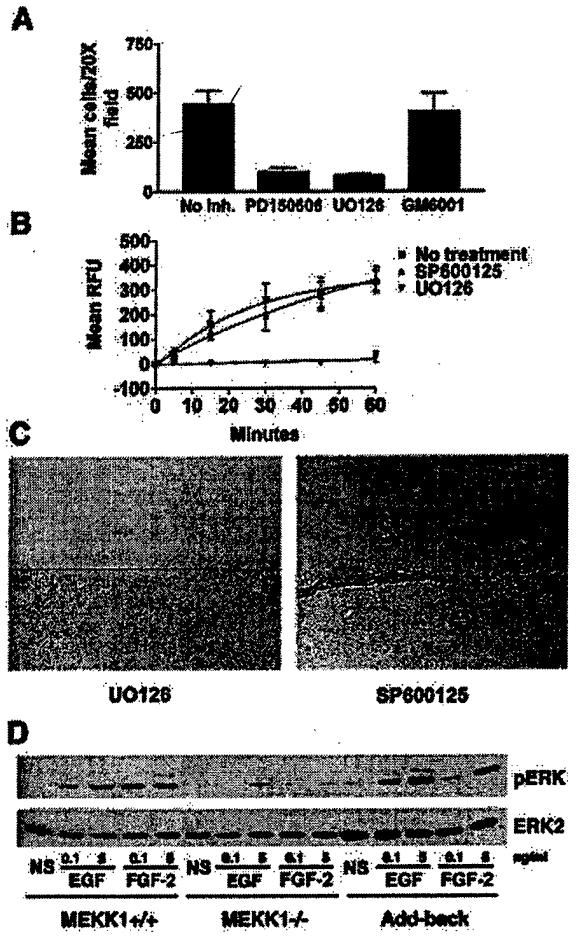

Fig. 7. Fibroblast migration and calpain activity are dependent on MEK, but not JNK activity. (A) Wild-type fibroblasts were loaded into Transwell migration chambers (10^5 cells/well) and allowed to migrate for 5 h, using 5% serum as a chemotactic agent. Calpain inhibitor PD150606 (50 μM), MEK inhibitor UO126 (10 μM) or matrix metalloproteinase inhibitor GM6001 (2 μM) were added to both the upper and lower chambers of the designated wells. (B) Wild-type fibroblasts were pre-incubated for 1 h with JNK inhibitor SP600125 (10 μM) or MEK inhibitor UO126 (10 μM), and calpain activity was assessed by SLLVY-AMC cleavage, and compared with that of non-treated cells. The results of both (A) and (B) are the mean ± SEM of at least three independent experiments. (C) Wild-type fibroblasts were pre-incubated with 10 μM SP600125 or 10 μM UO126 for 1 h and then analyzed for migration using the *in vitro* wound healing assay in the continuous presence of inhibitor. (D) Serum-starved wild-type, MEKK1–/– or MEKK1 add-back fibroblasts were treated with EGF or FGF-2 for 10 min and then lysed. ERK1/2 activation was then assessed by phospho-ERK immunoblotting. The membrane was then stripped and the total ERK2 level determined by ERK2 immunoblotting. The data are representative of at least three independent experiments. NS, no stimulus.

thereby possibly alter calpain activity, we tested the effect of UO126, an unrelated MEK inhibitor that does not non-specifically alter Ca^{2+} levels (Pereira *et al.*, 2002) (Figure 7). U0126 inhibits calpain activation (Figure 7B) and dramatically reduces fibroblast chemotaxis towards serum (Figure 7A). In contrast, SP600125, a JNK inhibitor, does not diminish fibroblast migration or calpain activity (Figure 7B and C). Thus, while MEKK1 has been shown to regulate both the ERK1/2 and JNK signaling pathways, calpain activation and consequent cell migration may be attributed specifically to MEKK1 regulation of ERK1/2 signaling.

Given that numerous studies have identified Raf as the MAPK kinase kinase responsible for growth factor-mediated ERK1/2 activation, what role might MEKK1 play in EGF-induced ERK1/2 activation? We asked whether a portion of EGF-induced ERK1/2 activation might actually be attributable to MEKK1. By treating the cells with low (0.1–5 ng/ml) concentrations of EGF or FGF-2, we found that induced ERK1/2 phosphorylation and consequent activation by low levels of growth factors in mouse embryo fibroblasts is significantly dependent on MEKK1 expression (Figure 7D), while at higher levels of growth factor (100 ng/ml or higher), ERK1/2 phosphorylation levels of MEKK1+/+ and MEKK1–/– MEFs were similar (data not shown). Thus, MEKK1 control of ERK1/2 activation is readily apparent at low growth factor concentrations and verified by comparison of wild-type and MEKK1–/– fibroblasts. Further, densitometric analysis of Figure 7D reveals that MEKK1+/+ cells stimulated with the level of EGF used in our migration experiments (5 ng/ml) (Figure 2B) display a 2.5-fold greater level of pERK than the MEKK1–/– MEFs. Our data show that the loss of MEKK1 regulation of ERK1/2 signaling in MEKK1–/– fibroblasts contributes significantly to inhibition of calpain activation required for regulation of adherence and rear-end detachment of migrating cells. Importantly, the add-back of MEKK1 completely restores ERK1/2 activation by low doses of growth factor.

Discussion

Cell adhesion to the extracellular matrix is mediated by integrins, which, in turn, are linked to the cytoskeleton through proteins in focal adhesion complexes (Yamada and Miyamoto, 1995). The strength of cell adherence to the extracellular matrix is modulated by signal transduction pathways involving proteins within focal adhesions (Yamada and Miyamoto, 1995). One such pathway of particular importance to adhesion-mediated signaling is the ERK1/2 pathway. v-Src, a potent activator of ERK1/2 signaling, has been shown to drive MEK-dependent ERK activation and localization to focal adhesions in chicken embryo fibroblasts (Fincham *et al.*, 2000). One explanation for the importance of membrane-localized ERK activity in cell adhesion, and by extension cell migration, is that ERK1/2 signaling is required for efficient release of cellular adhesion to the matrix substratum (Glading *et al.*, 2000). We have previously reported that MEKK1 regulates ERK1/2 activation, and that MEKK1-deficient cells display reduced motility (Yujiri *et al.*, 1998, 2000). In this paper, our findings demonstrate that MEKK1–/– fibroblasts have an increased adherence but display normal extension of the leading edge during migration. Thus, the loss of migration in MEKK1–/– fibroblasts is due to the increased adherence and a diminished ability to detach the trailing end of the cell, rather than decreased forward extension. We have demonstrated by co-immunoprecipitation that MEKK1 is associated with FAK-associated protein complexes, and that these complexes were localized in adhesion complexes. MEKK1 has also been proposed to co-localize with α-actinin and actin stress

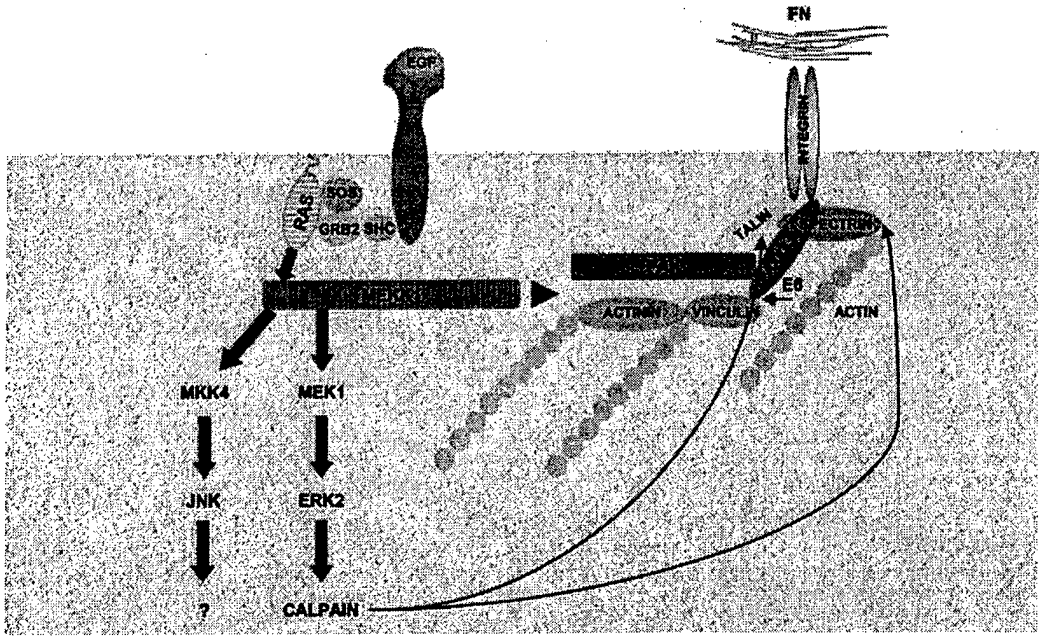

Fig. 8. Model depicting the FAK–MEKK1–MEK1/2–ERK2 pathway controlling calpain activation and the disruption of focal adhesion-actin cytoskeletal complexes. MEKK1–/– cells are defective in focal adhesion composition and regulation of the ERK2–calpain activation pathway (see text for details).

fibers (Christerson *et al.*, 1999), and our immunofluorescence studies support that contention. Thus, our findings reveal that the cellular location of MEKK1 is well suited to regulate signal transduction in response to cell adhesion or cytoskeletal changes. Indeed, we have previously shown MEKK1 to regulate signaling in response to cytoskeletal alteration (Yujiri *et al.*, 1999, 2000). Activation of the MEK–ERK1/2 pathway initiated by changes in integrin interactions with focal adhesion proteins is well characterized (Howe *et al.*, 2002), and our findings with MEKK1 knockout fibroblasts demonstrate this response is, in part, dependent on the expression of MEKK1.

The protease calpain has recently been implicated in the control of cell migration through regulation of de-adhesion from matrix substratum. We have demonstrated that MEKK1 expression is critical for calpain activity regulation. Glading *et al.* (2001) have recently shown that membrane-proximal ERK1/2 activity is required for EGF-induced m-calpain activity, and we demonstrate that MEKK1 is required for regulation of calpain activation. While our studies did not rule out that MEKK1-dependent MEK activity might phosphorylate proteins other than ERK1/2 that are required for calpain activity, recent studies (Glading *et al.*, 2001) indicate that appropriate localization of ERK activity is the key MEK-dependent factor in calpain activation. It is possible that MEKK1 might also influence calpain cellular location, but we were unable to detect any MEKK1-dependent calpain localization (data not shown). Importantly, reconstitution of the wild-type phenotype by expression of MEKK1 confirms that the defects we have measured in MEKK1–/– fibroblasts are a direct consequence of MEKK1 deficiency and not an epigenetic difference between cell lines.

Calpain has been shown to be associated with focal adhesions, and two primary substrates for calpain in fibroblasts are the structural proteins spectrin and talin (Glading *et al.*, 2002). Through vinculin, both spectrin and talin are linked to α-actinin and the actin cytoskeleton (Petit and Thiery, 2000). Calpain-dependent cleavage of these two proteins thus alters the tethering of the cytoskeleton to focal adhesion complexes and the plasma membrane. Regulation of limited calpain cleavage of these proteins requires MEKK1 regulation of the ERK1/2 pathway. The requirement of MEKK1 expression for the control of adhesion probably explains, at least in part, the defective eyelid closure of MEKK1-deficient mice due to impaired epithelial cell migration. Furthermore, other MEKK1–/– cell types including neutrophils and macrophages appear to have compromised migration (our unpublished observations), indicating that MEKK1 contributes to the regulation of migration of mutiple cell types.

The significance of our work is that a focal adhesion-regulated pathway controlling cell adherence and migration has now been genetically defined. Targeted disruption of FAK (Ilic *et al.*, 1995), MEKK1 (Yujiri *et al.*, 2000), MEK1 (Giroux *et al.*, 1999), ERK2 (Saba El-Leil, 2002) and calpain (Dourdin *et al.*, 2001) demonstrates defects in cell migration (Figure 8). Pharmacological inhibitors of MEK1 and calpain mimic the loss of expression of component members of this pathway by blocking migration and influencing adherence. Interestingly, only the loss of MEKK1 expression yields viable animals, the other knockouts are embryonic lethal. This result is most likely related to the requirement of FAK to initiate multiple signals from focal adhesions, and the involvement of MEK1 and ERK2 in many diverse functions regulated by members of the Raf family (A-Raf, B-Raf and c-Raf1), Mos, Tpl-2 and MEKK1, all MAPK kinase kinases defined genetically to regulate the ERK1/2 pathway (Schlesinger

et al., 1998). At low growth factor levels, which are most likely physiologically relevant, it is apparent that MEKK1 is critical for normal ERK1/2 activation. At higher growth factor concentrations, the activation of Raf proteins probably rescues the MEKK1 deficiency by activating the ERK1/2 pathway. Thus, pharmacological inhibition of MAPK kinase kinases such as MEKK1 would predictably have greater specificity in selectively inhibiting migration in pathological states such as cancer metastasis than inhibition of MEK1, ERK1/2 or calpain.

Materials and methods

Antibodies and reagents

Anti-phospho ERK, ERK2 and FAK (C-terminal) antibodies used for immunoblotting were from Santa Cruz Biotechnology, Inc. (Santa Cruz, CA). Anti-phosphotyrosine and anti-FAK (N-terminal) antibodies were from Upstate Biotechnology (Lake Placid, NY). Fibronectin-coated tissue culture plates were from BD Biosciences (Bedford, MA). Anti-vinculin (V-4505) and FITC-conjugated donkey anti-mouse antibodies were from Sigma (St Louis, MO). HRP–sheep anti-mouse IgG was from Amersham (Piscataway, NJ). Protein A–HRP conjugate was from Zymed Laboratories (San Francisco, CA). PKH67 and PKH26 vital dyes were from Sigma. PD150606 and SP600125 were from Calbiochem (San Diego, CA). UO126 was from Promega (Madison, WI). SLLVY-AMC was from Peptides International (Louisville, KY). The MEKK1 sequence DTVD (amino acids 871–874) was substituted with alanines by a PCR strategy, and then subcloned into pEGFP-C1 (BD Biosciences Clontech, Palo Alto, CA).

Fibroblasts

The development of MEKK1–/– mice has been described previously (Yujiri *et al.*, 2000). Mouse embryo fibroblasts were isolated from E14.5 embryos. Immortalized fibroblasts were isolated after continuous passage for 3 months or by expression of papilloma E6/E7 oncoproteins. All results comparing wild-type fibroblasts and MEKK1–/– fibroblasts were characterized with similar results in primary and immortalized fibroblasts. The MEKK1 add-back fibroblasts were made by stable transfection of immortalized MEKK1–/– fibroblasts using a full-length mouse MEKK1 cDNA in pLHCX. MEKK1 expression as determined by immunoblotting was ~20% of the MEKK1 expression of wild-type fibroblasts. The FAK–/– fibroblasts were a generous gift from Dr Dusko Ilic, University of California at San Francisco.

Cell culture

Fibroblasts were cultured in IMDM medium (Gibco, Grand Island, NY) containing penicillin/streptomycin (1%; Gibco), L-glutamine (2 mM; Gibco), monothioglycerol (0.0012%; Sigma) and 10% (v/v) fetal calf serum (Gemini Bioproducts, Woodland, CA) at 37°C in a humidified atmosphere. Human FGF-2 was purchased from Upstate Biotechnology (Lake Placid, NY) and murine EGF from Sigma.

Immunoprecipitation

After stimulation, fibroblasts were washed twice with cold PBS and lysed in 20 mM Tris–HCl pH 7.6, 0.5% NP-40, 250 mM NaCl, 3 mM EDTA, 3 mM EGTA, 1 mM PMSF, 2 mM sodium orthovanadate, 20 μg/ml aprotinin, 1 mM DTT and 5 μg/ml leupeptin. Lysates were cleared by centrifugation at 14 000 *g* for 10 min at 4°C, incubated with the appropriate antibody for 16 h at 4°C, and then with protein G–Sepharose for 1 h. The beads were washed three times, then resuspended in sample buffer (125 mM Tris–HCl pH 6.8, 20% glycerol, 4.6% SDS, 0.1% bromophenol blue and 10% 2-mercaptoethanol) for SDS–PAGE.

Immunoblotting

After stimulation, cells were lysed in 0.5 ml of sample buffer and incubated at room temperature for 20 min. After centrifugation at 14 000 *g* for 5 min, post-nuclear detergent cell lysates were collected. Proteins were separated by SDS–PAGE and transferred to nitrocellulose (Scleicher & Schuell, Keene, NH). Membranes were blocked in 5% milk (diluted in Tris-buffered saline and 0.1% Tween-20) and incubated with the appropriate antibody at 4°C overnight. HRP–protein A or HRP–sheep anti-mouse IgG was used as secondary reagent. After extensive washing, the targeted proteins were detected by enhanced chemiluminescence (ECL). Where indicated, blots were stripped by treatment with 2% SDS and 100 mM 2-mercaptoethanol in TBS, and then reprobed with desired antibodies and detected by ECL.

In vitro wound healing assessment

Fibroblasts were grown on coverslips (10^6 cells) until confluent. The culture was 'wounded' with a razor blade by swiping the coverslip to generate an open area with no cells. The coverslips were rinsed and cells allowed to migrate into the wound site in complete media with or without inhibitors for 5 h unless noted otherwise. Fibroblast migration was assessed by live cell microscopy. For the mixed cell experiments, the fibroblasts were stained with either PKH26 or PKH67 fluorescent vital dyes (Sigma), mixed and allowed to grow together overnight before wounding and assessment by fluorescence microscopy. To measure healing time, cells were grown in tissue culture dishes until confluent, wounded with an 18g needle and then periodically examined until the wound was completely sealed. The data were analyzed by Student's *t*-test.

Transwell chemotaxis assay

Fibroblasts were typsinized, washed and suspended in IMDM with 5% BSA. A total of 10^5 cells were then loaded into the upper chamber of a Transwell (Corning, Corning, NY) migration plate (8 μm pore) and allowed to migrate toward IMDM ± 5% fetal bovine serum for 5 h at 37°C. After migration, the upper surface of the membrane was thoroughly cleaned with a cotton swab, stained with Wright stain (Sigma) and the cells that migrated to the lower surface counted (five random 20× fields/well).

Calpain fluorescence assay

Fibroblasts were seeded into 96-well plates (10^4 cells/well) and allowed to attach overnight. The cells were then serum starved for 8 h before treatment with 10% FBS in IMDM for 30 min. The medium was removed and 200 μl of 62.5 mM SLLVY-AMC, a cell-permeable calpain substrate, in reaction buffer (115 mM NaCl, 1 mM KH_2PO_4, 5 mM KCl, 2 mM $CaCl_2$ 1.2 mM $MgSO_4$ and 25 mM HEPES pH 7.25) were added and fluorescence assessed using a Perkin Elmer 7000 BioAssay Reader (360/465 nm). When inhibitors were used, the cells were incubated with the inhibitor for 1 h prior to addition of the substrate, and the assay conducted in the presence of the inhibitor.

Centrifugation adherence assay

Cells were seeded into a 96-well plate (2000 cells/well) and allowed to attach overnight. Cells were serum starved for 8 h before treatment with or without 10% FBS in IMDM for 30 min. The plate was then sealed, inverted and centrifuged at 2300 *g* for 5 min at 37°C. After rinsing, the remaining attached cells were stained with Wright stain (Sigma) and counted. Cell adherence is represented as the percent of the total remaining serum-treated cells compared with the non-treated cells.

Fibroblast attachment rate

MEKK1+/+ (wild-type) or MEKK1-deficient fibroblasts were resuspended in complete media and allowed to attach in either untreated or fibronectin-coated tissue culture plates (Becton Dickinson, Bedford, MA). The number of attached cells was determined over the course of 2 h by phase microscopy of a defined plate area.

Immunofluorescence

Cells were transfected with lipofectamine and grown on glass coverslips. Two days after transfection, the cells were treated with 50 ng/ml EGF or serum-free medium alone for 30 min, then the medium was removed and the cells fixed in 3% paraformaldehyde/3% sucrose in phosphate-buffered saline (PBS) for 10 min. Following three PBS washes, the cells were permeabilized for 10 min with 0.1%Triton X-100 in PBS. After washing, the cells were blocked in 10% donkey serum in PBS for 1 h at room temperature. The coverslips were then incubated with anti-FAK (BD Transduction Laboratories) in 3% BSA/PBS for 1 h. After three washes, the coverslips were incubated with Cy5-conjugated anti-mouse antibodies (Jackson Immunoresearch) and rhodamine–phalloidin (Molecular Probes) in 3% BSA/PBS for 1 h. Following washing, cells were mounted in 75% glycerol/25% PBS/Tris pH 7.5.

Quantitation of vinculin in focal adhesions

Cells migrating into the wound area resulting from the razor swipe of a confluent monolayer of fibroblasts were paraformaldehyde fixed at 12 h post-wounding. Cells were stained with the mouse anti-vinculin antibody followed by FITC-conjugated donkey anti-mouse antibody. Images were taken every 0.4 μm along the *Z*-axis and deconvolved using the nearest-

neighbors algorithm Slidebook program from Intelligent Imaging, Inc. (Denver, CO). The section at the substratum interface with the best in-focus vinculin staining was selected for measurement of the integrated fluorescence intensity in focal adhesions. The cell area for the section was also determined using Slidebook. The fluorescence intensity of vinculin per cell area was calculated for MEKK1+/+, MEKK1−/− and add-back clones from three independent experiments. The data were pooled and analyzed statistically using Student's *t*-test.

Supplementary data

Supplementary data are available at *The EMBO Journal* Online.

References

Arthur,J.S., Elce,J.S., Hegadorn,C., Williams,K. and Greer,P.A. (2000) Disruption of the murine calpain small subunit gene, *Capn4*: calpain is essential for embryonic development but not for cell growth and division. *Mol. Cell. Biol.*, **20**, 4474–4481.

Beckerle,M.C., Burridge,K., DeMartino,G.N. and Croall,D.E. (1987) Colocalization of calcium-dependent protease II and one of its substrates at sites of cell adhesion. *Cell*, **51**, 569–577.

Bialkowska,K., Kulkarni,S., Du,X., Goll,D.E., Saido,T.C. and Fox,J.E. (2000) Evidence that β3 integrin-induced Rac activation involves the calpain-dependent formation of integrin clusters that are distinct from the focal complexes and focal adhesions that form as Rac and RhoA become active. *J. Cell Biol.*, **151**, 685–696.

Cary,L.A., Klinghoffer,R.A., Sachsenmaier,C. and Cooper,J.A. (2002) SRC catalytic but not scaffolding function is needed for integrin-regulated tyrosine phosphorylation, cell migration and cell spreading. *Mol. Cell. Biol.*, **22**, 2427–2440.

Christerson,L.B., Vanderbilt,C.A. and Cobb,M.H. (1999) MEKK1 interacts with α-actinin and localizes to stress fibers and focal adhesions. *Cell Motil. Cytoskeleton*, **43**, 186–198.

Cooray,P., Yuan,Y., Schoenwaelder,S.M., Mitchell,C.A., Salem,H.H. and Jackson,S.P. (1996) Focal adhesion kinase (pp125FAK) cleavage and regulation by calpain. *Biochem. J.*, **318**, 41–47.

Dourdin,N., Bhatt,A.K., Dutt,P., Greer,P.A., Arthur,J.S., Elce,J.S. and Huttenlocher,A. (2001) Reduced cell migration and disruption of the actin cytoskeleton in calpain-deficient embryonic fibroblasts. *J. Biol. Chem.*, **276**, 48382–48388.

Fanger,G.R., Johnson,N.L. and Johnson,G.L. (1997) MEK kinases are regulated by EGF and selectively interact with Rac/Cdc42. *EMBO J.*, **16**, 4961–4972.

Fincham,V.J., James,M., Frame,M.C. and Winder,S.J. (2000) Active ERK/MAP kinase is targeted to newly forming cell-matrix adhesions by integrin engagement and v-Src. *EMBO J.*, **19**, 2911–2923.

Frame,M.C., Fincham,V.J., Carragher,N.O. and Wyke,J.A. (2002) v-Src's hold over actin and cell adhesions. *Nat. Rev. Mol. Cell Biol.*, **3**, 233–245.

Giroux,S. *et al.* (1999) Embryonic death of Mek1-deficient mice reveals a role for this kinase in angiogenesis in the labyrinthine region of the placenta. *Curr. Biol.*, **9**, 369–372.

Glading,A., Chang,P., Lauffenburger,D.A. and Wells,A. (2000) Epidermal growth factor receptor activation of calpain is required for fibroblast motility and occurs via an ERK/MAP kinase signaling pathway. *J. Biol. Chem.*, **275**, 2390–2398.

Glading,A., Uberall,F., Keyse,S.M., Lauffenburger,D.A. and Wells,A. (2001) Membrane proximal ERK signaling is required for M-calpain activation downstream of epidermal growth factor receptor signaling. *J. Biol. Chem.*, **276**, 23341–23348.

Glading,A., Lauffenburger,D.A. and Wells,A. (2002) Cutting to the chase: calpain proteases in cell motility. *Trends Cell Biol.*, **12**, 46–54.

Howe,A.K., Aplin,A.E. and Juliano,R.L. (2002) Anchorage-dependent ERK signaling—mechanisms and consequences. *Curr. Opin. Genet. Dev.*, **12**, 30–35.

Huang,Y. and Wang,K.K. (2001) The calpain family and human disease. *Trends Mol. Med.*, **7**, 355–362.

Huttenlocher,A., Palecek,S.P., Lu,Q., Zhang,W., Mellgren,R.L., Lauffenburger,D.A., Ginsberg,M.H. and Horwitz,A.F. (1997) Regulation of cell migration by the calcium-dependent protease calpain. *J. Biol. Chem.*, **272**, 32719–32722.

Ilic,D. *et al.* (1995) Reduced cell motility and enhanced focal adhesion contact formation in cells from FAK-deficient mice. *Nature*, **377**, 539–544.

Lotz,M.M., Burdsal,C.A., Erickson,H.P. and McClay,D.R. (1989) Cell adhesion to fibronectin and tenascin: quantitative measurements of initial binding and subsequent strengthening response. *J. Cell Biol.*, **109**, 1795–1805.

Maheshwari,G., Wells,A., Griffith,L.G. and Lauffenburger,D.A. (1999) Biophysical integration of effects of epidermal growth factor and fibronectin on fibroblast migration. *Biophys. J.*, **76**, 2814–2823.

Palecek,S.P., Huttenlocher,A., Horwitz,A.F. and Lauffenburger,D.A. (1998) Physical and biochemical regulation of integrin release during rear detachment of migrating cells. *J. Cell Sci.*, **111**, 929–940.

Pereira,D.B., Carvalho,A.P. and Duarte,C.B. (2002) Non-specific effects of the MEK inhibitors PD098,059 and U0126 on glutamate release from hippocampal synaptosomes. *Neuropharmacology*, **42**, 9–19.

Petit,V. and Thiery,J.P. (2000) Focal adhesions: structure and dynamics. *Biol. Cell*, **92**, 477–494.

Pfaff,M., Du,X. and Ginsberg,M.H. (1999) Calpain cleavage of integrin β cytoplasmic domains. *FEBS Lett.*, **460**, 17–22.

Potter,D.A., Tirnauer,J.S., Janssen,R., Croall,D.E., Hughes,C.N., Fiacco,K.A., Mier,J.W., Maki,M. and Herman,I.M. (1998) Calpain regulates actin remodeling during cell spreading. *J. Cell Biol.*, **141**, 647–662.

Saba El-Leil,M.K. (2002) Targeted inactivation of the Erk2 MAP kinase gene in the mouse. In *Abstracts of the Meeting on Protein Phosphorylation and Mechanisms of Cellular Regulation*, March 5–10, 2002, Taos, NM. Keystone Symposia.

Schlesinger,T.K., Fanger,G.R., Yujiri,T. and Johnson,G.L. (1998) The TAO of MEKK. *Front. Biosci.*, **3**, D1181–D1186.

Tong,X., Salgia,R., Li,J.L., Griffin,J.D. and Howley,P.M. (1997) The bovine papillomavirus E6 protein binds to the LD motif repeats of paxillin and blocks its interaction with vinculin and the focal adhesion kinase. *J. Biol. Chem.*, **272**, 33373–33376.

Turner,C.E. (2000) Paxillin and focal adhesion signalling. *Nat. Cell Biol.*, **2**, E231–E236.

Wang,K.K. (2000) Calpain and caspase: can you tell the difference? *Trends Neurosci.*, **23**, 20–26.

Wang,K.K.W. and Yuen,P.-w. (1999) *Calpain: Pharmacology and Toxicology of a Cellular Protease*. Taylor & Francis, London, UK.

Wang,K.K. *et al.* (1996) An α-mercaptoacrylic acid derivative is a selective nonpeptide cell-permeable calpain inhibitor and is neuroprotective. *Proc. Natl Acad. Sci. USA*, **93**, 6687–6692.

Widmann,C., Gerwins,P., Johnson,N.L., Jarpe,M.B. and Johnson,G.L. (1998) MEK kinase 1, a substrate for DEVD-directed caspases, is involved in genotoxin-induced apoptosis. *Mol. Cell. Biol.*, **18**, 2416–2429.

Yamada,K.M. and Miyamoto,S. (1995) Integrin transmembrane signaling and cytoskeletal control. *Curr. Opin. Cell Biol.*, **7**, 681–689.

Yujiri,T., Sather,S., Fanger,G.R. and Johnson,G.L. (1998) Role of MEKK1 in cell survival and activation of JNK and ERK pathways defined by targeted gene disruption. *Science*, **282**, 1911–1914.

Yujiri,T., Fanger,G.R., Garrington,T.P., Schlesinger,T.K., Gibson,S. and Johnson,G.L. (1999) MEK kinase 1 (MEKK1) transduces c-Jun NH2-terminal kinase activation in response to changes in the microtubule cytoskeleton. *J. Biol. Chem.*, **274**, 12605–12610.

Yujiri,T. *et al.* (2000) MEK kinase 1 gene disruption alters cell migration and c-Jun NH_2-terminal kinase regulation but does not cause a measurable defect in NF-κB activation. *Proc. Natl Acad. Sci. USA*, **97**, 7272–7277.

Yujiri,T., Nawata,R., Takahashi,T., Sato,Y., Tanizawa,Y., Kitamura,T. and Oka,Y. (2003) MEK kinase 1 interacts with focal adhesion kinase and regulates insulin receptor substrate-1 expression. *J. Biol. Chem.*, **278**, 3846–3851.

Received September 19, 2002; revised May 12, 2003; accepted May 13, 2003

Apoptosis 2003; 8: 141–150

Reovirus-induced apoptosis: A minireview*

P. Clarke and K. L. Tyler

Departments of Neurology (P. Clarke, K. L. Tyler), Medicine, Microbiology and Immunology (K. L. Tyler), University of Colorado Health Sciences, Denver, CO 80262 and Denver Veteran's Affairs Medical Center (K. L. Tyler), Denver, CO 80220, USA

Reoviruses infect a variety of mammalian hosts and serve as an important experimental system for studying the mechanisms of virus-induced injury. Reovirus infection induces apoptosis in cultured cells *in vitro* and in target tissues *in vivo*, including the heart and central nervous system (CNS). In epithelial cells, reovirus-induced apoptosis involves the release of tumor necrosis factor (TNF)-related apoptosis-inducing ligand (TRAIL) from infected cells and the activation of TRAIL-associated death receptors (DRs) DR4 and DR5. DR activation is followed by activation of caspase 8, cleavage of Bid, and the subsequent release of pro-apoptotic mitochondrial factors. By contrast, in neurons, reovirus-induced apoptosis involves a wider array of DRs, including TNFR and Fas, and the mitochondria appear to play a less critical role. These results show that reoviruses induce apoptotic pathways in a cell and tissue specific manner. *In vivo* there is an excellent correlation between the location of viral infection, the presence of tissue injury and apoptosis, indicating that apoptosis is a critical mechanism by which disease is triggered in the host. These studies suggest that inhibition of apoptosis may provide a novel strategy for limiting virus-induced tissue damage following infection.

Keywords: apoptosis; caspases; death receptors; mitochondria; reovirus.

Introduction: Mammalian reoviruses

Reoviruses are non-enveloped, cytoplasmically replicating viruses comprised of two concentric protein capsids surrounding a genome consisting of 10 segments of double-stranded (ds) RNA.[1] Each dsRNA segment encodes a single protein, except for the S1 gene segment, which is bicistronic. Reoviruses are ubiquitous viruses that have been isolated from a wide variety of mammalian species including humans. In humans, the viruses are still considered 'orphan viruses' as they have not been definitively linked to disease, although they have been associated with diarrheal illnesses, upper respiratory infections, hepatobiliary diseases, including biliary atresia, and rare cases of central nervous system (CNS) infection.[2] By contrast, natural and experimental infection of animals produces a wide variety of diseases. The most extensively studied experimental system involves infection of neonatal mice, where, depending on the viral strain and route of inoculation, reovirus infection in mice can produce disease in a variety of organs including the CNS and heart.[2]

Reovirus-induced apoptosis is determined by the reovirus S1 and M2 gene segments

One of the most useful properties of reoviruses is the capacity to generate reassortant viruses when cells or animals are simultaneously coinfected with two different strains of virus. Reassortants are progeny viruses that contain different combinations of gene segments derived from two infecting parental strains. By comparing the phenotype of these reassortant viruses to that of the parental viruses the role of specific virus genes in the determination of viral-induced phenotypes can be determined. This strategy has been employed to identify viral determinants of apoptosis in a variety of cultured cells. For example, the prototype reovirus strains, Type 1 Lang (T1L), Type 3 Dearing (T3D) and Type 3 Abney (T3A) differ in their ability to induce apoptosis in infected L929 fibroblasts, with T3D and T3A being significantly more apoptogenic than T1L. Analysis of two independent sets of reassortant viruses generated from T1L × T3D and T1L × T3A both identified a significant association between the capacity of viral reassortants to induce apoptosis and the presence of the T3 S1 and M2 gene segments.[3,4] These same two gene segments were also identified as important determinants

*This work was supported by Public Health Service grant 1RO1AG14071 from the National Institute of Health (KLT), Merit and REAP grants from the Department of Veterans Affairs (KLT), a U.S. Army Medical Research and Material Command grant #DAMD17-98-1-8614 (KLT), the Reuler-Lewin Family Professorship of Neurology (KLT) and the Ovarian Cancer Research Fund (PC).

Correspondence to: Dr. K. L. Tyler, Department of Neurology (B 182), University of Colorado, Health Sciences Center, 4200 East 9th Ave., Denver, CO 80262, USA. Tel: (+1) 303 393 2874; Fax: (+1) 303 393 4686; e-mail: Ken.Tyler@uchsc.edu

of apoptosis in Madin-Darby canine kidney (MDCK) cells and the S1 gene segment alone as a determinant of apoptosis in HeLa cells.[5,6]

In addition to determining the ability of reoviruses to induce apoptosis in infected cells the S1 gene segment is also a key determinant of reovirus-induced G_2/M cell cycle arrest, an effect that results from inhibition of the G_2/M regulatory kinase $p34^{cdc2}$ and the resulting inhibition of cellular DNA synthesis.[4,7,8] G_2/M cell cycle arrest has recently been shown to be the result of the activity of the non-structural S1-encoded protein σ1s.[7] Infection of cells with a reovirus σ1s null-mutant virus (clone 84 MA) results in apoptosis without associated cell cycle arrest indicating that apoptosis and cell cycle dysregulation can be dissociated.[7,9] In addition, treatment of infected cells with caspase inhibitors, calpain inhibitors, or inhibition of NF-κB activation, all of which prevent apoptosis (see below), have no effect on reovirus-induced cell cycle arrest.[7]

In distinction to the key role played by the σ1s protein in reovirus-induced cell cycle arrest, several lines of evidence suggest that it is the S1-encoded σ1 protein that is the major determinant of reovirus-induced apoptosis. First, apoptosis can be induced by UV-inactivated replication-incompetent virions, which lack σ1s.[3] Second, apoptosis can also be induced at non-permissive temperatures by a variety of reovirus temperature-sensitive (ts)-mutants, which are arrested at defined steps in viral replication and fail to synthesize σ1s in infected cells.[10] Finally, the reovirus σ1s-null mutant clone 84MA fails to induce G_2/M arrest in infected cells, but retains the capacity to induce apoptosis, indicating that σ1s is not required for this process.[7,9]

In both L929 cells and MDCK cells, but not HeLa cells, the reovirus M2 gene is associated with the S1 gene as a determinant of apoptosis. The M2 gene encodes the major viral outer capsid protein μ1/μ1c.[3–6] Linear regression analysis indicates that both the S1 and M2 genes contribute to the apoptotic phenotype and that the M2 effects are not simply the result of S1 and M2 being linked or co-segregating in the reassortant pools.[3–5] Incubation of infected cells with monoclonal antibodies (MAbs) directed against either the σ1 (viral attachment), σ3 or μ1 proteins (outer capsid) can inhibit apoptosis.[3] In the case of the σ1 MAbs this almost certainly reflects their capacity to inhibit viral cell attachment. However, both anti-μ1 and anti-σ3 MAbs, which do not inhibit viral cell attachment, but which do prevent virion-uncoating, can inhibit apoptosis.[11] These MAb studies and the determination of the M2 gene as a determinant of apoptosis, suggest that early events during viral entry, but subsequent to virus engagement of cellular receptors, are required for apoptosis. This interpretation has subsequently been supported by experiments using temperature sensitive (ts)-mutants blocked at different stages in the reovirus replication cycle and pharmacological inhibitors of reovirus uncoating.[10]

The reovirus attachment protein σ1

In virions, the reovirus σ1 protein is a homotrimer comprised of an elongated fibrous tail, which inserts into the virion, and an externally facing globular head.[12] The head of both the T1L and T3D σ1 proteins contain an independent receptor-binding domain that binds junction adhesion molecule (JAM).[13] The fibrous tail of the reovirus σ1 protein also contains receptor-binding domains.[14] In T3σ1 this additional region binds α-linked sialic acid, whereas a separate region of the T1 σ1 mediates the binding of T1L to an as yet unidentified cell surface carbohydrate.[13–15]

To investigate the contribution of the JAM and sialic acid binding domains during T3 reovirus infection monoreassortant viruses were constructed containing the S1 gene from either the non-sialic-acid-binding strain T3C44 (strain T3SA−) or from the sialic-acid-binding strain T3C44-MA (strain T3SA+) on a T1L background.[16–18] As expected, experiments using these reassortant viruses show that T3SA− binds JAM while T3SA+ binds both JAM and sialic acid.[13] In addition, it was found that MAbs directed against hJAM (J10.4) completely block the ability of T3SA− to bind to human neuronal precursor (NT2) cells, indicating the requirement of JAM for T3 reovirus binding in the absence of sialic acid.[13] Antibodies directed against hJAM also significantly block the ability of T3SA+ to bind to NT2 cells and HeLa cells, although residual binding activity above background remained.[13,18] The fact that growth of T3SA+ in HeLa cells in the presence of mAb J10.4 is only minimally reduced (less than 2-fold at 48 hr) suggests that this residual binding activity is sufficient to act as a functional receptor when hJAM is absent or inaccessible.[13] T3SA− and T3SA+ grow equally well in L929 cells, however in HeLa cells T3SA− growth is reduced compared to that of T3SA+.[6] The binding of sialic acid in addition to JAM at early times post attachment is thus proposed to enhance both reovirus-attachment and growth in some cell types.[6,18]

Whereas there seems to be some flexibility on the binding of sialic acid and JAM for reovirus growth both of these receptors are required for the ability of reovirus to induced apoptosis in infected cells. Thus, T3SA+ induces high levels of apoptosis in both HeLa and L929 cells, whereas T3SA− induces little or no apoptosis in these cell types.[6] In addition, the removal of cell surface sialic acid with neuraminidase or the incubation of virus with sialyllactose, a trisaccharide comprised of lactose and sialic acid abolishes the capacity of T3SA+ to induce apoptosis.[6]

Reovirus-induced apoptosis requires viral disassembly but not viral replication

Although the induction of apoptosis in reovirus-infected cells is dependent on viral binding to both the JAM receptor and sialic acid co-receptors, engagement of these receptors alone is not sufficient to elicit apoptosis and early steps in the viral replication cycle are also required. Following viral cell attachment and subsequent receptor-mediated endocytosis, reovirions are proteolytically disassembled to form infectious sub-virion particles (ISVPs); a process characterized by the removal of the outer capsid protein $\sigma 3$, proteolytic cleavage of $\mu 1/\mu 1C$ and conformational changes in $\sigma 1$. Blocking proteolysis of reovirus virions with ammonium chloride, which inhibits endosomal acidification, or E64, which inhibits cysteine-containing endocytic proteases, blocks reovirus-induced apoptosis, indicating that viral disassembly is required for apoptosis in infected cells.[10] *In vitro* generated ISVPs are capable of inducing apoptosis, however like virions their ability to induce apoptosis is blocked by ammonium chloride suggesting that endosomal events are critical in inducing apoptosis and that this is not simply a result of the role endosomes play in mediating conversion of virions to ISVPs.[10]

Treatment of infected cells with the viral RNA synthesis inhibitor ribavirin does not prevent apoptosis.[10] In addition, particles lacking genomic dsRNA are capable of inducing apoptosis, indicating that the key apoptosis-initiating event precedes and does not require viral RNA synthesis.[10] Further, ts reovirus mutants with mutations resulting in defects in outer capsid assembly (tsB352/L2 gene), and in dsRNA synthesis (tsD357/L1 gene, tsE320/S3 gene) are capable of inducing similar levels of apoptosis at both non-permissive (39°C) and permissive (32°C) temperatures. Temperature sensitive mutants with defects in viral core (tsC447/S2 gene) and outer capsid assembly (tsG453/S4 gene) also still induce apoptosis at 39°C, but only about half as efficiently as they do at 32°C.[10] Since all these ts mutants undergo endosomal processing, their ability to induce apoptosis is consistent with a key role for endosomal vesicle-related events in apoptosis induction. However, the fact that assembly defects can influence the efficiency of this process suggests that non-endosomal factors also modulate this process.

The observation that UV-inactivated reovirions can induce apoptosis also indicates that replication is not absolutely required for induction of apoptosis, provided the inoculum size is sufficient.[3] Further support for the lack of a requirement for replication comes from studies in L929 and MDCK cells, which indicate that there is little correlation between the efficiency with which reovirus strains replicate in particular cells, and their capacity to induce apoptosis.[3,5] Consistent with these results, inhibition of apoptosis in reovirus-infected cells, typically has either no effect on viral titer or results in modest titer reduction on the order of 0.5 log.[19–21]

Reovirus induced apoptosis requires activation of the transcription factor NF-κB

Nuclear factor kappa B (NF-κB) is a transcription factor that is normally prevented form migrating to the nucleus and binding to DNA by its association in the cytoplasm with members of the IκB family of inhibitory proteins. Site specific phosphorylation, followed by ubiquitination and proteosomal degradation of IκB, allow for NF-κB activation. Reovirus-infection transiently activates NF-κB in a variety of cell types, including L929, MDCK and HeLa cells.[20] This activation can be detected by electrophoretic mobility shift assays (EMSA) as early as 4 h post infection (pi) and peaks at 10 h pi.[20] Similarly, expression of an NF-κB-dependent luciferase reporter gene is transient in reovirus-infected cells where expression is detectable at 12 h pi and peaks at 18 h pi.[20] Inhibition of NF-κB by stable over-expression of an IκB super-repressor or treatment of cells with a proteasome inhibitor that blocks IκB degradation (Z-L_sVS) inhibits reovirus-induced apoptosis.[20] Apoptosis is also inhibited in immortalized mouse embryo fibroblasts (MEFs) with targeted disruptions in the genes encoding the p50 or p65 subunits of NF-κB.[20] These results suggest, in contradistinction to many other models of apoptosis, that at early hmes following reovirus infection NF-κB exerts a pro- rather than anti-apoptotic influence.

Similar to reovirus-induced apoptosis, NF-κB activation in reovirus-infected cells requires the engagement of both the sialic acid and JAM receptors by the reovirus viral attachment protein, $\sigma 1$.[6,13] This observation, suggests that only sialic acid-binding reovirus strains, including most T3 strains, but no T1 strains, would activate NF-κB, a prediction that has not yet been tested. Again, similarly to reovirus-induced apoptosis, NF-κB activation in reovirus-infected cells requires viral disassembly but not viral replication.[10] The exact mechanism by which receptor engagement and viral disassembly activate NF-κB remains unknown although numerous potential mechanisms have been discussed.[10,13,23] It has been suggested that the conformational change in $\sigma 1$ that occurs during disassembly may enhance the affinity of $\sigma 1$ for sialic acid, JAM, or both receptors, leading to receptor aggregation and stimulation of intracellular signaling. Proteolytic processing of $\mu 1/\mu 1C$ during virion disassembly may also influence virus-receptor interactions and would provide a mechanistic explanation for the contribution of the M2 gene to the efficiency of apoptosis.[3–5] Finally, JAM exists in a complex of tight junction proteins that includes the

ras-interacting protein AF-6. Since ras-mediated pathways have been implicated in the activation of NF-κB this may also constitute a mechanism whereby NF-κB is activated in reovirus-infected cells.

Reovirus-induced apoptosis is associated with the activation of JNK and the JNK-dependent transcription factor c-Jun

Reovirus infection results in viral strain-specific patterns of selective activation of the c-Jun N-terminal kinase (JNK), extracellular-related kinase (ERK), and p38 mitogen-activated protein kinase (MAPK) signaling pathways in infected cells.[23] Activation of JNK can be detected within 10 h of T3−, but not T1L−, reovirus infection in L929 cells and increases steadily for the first 24 h. ERK shows a bimodal pattern of activation with an early phase resolving within 30 min of infection followed by a second activation phase detectable at 2 h pi. In distinction to JNK activation, the late phase of ERK activation appears equally robust in cells infected with T1L, T3A, and T3D.[23] In contrast to their activation of ERK and JNK, reovirus strains do not appear to activate p38 MAPKs.[23]

Pharmacologic inhibition of ERK activation does not either augment or inhibit reovirus-induced apoptosis indicating that the activation of this kinase is not required for reovirus-induced apoptosis.[23] By contrast, the capacity of reovirus strains to activate JNK correlates closely with their capacity to induce apoptosis.[23] In addition, experiments using T1L × T3D reassortants indicate that the same viral gene segments that determine apoptosis induction (S1 and M2) are also key determinants of JNK activation.[23] Preliminary studies also suggest that inhibition of JNK activation with pharmacologic inhibitors inhibits reovirus-induced apoptosis (unpublished).

Reovirus-induced JNK activation is associated with the subsequent activation-related phosphorylation of the JNK-dependent transcription factor c-Jun.[23] Increased activation of c-Jun is detectable by 12 h pi, peaks at 12–24 h pi and then gradually declines to baseline by 48 hrs pi.[23] Although the specific receptor requirement for JNK and c-Jun activation has not been identified, the results described above suggest that, like apoptosis, engagement of both JAM and sialic acid will be necessary for JNK activation.

The requirement for and association of transcription factor activation with reovirus-induced apoptosis suggests that *de novo* expression of cellular genes and/or the consequences of activation of cellular MAPK signaling pathways mediate this process. Oligonucleotide microarrays have been utilized to analyze reovirus-induced changes in gene expression in infected cells and application of this technology to identify changes in expression of apoptosis-related-genes and their transcription factor dependence is underway.[24]

Reovirus-induced apoptosis is initiated by activation of death receptors

Many types of apoptosis triggered by extrinsic stimuli are initiated by activation of members of the tumor necrosis factor receptor (TNFR) superfamily of cell surface death receptors. In a wide variety of non-neuronal cells including L929 cells, human embryonic kidney (HEK293) cells and several human cervical (HeLa), breast, and lung cancer derived cell lines, TNF-related apoptosis-inducing ligand (TRAIL) and its receptors play a key role in reovirus-induced apoptosis.[21,25] TRAIL is a widely expressed type-2 membrane protein that was identified by its homology to Fas ligand (FasL) and TNFα. Following its release from cells TRAIL can induce apoptosis by binding to specific cell surface death receptors (DRs), DR4 (also called TRAIL-R1) and DR5 (also called Apo2, TRAIL-R2, TRACK2 or KILLER). TRAIL can also bind to the receptors DcR-1 (for Decoy Receptor 1) and DcR-2. These decoy receptors do not transduce apoptotic signals and can prevent the induction of apoptosis in TRAIL-treated cells. TRAIL-mediated activation of DR4 and DR5 triggers the onset of DR induced apoptosis, which involves DR oligomerization and the close association of their cytoplasmic death domains (DDs). This is followed by a DD-associated interaction with the cytosolic adapter molecule FADD (for Fas associated death domain), and the recruitment of pro-caspase 8 to form a death inducing signaling complex (DISC), where the cleavage of pro-caspase 8 results in the generation of the active initiator caspase, caspase 8. Caspase 8 then activates the effector caspases (caspases 3, 6 and 7), which are the proteolytic engines of cell death.[26]

In HEK293 cells, L929 cells and a variety of different cell lines derived from human cancers, reovirus-induced apoptosis is inhibited by the presence of anti-TRAIL antibodies or soluble TRAIL receptors (Fc:DR4 and Fc:DR5) and by the over-expression of the non-apoptosis-inducing TRAIL receptor DcR-1.[21,25] In contrast, antibodies directed against Fas and soluble TNF receptors appeared to have no effect on reovirus-induced apoptosis in these cells. Events downstream of TRAIL-receptor binding are also activated following reovirus infection. For example, pro-caspase 8 is cleaved to form the active initiator caspase, caspase 8.[25,27] In HEK293 cells the activation of caspase 8 occurs in two phases. An initial phase occurs between 8 and 14 h pi and a later phase occurs between 24 and 34 h pi, by which time all pro-caspase 8 has been cleaved.[27] Caspase-8-activity is required for reovirus-induced apoptosis in

HEK293 cells. Hence the expression of DN-FADD, and a peptide inhibitor of caspase 8-activity (IETD-FMK) block reovirus-induced apoptosis.[21,27] Caspase-8 activation following reovirus-infection is required for the activation of caspase 3, as demonstrated by the inhibition of reovirus-induced activation of caspase 3, in cells expressing FADD-DN.[27] Again reovirus-induced activation of caspase 3 is biphasic, with the first phase beginning around 8 hours pi and a second activation beginning at 24 h pi.[27] The kinetics of caspase 8 and caspase 3 activation suggest that these two events occur in rapid succession in reovirus-infected cells. Reovirus-induced caspase 3-activity corresponds closely to the cleavage of the cellular substrate PARP, indicating that caspase 3 has biological activity in infected cells and can participate in the cleavage of cellular substrates to induce the morphological hallmarks of apoptosis.[10,25,27]

Reovirus-infected cells release soluble TRAIL into the supernate, providing a potential mechanism for initiating both autocrine and exocrine (bystander) apoptosis. TRAIL release from infected cells can be detected using supernatant transfer experiments.[21,25] In these experiments cells are infected with reovirus and then, at various times following infection, the culture supernatant is removed and used to inoculate a TRAIL-sensitive indicator cell line (HeLa cells). Apoptosis is then determined 24 h following media-transfer. Apoptosis is induced in TRAIL-sensitive indicator cells following treatment with media taken from virus-infected HEK293 cells at 24, 38 and 48 h post-infection (18, 30 and 68% respectively).[21] This apoptosis is inhibited by soluble TRAIL receptors (Fc:DR5 or Fc:DR4) indicating it is TRAIL-specific. In contrast, apoptosis in the indicator cells is not blocked with a neutralizing polyclonal antireovirus antiserum that neutralizes both reovirus infection and apoptosis, indicating that apoptosis in the indicator line is not mediated by virus present in the transferred supernatant.

It has recently been shown that regulation of TRAIL and DR-expression is mediated by NF-κB in a variety of systems and that NF-κB activation is required for the up-regulation of TRAIL and DR-expression in cells undergoing apoptosis induced by HTLV-1 Tax and the chemotherapeutic agents etoposide and doxorubicin.[28–31] Studies are now underway to determine the role of NF-κB in mediating TRAIL and DR-expression during reovirus-induced apoptosis.

Binding of TRAIL to DR4/DR5 can induce activation of JNK and c-Jun through a TRAF 1/2-dependent process, providing a potential link between reovirus-induced death receptor activation and MAPK induction.[32] However, inhibition of TRAIL binding, using soluble Fc:DR5, inhibited reovirus-induced apoptosis but had no effect on reovirus-induced c-Jun activation.[23] In addition JNK activity in reovirus-infected cells precedes detectable TRAIL release.[21,23,25] These results indicate that JNK activation in reovirus-infected cells is not merely a consequence of TRAIL/receptor binding and that other mechanisms of activation must be present.

Reovirus-induced activation of mitochondrial apoptosis pathway

In addition to activating the effector caspases, caspase 8 can also cleave the pro-apoptotic Bcl-2 family member, Bid.[33,34] Cleaved Bid translocates to the mitochondria where, in conjunction with other pro-apoptotic Bcl-2 family proteins (e.g. Bak and Bax), it contributes to the opening, or modification, of channels in the mitochondrial membrane, allowing the release of pro-apoptotic factors, including cytochrome *c* and a second mitochondrial activator of apoptosis (Smac, also called DIABLO). Cytochrome *c* assists with the formation of a macromolecular complex (the apoptosome), which utilizes the apoptotic protease activating factor (APAF)-1 to mediate activation of the initiator caspase, caspase 9.[35] Smac/DIABLO binds to cellular inhibitor of apoptosis proteins (IAPs), preventing their inhibitory actions on caspase activity.[36] In addition to activating the effector caspases, caspase 9 can also cleave pro-caspase 8, through the activation of caspase 3, which may act to amplify the apoptotic response.[37] It is thought that in addition to releasing cytochrome *c* and Smac/DIABLO the mitochondria may also contribute to apoptosis by releasing stores of pro-caspase 8, which then become available for activation.[38] In some cell types activation of the mitochondrial pathway, through the caspase 8-dependent cleavage of Bid may be required for ligand-induced apoptosis, whereas other cells undergo ligand-mediated apoptosis without the involvement of the mitochondria. At the molecular level these cell types differ principally in the amount of caspase 8 recruited to the ligand-activated receptor.

The first indication that mitochondrial events were involved in reovirus-induced apoptosis came from the observation that reovirus-induced apoptosis is inhibited in MDCK cells that over-express Bcl-2, which inhibits the formation of pores in the mitochondrial membrane by binding to pro-apoptotic "pore-forming" Bcl-2 family members.[5] It was subsequently found that Bid is cleaved in HEK293 cells following infection with reovirus.[27] Similar to the activation of caspase 8, Bid cleavage is biphasic. The release of cytochrome *c* from the mitochondria of reovirus-infected cells at 10 hours pi and the associated activation of caspase 9 at approximately the same time, suggest that cleaved Bid is able to induce the activation of mitochondrial apoptotic pathways in reovirus-infected cells.[27] Both Bid cleavage and the release of cytochrome *c* are blocked in cells expressing DN-FADD, indicating that caspase 8 activity is required for activation of the mitochondrial apoptotic pathway in reovirus-infected cells.[27]

Smac/DIABLO is also released from the mitochondria of reovirus-infected cells with similar kinetics to the release of cytochrome *c* and, like cytochrome *c*, Smac/DIABLO release is blocked by the over-expression of Bcl-2.[27] Although reovirus-infection results in both cytochrome *c*-mediated caspase 9 activation and Smac/DIABLO release, recent studies suggest that it is likely that Smac/DIABLO release, rather than caspase 9 activation, plays a critical role in the mitochondrial-related augmentation of death-receptor initiated apoptotic pathways.[39] Thus, stable transfection of HEK293 cells with DN-caspase 9 (caspase 9b) only inhibits caspase 9-activation, unlike Bcl-2 over-expression, which blocks all mitochondrially-mediated events.[39] Similarly, caspase 9b expression prevents the activation of caspase 9 in reovirus-infected cells but does not affect reovirus-induced activation of caspase 3 or reovirus-induced PARP cleavage, suggesting that although caspase 9 is activated in reovirus-infected cells, other pathways are necessary for effector caspase activation.[39]

As noted, Smac/DIABLO acts as a pro-apoptotic factor by inhibiting IAP-mediated caspase inhibition.[36] This may be mediated through direct binding of Smac/DIABLO with target IAPs.[36,40–42] Alternatively, IAP degradation has also been shown to represent an important apoptotic event in both mammalian cells and in drosophila where proteins with regions homologous to Smac/DIABLO (Grim and REAPER) promote ubiquitin-mediated DIAP1 degradation.[43–46] The fact that in reovirus-infected cells some cellular IAPs (survivin, cIAP1 and XIAP) undergo proteolytic cleavage and degradation following reovirus-infection, and that this can be prevented in cells over-expressing Bcl-2, is consistent with a key role for Smac/DIABLO in mediating mitochondrial-related reovirus-induced apoptotic pathways.[39]

In addition to cytochrome *c* and Smac/DIABLO, a variety of other mitochondrial apoptotic factors have been identified, including apoptosis inducing factor (AIF). Reovirus infection is not associated with release of AIF in HEK293 cells.[39] Neither does it result in disruption of mitochondrial transmembrane potential, indicating that the release of pro-apoptotic factors from the mitochondria following reovirus infection is selective.[39] This is consistent with ultrastructural studies in reovirus-infected cells that suggest that disruption of mitochondrial architecture is not a typical feature of reovirus infection.

As previously described, activation of both caspase-8 and Bid show a biphasic pattern with an early-activation phase at 8–10 h pi followed by a later activation phase.[27] In contrast, reovirus-induced release of Smac/DIABLO is not biphasic and occurs just after the early phase and before the late phase of caspase 8-activation and Bid cleavage.[27] Over-expression of Bcl-2 inhibits the late phase of caspase 8 activation without affecting the early phase, suggesting that the late phase is mitochondrial-dependent. Taken together these results are consistent with a model in which death-receptor activation initiates reovirus apoptosis, and results in early low level activation of effector caspases. Mitochondrial-events, likely initiated by Bid translocation and involving release of Smac/DIABLO, then amplify the initial death receptor-initiated signal and dramatically augment effector caspase activation.

In addition to caspase 3, the effector caspase, caspase 7 is also activated following reovirus infection.[27] This activation occurs later than the first phase of caspase 3-activity and is less robust suggesting that caspase 7 activation may play a less critical role in reovirus-induced apoptosis than caspase 3. In addition, the observations that caspase 7 activation parallels that of caspase 9 and is not biphasic suggest that it may result from the activation of caspase 9.

Reovirus sensitizes cells to TRAIL—Induced apoptosis

In addition to inducing the release of TRAIL from infected cells, reovirus-infection also sensitizes cells to TRAIL-induced apoptosis.[21,25] This sensitization is detectable around 12 h pi and increases until 48 h pi when the majority of cells are apoptotic.[21] Reovirus infection and TRAIL treatment have synergistic rather than merely additive effects on apoptosis, and infection can confer TRAIL sensitivity to previously TRAIL-resistant cells as well as increasing the TRAIL sensitivity of partially resistant lines.[21,25] For example, reovirus infection increases apoptosis in TRAIL-treated HEK293 cells from 30% to 90%, in a TRAIL-treated human breast cancer cell line (ZR75-1) from <10% to 80%, in a TRAIL-treated human lung cancer cell line (H157) from 10% to 70% and in a TRAIL-treated human ovarian cancer cell line (OVCAR-3) from 10% to 80% (unpublished).[21,25] This finding may increase the potential utility of TRAIL as an agent for cancer therapy, which is currently limited by the fact that cancer cells of all types differ in sensitivity to TRAIL-induced apoptosis. Although TRAIL receptor expression may be up-regulated in HEK293 cells the ability of reovirus to sensitize cells to TRAIL does not appear to reflect an increase in the expression of TRAIL receptors in several human cancer cell lines.[21] In the human lung cancer cell line, H157, reovirus-induced sensitization of cells to TRAIL is associated with an increase in the activation of caspase 8 and caspase 3 and is blocked by the caspase 8 inhibitor IETD-FMK.[25]

Reovirus-induced apoptosis requires calpain

Although the caspase family of cellular proteases are central to reovirus-induced apoptosis, the calcium dependent

papain-like neutral cysteine protease, calpain, also plays a role in this process. Calpain is distributed widely throughout the cytosol of many cell types and exists as an inactive pro-enzyme in steady state with its endogenous inhibitor calpastatin. Calpains have been demonstrated to mediate differentiation and necrosis and to participate in caspase-dependent and caspase-independent apoptosis.

Reovirus-induced apoptosis in L929 cells and in myocardiocytes is associated with an increase in cellular calpain activity.[19,47] Increased calpain activity is seen in reovirus-infected cells, compared to mock-infected cells, as early as 2 h pi and this activation is suppressed by the addition of the calpain active-site inhibitor, N-acetyl-leucyl-leucyl-norleucinal (aLLN, calpain inhibitor 1) and by a second calpain inhibitor, PD150606, an α-mercapto-acrylic acid derivative that selectively blocks calpain's calcium-binding site inhibitor.[19] Calpain inhibitors also block apoptosis induced by T3A, T1L and UV-inactivated reovirus indicating the role of calpain in this process. Calpain activation has also been shown to occur in reovirus-infected primary cardiac myocytes and again treatment of these cells with a calpain inhibitor (Z-leu-aminobutyric acid-CONH$(CH_2)3$-morpholine, CX295) protects them from reovirus-induced apoptosis. Further, CX295 also dramatically reduces the extent of apoptotic myocardial injury in reovirus-infected mice (see below).[47] The precise step in reovirus-induced apoptosis at which calpains act is unclear. In most models of apoptosis calpains act upstream of caspases and the early onset of calpain activity in reovirus-infected cells suggests that this may is also be true for reovirus-induced apoptosis. Experiments showing the effect of calpain inhibitors on caspase-activation would be useful to confirm this possibility. Calpain has also been implicated in the regulation of a variety of cellular transcription factors, including NF-κB and c-Jun activation, which may both play a role in reovirus-induced apoptosis.[48–50]

Reovirus-induced apoptosis in the mouse CNS

It has long been known that T3 reovirus strains infect neurons within specific regions of neonatal mouse brain producing a lethal meningoencephalitis. Viral replication and pathology co-localize in the brain and have a predilection for the cortex hippocampus and thalamus. It has now been shown that reovirus induces apoptosis in the brain following intracerebral inoculation of newborn mice with T3D and fragmentation of DNA into oligonucleosomal length ladders can be detected in tissue samples prepared from T3D− but not mock-infected brain (8–9 days pi), coinciding with maximal viral growth.

In an effort to determine the relationship between pathology, apoptosis, and viral infection, brain sections have been stained with TUNEL and antibodies specific for activated caspase 3 to detect apoptosis, and with polyclonal anti-reovirus antisera to detect viral antigen. At a macroscopic level there is an excellent correlation between areas of tissue injury, the presence of apoptotic cells, and the localization of viral infection.[51,52] At a microscopic level, individual cells can also be analyzed for the presence of viral antigen and apoptosis. In brain, most cells in infected regions are both TUNEL-positive and reovirus antigen-positive, however there are cells in these regions that are apoptotic but antigen negative.[51,52] This suggests that apoptosis occurs both as a result of direct viral infection, and in uninfected 'bystander' cells adjacent to productively infected cells.

Studies of reovirus-infection in a mouse neuroblastoma-derived cell line (NB41a3) and in primary mouse cortical cultures (MCC) derived from embryonic (E20) mice indicate that reovirus-induced apoptosis of neurons is similar to reovirus-induced apoptosis of non-neuronal cells in that it is associated with increased levels of caspase 3-activity and is blocked with the caspase 3-inhibitor DEVD-FMK.[52]

Again, similar to the mechanism of reovirus-induced apoptosis in epithelial cells reovirus infection induces increased caspase 8 activation in infected neurons, indicating that neuronal apoptosis, like that in its epithelial cell counterparts, involves death-receptor activation.[52] However, the ligand-receptor trigger for this activation appears to be less specific than that observed in epithelial cells. Thus, whereas reovirus-induced apoptosis in HEK293 cells is selectively inhibited by blocking TRAIL ligand/receptor interaction, reovirus-induced apoptosis in NB4 cells is inhibited by treating cells with both soluble TRAIL receptors (Fc:DR5) and soluble TNFR (FcTNFR-1), and reovirus-induced apoptosis in MCCs is inhibited by Fc:TNFR-1 and Fc:Fas.[52]

Another distinction between reovirus-induced apoptosis in neuronal and epithelial cells may be the extent of involvement of the mitochondrial pathway. In contrast to HEK cells, in which reovirus infection is associated with robust release of cytochrome *c* and the subsequent activation of caspase 9, in neuronal cultures cytochrome *c* release appears to occur only at low levels and at later times following infection.[52] As would be predicted from this result, there is only low level activation of caspase 9 in these cells.[52] Consistent with these findings, the caspase 9 inhibitor Z-LEHD-FMK has little effect on reovirus-induced neuronal apoptosis, which is significantly inhibited by either caspase 8 (Z-IETD-FMK), caspase 3 (Z-DEVD-FMK) or pan-caspase inhibitors.[52] Studies are currently underway to determine if Smac/DIABLO or other pro-apoptotic factors are released during reovirus-induced neuronal apoptosis.

Studies of reovirus-infection in neuronal cultures also provide further evidence of bystander apoptosis seen

following reovirus infection and in both MCC and NB4 cells dual labeling with imunocytochemistry and TUNEL showed that although a great majority of infected cells were undergoing apoptosis there was also a subset of apoptotic cells that were uninfected but located in proximity to virus-infected cells.[52] Bystander apoptosis could result from the release of TRAIL, or other death ligands, from reovirus-infected cells. If this is the case the amount of bystander apoptosis would reflect the sensitivity of the surrounding cells to the released ligand.

Reovirus-induced apoptosis is responsible for tissue injury

Although studies in the mouse CNS show that apoptotic cells are restricted to the same regions of the brain in which infected cells and tissue damage occur, the actual demonstration that reovirus-induced disease results from apoptosis came from studies using reovirus strain 8B, a virus that efficiently produces myocarditis in infected neonatal mice.[43] In this model, reovirus infection results in apoptosis in the heart. Similar to results seen in the mouse brain, DNA extracted from the hearts of reovirus-infected mice is fragmented into oligonucleosomal-length ladders, indicative of apoptosis.[47] Also similar to results seen in reovirus-infected brain tissue, areas of TUNEL positive cells in 8B infected hearts correlate with areas of histologic damage and reovirus antigen.[47] Injury to the heart following reovirus-infection occurred in the absence of an inflammatory response, also suggesting that it results from apoptotic cell death.[47]

Treatment of mice with the calpain inhibitor CX295 (dipeptide alpha-ketoamide calapin inhibitor z-Leu-aminobutyric acid-CONH(CH_2)3-morpoline) is protective against reovirus induced-myocarditis and produces a dramatic reduction in histopathologic evidence of myocardial injury, a reduction in serum creatine phosphokinase (an intracellular enzyme whose release into the serum is a quantitative marker of skeletal and cardiac muscle damage) and improved weight gain.[47] Prevention of myocardial injury is accompanied by a virtually complete inhibition of apoptotic myocardial cell death, strongly suggesting that virus-induced apoptosis is a key mechanism of cell death, tissue injury and mortality in reovirus-infected mice.

Although treatment of reovirus-infected animals results in a marked decrease in apoptosis in infected tissues, the impact on viral titer is less dramatic, and only a 0.5 $\log_{10}$ PFU/ml reduction is observed at the site of primary replication primary (hind limb) and only a 0.7 $\log_{10}$ PFU/ml reduction is observed in the heart.[47] These

Figure 1. TRAIL mediated apoptosis in reovirus-infected epithelial cells. Reovirus induces the release of TRAIL from infected cells. TRAIL binds to DR4 and DR5 initiating their association with FADD and pro-caspase 8. Cleavage of pro-caspase 8 results in the activation of caspase 8, which then activates caspase 3 to induce apoptosis. Caspase 8 also cleaves Bid to activate the mitochondrial apoptotic pathway resulting in the release of cyctochrome *c* and Smac/DIABLO into the cytosol. Cytochrome *c* assists with the formation of the apoptosome, which utilizes APAF-1 to mediate activation of caspase 9. The release of Smac/DIABLO from the mitochondria results in the release of IAP inhibition of caspase 3-activity and leads to the onset of apoptosis. The broad arrows indicate events that are thought to be critical for reovirus-induced apoptosis in HEK cells, whereas the thin arrows represent events that may be less important.

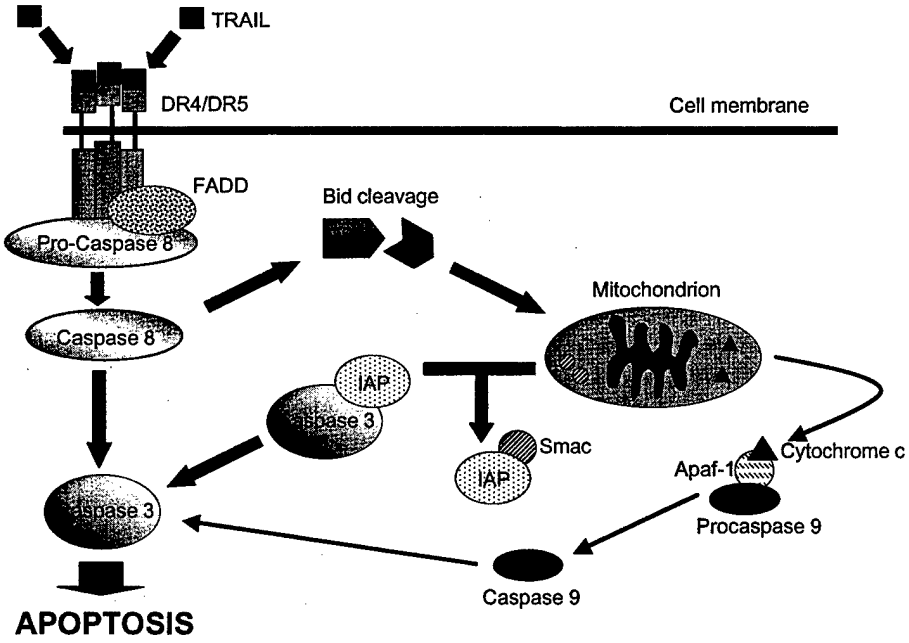

results are similar to those obtained *in vitro* and indicate that inhibiting apoptosis has only a modest effect on virus growth.

Conclusions and future directions

Over the past few years considerable advances have been made in our knowledge of reovirus-induced apoptosis, both *in vitro* and *in vivo*. Reovirus triggers apoptosis during its attachment and disassembly in infected cells. In epithelial cells, these events stimulate a variety of cellular pathways, including the activation of the cellular transcription factors NF-κB and c-Jun, the release of TRAIL from infected cells and the subsequent activation of TRAIL-apoptotic pathway. TRAIL-induced apoptosis in reovirus-infected cells is associated with the activation of the death-receptor associated caspases, caspase 8 and 3 (Figure 1). The subsequent activation of the mitochondrial apoptotic pathway in reovirus-infected cells, which requires caspase 8 activity, releases both cytochrome *c* and Smac/DIABLO into the cytoplasm. The action of Smac/DIABLO appears to be a key mitochondrial event in augmenting reovirus induced apoptosis, presumably through its action on cellular IAPs. In neurons, the pathways of virus-induced apoptosis are also initiated through death receptors, although both TNFR and Fas may play a role in addition to DR4/DR5. In addition, the mitochondrial pathway may be less important in augmenting DR-initiated apoptosis in neurons, as compared to epithelial cells, although the precise role of Smac/DIABLO remains to be established in these cells. The differences between neurons and non-neuronal cells clearly indicate that the same virus may differentially activate cellular apoptotic pathways in a cell and tissue specific manner.

Although the mechanisms of reovirus-induced apoptosis are becoming increasingly understood, a number of important questions remain. For example: (1) What are the specific links between the requirement for cellular transcription factors such as NF-κB and c-Jun and the initiation of cellular apoptotic pathways? (2) What role does the selective activation of MAPK cascades play in reovirus-induced apoptosis and how is this mediated? (3) What role does calpain play in reovirus-induced apoptosis, and how is this linked to caspase cascades, transcription factor activation, and MAPK cascades? (4) Can organ specific differences in apoptotic pathways be identified, and will this influence the response of these organs to specific anti-apoptotic therapies?

References

1. Nibert ML, Schiff, LA. Reoviruses and their replication. In: Fields BN, Knipe DM, Howley PM, eds. *Fields Virology.* Philadelphia: Lippincott-Raven Publisher, 2001: 1679–1728.
2. Tyler KL. Mammalian reoviruses. In: Fields BN, Knipe DM, Howley PM, eds. *Fields Virology.* Philadelphia: Lippincott-Raven Publisher, 2001: 1729–1747.
3. Tyler KL, Squier MKT, Rodgers SE, *et al.* Differences in the capacity of reovirus strains to induce apoptosis are determined by the viral attachment protein sigma 1. *J Virol* 1995; 69: 6972–6979.
4. Tyler KL, Squier MKT, Brown AL, *et al.* Linkage between reovirus-induced apoptosis and inhibition of cellular DNA synthesis: Role of the S1 and M2 genes. *J Virol* 1996; 70: 7984–7991.
5. Rodgers SE, Barton ES, Oberhaus SM, *et al.* Reovirus-induced apoptosis of MDCK cells is not linked to viral yield and is blocked by Bcl-2. *J Virol* 1997; 71: 2540–2546.
6. Connolly JL, Barton ES, Dermody TS. Reovirus binding to cell surface sialic acid potentiates virus-induced apoptosis. *J Virol* 2001; 75: 4029–4039.
7. Poggioli GJ, Keefer C, Connolly JL, Dermody TS, Tyler KL. Reovirus-induced G_2/M cell cycle arrest requires σ1s and occurs in the absence of apoptosis. *J Virol* 2000; 74: 9562–9570.
8. Poggioli GJ, Dermody TS, Tyler KL. Reovirus-induced G_2/M cell cycle arrest is associated with inhibition of $p34^{cdc2}$. *J Virol* 2001; 74: 9562–9570.
9. Rodgers SE, Connolly JL, Chappell JD, Dermody TS. Reovirus growth in cell culture does not require a full complement of viral proteins: Identification of a σ1s-null mutant. *J Virol* 1998; 72: 8597–8604.
10. Connolly JL, Dermody TS. Virion disassembly is required for apoptosis induced by reovirus. *J Virol* 2002; 76: 1632–1641.
11. Virgin HW 4th, Mann MA, Tyler KL. Protective antibodies inhibit reovirus internalization and uncoating by intracellular proteases. *J Virol* 1994; 68: 6719–6729.
12. Chappell JD, Prota AE, Dermody TS, Stehle T. Crystal structure of reovirus attachment protein sigma 1 reveals evolutionary relationship to adenovirus fiber. *EMBO J* 2002; 15: 1–11.
13. Barton ES, Forrest JC, Connolly JL, *et al.* Junction adhesion molecule is a receptor for reovirus. *Cell* 2001; 104: 441–451.
14. Chappell JD, Duong JL, Wright BW, Dermody TS. Identification of carbohydrate-binding domains in the attachment proteins of Type 1 and Type 3 reoviruses. *J Virol* 2000; 74: 8472–8479.
15. Lerner AM, Cherry JD, Finland M. Haemagglutination with reoviruses. *Virology* 1963; 19: 58–65.
16. Dermody TS, Nibert ML, Bassel-Duby R, Fields BN. A σ1 region important for haemagglutination by serotype 3 reovirus strains. *J Virol* 1990; 64: 5173–5176.
17. Chappell JD, Gunn VL, Wetzel JD, Baer GS, Dermody TS. Mutations in type 3 reovirus that determine binding to sialic acid are contained in the fibrous tail domain of viral attachment protein σ1. *J Virol* 1997; 71: 1834–1841.
18. Barton ES, Connolly JL, Forrest JC, Chappell JD, Dermody TS. Utilization of sialic acid as a coreceptor enhances reovirus attachment by multistep adhesion strengthening. *J Biol Chem* 2001; 276: 2200–2211.
19. DeBiasi RL, Squier MKT, Pike B, *et al.* Reovirus-induced apoptosis is preceded by increased cellular calpain activity and is blocked by calpain inhibitors. *J Virol* 1999; 73: 695–701.
20. Connolly JL, Rodgers SE, Clarke P, *et al.* Reovirus-induced apoptosis requires activation of transcription factor NF-κB. *J Virol* 2000; 74: 2981–2989.
21. Clarke P, Meintzer SM, Gibson S, *et al.* Reovirus-induced apoptosis is mediated by TRAIL. *J Virol* 2000; 74: 8135–8139.

22. Tyler KL, Clarke P, DeBiasi RL, Kominsky D, Poggioli GJ. Reoviruses and the host cell. *TRENDS in Microbiology* 2001; 9: 560–564.
23. Clarke P, Meintzer SM, Widmann C, Johnson GL, Tyler KL. Reovirus infection activates JNK and the JNK-dependent transcription factor c-Jun. *J Virol* 2001; 75: 11275–11283.
24. Pogioli GJ, DeBiasi RL, Bickel RB, *et al.* Reovirus-induced alterations in gene expression related to cell cycle regulation. *J Virol* 2002; 76: 2582–2594.
25. Clarke P, Meintzer SM, Spalding AC, Johnson GL, Tyler KL. Caspase 8-dependent sensitization of cancer cells to TRAIL-induced apoptosis following reovirus-infection. *Oncogene* 2001; 20: 6910–6919.
26. Ashkenazi A, Dixit VM. Death receptors: Signaling and modulation. *Science* 1998; 281: 1305–1308.
27. Kominsky DJ, Bickel RJ, Tyler KL. Reovirus-induced apoptosis requires both death receptor- and mitochondrial-mediated caspase-dependent pathways of cell death. *Cell Death and Differentiation* 2002; 9: 926–933.
28. Ravi R, Bedi GC, Engstrom LW, *et al.* Regulation of death receptor expression and TRAIL/Apo2L-induced apoptosis by NF-κB. *Nature Cell Biol* 2001; 3: 409–415.
29. Gibson SB, Oyer R, Spalding AC, Anderson SM, Johnson GL. Increased expression of death receptors 4 and 5 synergizes the apoptosis response to combined treatment with etoposide and TRAIL. *Mol Cell Biol* 2000; 20: 205–212.
30. Spalding AC, Jotte RM, Scheinman RI, *et al.* TRAIL and inhibitors of apoptosis are opposing determinants for NF-κB-dependent, genotoxin-induced apoptosis of cancer cells. *Oncogene* 2002; 21: 260–271.
31. Rivera-Walsh I, Waterfield M, Xiao G, Fong A, Sun S-C. NF-κB signaling pathway governs TRAIL gene expression and HTLV-1 Tax-induced T-cell death. *J Biol Chem* 2001.
32. Hu WH, Johnson H, Shu HB. Tumor necrosis factor related apoptosis inducing ligand signals NF-κB and JNK activation and apoptosis through distinct pathways. *J Biol Chem* 1999; 274: 30603–30610.
33. Li H, Zhu H, Xu CJ, Yuan J. Cleavage of Bid by caspase 8 mediates the mitochondrial damage in the Fas pathway of apoptosis. *Cell* 1998; 91: 479–489.
34. Luo X, Budihardjo I, Zou H, Slaughter C, Wang X. Bid, a Bcl-2 interactibg protein, mediates cytochrome *c* release from mitochondria in response to activation of cell surface death receptors. *Cell* 1998; 94: 481–490.
35. Zou H, Li Y, Liu X, Wang X. An APAF-1 cytochrome *c* multimeric complex is a functional apoptosome that activates procaspase 9. *J Biol Chem* 1999; 274: 11549–11556.
36. Verhagen AM, Ekert PG, Pakusch M, *et al.* Identification of DIABLO, a mammalian protein that promotes apoptosis by binding to and antagonizing IAP proteins. *Cell* 2000; 102: 43–53.
37. Slee EA, Harte MT, Kluck RM, *et al.* Ordering the cytochrome c-initiated caspase cascade: Hierarchical activation of caspases -2, -3, -6, -7, -8, and -10 in a caspase-9-dependent manner. *J Cell Biol* 1999; 144: 281–292.
38. Qin Z-H, Wang Y, Kikly KK, *et al.* Procaspase 8 is predominantly localized in mitochondria and released into cytoplasm upon apoptotic stimulation. *J Biol Chem* 2001; 276: 8079–8086.
39. Kominsky DJ, Bickel RJ, Tyler KL. Reovirus-induced apoptosis requires mitochondrial release of Smac-DIABLO and involves reduction of cellular inhibitor of apoptosis protein levels. *J Virol* 2002; 76: in press.
40. Chai J, Shiozaki E, Srinivasula SM, *et al.* Structural basis of caspase 7-inhibition by XIAP. *Cell* 2001; 104: 769–780.
41. Huang Y, Park YC, Rich RL, Segal D, Myszka DG, Wu H. Structural basis of caspase inhibition by XIAP: Differential roles of the linker versus the BIR domain. *Cell* 2001; 104: 781–790.
42. Riedl SJ, Renatus M, Schwartzenbacher R, *et al.* Structural basis for the inhibition of caspase-3 by XIAP. *Cell* 2001; 104: 791–800.
43. Johnson DE, Gastman BR, Wieckowski E, *et al.* Inhibitor of apoptosis protein hILP undergoes caspase-mediated cleavage during T lymphocyte apoptosis. *Cancer Res* 2000; 60: 1818–1823.
44. Deveraux QL, Leo E, Stennicke HR, Welsh K, Salvesen GS, Reed JC. Cleavage of human inhibitor of apoptosis protein XIAP results in fragments with distinct specificities for caspases. *EMBO J* 1999; 18: 5242–5251.
45. Yang Y, Fang S, Jensen JP, Weissman AM, Ashwell JD. Ubiquitin protein ligase activity of IAPs and their degradation in proteasomes in response to apoptotic stimuli. *Science* 2000; 288: 874–877.
46. Palaga T, Osborne B. The 3Ds of apoptosis: Death degradation and DIAPs. *Nature Cell Biol* 2002; 4: E149–151.
47. DeBiasi RL, Edelstein CL, Sherry B, Tyler KL. Calpain inhibition protects against virus-induced apoptotic myocardial injury. *J Virol* 2001; 75: 351–361.
48. Baghdiguian S, Martin M, Richard I, *et al.* Calpain 3 deficiency is associated with myonuclear apoptosis and profound perturbation of the IκB/NF-κB pathway in limb-girdle muscular dystrophy type 2A. *Nature Med* 1999; 5: 503–511.
49. Chen F, Lu Y, Kuhn DC, Maki M, Shi X, Demers LM. Calpain contributes to silica-induced IκB degradation and nuclear factor κB activation. *Arch Biochem Biophys* 1997; 34: 383–388.
50. Watt F, Molloy PL. Specific cleavage of transcription factors by the thiol protease m-calpain. *Nucleic Acids Res* 1993; 21: 5092–5100.
51. Oberhaus SM, Smith RL, Clayton GH, Dermody TS, Tyler KL. Reovirus infection and tissue injury in mouse central nervous system are associated with apoptosis. *J Virol* 1997; 71: 2100–2106.
52. Richardson-Burns SM, Kominsky DJ, Tyler KL. Reovirus-induced neuronal apoptosis is mediated by caspase 3 and is associated with the activation of death receptors. *J NeuroVirol* 2002; 8: 1–16.

THE JOURNAL OF BIOLOGICAL CHEMISTRY

Vol. 278, No. 20, Issue of May 16, pp. 18092–18100, 2003
Printed in U.S.A.

Two Distinct Phases of Virus-induced Nuclear Factor κB Regulation Enhance Tumor Necrosis Factor-related Apoptosis-inducing Ligand-mediated Apoptosis in Virus-infected Cells*

Received for publication, January 9, 2003, and in revised form, February 25, 2003
Published, JBC Papers in Press, March 13, 2003, DOI 10.1074/jbc.M300265200

Penny Clarke‡, Suzanne M. Meintzer, Lisa A. Moffitt, and Kenneth L. Tyler§¶

From the Departments of Neurology, §Medicine, Microbiology, and Immunology, University of Colorado Health Science Center, Denver, Colorado 80262 and Denver Veterans Affairs Medical Center, Denver, Colorado 80220

Cellular transcription factors are often utilized by infecting viruses to promote viral growth and influence cell fate. We have previously shown that nuclear factor κB (NF-κB) is activated after reovirus infection and that this activation is required for virus-induced apoptosis. In this report we identify a second phase of reovirus-induced NF-κB regulation. We show that at later times post-infection NF-κB activation is blocked in reovirus-infected cells. This results in the termination of virus-induced NF-κB activity and the inhibition of tumor necrosis factor α and etoposide-induced NF-κB activation in infected cells. Reovirus-induced inhibition of NF-κB activation occurs by a mechanism that prevents IκBα degradation and that is blocked in the presence of the viral RNA synthesis inhibitor, ribavirin. Reovirus-induced apoptosis is mediated by tumor necrosis factor-related apoptosis inducing ligand (TRAIL) in a variety of epithelial cell lines. Herein we show that ribavirin inhibits reovirus-induced apoptosis in TRAIL-resistant HEK293 cells and prevents the ability of reovirus infection to sensitize TRAIL-resistant cells to TRAIL-induced apoptosis. Furthermore, TRAIL-induced apoptosis is enhanced in HEK293 cells expressing IκBΔN2, which blocks NF-κB activation. These results indicate that the ability of reovirus to inhibit NF-κB activation sensitizes HEK293 cells to TRAIL and facilitates virus-induced apoptosis in TRAIL-resistant cells. Our findings demonstrate that two distinct phases of virus-induced NF-κB regulation are required to efficiently activate host cell apoptotic responses to reovirus infection.

Experimental infection with mammalian reoviruses has provided a classic model of viral pathogenesis (for review, see Ref. 1). Reovirus induces apoptosis both in cultured cells and in target tissues (for review, see Ref. 2). In the central nervous system and heart, virus-induced apoptosis correlates with pathology and is a critical mechanism by which disease is triggered in the host (3–5). Reovirus induces apoptosis by a p53-independent mechanism that involves cellular proteases, including calpains (3, 6) and caspases (5, 7, 8).

We have previously shown that in a variety of human epithelial cell lines (7, 9) reovirus-induced apoptosis is mediated by tumor necrosis factor (TNF)[1]-related apoptosis-inducing ligand (TRAIL) (for review, see Ref. 10). However, reovirus infection triggers apoptosis in both TRAIL-sensitive (7, 9) and TRAIL-resistant cells (7). The question as to how reovirus induces apoptosis in TRAIL-resistant lines has been answered in part by the observation that reovirus can sensitize previously resistant cells to killing by TRAIL (7, 9). Reovirus-induced sensitization of cells to TRAIL requires caspase 8 activity and is associated with an increase in the cleavage of procaspase 8 in cells treated with TRAIL and reovirus compared with cells treated with TRAIL alone (9). The mechanism by which reovirus induces increased caspase 8 activation in TRAIL-treated cells is, however, unknown.

The NF-κB family of cellular transcription factors promotes the expression of a variety of cellular genes, including genes that have either pro- or anti-apoptotic effects, and it is thought that the balance of expression of NF-κB-regulated genes may determine cell fate (12). The prototypical form of NF-κB exists as a heterodimer of proteins p50 and p65 (RelA) (13, 14). NF-κB is normally sequestered in the cytoplasm by its binding to a family of inhibitor proteins, collectively known as IκB (15, 16). In response to a variety of stimuli, IκB is phosphorylated, resulting in its ubiquitination and subsequent degradation (17–20). This allows the release of NF-κB, which translocates to the nucleus (21), where it stimulates cellular gene transcription (for review, see Refs. 22 and 23). In a variety of cell types, the binding of reovirus to the cell surface receptors junctional adhesion molecule and sialic acid induces the activation of NF-κB (24, 25). In TRAIL-sensitive HeLa cells this activation is detected 2–12 h post-infection (pi), involves both the p65 and p50 subunits of NF-κB, and is required for reovirus-induced apoptosis (26). In HeLa cells reovirus-induced NF-κB activation and apoptosis require viral disassembly but not subsequent events of reovirus replication and are not inhibited by the viral RNA synthesis inhibitor ribavirin or by replication incompetent viruses (27).

The experiments described below investigate the role of NF-κB in reovirus-induced apoptosis in TRAIL-resistant HEK293 cells. These studies show that reovirus infection of HEK293 cells results in an initial, transient phase of NF-κB activation that is required for reovirus-induced apoptosis in

* This work was supported by National Institute of Health Public Health Service Grant 1RO1AG14071, Merit and Research Enhancement Award Program (REAP) grants from the Department of Veterans Affairs, U. S. Army Medical Research and Material Command Grant DAMD17-98-1-8614, and by the Reuler-Lewin Family Professorship of Neurology. The costs of publication of this article were defrayed in part by the payment of page charges. This article must therefore be hereby marked "*advertisement*" in accordance with 18 U.S.C. Section 1734 solely to indicate this fact.

‡ Supported by the Ovarian Cancer Research Fund.

¶ To whom correspondence should be addressed: Dept. of Neurology (B 182), University of Colorado Health Sciences Center, 4200 East 9th Ave., Denver CO 80262. Tel.: 303-393-2874; Fax: 303-393-4686; E-mail: Ken.Tyler@uchsc.edu.

[1] The abbreviations used are: TNF, tumor necrosis factor; TRAIL, TNF-related apoptosis-inducing ligand; NF-κB, nuclear factor κB; IκB, inhibitor κB; pi, post-infection; EMSA, electrophoretic mobility shift assay; m.o.i., multiplicity of infection; HIV-1, human immunodeficiency virus type.

these cells. This is followed by a later phase of virus-induced NF-κB inhibition. Reovirus-induced inhibition of NF-κB activation is associated with impaired degradation of IκB and is inhibited by the viral RNA synthesis inhibitor, ribavirin. In contrast to findings in TRAIL-sensitive HeLa cells, in which ribavirin blocks reovirus replication but not apoptosis, both these events are blocked by ribavirin in TRAIL-resistant HEK293 cells. Ribavirin also inhibits reovirus-induced sensitization of HEK293 cells to TRAIL-induced apoptosis. We further show that HEK293 cells are sensitized to TRAIL-induced apoptosis by the expression of IκBΔN2, which blocks the activation of NF-κB. This suggests that the ability of reovirus to block NF-κB activation at later times post-infection sensitizes HEK293 cells to TRAIL-induced apoptosis and is critical for apoptosis in TRAIL-resistant cells. The demonstration that multiple levels of virus-induced NF-κB regulation are required to efficiently activate host cell apoptotic responses to reovirus infection represents a novel mechanism of viral-induced apoptosis.

EXPERIMENTAL PROCEDURES

Cells, Viruses, and Reagents—HEK293 (ATCC CRL1573) were grown in Dulbecco's modified Eagle's medium supplemented with 100 units/ml each penicillin and streptomycin and containing 10% fetal bovine serum. HeLa cells (ATCC CCL2) were grown in Eagle's minimal essential medium supplemented with 2.4 mM L-glutamine, nonessential amino acids, 60 units/ml each penicillin and streptomycin and containing 10% fetal bovine serum (Invitrogen). HEK293 cells expressing IκBΔN2, a strong dominant negative IκB mutant lacking the NH_2-terminal phosphorylation sites that regulate IκB degradation and the consequent activation of NF-κB, were a kind gift from Dr. G. Johnson). Reovirus strain Type 3 Abney (T3A) was used for all experiments. T3A is a laboratory stock that has been plaque-purified and passaged (twice) in L929 (ATCC CCL1) cells to generate working stocks (28). TRAIL was obtained from Upstate Biotechnology and Sigma, TNFα was obtained from Invitrogen, and etoposide and ribavirin were obtained from Sigma. Ribavirin was used at a concentration of 200 μM.

Apoptosis Assays—Cells were assayed for apoptosis by staining with acridine orange for determination of nuclear morphology and ethidium bromide to distinguish cell viability at a final concentration of 1 μg/ml each (29). After staining, cells were examined by epifluorescence microscopy (Nikon Labophot-2, B-2A filter; excitation, 450–490 nm; barrier, 520 nm; dichroic mirror, 505 nm). The percentage of cells containing condensed nuclei and/or marginated chromatin in a population of 100 cells was recorded. The specificity of this assay has been previously established in reovirus-infected cells using DNA laddering techniques and electron microscopy (9, 30).

Caspase 3 Activity Assays—Caspase 3 activation assays were performed using a kit obtained from Clontech. Cells (1×10^6) were centrifuged at 200 × *g* for 10 min, supernatants were removed, and cell pellets were frozen at −70 °C until all time points were collected. Assays were performed in 96-well plates and analyzed using a fluorescent plate reader (CytoFluor 4000, PerSeptive Biosystems). Cleavage of DEVD-aminofluoromethylcoumarin, a synthetic caspase-3 substrate, was used to measure caspase 3 activation in reovirus-infected cells. Cleavage after the second Asp residue produces free aminofluoromethylcoumarin that can be detected using a fluorescent plate reader. The amount of fluorescence detected is directly proportional to the amount of caspase 3 activity.

Electrophoretic Mobility Shift Assay (EMSA)—Nuclear extracts were prepared from treated cells (5×10^6) by washing cells in phosphate-buffered saline followed by incubation in hypotonic lysis buffer (10 mM HEPES (pH 7.9), 10 mM KCl, 1.5 mM $MgCl_2$, 0.5 mM dithiothreitol, 0.5 mM phenylmethylsulfonyl fluoride, and a protease inhibitor mixture (Roche Applied Science)) at 4 °C for 15 min. One-twentieth volume 10% Nonidet P-40 was added to the cell lysate, and the sample was vortexed for 10 s and centrifuged at 10,000 × *g* for 5 min. The nuclear pellet was washed once in hypotonic buffer, resuspended in high salt buffer (25% glycerol, 20 mM HEPES (pH 7.9), 0.42 M NaCl, 1.5 mM $MgCl_2$, 0.2 mM EDTA, 0.5 mM dithiothreitol, 0.5 mM phenylmethylsulfonyl fluoride, and protease inhibitor mixture), and incubated at 4 °C for 2–3 h. Samples were centrifuged at 10,000 × *g* for 10 min, and the supernatant was used as the nuclear extract.

Nuclear extracts were assayed for NF-κB activation by EMSA using a ^{32}P-labeled oligonucleotide consisting of the NF-κB consensus binding sequence (Santa Cruz Biotechnology). Nuclear extracts (5–10 μg of total protein) were incubated with a binding reaction buffer containing 2 μg of poly(dI-dC) (Sigma) in the presence of 20 mM HEPES (pH 7.9), 60 mM KCl, 1 mM EDTA, 1 mM dithiothreitol, and 5% glycerol at 4 °C for 20 min. Radiolabeled NF-κB consensus oligonucleotide (0.1–1.0 ng) was added, and the mixture was incubated at room temperature for 20 min. For competition experiments, a 10-fold excess of unlabeled consensus oligonucleotide or an oligonucleotide containing the SP-1 consensussite (Santa Cruz Biotechnology) were added to reaction mixtures. Nucleoprotein complexes were subjected to electrophoresis on native 5% polyacrylamide gels at 180 V, dried under vacuum, and exposed to Biomax MR film (Eastman Kodak Co.).

Luciferase Gene Reporter Assays—The NF-κB-dependent luciferase reporter construct was a gift from Dr. B. Sugden. The construct contains four NF-κB binding sites upstream of the luciferase gene. HEK293 cells (1.5×10^5) in 6-well tissue culture plates (Costar) were incubated for 24 h before being transfected with 1 μg of the luciferase reporter construct and 1 μg of a cytomegalovirus-β-galactosidase reporter construct (Clontech) using LipofectAMINE (Invitrogen). After an additional 24-h incubation, cells were either mock-infected or infected with T3A at an m.o.i. of 100 plaque-forming units per cell and incubated at 37 °C for various intervals. Cells were then harvested and resuspended in 1 ml of sonication buffer (91 mM dithiothreitol, 0.91 M K_2HPO_4 (pH 7.8), centrifuged at 2000 × *g* for 10 min, and resuspended in 100 μl of sonication buffer. Cells were vortexed, frozen (−20 °C) and thawed three times, and centrifuged at 14,000 × *g* for 10 min. Samples (10 μl) were assessed for luciferase activity after the addition of 350 μl of luciferase assay buffer (85 mM dithiothreitol, 0.85 M K_2HPO_4 (pH 7.8), 50 mM ATP, 15 mM $MgSO_4$) by determining optical density in a luminometer (Monolight 2010, Analytical Luminescence Laboratory). Samples were assayed for β-galactosidase activity using standard procedures (32) to normalize for transfection efficiency.

Western Blot Analysis—After infection with reovirus, cells were pelleted by centrifugation, washed twice with ice-cold phosphate-buffered saline, and lysed by sonication in 200 μl of a buffer containing 15 mM Tris, pH 7.5, 2 mM EDTA, 10 mM EGTA, 20% glycerol, 0.1% Nonidet P-40, 50 mM β-mercaptoethanol, 100 μg/ml leupeptin, 2 μg/ml aprotinin, 40 μM Z-Asp-2,6-dichlorobenzoyloxime, and 1 mM phenylmethylsulfonyl fluoride. The lysates were then cleared by centrifugation at 16,000 × *g* for 5 min, normalized for the protein amount, mixed 1:1 with SDS sample buffer (100 mM Tris, pH 6.8, 2% SDS, 300 mM β-mercaptoethanol, 30% glycerol, and 5% pyronine Y), boiled for 5 min, and stored at −70 °C. Proteins were electrophoresed by SDS-PAGE (10% gels) and probed with antibodies directed against IκBα (Santa Cruz No. 203). All lysates were standardized for protein concentration with antibodies directed against actin (Oncogene No. CP01). Autoradiographs were quantitated by densitometric analysis using a Fluor-S MultiImager (Bio-Rad).

RESULTS

Reovirus Induces the Activation of NF-κB in TRAIL-resistant HEK293 Cells—Reovirus-induced apoptosis in a variety of epithelial cell lines, including HEK293 cells and HeLa cells, is mediated by TRAIL (7, 9). However, whereas reovirus induces similar levels of apoptosis 48 h pi in HeLa and HEK293 cells (Fig. 1*A*), these cell types differ substantially in their sensitivity to TRAIL-induced apoptosis (Fig. 1*B*).

We have previously shown that reovirus activates NF-κB in TRAIL-sensitive (HeLa) cells and that this activation is required for reovirus-induced apoptosis in these cells (15). To determine the role of NF-κB in reovirus-induced apoptosis in TRAIL-resistant cells we first investigated whether NF-κB is activated after reovirus infection of these cells. HEK293 cells were infected with reovirus (m.o.i. 100), and at various times pi nuclear extracts were prepared and incubated with a ^{32}P-labeled oligonucleotide probe comprising NF-κB binding sequences. After incubation with nuclear extracts from reovirus-infected cells the mobility of the oligonucleotide probe during electrophoresis was retarded, indicating the binding of activated NF-κB to the probe sequences (Fig. 2*A*). Activated NF-κB-probe complexes in reovirus-infected cells were present 2–4 h pi and were undetectable at later times pi. Binding specificity was demonstrated by the fact that an excess of cold NF-κB, but not SP-1, sequences prevented the appearance of

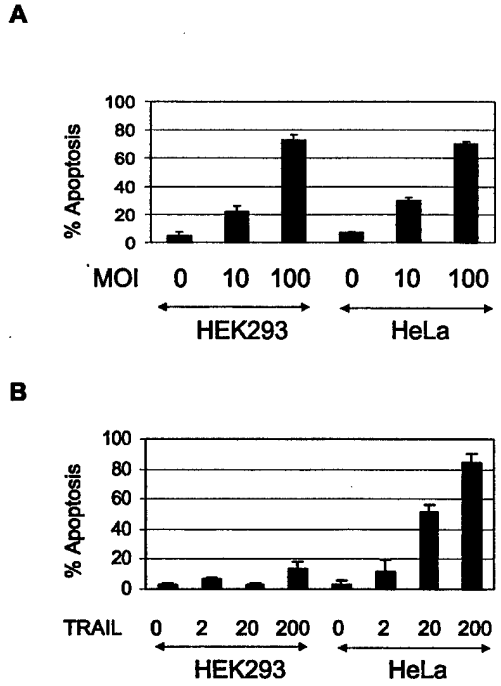

FIG. 1. **Reovirus and TRAIL-induced apoptosis in HeLa and HEK293 cells.** HEK293 and HeLa cells were treated with reovirus (m.o.i. 0, 10, 100) for 48 h (*A*) or TRAIL (0–200 ng/ml) for 24 h (*B*). The *graph* shows the mean percentage apoptosis obtained from three independent experiments. *Error bars* represent S.E.

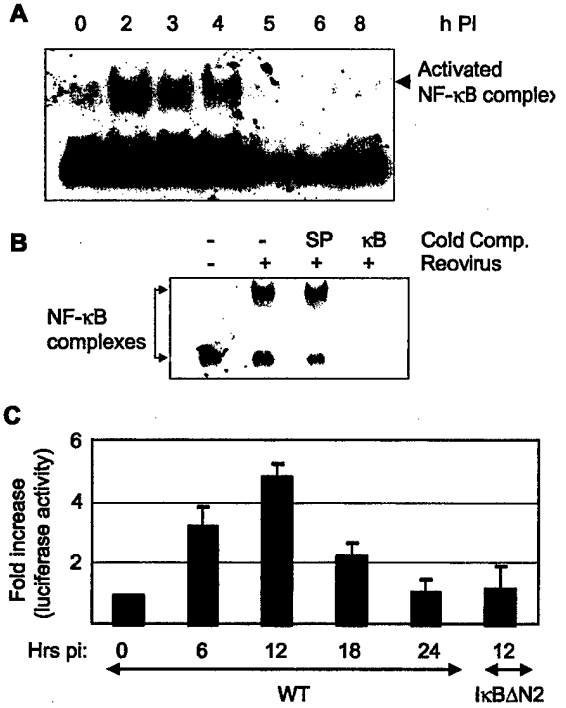

FIG. 2. **Activation of NF-κB after reovirus infection of HEK293 cells.** *A*, EMSA of reovirus-infected HEK293 cells. Nuclear extracts were prepared at various times after infection with reovirus (m.o.i. 100) and were incubated with a ^{32}P-labeled oligonucleotide consisting of the NF-κB consensus binding sequence. Incubation mixtures were resolved by acrylamide gel electrophoresis, dried, and exposed to film. Reovirus-induced NF-κB·DNA complexes are indicated. *B*, specificity of reovirus-induced NF-κB·DNA complexes. HEK293 cells were infected with reovirus or were mock-infected. Nuclear extracts were prepared 4 h after infection, and EMSA analysis was performed using a ^{32}P-labeled oligonucleotide consisting of the NF-κB consensus binding sequence. The gel shows NF-κB·DNA complexes present in nuclear extracts prepared from mock (*lane 1*) and reovirus (*lane 2*)-infected cells. Also shown are reactions from reovirus-infected cells incubated with an excess of cold oligonucleotide sequences comprising SP1 (*lane 3*) and NF-κB (*lane 4*) consensus binding sequences. *C*, NF-κB-dependent luciferase expression in reovirus-infected HEK293 cells. HEK293 cells (1.5×10^5) expressing wild type (*WT*) IκB or IκBΔN2 were transfected with 1 μg of a luciferase reporter construct containing NF-κB binding sites. After 24 h, cells were infected with T3A (m.o.i. 100) and incubated at 37 °C for the times shown. Cell extracts were then prepared, and luciferase activity was determined. The results are expressed as the mean luciferase units for three independent experiments. *Error bars* indicate S.E.

both the reovirus-induced (Fig. 2, *upper band*) and non-stimulus-induced (Fig. 2, *lower band*) NF-κB-probe complexes (Fig. 2*B*).

Luciferase reporter gene assays were also used to show that NF-κB is activated after infection of HEK293 cells with reovirus infection. Cells were transfected with a construct containing the luciferase gene under the control of NF-κB binding sequences. After transfection, cells were infected with reovirus (m.o.i. 100), and at various times pi cells were harvested and assayed for luciferase activity. Fig. 2*C* shows that luciferase gene expression is increased after infection with reovirus. A 3-fold increase in reporter gene activity was detected as early as 6 h pi, peaked at 12 h pi (5-fold increase), and then declined (Fig. 2*C*). Luciferase reporter gene activity was not detected 12 h after reovirus infection of cells expressing a dominant negative form of IκBΔN2, which lacks the sites necessary for IκB phosphorylation. The subsequent ubiquitination and degradation of IκB, which is necessary for NF-κB activation, is thus blocked in these cells. These results indicate that NF-κB is activated in a transient manner after reovirus-infection of HEK293 cells.

NF-κB Activation Is Required for Reovirus-induced Apoptosis—After having shown that NF-κB is activated after reovirus infection of TRAIL-resistant cells we next wished to determine whether NF-κB is required for reovirus-induced apoptosis in these cells. HEK293 were infected with reovirus, and at various times post-infection were harvested and assayed for apoptosis. Compared with mock-infected cells, reovirus infection resulted in a significant increase in the number of apoptotic cells at both 24 and 48 h pi. However, reovirus-induced apoptosis was blocked in cells expressing IκBΔN2 (Fig. 3A). Reovirus-induced apoptosis was also assayed by measuring caspase 3-activity using a fluorogenic substrate assay. Increased caspase 3 activity, compared with mock-infected cells, was detected at 18 h (3-fold) and 24 h (7.5-fold) pi. Again, reovirus-induced caspase 3-activity was blocked in cells expressing IκBΔN2 (Fig. 3*B*). These results indicate that NF-κB activation is required for reovirus-induced activation of caspase 3 and apoptosis.

Reovirus Prevents the Activation of NF-κB by TNFα and Etoposide—Although reovirus induces NF-κB after infection of HEK293 cells, this activation is transient in nature. We next investigated whether the transient nature of reovirus-induced NF-κB activation resulted from a block in NF-κB activation at later times pi. Both TNFα (100 ng/ml) and etoposide (100 μM) are classic inducers of NF-κB and cause a rapid and robust activation of NF-κB in HEK293 cells as determined by the appearance of a shifted probe band after EMSA in treated, but not untreated cells (Fig. 4*A*). NF-κB binding was seen as early as 1 h after treatment with TNFα and etoposide and was persistent. Prior infection of cells with reovirus blocked the appearance of the TNFα and etoposide-induced-shifted probe band compared with that seen in mock-infected cells (Fig. 4*B*). In contrast, there was no difference in the intensity of the lower NF-κB-probe complex after etoposide or TNFα treatment in either mock or reovirus-infected cells. These results indicate that reovirus infection blocks the activation of NF-κB after treatment of HEK293 cells with TNFα or etoposide, indicating

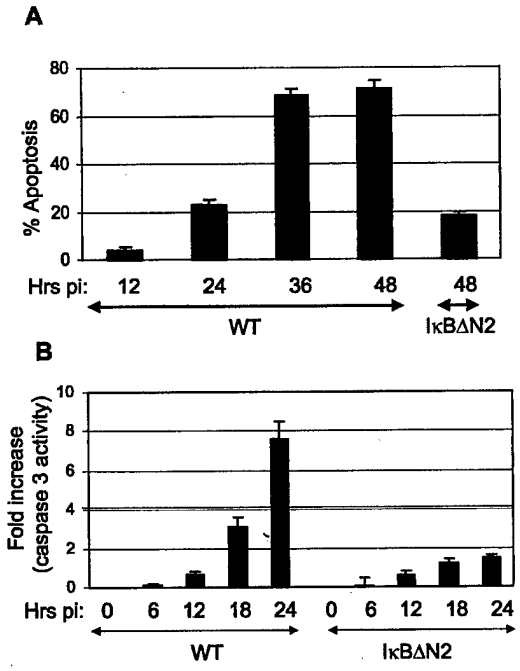

FIG. 3. **NF-κB activation is required for reovirus-induced apoptosis and caspase 3 activity.** HEK293 cells expressing wild type (*WT*) IκB or IκBΔN2 were infected with reovirus (m.o.i. 100) and assayed for apoptosis (*A*) and caspase 3 activity (*B*) at various times pi. The results are expressed as the mean percentage apoptosis or fold-activation obtained from three independent experiments. *Error bars* indicate S.E.

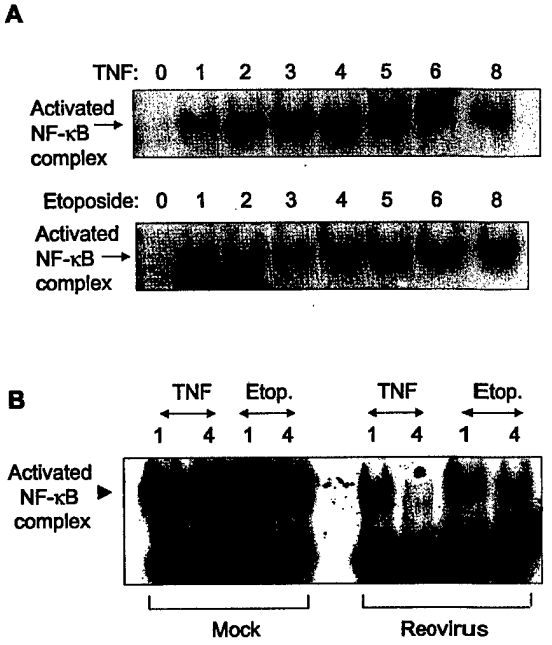

FIG. 4. **Reovirus prevents TNFα and etoposide-induced activation of NF-κB.** *A*, time course of NF-κB activation after treatment with TNFα and etoposide. HEK293 cells were treated with TNFα (100 ng/ml) or etoposide (100 μM) for the indicated times. Nuclear extracts were then prepared, and EMSA analysis was performed using an oligonucleotide probe comprising NF-κB binding sequences. Shifted bands, corresponding to activated NF-κB·DNA complexes, are indicated. *B*, prior infection with reovirus prevents TNFα- and etoposide-induced NF-κB activation. HEK293 cells were infected with reovirus or were mock-infected. 12 h pi cells were treated with TNFα (100 ng/ml) or etoposide (100 μM) (*Etop.*). Nuclear extracts were prepared after treatment at the times indicated, and EMSA was performed using an oligonucleotide probe comprising NF-κB binding sequences. Stimulus-induced NF-κB·DNA complexes are indicated.

that reovirus infection both induces and then inhibits the activation of NF-κB.

Reovirus Blocks the Degradation of IκB after Treatment of Cells with Etoposide and TNF—Activation of NF-κB results from the stimulus-induced degradation of the inhibitor family of proteins, collectively known as IκB. Treatment of HEK293 cells with the NF-κB-inducing stimuli etoposide (100 μM) and TNF (100 ng/ml) thus causes the degradation of IκB as detected by Western blot analysis using an antibody directed against IκBα (Fig. 5*A*). Degradation of IκBα is detectable around 1 h after treatment with both TNF and etoposide, and levels gradually decline over a 24-h period. In contrast, no changes in levels of IκBα were detected after reovirus infection (Fig. 5*B*). We next determined whether reovirus blocked etoposide- and TNF-induced activation of NF-κB by inhibiting IκBα degradation. Cells were infected with reovirus (m.o.i. 100). Then, at various times pi cells were treated with etoposide (100 μM) or TNF (100 ng/ml). After a further 3 h, to allow etoposide and TNF-induced IκBα degradation, cells were harvested and assayed for the presence of IκBα by Western blot analysis. When etoposide was added 2 h after reovirus infection etoposide induced the degradation of IκBα as expected. However, by 4 h pi the ability of etoposide to induce the degradation of IκBα was inhibited, and at 12 h pi there was no degradation of IκBα after etoposide treatment (Fig. 5*B*). Similar results were obtained after TNF treatment of reovirus-infected cells (Fig. 5*B*). These results indicate that the mechanism by which reovirus inhibits NF-κB activation at later times pi involves inhibition of IκB degradation in reovirus-infected cells.

Reovirus-induced Inhibition of Stimulus-induced IκBα Degradation Requires Viral RNA Synthesis—The ability of reovirus to inhibit stimulus-induced IκBα degradation and subsequent NF-κB activation occurs somewhat later than would be expected for the initial events of viral infection, including receptor binding, viral entry, and disassembly, and is more concurrent with the time at which viral proteins are produced in reovirus-infected HEK293 cells (not shown). Therefore we next investigated whether viral replication was required for reovirus-induced inhibition of IκB degradation. Ribavirin is a viral RNA synthesis inhibitor that inhibits reovirus replication (27). Cells were infected with reovirus (m.o.i. 100) in the presence or absence of ribavirin. 12 h after infection cells were treated with etoposide (100 μM) for 3 h. They were then harvested and analyzed by Western blot analysis using an IκB antibody. Fig. 6*A* shows that etoposide treatment of mock-infected cells in the presence or absence of ribavirin, results in the degradation of IκB. As expected, in reovirus-infected cells the ability of etoposide to induce the degradation of IκB is blocked. However, etoposide does induce IκB degradation in cells treated with both reovirus and ribavirin, indicating that viral RNA synthesis is required for reovirus-induced inhibition of stimulus-induced IκB degradation.

Reovirus-induced Apoptosis in HEK293 Cells Requires Viral RNA Synthesis—Having shown that reovirus-induced inhibition of IκB degradation requires viral replication and is blocked in the presence of ribavirin, we investigated the effect of ribavirin on reovirus-induced apoptosis. HEK293 cells were infected with reovirus in the presence or absence of ribavirin. After 48 h cells were harvested and assayed for apoptosis. Ribavirin significantly inhibited reovirus (m.o.i. 100)-induced apoptosis in HEK293 cells (Fig. 6*B*), indicating that reovirus-induced inhibition of apoptosis of HEK293 cells requires viral RNA replication. In contrast, ribavirin did not inhibit reovirus-induced apoptosis in TRAIL-sensitive HeLa cells, as has previously been shown (27).

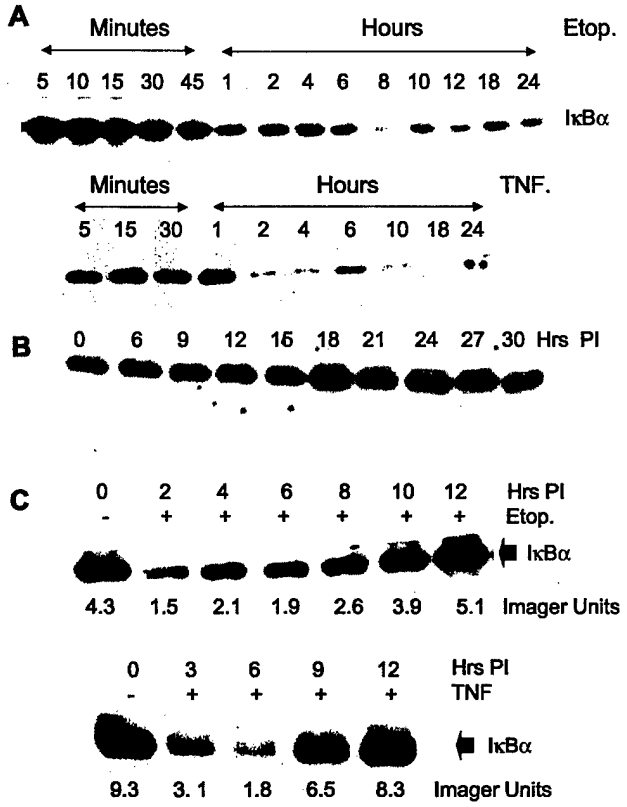

FIG. 5. **Reovirus prevents etoposide-induced degradation of IκBα.** *A*, time course of etoposide- and TNF-induced IκBα degradation. HEK293 cells were treated with etoposide (*Etop.*, 100 μM) or TNF (100 ng/ml). After the indicated times cells were harvested for Western blot analysis. After SDS-PAGE, blots were probed with an anti-IκBα antibody. *B*, time course of levels of IκBα in reovirus-infected cells. HEK293 cells were infected with reovirus (m.o.i. 100). After the indicated times cells were harvested for Western blot analysis. After SDS-PAGE, blots were probed with an anti-IκBα antibody. *C*, reovirus prevents etoposide- and TNF-induced degradation of IκBα. HEK293 cells were infected with reovirus (m.o.i. 100). At the times indicated pi cells were treated with etoposide (100 μM) or TNF (100 ng/ml). After a further 3 h, to allow these reagents to induce IκBα degradation, cells were harvested for Western blot analysis. After SDS-PAGE, blots were probed with an anti-IκBα antibody. Also shown are the results from densitometric analysis.

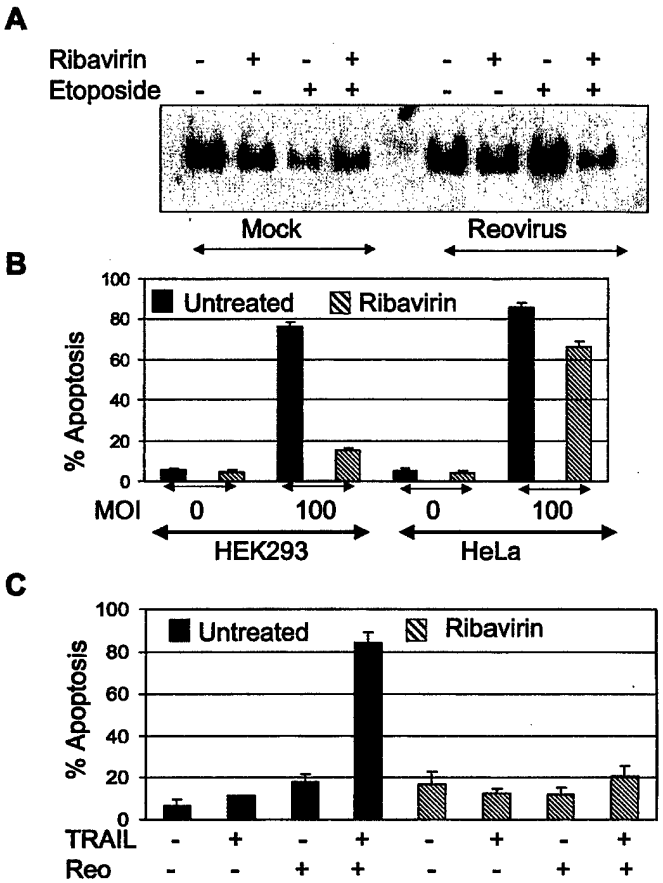

FIG. 6. **In HEK293 cells reovirus replication is required for reovirus-induced inhibition of NF-κB activation by etoposide, reovirus-induced apoptosis, and reovirus-induced sensitization of cells to TRAIL.** *A*, ribavirin blocks the ability of reovirus to inhibit etoposide-induced IκBα degradation. Cells were infected with reovirus or were mock-infected in the presence or absence of ribavirin. 12 h after infection, cells were treated with etoposide or were left untreated for 3 h before cells were harvested for Western blot analysis using an anti-IκBα antibody. *B*, ribavirin blocks reovirus-induced apoptosis in HEK293 cells. HEK293 cells and HeLa cells were infected with reovirus (m.o.i. 100) or were mock-infected (m.o.i. 0) in the absence (*black bars*) or presence (*shaded bars*) of ribavirin. After 48 h cells were harvested and assayed for apoptosis. The *graph* shows the mean percentage apoptosis obtained from three independent experiments. *Error bars* represent S.E. *C*, ribavirin blocks reovirus-induced sensitization of cells to TRAIL. HEK293 cells were infected with reovirus (m.o.i. 10) or were mock-infected in the absence (*black bars*) or presence (*shaded bars*) of ribavirin. 24 h after infection, cells were treated with TRAIL (20 ng/ml). After a further 24 h cells were harvested and assayed for apoptosis. The *graph* shows the mean percentage apoptosis obtained from three independent experiments. *REO*, reovirus. *Error bars* represent S.E.

Viral RNA Synthesis Is Required for Reovirus-induced Sensitization of Cells to TRAIL—We have previously shown that reovirus sensitizes cells to TRAIL-induced apoptosis (7, 9). The fact that ribavirin blocks reovirus-induced apoptosis in TRAIL-resistant but not TRAIL-sensitive cells suggests the mechanism by which reovirus sensitizes cells to TRAIL requires viral RNA synthesis. HEK293 cells were thus infected with reovirus with or without ribavirin. 24 h post-infection cells were then treated with TRAIL, and apoptosis was assayed after a further 24 h. Fig. 6*C* shows that reovirus-induced sensitization of cells to TRAIL is inhibited in the presence of ribavirin, indicating that reovirus-induced sensitization of cells to TRAIL is dependent on viral RNA synthesis.

Inhibition of NF-κB Activation Sensitizes Cells to Apoptosis Induced by TRAIL and TNFα—Our results indicate that ribavirin blocks both reovirus-induced apoptosis in TRAIL-resistant cells and reovirus-induced sensitization of TRAIL-resistant cells to TRAIL-induced apoptosis. Because ribavirin also blocks the ability of reovirus to inhibit NF-κB activation in infected cells at later times pi we wished to determine whether inhibition of NF-κB activation was the mechanism by which reovirus sensitizes TRAIL-resistant cells to TRAIL-induced apoptosis. HEK293 cells expressing IκBΔN2 were treated with various concentrations of TRAIL. At 24 h after treatment cells were harvested and assayed for apoptosis. High concentrations of TRAIL (200 ng/ml) did not induce significant levels of apoptosis in HEK293 cells expressing vector alone compared with untreated cells. In contrast, both 20 and 200 ng/ml TRAIL induced significant apoptosis in HEK293 cells expressing IκBΔN2 (Fig. 7*A*). Apoptosis was also determined using caspase 3 activity assays. Cells were treated with similar concentrations of TRAIL and were harvested 4 h after treatment for caspase 3 activity assays. At 4 h pi TRAIL (20 and 200 ng/ml) induced caspase 3 activity in HEK293 cells expressing IκBΔN2 but not in cells expressing vector alone (Fig. 7*A*). An 8-fold increase in caspase 3 activity was seen in TRAIL (20 ng/ml)-treated cells expressing IκBΔN2 compared with cells expressing vector alone, and at 200 ng/ml TRAIL induced a 20-fold increase. The expression of IκBΔN2, thus, sensitizes HEK293 cells to TRAIL-induced apoptosis, sug-

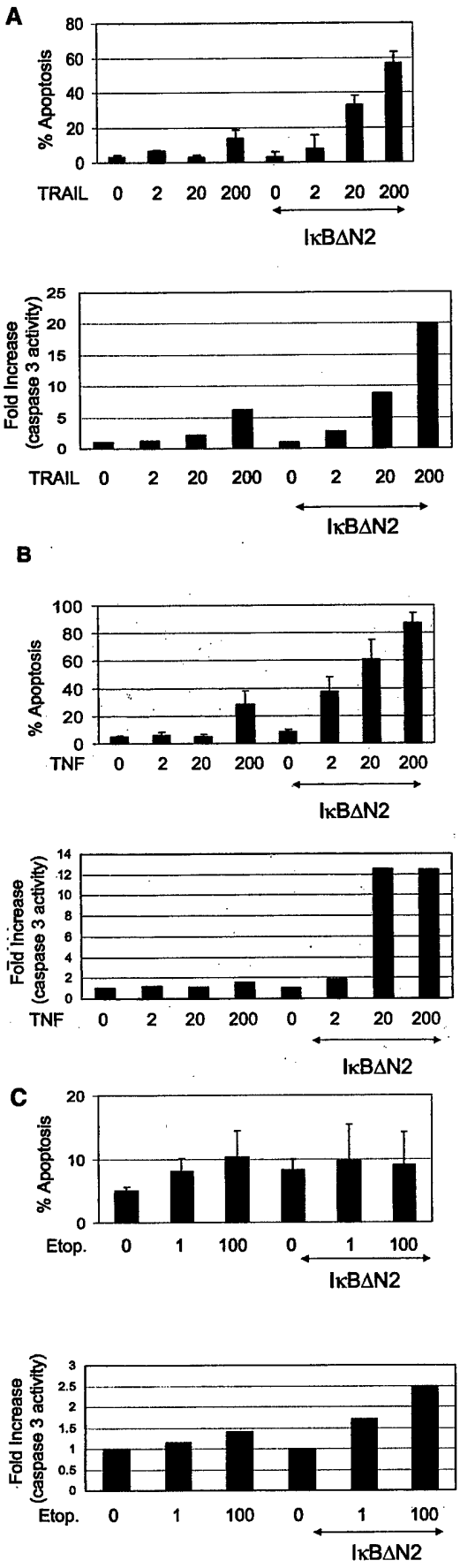

FIG. 7. **Expression of IκBΔN2 sensitizes cells to TRAIL and TNFα-induced apoptosis.** HEK293 cells expressing WT IκB or IκBΔN2 were treated with the indicated concentrations of TRAIL (*A*), TNFα (*B*), and etoposide (*Etop.*, *C*). After treatment cells were harvested and assayed for apoptosis or caspase 3 activity. The *graph* shows the mean percentage apoptosis and fold-increase in caspase 3 activity obtained from three independent experiments. *Error bars* represent S.E.

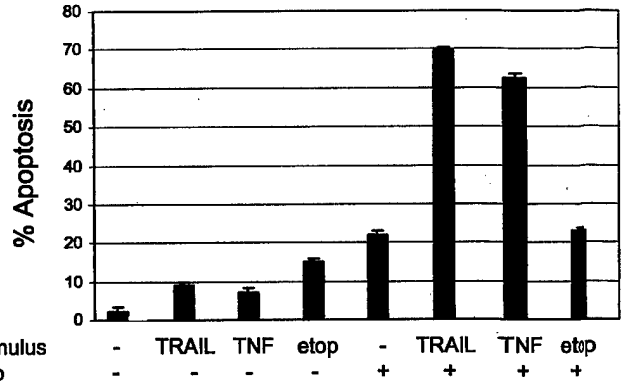

FIG. 8. **Reovirus sensitizes HEK293 cells to TRAIL and TNFα-induced apoptosis.** HEK293 cells were infected with reovirus (m.o.i. 10) or were mock-infected. 24 h after infection, cells were treated with TRAIL, TNFα, or etoposide (*etop*) or were left untreated. After a further 24 h, cells were harvested and assayed for apoptosis. The *graph* shows the mean percentage apoptosis obtained from three independent experiments. *Error bars* represent S.E. *Reo*, reovirus.

gesting that reovirus-induced inhibition of NF-κB activation is the mechanism by which reovirus sensitizes of cells to TRAIL.

Fig. 4 shows that TNFα and etoposide induce the activation of NF-κB in HEK293 cells. TRAIL also induces NF-κB activation in these cells (31). Having shown that the expression of IκBΔN2 sensitizes cells to TRAIL-induced apoptosis, we next determined whether the expression of IκBΔN2 would also sensitize HEK293 cells to TNF and etoposide-induced apoptosis. Neither TNFα (200 ng/ml) nor etoposide (100 μM) induced apoptosis in HEK293 cells. However, whereas levels of TNFα as low as 2 ng/ml induced significant apoptosis in cells expressing IκBΔN2 (Fig. 7*B*), the expression of IκBΔN2 did not sensitize cells to etoposide (100 μM)-induced apoptosis (Fig. 7*C*). Similarly a 12-fold increase in caspase 3 activation was seen 24 h after TNFα (20 and 200 ng/ml) treatment of cells expressing IκBΔN2 but not after TNFα treatment of cells expressing vector alone (Fig. 7*B*). Again, caspase-3 activation was not enhanced in etoposide-treated cells expressing IκBΔN2 compared with cells expressing vector alone (Fig. 7*C*). These results indicate that the expression of IκBΔN2 sensitizes HEK293 cells to TRAIL and TNFα but not etoposide-induced apoptosis.

Virus Infection Sensitizes HEK293 Cells to Apoptosis Induced by TNFα and TRAIL—We have previously shown that reovirus infection sensitizes HEK293 cells to TRAIL-induced apoptosis. Results described above show that blocking NF-κB activation sensitizes cells to both TRAIL- and TNFα-induced apoptosis. Because reovirus-induced inhibition of NF-κB activation is the mechanism by which reovirus sensitizes cells to TRAIL-induced apoptosis, we wanted to determine whether the inhibition of NF-κB activation after reovirus infection would also sensitize these cells to TNFα-induced apoptosis. Cells were incubated with reovirus (m.o.i. 10). 24 h post-infection cells were then treated with TRAIL (20 ng/ml) or TNFα (20 ng/ml). Apoptosis was then determined after a further 24 h. Fig. 8 shows that TRAIL and TNFα alone do not induce apoptosis in HEK293 cells, as previously shown (Fig. 7). Infection of HEK293 cells with reovirus (m.o.i. 10) also induces only low levels (22%) of apoptosis in HEK293 cells (see Fig. 1). However, treatment of cells with TRAIL or TNFα in the presence of

reovirus produces high levels (70 and 63%) of apoptosis in HEK293 cells. These values are significantly greater than the sum of apoptosis induced by TRAIL and reovirus or TNFα and reovirus when these agents are used alone, indicating that reovirus infection acts synergistically with TRAIL and TNFα to induce apoptosis. In contrast, reovirus did not sensitize cells to etoposide-induced apoptosis, in agreement with the observation that the expression of IκBΔN2 also does not sensitize these cells to etoposide.

DISCUSSION

Reovirus-induced apoptosis in human epithelial HEK293 cells and in several human cancer cell lines is mediated by TRAIL and is blocked by the presence of soluble TRAIL receptors and by anti-TRAIL antibodies (7, 9). However, reovirus can induce apoptosis in both TRAIL-sensitive and TRAIL-resistant cells. Reovirus, therefore, has the ability to sensitize TRAIL-resistant cells to TRAIL-induced apoptosis (7, 9). We have previously shown that in TRAIL-sensitive HeLa cells reovirus infection results in the activation of NF-κB and that this activation is required for reovirus-induced apoptosis (26). The results presented in this report describe the role of NF-κB in reovirus-induced apoptosis in TRAIL-resistant (HEK293) cells. We show that reovirus-induced NF-κB activation is highly regulated in these cells. At early times pi (2–4 h) reovirus activates NF-κB, as demonstrated by the presence of NF-κB in the nucleus of reovirus-infected cells and by the ability of this NF-κB to bind to radiolabeled oligonucleotide probe sequences comprising NF-κB binding sites. Activation of NF-κB-responsive genes after reovirus infection of HEK293 cells is also demonstrated by luciferase reporter gene assays. NF-κB activation is required for reovirus-induced apoptosis since reovirus-infection does not result in caspase 3 activity or apoptosis-associated changes in nuclear morphology in HEK293 cells expressing IκBΔN2. These results are similar to those observed for TRAIL-sensitive HeLa cells and suggest that reovirus-induced apoptosis in TRAIL resistant cells also requires the expression of pro-apoptotic NF-κB-regulated genes.

Although required for virus-induced apoptosis, NF-κB activation is transient in both reovirus-infected TRAIL-sensitive and TRAIL-resistant cells. The transient nature of NF-κB activation in HEK293 cells results from the inhibition of NF-κB activation at later times pi since reovirus can block the ability of both etoposide and TNFα to induce NF-κB activation. This inhibition of NF-κB activation results from the inhibition of stimulus-induced IκB degradation and is time-dependent. Thus, at early times post-infection (2, 4 h) etoposide or TNF are still able to induce the degradation of IκBα. However, at later times post-infection (8–12 h) neither reagent induces IκBα degradation. These results are consistent with the fact that reovirus only activates NF-κB at early times pi.

Although the inhibition of NF-κB activation in reovirus-infected cells might be expected to induce a concordant increase in levels of IκBα at later times pi, we were unable to detect such a change. We predict that this is because of the low levels of NF-κB that are activated in reovirus-infected cells and the relative insensitivity of Western blotting compared with EMSA.

Reovirus-induced activation of NF-κB is not dependent on viral replication and occurs in the presence of ribavirin in both HeLa (27) and HEK293 cells.[2] Because the ability of reovirus to inhibit stimulus-induced NF-κB activation occurs somewhat later than the initial infection events (receptor binding, viral entry, and disassembly) and occurs around the time that viral proteins are produced in reovirus-infected HEK293 cells (not shown), we next investigated whether viral RNA synthesis was required. In the presence of the viral RNA synthesis inhibitor ribavirin the ability of etoposide to induce the degradation of IκB was completely blocked, indicating that viral RNA synthesis is required for this process.

NF-κB regulates genes with both pro- and anti-apoptotic effects. The ability of reovirus to block NF-κB activation at later times post-infection enhances virus-induced apoptosis in TRAIL-resistant cells, as demonstrated by three lines of investigation. First, TRAIL-induced apoptosis is enhanced in HEK293 cells expressing IκBΔN2. This indicates that blocking NF-κB activation sensitizes cells to TRAIL-induced apoptosis. Second, ribavirin, which blocks the ability of reovirus to inhibit stimulus-induced IκB degradation, blocks reovirus-induced apoptosis in TRAIL-resistant, but not TRAIL-sensitive cells. Finally, ribavirin also blocks the ability of reovirus to sensitize cells to TRAIL-induced apoptosis.

In neurons TNFα may be more important in mediating reovirus-induced apoptosis than TRAIL (5). The results presented here indicate that reovirus can also sensitize cells to TNFα-induced apoptosis by inhibiting NF-κB activation at later times pi, which may have important consequences for the ability of reovirus to induce apoptosis in these cells and to cause disease of the central nervous system in infected animals. The expression of IκBΔN2 was not found to sensitize cells to etoposide-induced apoptosis. This suggests that etoposide induces apoptosis by a mechanism that is different from that induced by TRAIL and TNFα. Previous studies show that NF-κB activation is required for etoposide-induced apoptosis (32), supporting our observation that the expression of IκBΔN2 does not sensitize HEK293 cells to etoposide-induced apoptosis.

Reovirus-induced apoptosis is mediated by TRAIL and involves the release of TRAIL from infected cells (7). Thus, the supernatant from reovirus-infected cells contains TRAIL and can induce apoptosis in TRAIL-sensitive cells (7). This apoptosis is blocked in the presence of soluble TRAIL receptors, indicating that it is specific to TRAIL and is not blocked in the presence of a neutralizing reovirus antibody, indicating that it is not due to residual virus in the supernatant. TRAIL released from reovirus-infected cells, thus, induces apoptosis by inducing receptor-mediated activation of caspase 8 (10). These results show that reovirus regulation of NF-κB is also critical for virus-induced apoptosis. NF-κB is first activated at early times after reovirus infection, an event that is required for apoptosis in both TRAIL-sensitive and TRAIL-resistant cells and which presumably acts to up-regulate the expression of pro-apoptotic NF-κB-regulated genes. Both TRAIL and its receptors are regulated by NF-κB (32–34). It is, thus, likely that the pro-apoptotic effects of NF-κB activation that are required for reovirus-induced apoptosis include the up-regulation of these genes. TRAIL, DR4, and DR5 are up-regulated after reovirus-infection (7), although the involvement of NF-κB in this process has yet to be established. At later times pi, reovirus inhibits the activation of NF-κB in infected cells. This has the effect of blocking stimulus-induced NF-κB activation. In uninfected HEK293 cells TRAIL induces the activation of NF-κB (31). Our results suggest that TRAIL-induced NF-κB activation has an inhibitory effect on TRAIL-induced apoptosis in these cells. Thus, the ability of reovirus to block TRAIL-induced NF-κB activation will sensitize cells to TRAIL-induced apoptosis, therefore allowing both TRAIL and reovirus-induced apoptosis in TRAIL-resistant cells. The timing of reovirus-induced inhibition of stimulus-induced NF-κB activation is in accordance with TRAIL release from reovirus-infected cells, which occurs

[2] P. Clarke, S. M. Meintzer, L. Moffitt, and K. L. Tyler, unpublished data.

at later times pi (7). Thus, it appears that NF-κB activation is turned off in reovirus-infected cells before TRAIL is released to facilitate reovirus-induced apoptosis in TRAIL-resistant cells.

The ability of TRAIL to induce apoptosis in a variety of human cancer cells but not in normal cells has triggered the investigation of this reagent as a potential therapeutic agent for human cancers. However, many cancer cells are resistant to TRAIL-induced apoptosis. We have previously shown that reovirus can sensitize TRAIL-resistant human cancer cell lines to TRAIL-induced apoptosis. The results presented here suggest that the mechanism for this sensitization results from the ability of reovirus to block NF-κB activation. Other studies also indicate that blocking NF-κB activation can sensitize human cancer cells to TRAIL-induced apoptosis (35–37). Together these findings could have an important impact on the use of TRAIL as a potential cancer therapeutic in combination with other agents that inhibit NF-κB.

The NF-κB pathway provides an attractive target to viral pathogens for modulating host cell events. NF-κB promotes the expression of more than 100 genes that participate in the host immune response, oncogenesis, and regulation of apoptosis. In addition, activation of NF-κB is a rapid immediate early response that occurs within minutes after exposure to a relevant inducer, does not require *de novo* protein synthesis, and results in a strong transcriptional stimulation of several early viral as well as cellular genes. NF-κB is, thus, activated by multiple families of viruses, including human immunodeficiency virus type 1 (HIV-1) (38), human T-cell lymphotrophic virus- (39), hepatitis B virus (40), hepatitis C virus (41, 42), Epstein-Barr virus (43), rotavirus (44), and influenza virus (45) to promote viral replication, prevent virus-induced apoptosis, and mediate the immune response to the invading pathogen (for review, see Ref. 46). In contrast, activation of NF-κB by Sindbis (47, 48) and Dengue virus (49) is associated with the induction of apoptosis, which may increase viral spread. In still other cases, proteins encoded by adenovirus (50), hepatitis C virus (51), and African swine fever virus (52) inhibit NF-κB activity to enhance replication or contribute to viral pathogenicity.

The results demonstrated here indicate that reovirus both activates and then inhibits NF-κB activity to efficiently induce apoptosis in infected cells. This is the first time that two phases of NF-κB regulation have been shown to be required to modulate viral-host interactions within a specific cell type. We propose that the complex regulation of NF-κB by reovirus is critical for TRAIL- and TNFα-induced apoptosis in reovirus-infected cells. Death receptor ligands are commonly used by viruses to induce apoptosis. For example, HIV infection increases the expression of TRAIL and sensitizes T-cells to TRAIL-mediated apoptosis (53). In addition, alteration of the cell surface expression of Fas may be involved in virus-induced or viral regulation of apoptosis in cells infected with influenza virus (54, 55), herpes simplex virus type 2 (56), bovine herpesvirus 4 (57), adenovirus (58) and HIV 1 (59, 60). Similarly, apoptosis induced by hepatitis B (61), HIV-1 (62), bovine herpesvirus 4 (57), and parvovirus H-1 (63) may involve the TNF receptor signaling pathway. NF-κB regulation is, thus, likely to have implications for apoptosis and disease resulting from a variety of viral infections.

REFERENCES

1. Tyler, K. L., Clarke, P., DeBiasi, R. L., Kominsky, D. J., and Poggioli, G. J. (2001) *Trends Microbiol.* **9,** 560–564
2. Clarke, P., and Tyler, K. L. (2003) *Apoptosis* **8,** 141–150
3. DeBiasi, R. L., Edelstein, C. L., Sherry, B., and Tyler, K. L. (2001) *J. Virol.* **75,** 351–361
4. Oberhaus, S. M., Smith, R. L., Clayton, G. H., Dermody, T. S., and Tyler, K. L. (1997) *J. Virol.* **71,** 2100–2106
5. Richardson-Burns, S. M., Kominsky, D. J., and Tyler, K. L. (2002) *J. Neurovirol.* **8,** 365–380
6. DeBiasi, R. L., Squier, M. K. T., Pike, B., Wynes, W. M., Dermody, T. S., Cohen, J. J., and Tyler, K. L. (1999) *J. Virol.* **73,** 695–701
7. Clarke, P., Meintzer, S. M., Gibson, S. B., Widmann, C., Garrington, T. P., Johnson, G. L., and Tyler, K. L. (2000) *J. Virol.* **74,** 8135–8139
8. Kominsky, D. J., Bickel, R. J., and Tyler, K. L. (2002) *Cell Death Differ.* **9,** 926–933
9. Clarke, P., Meintzer, S. M., Spalding, A. C., Johnson, G. L., and Tyler, K. L. (2001) *Oncogene* **20,** 6910–6919
10. Ashkenazi, A., and Dixit, V. M. (1998) *Science* **281,** 1305–1308
11. Deleted in proof
12. Karin, M., and Lin, A. (2002) *Nat. Immunol.* **3,** 221–227
13. Baeuerle, P., and Baltimore, D. (1989) *Genes Dev.* **3,** 1689–1698
14. Ghosh, S., Gifford, A., Riviere, L., Tempst, P., Nolan, G., and Baltimore, D. (1990) *Cell* **62,** 1019–1029
15. Baeuerle, P., and Baltimore, D. (1988) *Science* **242,** 540–546
16. Verma, I. M., Stevenson, J. K., Schwarz, E. M., van Antwerp, D., and Miyamoto, S. (1995) *Genes Dev.* **9,** 2723–2735
17. Brockman, J. A., Scherer, D. C., McKinsey, T. A., Hall, S. M., Qi, X., Lee, W. Y., and Ballard, D. W. (1995) *Mol. Cell. Biol.* **15,** 2809–2818
18. Brown, K., Gerstberger, S., Carlson, L., Franzoso, G., and Siebenlist, U. (1995) *Science* **267,** 1485–1488
19. Chen, Z., Hagler, J., Palombella, V. J., Melandri, F., Scherer, D., Ballard, D., and Maniatis, T. (1995) *Genes Dev.* **9,** 1585–1597
20. Traencker, E. B., Pahl, H. L., Henkel, T., Schmidt, K. N., Wilk, S., and Baeuerle, P. A. (1995) *EMBO J.* **14,** 2876–2883
21. Beg, A. A., Ruben, S. M., Scheinman, R. I., Haskill, S., Rosen, C. A., and Baldwin, A. J. (1992) *Genes Dev.* **6,** 1899–1913
22. May, M. J., and Ghosh, S. (1997) *Semin. Cancer Biol.* **8,** 63–73
23. Teodoro, J. G., and Branton, P. E. (1997) *J. Virol.* **71,** 1739–1746
24. Connolly, J. L., Barton, E. S., and Dermody, T. S. (2001) *J. Virol.* **75,** 4029–4039
25. Barton, E. S., Forrest, J. C., Connolly, J. L., Chappell, J. D., Liu, Y., Schnell, F. J., Nusrat, A., Parkos, C. A., and Dermody, T. S. (2001) *Cell* **104,** 441–451
26. Connolly, J. L., Rodgers, S. E., Clarke, P., Ballard, D. W., Kerr, L. D., Tyler, K. L., and Dermody, T. S. (2000) *J. Virol.* **74,** 2981–2989
27. Connolly, J. L., and Dermody, T. S. (2002) *J. Virol.* **76,** 1632–1641
28. Tyler, K. L., Squier, M. K. T., Brown, A. L., Pike, B., Willis, D., Oberhaus, S. M., Dermody, T. S., and Cohen, J. J. (1996) *J. Virol.* **70,** 7984–7991
29. Duke, R. C., and J. J. Cohen. (1992). *Current Protocols in Immunology*, pp. 3.17.1–3.17.16, John Wiley & Sons, Inc., New York
30. Tyler, K. L., Squier, M. K. T., Rodgers, S. E., Schneider, B. E., Oberhaus, S. M., Grdina, T. A., Cohen, J. J., and Dermody, T. S. (1995) *J. Virol.* **69,** 6972–6979
31. Shetty, S., Gladden, J. B., Henson, E. S., Hu, X., Villanueva, J., Haney, N., and Gibson, S. B. (2002) *Apoptosis* **7,** 413–420
32. Gibson, S. B., Oyer, R., Spalding, A. C., Anderson, S. M., and Johnson, G. L. (2000) *Mol. Cell. Biol.* **20,** 205–212
33. Ravi, R., Bedi, G. C., Engstrom, W., Zeng, Q., Mookerjee, B., Gelinas, C., Fuchs, E. J., and Bedi, A. (2001) *Nat. Cell Biol.* **3,** 409–416
34. Spalding, A. C., Jotte, R. M., Scheinman, R. I., Geraci, M. W., Clarke, P., Tyler, K. L., and Johnson, G. L. (2002) *Oncogene* **21,** 260–271
35. Thomas, R. P., Farrow, B. J., Kim, S., May, M. J., Hellmich, M. R., and Evers, B. M. (2002) *Surgery* **132,** 127–134
36. Keane, M. M., Rubinstein, Y., Cuello, M., Ettenberg, S. A., Banerjee, P., Nau, M. M., and Lipkowitz, S. (2000) *Breast Cancer Res. Treat.* **64,** 211–219
37. Oya, M., Ohtsubo, M., Takayanagi, A., Tachibana, M., Shimizu, N., and Murai, M. (2001) *Oncogene* **20,** 3888–3896
38. Roulston, A., Lin, R., Beauparlant, P., and Wainberg, J. (1995) *Microbiol. Rev.* **59,** 481–505
39. Sun, S. C., and Ballard, D. W. (1999) *Oncogene* **18,** 6948–6958
40. Weil, R., Sirma, H., Giannini, C., Kremsdorf, D., Bessia, C., Dargemont, C., Brechot, C., and Israel, A. (1999) *Mol. Cell. Biol.* **19,** 6345–6354
41. You, L. R., Chen, C. M., and Lee, Y. H. W. (1999) *J. Virol.* **73,** 1672–1681
42. Tai, D. I., Tsai, S. L., Chen, Y. M., Chuang, Y. L., Peng, C. Y., Sheen, I. S., Yeh, C. T., Chang, K. S., Huang, S. N., Kuo, G. C., and Liaw, Y. F. (2000) *Hepatology* **31,** 656–664
43. Sylla, B. S., Hung, S. C., Davidson, D. M., Hatzivassiliou, E., Malinin, N. L., Wallach, D., Gilmore, T. D., Kieff, E., and Mosialos, G. (1998) *Proc. Natl. Acad. Sci. U. S. A.* **95,** 10106–10111
44. Casola, A., Garofalo, R. P., Crawford, S. E., Estes, M. K., Mercurio, F., Crowe, S. E., and Brasier, A. R. (2002) *Virology* **298,** 8–19
45. Pahl, H. L., and Baeuerle, P. A. (1997) *Trends Biochem. Sci.* **22,** 63–67
46. Hiscott, J., Kwon, H., and Genin, P. (2001). *J. Biol. Chem.* **107,** 143–151
47. Lin, K. I., Lee, S. H., Narayanan, R., Baraban, J. M., Hardwick, J. M., and Ratan, R. R. (1995) *J. Cell Biol.* **131,** 1149–1161
48. Lin, K. I., DiDonato, J. A., Hoffmann, A., Hardwick, J. M., and Ratan, R. R. (1998) *J. Cell Biol.* **141,** 1479–1487
49. Jan, J. T., Chen, B. H., Ma, S. H., Liu, C. I., Tsai, H. P., Wu, H. C., Jiang, S. Y., Yang, K. D., and Shaio, M. F. (2000) *J. Virol.* **74,** 8680–8691
50. Shao, R., Hu, M. C. T., Zhou, B. P., Lin, S. Y., Chiao, P. J., von Lindern, R. H., Spohn, B., and Hung, M. C. (1999) *J. Biol. Chem.* **274,** 21495–21498
51. Shrivastava, A., Manna, S. K., Ray, R., and Aggarwal, B. B. (1998) *J. Virol.* **72,** 9722–9728
52. Powell, P. P. Dixon, L. K., and Parkhouse, M. E. (1996) *J. Virol.* **70,** 8527–8533
53. Jeremias, I., Herr, I., Boehler, T., and Debatin, K.-M. (1998). *Eur. J. Immunol.* **28,** 143–152
54. Takizawa, T., Matsukawa, S., Higuchi, Y., Nakamura, S., Nakanishi, Y., and Fukuda R. (1993) *J. Gen. Virol.* **74,** 2347–2355
55. Takizawa, T., Fukuda, R., Miyawaki, T., Ohashi, K., and Nakanishi, Y. (1995) *Virology* **209,** 288–296
56. Sieg, S., Yildirim, Z., Smith, D., Kayagaki, N., Yagita, H., Huang, Y., and

Kaplan, D. (1996) *J. Virol.* **70,** 8747–8751
57. Wang, G. H., Bertin, J., Wang, Y., Martin, D. A., Wang, J., Tomaselli, K. J., Armstrong, R. C., and Cohen, J. I. (1997) *J. Virol.* **71,** 8928–8932
58. Tollefson, A. E., Hermiston, T. W., Lichtenstein, D. L., Colle, C. F., Tripp, R. A., Dimitrov. T., Toth, K., Wells, C. E., Doherty, P. C., and Wold, W. S. (1998) *Nature* **392,** 726–730
59. Conaldi, P. G., Biancone, L., Bottelli, A., Wade-Evans, A., Racusen, L. C., Boccellino, M., Orlandi, V., Serra, C., Camussi, G., and Toniolo, A. (1998) *J. Clin. Invest.* **102,** 2041–2049
60. Kaplan, D., and Sieg, S. (1998) *J. Virol.* **72,** 6279–6282
61. Su, F., and Schneider, R. J. (1997) *Proc. Natl. Acad. Sci. U. S. A.* **94,** 8744–8749
62. Herbein, G., Mahlknecht, U., Batliwalla, F., Gregerson, P., Pappas, T., Butler, J., O'Brian, W. A., and Verdin, E. (1999) *Nature* **395,** 189–194
63. Rayet, B., Lopez-Guerrero, J.-A., Rommelaere, J., and Dinsart, C. (1998) *J. Virol.* **72,** 8893–8903

Virology 303, 213–221 (2002)
doi:10.1006/viro.2002.1698

Type 3 Reovirus Neuroinvasion after Intramuscular Inoculation: Viral Genetic Determinants of Lethality and Spinal Cord Infection

Mary Anne Mann,*,†,[1,2] Kenneth L Tyler,‡ David M. Knipe,† and Bernard N. Fields†,[3]

*Department of Biology, Northeastern University, 360 Huntington Avenue, Boston, Massachusetts 02115; †Department of Microbiology and Molecular Genetics, Harvard Medical School, 200 Longwood Avenue, Boston, MA 02115; and ‡Department of Neurology, Department of Medicine, Department of Microbiology, and Department of Immunology, University of Colorado Health Science Center, and Neurology Service, Denver VA Medical Center, Denver, Colorado 80262

Received April 2, 2001; returned to author for revision July 13, 2001; accepted July 16, 2002

To better understand the mechanisms by which neurotropic viruses invade peripheral nerve pathways and produce CNS disease, we defined the type 3 (T3) reovirus genes that are determinants of the capacity of reovirus T3 strain Dearing (T3D) and T3 clone 9 (C9) to infect the spinal cord and kill mice after hindlimb injection. T3D and C9 viruses are both highly virulent ($LD_{50} < 10^1$ PFU) after intracranial injection of neonatal mice. However, C9 is significantly more lethal than T3D after either intramuscular injection ($LD_{50} < 10^1$ vs LD_{50} 10^4 PFU) or peroral injection (LD_{50} $10^{3.4}$ vs $LD_{50} > 10^{8.3}$ PFU). Using reassortant viruses containing different combinations of genes derived from T3D and C9, we found that the *S1* gene, encoding the cell attachment protein sigma 1 and the nonstructural protein sigma 1s, and the *L3* gene, encoding the core shell protein lambda 1 were the primary determinants of lethality after intramuscular injection. The *L3* gene and the *L2* gene encoding spike protein, lambda 2, determined differences in spinal cord titer after intramuscular injection. A C9 × T3D mono-reassortant containing all T3D genes except for the C9-derived *L3* was lethal after peroral injection. These studies indicate that the *S1*, *L2*, and *L3* genes all play a potential role in neuroinvasiveness and provide the first identification of a role in pathogenesis for the *L3* gene. © 2002 Elsevier Science (USA)

INTRODUCTION

The central nervous system (CNS) is partially protected from systemic infections by the blood–brain barrier. Neurotropic viruses employ several strategies to penetrate this defense and produce neurological disease (Mims, 1987). Bloodborne viruses may invade neural tissue after infecting vessels in the brain or spinal cord or may spread to neural sites through the cerebrospinal fluid (CSF) by crossing the blood– (CSF) junction in the meninges or choroid plexus. Neurally spreading viruses can evade the blood–brain barrier by utilizing peripheral nerve fibers as direct pathways into the CNS. Rabies virus, poliovirus, herpes simplex virus, and reovirus travel via the fast axonal transport system in motor, sensory, or autonomic fibers to spread through the nervous system from extraneural sites of infection (Nathanson and Tyler, 1997).

Reovirus infection of neonatal mice has provided an important animal model for studying the pathogenesis of virus-induced CNS disease. Different reovirus serotypes have been identified based on neutralization and hemagglutination-inhibition assays (Nibert and Schiff, 2001), and viruses belonging to these serotypes differ in their pattern of CNS infection. Serotype 1 reoviruses primarily spread to the CNS by hematogenous routes, infect ependymal cells, and produce a generally nonlethal ependymitis (Tyler and Fields, 1996). However, after intramuscular or peroral injection serotype 3 viruses utilize peripheral nerve pathways to invade the CNS, infect neurons, and produce lethal encephalitis (Tyler *et al.*, 1986; Morrison *et al.*, 1991). Because reoviruses contain 10 segments of dsRNA, most encoding a single major protein, reassortant viruses may be generated from parents exhibiting unique patterns of disease (Nibert and Schift, 2001). Analysis of the pathogenesis of reassortant viruses after intracranial injection (IC) has shown that the major product of the *S1* gene, virus cell attachment protein, sigma 1, determines tropism for neurons or ependymal cells by serotype 3 and serotype 1 viruses, respectively (Weiner *et al.*, 1977). Among serotype 3 strains, the product of the *M2* gene, a major outer capsid structural protein, mu 1, influences differences in the capacity of these viruses to grow in the brain (Hrdy *et al.*, 1982). Thus, at least two reovirus genes play distinct roles in determining neurovirulence after IC injection.

After hindlimb injection, type 3 reovirus travels to the spinal cord via the sciatic nerve (Tyler *et al.*, 1986). Viruses are carried to the spinal cord by fast axonal

[1] Present address: College of Physicians and Surgeons 11-519, Columbia University, 630 West 168th Street, New York, NY 10032.

[2] To whom correspondence and reprint requests should be addressed. Fax: 212 305-5775. E-mail: mam2012@columbia.edu.

[3] Deceased.

0042-6822/02 $35.00

transport (Tyler *et al.*, 1986) and within 14 h viral antigens are detected in spinal cord motor neurons ipsilateral to the injection site (Flamand *et al.*, 1991). To identify genes that influence type 3 reovirus neuroinvasiveness, we first identified two neurotropic type 3 viruses that differ in lethality when injected into the hindlimb but not after injection into the brain. We reasoned that such viruses might differ at early steps in pathogenesis (primary replication and/or spread to the nervous system), yet be similar at later steps (tropism and growth in the brain). By analysis of the pathogenesis of reassortant viruses generated from these viruses, we identified reovirus genes important for type 3 reovirus invasion of the central nervous system after peripheral injection.

RESULTS

Characterization of reassortant viruses

In 1-day old mice, we found that two type 3 reoviruses, strain Dearing (T3D) and clone 9 (C9), had similar 50% lethal doses (LD_{50}) by the intracranial (IC) route of injection ($LD_{50} < 5$ plaque-forming units (PFU)/mouse). However, 1000 times more T3D than C9 virus was required for an LD_{50} after intramuscular (IM) injection (LD_{50} for T3D $> 10^4$ vs LD_{50} for C9 $< 10^1$). To determine the genetic basis for this difference in neuroinvasiveness, we characterized a panel of T3D × C9 reassortant viruses generated by coinfection of murine L929 cells (Table 1). Viral genotypes were defined by analysis of the migration patterns of the dsRNA gene segments in polyacrylamide gels. As reported previously for intertypic (Type 1 × Type 3) reovirus reassortants (Nibert *et al.*, 1996), we found a nonrandom distribution of certain genes in the intratypic T3D × C9 reassortants. The *M1* and *M2* genes cosegregated in all reassortants and the T3D *L2* gene was present in all but two reassortants.

TABLE 1

T3D × C9 Reassortants

Virus strain	Origin of the gene segment[a]										LD_{50}[b]	Titer[c]	PO[d] %
	L1	*L2*	*L3*	*M1*	*M2*	*M3*	*S1*	*S2*	*S3*	*S4*			
C9	9	9	9	9	9	9	9	9	9	9	0.5	5.5	0
56	9	3	9	9	9	9	9	9	3	9	1.4	1.2	0
42	9	3	9	3	3	9	9	3	3	3	1.5	2.3	100
1.84	9	3	9	3	3	9	9	9	9	9	1.7	3.9	40
Z10	9	3	9	9	9	9	9	9	9	9	1.7	1.6	60
2.11	3	3	9	3	3	3	3	3	3	3	1.7	2.2	20
1.46	3	3	9	3	3	3	9	3	3	3	1.9	4.8	0
1.217	3	3	9	3	3	3	9	3	3	9	2.1	3.5	0
1.211	9	3	3	3	3	3	9	3	3	9	2.2	0.0	0
1.4	3	9	3	3	3	9	9	3	3	9	2.3	4.4	75
1.5	3	3	9	3	3	3	9	3	9	9	2.3	3.7	40
1.118	3	3	9	3	3	3	3	3	9	9	2.6	1.4	40
65	3	3	9	9	9	9	9	3	9	9	2.6	3.9	75
1.77	3	3	3	3	3	3	9	3	3	9	2.8	2.2	60
3.8	3	3	3	3	3	3	9	9	3	9	3.0	0.0	0
1.54	9	3	9	3	3	9	3	3	3	9	3.1	4.9	100
1.9	3	3	9	3	3	9	9	3	9	9	3.2	0.8	20
48	3	3	9	3	3	9	3	3	3	9	3.3	2.7	100
62	3	3	3	3	3	9	9	3	9	9	3.4	2.0	100
1.33	3	3	9	3	3	3	3	3	9	3	3.8	1.8	100
T3D	3	3	3	3	3	3	3	3	3	3	4.0	1.9	100
45	3	3	3	3	3	3	3	3	3	9	4.2	1.2	75
1.39	9	3	3	9	9	3	9	3	3	3	4.5	1.0	100
57	3	3	9	9	9	9	3	3	9	9	4.7	1.6	100
1.219	3	9	3	3	3	9	3	3	3	9	5.0	3.6	100
4.19	9	3	9	3	3	9	9	9	9	3	5.0	0.0	100
1.109	3	3	3	9	9	3	9	3	3	9	5.0	0.0	100
82	3	3	9	9	9	3	3	3	3	9	5.1	2.3	100
1.6	3	3	9	9	9	3	3	3	9	9	6.0	0.7	100
1.71	3	3	3	9	9	9	3	3	3	9	6.0	0.0	100
26	9	3	3	3	3	9	3	3	9	9	6.0	1.3	100
32	9	3	3	9	9	3	3	3	3	9	6.0	0.0	100

[a] Parental origin of gene segment: 3, gene derived from T3D; 9, gene derived from C9.

[b] Lethality expressed as median lethal dose (LD_{50}) in $\log_{10}$ PFU/mouse.

[c] Titer of virus in spinal cord on day 5 postinoculation ($\log_{10}$ PFU/ml).

[d] Percentage of injected animals surviving after peroral injection.

Genetic determinants of lethality after im injection

To identify the gene(s) associated with route-specific lethality differences, we determined the LD_{50} of each reassortant after hindlimb injection of 1-day old mice. Three to five dilutions of each of the 32 viruses were injected into groups of four to six mice (total 768 mice). The resulting LD_{50}s exhibited a range of values (lethal viruses having the lowest LD_{50}), with no clear gap between more and less lethal groups (Table 1). No reassortant was more lethal than the parental C9; however, several were less lethal than T3D. Statistical analysis demonstrated a significant association between lethality and the derivation of the *S1* (MW test, $P = 0.002$; *t* test, $P = 0.001$) and the *L3* (MW test, $P = 0.016$; *t* test, $P = 0.016$) genes and a possible but less significant association between lethality and the *S2* gene (MW test, $P = 0.03$; *t* test, $P = 0.4$). To calculate the influence on lethality of individual C9 genes in the context of all other genes, we subjected the data to linear regression analysis with each gene an independent variable, except for the cosegregating genes, *M1* and *M2*, which were treated as a single variable (Fig. 1). Two C9 genes were associated with significant increases in virus lethality. The presence of a C9-derived *L3* gene was associated with an approximate reduction in LD_{50} of 1.8 log ($P = 0.001$), while the presence of a C9-derived *S1* gene reduced LD_{50} by 1.6 log ($P = 0.001$). Conversely, the presence of a C9-derived *M1/M2* gene pair tended to make reassortants less lethal, increasing LD_{50} by about 1 log ($P = 0.03$). The regression equation accounted for 67% of the variance seen in the data ($R^2 = 0.67$, $P = 0.001$, where R^2, the square of the multiple correlation, represents the proportion of the variance in the depen-

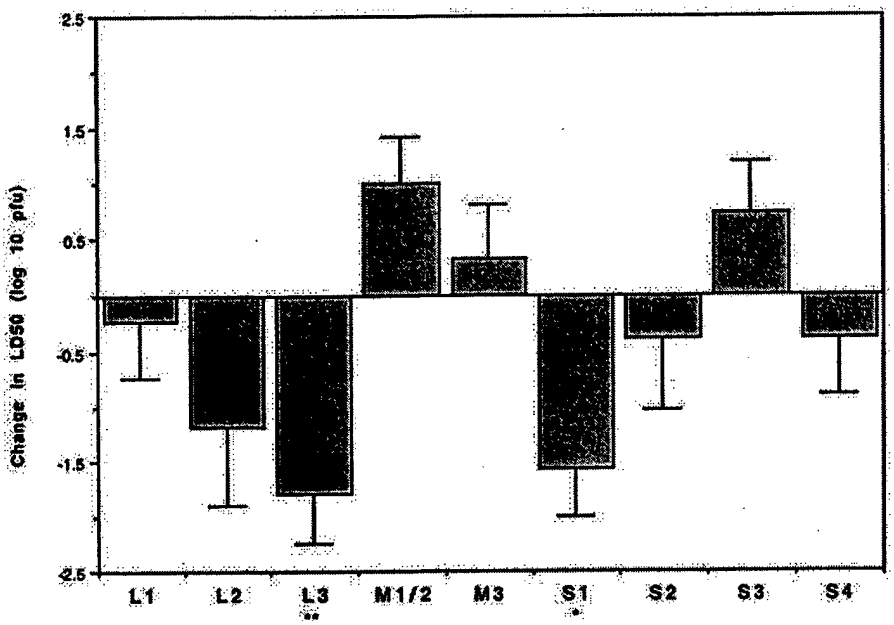

FIG. 1. Contribution of individual C9 genes to virus lethality. Each bar represents the difference in LD_{50} contributed by a single gene in association with all other genes after im injection of T3D × C9 reassortants in 1-day old mice. $^{**}P = 0.0008$; $^{*}P = 0.001$.

dent variable accounted for by the independent variables). Taken together, these results suggested that the difference in T3D and C9 lethality after skeletal muscle injection was multigenic, i.e., the C9 *L3* and S1 genes increased virus lethality, while the C9 *M1* and/or *M2* gene(s) tended to decrease lethality.

Because the substitution of certain C9 genes increased T3D lethality after IM injection, we analyzed separately the subset of viruses carrying the T3D *S1* gene (Table 2). All viruses more lethal than T3D contained the C9 *L3* gene, and the most lethal virus was mono-reassortant 2.11, with an LD_{50} 2.3 log lower than that of T3D. Conversely, all reassortants containing the C9 *M1/M2* gene pair were less lethal than T3D. In those reassortants with both the C9 *L3* and the C9 *M1/M2* genes, the *M1/M2* decrease in lethality was dominant. Thus while the association between lethality and the derivation of the *M1/M2* gene pair (MW test, $P = 0.015$; *t* test, $P = 0.012$) was statistically significant in this set of reassortants, the association between lethality and the derivation of the *L3* gene was not (MW test, 0.058; *t* test, $P = 0.055$). However, regression analysis, which identifies the contribution of each variable while allowing for the contribution of the other independent variables, suggested that the C9 *L3* gene was associated with increased lethality (LD_{50} reduced by 1.5 log, $P = 0.02$), while the C9 *M1/M2* decreased lethality (LD_{50} increased by 1.8 log, $P = 0.01$). The regression equation accounted for 85% ($P = 0.03$) of the variance in LD_{50}. Thus, while substitution of the C9 *L3* gene increased T3D lethality, the C9 *M1/M2* pair had an opposite, and dominant, effect.

Lethality after peroral injection

C9 reovirus is lethal after peroral (PO) injection while T3D is not (Rubin and Fields, 1980; Morrison *et al.*, 1991; Tyler *et al.*, 1989); however, the genetic basis of this difference has not been identified. To determine whether the reassortants shown to be more lethal after skeletal

TABLE 2

Lethality[a] of T3D × C9 Reassortants Carrying the T3D *S1* Gene Segment

Virus strain	Origin of the gene segment[b]										LD_{50}
	L1	*L2*	*L3*	*M1*	*M2*	*M3*	*S1*	*S2*	*S3*	*S4*	
C9	9	9	9	9	9	9	9	9	9	9	0.5
2.11	3	3	9	3	3	3	3	3	3	3	1.7
1.118	3	3	9	3	3	3	3	3	9	9	2.6
1.54	9	3	9	3	3	9	3	3	3	9	3.1
48	3	3	9	3	3	9	3	3	3	9	3.3
1.33	3	3	9	3	3	3	3	3	9	3	3.8
T3D	3	3	3	3	3	3	3	3	3	3	4.0
45	3	3	3	3	3	3	3	3	3	9	4.2
57	3	3	9	9	9	9	3	3	9	9	4.7
1.219	3	9	3	3	3	9	3	3	3	9	5.0
82	3	3	9	9	9	3	3	3	3	9	5.1
1.6	3	3	9	9	9	3	3	3	9	9	6.0
1.71	3	3	3	9	9	9	3	3	3	9	6.0
26	9	3	3	3	3	9	3	3	9	9	6.0
32	9	3	3	9	9	3	3	3	3	9	6.0

[a] Lethal dose 50 (LD_{50}) in $\log_{10}$ PFU/mouse, after im injection of 1-day old mice.

[b] Parental origin of gene segment: 3, gene derived from T3D: 9, gene derived from C9.

TABLE 3

Comparison of Lethality[a] after Intramuscular (IM) and Peroral (PO) Injection of T3D × C9 Reassortants Carrying the T3D *S1* Gene Segment

	Origin of the gene segment[b]											
Virus name	*L1*	*L2*	*L3*	*M1*	*M2*	*M3*	*S1*	*S2*	*S3*	*S4*	IM LD_{50}	PO LD_{50}
C9	9	9	9	9	9	9	9	9	9	9	0.5	3.4
2.11	3	3	9	3	3	3	3	3	3	3	1.7	6.4
1.118	3	3	9	3	3	3	3	3	9	9	2.6	6.3
T3D	3	3	3	3	3	3	3	3	3	3	4.0	>8.3

[a] Lethal dose 50 (LD_{50}) in $\log_{10}$ PFU/mouse, after IM or PO injection of 1-day old mice.

[b] Parental origin of gene segment: 3, gene derived from T3D: 9, gene derived from C9.

muscle injection were also more lethal after peroral injection, we injected groups of four to five 1-day old mice with each reassortant (135 mice) at a dose at which C9 killed 100% of injected mice while T3D killed few mice. Results were calculated as percentage survival and compared with LD_{50} after IM injection (Table 1). As was seen after IM injection, reassortants carrying the C9 *S1* gene tended to be most virulent after PO injection. However, two viruses carrying the T3D *S1* gene killed more than 50% of the mice: 2.11, the mono-reassortant carrying the C9 *L3* gene, and 1.118, carrying the C9 *L3*, *S3*, and *S4* genes. These also were the T3D reassortants most virulent after IM injection. To quantify this result, PO LD_{50}s were calculated for these two reassortants, as well as for T3D and C9 (Table 3). LD_{50}s were 3.4, 6.3, and 6.4 $\log_{10}$ PFU per mouse for C9, 2.11, and 1.118, respectively. However, the highest dose of T3D (8.3 $\log_{10}$ PFU) was insufficient for an LD_{50}. Thus, substitution of the C9 *L3* gene alone was sufficient to confer lethality after peroral injection to T3D, a virus normally avirulent by this route.

Spinal cord infection after IM injection

Ventral spinal cord neurons ipsilateral to the injection site are the first site of virus replication in the CNS after hindlimb injection (Tyler *et al.*, 1986; Flamand *et al.*, 1991). To determine whether T3D and C9 differed in their capacity for spinal cord infection after IM injection, we injected groups of 1-day old mice with 10^2 PFU of virus, a dose expected to kill all C9- and a few T3D-infected pups. Viral titer was measured in muscle, spinal cord, and brain tissue collected on alternate days after injection (Figs. 2A and 2B). Both viruses replicated well in muscle, suggesting that differences in the capacity of these viruses to replicate in skeletal muscle were not responsible for differences in neuroinvasiveness or lethality. In contrast, by 5 days postinjection there was a 4 log difference between T3D and C9 titers in spinal cord and brain. This suggested that there was a difference in either the capacity of these viruses to spread or the capacity to replicate within the spinal cord. To distinguish between these possibilities, and because direct spinal cord injection of virus was not feasible in newborn mice, we injected 1-day-old mice in the hindlimb with a 100 times larger dose of each virus (10^4 PFU) than was used in our initial experiments. This dose of virus produced measurable spinal cord titers by 24 h postinjection (Fig. 2C), suggesting that if there is a defect in spread it is relative rather than absolute. At this dose, T3D and C9 grew at a similar rate over the first 5 days after injection. However, at each time point, the titer of T3D was about 10-fold less than that of C9. These results suggested either that T3D might be less efficient than C9 in the initiation of spinal cord infection, that is, while both grew well once infection was established, higher doses of T3D were required to produce comparable spinal cord titers, or that less virus was produced per infected cell.

To identify the gene(s) responsible for differences in

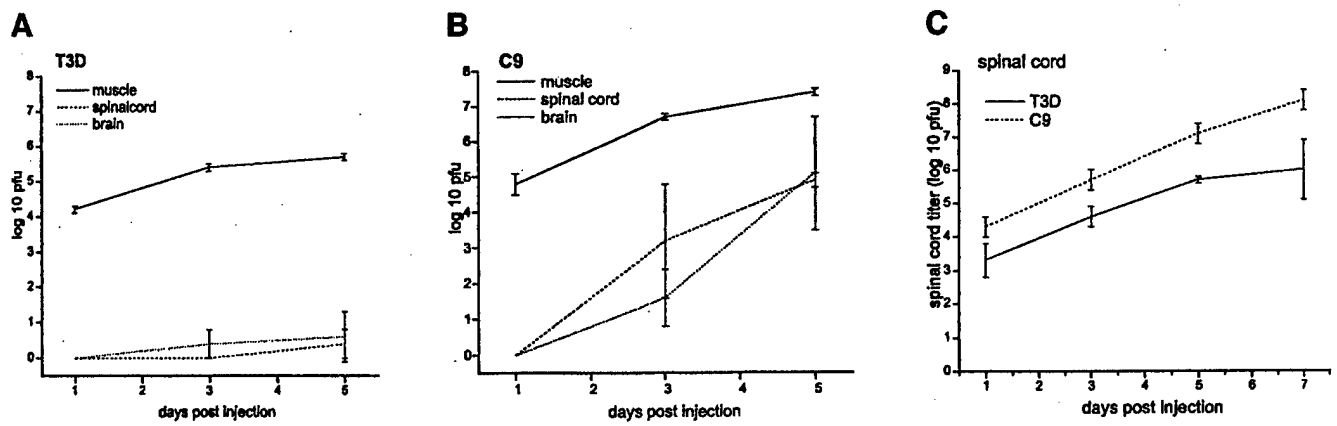

FIG. 2. Virus growth after IM injection. (A, B) One-day old pups were injected with a low dose (10^2 PFU) T3D (A) or C9 (B) virus, and tissue collected for titer at various times after injection. Each point represents the mean virus titer ± standard error in muscle, spinal cord, and brain of three mice, from one of two experiments. (C) One-day old mice were injected with a higher dose (10^4 PFU) of T3D or C9. Each point represents average spinal cord titer ± standard error ($n = 3$).

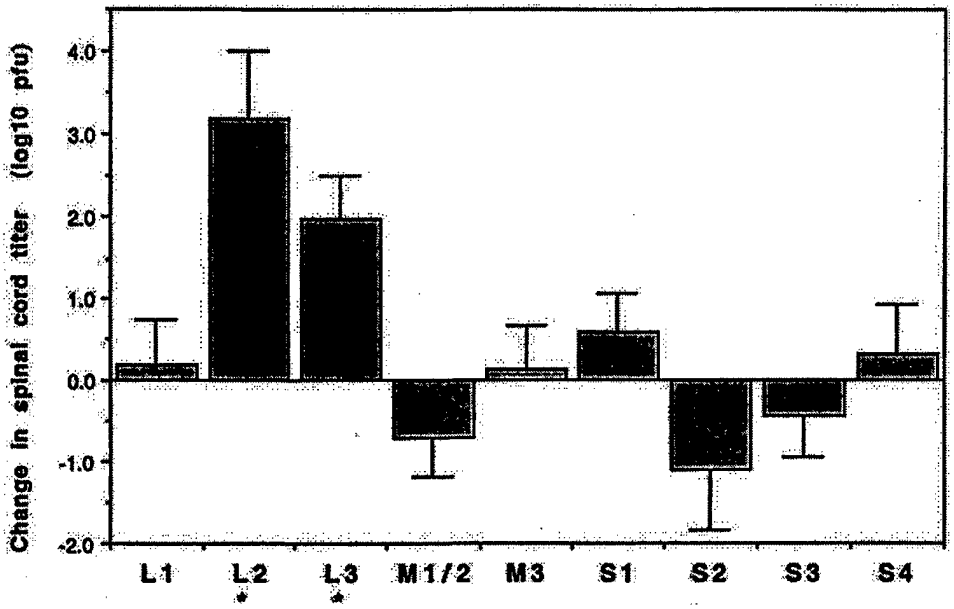

FIG. 3. Regression analysis of the contribution of C9 genes to spinal cord titer. Each bar represents the difference in spinal cord titer contributed a single gene in association with all other genes 5 days after IM injection of T3D × C9 reassortants in 1-day old mice. *P = 0.001.

T3D and C9 spinal cord infection, we measured viral titers in spinal cord tissue collected 5 days after hindlimb injection of three to six 1-day-old mice with 10^2 PFU of each reassortant (total 195 mice). This time point had shown clear differences between T3D and C9 spinal cord titers but lower standard deviations than Day 3 (Fig. 2). The panel of reassortants produced a range of titers (Table 1). C9 produced the highest titer, while T3D fell midway between C9 and reassortants producing no detectable spinal cord titer at Day 5. Reassortants with the highest titers tended to carry the C9 *L3* gene. Statistical analysis demonstrated a significant association between spinal cord titer and the derivation of the *L3* (MW test, $P = 0.028$, t test, $P = 0.033$) and *L2* (MW test, $P = 0.018$, t test, $P = 0.004$) genes. Because few reassortants carried the *L2* gene, additional reassortants will be required to confirm this result. However, the behavior of the C9 mono-reassortant carrying the T3D *L2* gene (spinal cord titer 3.9 logs lower than C9) supported a role for the *L2* gene in spinal cord infection. Although the *S1* gene was implicated in lethality, it was not associated with differences in spinal cord infection. To determine the influence of individual genes on Day 5 spinal cord titers, we subjected the data to linear regression analysis (Fig. 3). The C9 *L2* gene increased spinal cord titer by 3.2 log (P = 0.001). The C9 *L3* gene increased titer by 2.0 log (P = 0.001). The regression equation accounted for 59% of the variation seen in the data ($R^2 = 0.59$, $P = 0.007$). Thus, after IM injection, the *L3* gene influenced spinal cord infection, as it had virus lethality. The correlation between Day 5 spinal cord titer and virus lethality was significant (Spearmann rank correlation, $P = 0.005$; simple regression, $P = 0.001$) but accounted for only 31% of the variance. Thus, spread to the spinal cord after IM injection, as measured by Day 5 virus titer, was a weak predictor of reassortant lethality.

DISCUSSION

The neurotropic type 3 reoviruses use peripheral nerve fibers to invade the CNS from extraneural sites of infection (Tyler *et al.*, 1986; Morrison *et al.*, 1991). Field isolates, T3D and C9, are highly virulent after intracranial injection of neonatal mice; however, C9 is significantly more lethal than T3D after intramuscular injection. To better understand the mechanisms by which viruses invade peripheral nerve pathways to produce CNS disease, we used reassortant viruses to identify virus genes important for differences in type 3 reovirus neuroinvasion following inoculation at different sites in the mouse.

Nonrandom segregation of T3D × C9 genes

This article is the first characterization and usage of T3D × C9 intratypic reassortants to identify differences in neuroinvasion between type 3 viruses with similar tropism and neurovirulence. In the panel of reassortants we found that certain genes cosegregated (*M1* and *M2*) or were underrepresented (C9 *L2*). In addition, none of the T3D reassortants (carrying T3D *S1*) incorporated the C9 *S2* gene. Nonrandom distribution of reovirus gene segments has been reported previously for intertypic serotype 1, Lang (T1L) × serotype 3 (T3D) reovirus reassortants (Nibert *et al.*, 1996). As in our T3D × C9 reassortants, the T3D *L2* gene was found in most of the intertypic reassortants, and the T3D *L3* and T3D *S4* genes were somewhat underrepresented. Interestingly,

in our panel, the two reassortants carrying the C9 *L2* gene had the same genotype except for the S1 gene. Thus, a specific interaction between lambda 2 and one or more C9 proteins other than, or in addition to, sigma 1 may be necessary to produce a viable reassortant. An increased frequency of homologous pairing of certain parental alleles was reported for the T1L × T3D reassortants, but not of *M1* and *M2*, and, in no case did the parental alleles invariably cosegregate. The mechanisms responsible for the nonrandom nature of reovirus reassortment are unknown. Evidence for structural and/or functional interactions between reovirus proteins has been demonstrated by extragenic suppression of temperature-sensitive phenotypes (McPhillips and Ramig, 1984) and by identification of serotype-associated patterns of monoclonal antibody binding to outer capsid reovirus proteins (Virgin *et al.*, 1991).

Lethality after IM injection

Two genes, *S1* and *L3*, were primarily associated with lethality differences between T3D and C9 after hindlimb injection. The *S1* gene, encoding the viral cell attachment protein, sigma 1, defines reovirus serotype and is responsible for serotype-specific differences in disease phenotype after intracranial injection (Weiner *et al.*, 1980). Type 1 reovirus infection produces a generally nonlethal ependymitis, while type 3 infection produces a lethal encephalitis (Tyler and Fields, 1996). Thus, an association of *S1* with differences in reassortant lethality is not surprising. Previous associations of the *S1* gene with differences in neuroinvasion using intertypic T1L × T3D reassortants (Tyler *et al.*, 1986; Bodkin and Fields, 1989), reassortants made using T3D and an immune selected variant (Kaye *et al.*, 1986), and variants selected in severe combined immunodeficient (SCID) mice (Haller *et al.*, 1995), all correlated with differences in virulence after intracranial injection. However, the difference between T3D and C9 lethality after IM injection was not associated with a difference in lethality after IC inoculation. After IC injection, the LD_{50} values for both T3D and C9 are less than 10 PFU/mouse. Thus, the present identification of the *S1* gene contribution to lethality after hindlimb injection suggests additional roles of the sigma 1 protein that are specific to the routes of neuroinvasion studied here.

The reovirus *L3* gene was a determinant of reovirus lethality for the IM, as well as the PO (see below), routes. The *L3* gene product, lambda 1, is the major structural component of the inner shell of the viral capsid, which organizes the packing of the genomic RNA. Lambda 1 is believed to act as a helicase during transcription by the lambda 3 protein (Reinisch *et al.*, 2000; Bisaillon *et al.*, 1997; Noble and Nibert, 1997). Differences in the lambda 1 protein may affect the stability of the virus core, a multienzyme protein shell which must remain intact during virus uncoating and transcription of single-stranded RNA and/or may affect enzymatic activities required for viral transcription in different cell types. Strain-specific differences in the ATPase activities associated with the lambda 1 protein have been found *in vitro,* but T3D and C9 have not been compared (Noble and Nibert, 1997). Genes encoding core proteins, including *L3*, have been shown to influence virus growth in cultured mouse heart cells (Matoba *et al.*, 1991). However, no *in vivo* phenotype had been mapped to the *L3* gene previously.

The *M1* and/or *M2* gene(s) also contributed to differences in T3D and C9 lethality and had the opposite effect of *S1* and *L3*. The *M1* gene encodes inner capsid protein, mu 2, an NTPase with RNA-binding activity that forms part of the virus transcription complex (Brentano *et al.*, 1998). Reassortant analysis has linked a group of genes, including *M1*, with virus induction of myocarditis in newborn mice (Sherry and Blum, 1994) and with the extent of replication in cultured mouse heart cells and bovine aortic endothelial cells (Matoba *et al.*, 1993). The *M2* gene encodes a major outer capsid protein, mu 1. The *M2* gene has been shown to influence neurovirulence among Type 3 strains when injected into the brain of newborn mice (Hrdy *et al.*, 1982). Growth in the CNS and virulence was decreased in virus T3H/Ta (now T3 clone 8), a phenotype that mapped to the *M2* gene. Interestingly, a close relationship between the type 3 *M1* and *M2* genes has been suggested by the extragenic suppression of *M2* attenuation by the *M1* gene and restoration of T3, clone 8 virulence (Jayasuriya, 1991).

Lethality after PO injection

In addition to demonstrating a role for the lambda 1 protein in neuroinvasion after skeletal muscle injection, we also found that the C9 *L3* gene confers lethality to T3D after peroral injection, the natural route of reovirus infection. T3D avirulence has been attributed to the sigma 1 protein, which is sensitive to cleavage by proteases and is associated with reduced virus growth in the intestine (Bodkin and Fields, 1989; Nibert *et al.*, 1995). However, in our reassortants, a single C9 gene, *L3*, was sufficient to confer lethality after PO injection to a T3D mono-reassortant carrying the protease-sensitive T3D sigma 1 protein. Because the lambda 1 protein is located in the inner capsid, this result is not likely the result of a steric protection of the sigma 1 cleavage site, as has been suggested for the lambda 2 spike protein (Bodkin and Fields, 1989). However, the lambda 1, lambda 2, lambda 3, and sigma 1 proteins together comprise the structurally dynamic vertex of the viral capsid where cell binding, viral transcription, and extrusion of mRNA are localized. Thus a change in one protein in the complex may affect the function of another. A contribution of genes other than *S1* to T3D lethality after PO injection was also suggested in previous studies by Chappell *et*

al. (1997). The sigma 1 protein of a T3D variant isolated from SCID mice revealed a single amino acid change associated with resistance to protease cleavage. Compared to T3D, this virus showed increased growth in intestine but decreased growth in the brain in SCID mice. In neonatal mice, growth in intestine and the spread to the brain after PO injection were increased, but growth in the brain and virulence were decreased after IM injection.

Spinal cord infection after IM injection

At low doses, T3D appeared to infect the CNS more slowly than C9 after hindlimb injection. However, when tested at higher doses, the rate of virus growth in the spinal cord was similar for both T3D and C9, but 10-fold more infectious virus particles were required to produce similar titers. Other studies suggest that T3D and C9 are both rapidly transported to the neural soma, producing antigen-positive neurons 14–15 h after hindlimb injection (Flamand *et al.,* 1991; Mann *et al.*, 2002). Thus T3D and C9 may differ in efficiency of invasion of neonatal nerve terminals, or at an early step in replication in motor neurons.

The difference in Day 5 spinal cord titer was associated with the *L3*, and possibly the *L2*, gene. Together, the *L3* and *L2* genes have been associated previously with differences in virus growth in cardiac cell cultures (Matoba *et al.,* 1991). Pentameric complexes of the *L2* product, lambda 2, form hollow spikes through which internally transcribed mRNA exits the viral particle (Nibert and Schift, 2001). Because lambda 2 anchors sigma 1 in the outer capsid and caps nascent mRNAs as they exit the inner core (Reinisch *et al.,* 2000), this protein may influence the efficiency and/or stability of the capsid during binding, uptake, and targeting to endosomes, as well as the production of viral mRNA and its delivery to the host cytoplasm. The *L2* gene has been previously associated genetically with differences in the efficiency of reovirus horizontal spread between infected and uninfected littermates (Keroack and Fields, 1986) and in association with the *S1* and *M1* genes with differences in reovirus growth in the intestine early in PO infection (Bodkin and Fields, 1989). In association with the *M1* gene, the *L2* gene has been associated genetically with induction of myocarditis (Sherry and Blum, 1994).

Lethality and spinal cord infection

The set of genes determining differences in viral titers in Day 5 spinal cord after IM injection was somewhat different from that determining lethality differences by the same route. The *L2* gene appeared to be the stronger determinant of spinal cord infection, yet did not significantly affect virus lethality. Conversely, the *S1* gene was the stronger determinant of lethality after IM injection, yet had no significant effect on differences in spinal cord titers. The *M1/M2* gene pair also influenced lethality but not spinal cord invasion. Only the *L3* gene influenced both lethality and spinal cord infection and was sufficient to rescue T3D lethality after PO injection. However, after im injection, the paired contribution of *S1* and *L3* to lethality and of *L2* and *L3* to spread outweighed the independent contribution of *L3* to each, and in the subset of T3D reassortants, the decrease in lethality associated with the C9 *M1/M2* genes negated the increase associated with *L3*. Functional interdependence among type 3 proteins is suggested by the nonrandom reassortment of T3D and C9 genes (see above). In addition, the identification of serotype-specific sets of reovirus genes suggests that structure/function relationships evolve in association with particular virus strains (Virgin *et al.,* 1991).

The correlation between Day 5 spinal cord titer and reassortant lethality was statistically significant but low. Thus, these may reflect independent properties of type 3 reovirus neuroinvasiveness. For example, virus spread from spinal cord to brain may occur soon after infection of motor neurons and thus is not directly related to subsequent growth in the spinal cord. Alternatively, for some reassortants, early replication in the spinal cord may be dampened by Day 5 and thus would not be detected in our study, or some reassortants may better utilize other pathways to infect the brain; for example, certain gene combinations may facilitate bloodborne spread. T3D and C9 also differ in their induction of apoptosis (Tyler, in press), and this mechanism is independent of virus growth. Further experiments are needed to determine the contributions of these mechanisms to spinal cord infection and lethality.

Virus genes determining neuroinvasion after IM injection have been identified in the herpes simplex virus. Two viruses, nonlethal ANG and a lethal mouse brain-passage derivative, ANGpath, showed similar virulence after IC injection of adult mice (LD_{50} ~ 1 PFU), yet differed in neuroinvasiveness (LD_{50} 10^5 vs $>10^8$) after hindlimb injection (Izumi and Stevens, 1990). This difference correlated with restricted entry into the nervous system after footpad injection and mapped to the gene encoding glycoprotein D (gD), an envelope glycoprotein required for postattachment binding to a coreceptor. Because replacement of the ANG gD with ANGpath gD did not fully rescue ANGpath gD × ANG recombinant viruses to ANGpath LD_{50} levels, other genes may also be involved.

Taken together, our results suggest that both inner and outer capsid proteins influence reovirus neuroinvasiveness. In combination with sigma 1 and mu 1 and/or mu 2, inner capsid protein lambda 1 influences virus lethality, and with lambda 2, influences spinal cord infection after IM injection. Lambda 1 also can increase the lethality of T3D by the natural route of infection.

MATERIALS AND METHODS

Cells

Spinner-adapted mouse L929 (L) cells (ATCC) were grown in suspension or monolayer cultures in Joklik's modified Eagle's minimal essential medium (MEM, Irvine Scientific) supplemented with 5% fetal bovine serum (HyClone Laboratories) and 2 mM L-glutamine, 1 U penicillin, and 1 μg streptomycin (Irvine Scientific) per milliliter.

Viruses

Reovirus type 3, strain Dearing (T3D), and clone 9 (C9) were laboratory stocks described previously (Tyler *et al.*, 1989; Hrdy *et al.*, 1979). T3D × C9 reassortant viruses were grown from stocks originally isolated by Ken Tyler and Dinah Bodkin in our laboratory. Viruses were doubly plaque purified and passaged in L cells to generate working stocks as described previously (Tyler *et al.*, 1985). T3D and C9 viruses were purified from infected L cell lysates by cesium chloride gradient centrifugation (Furlong *et al.*, 1988).

Animals and inoculations

One-day-old Swiss Webster (Taconic) or NIH Swiss (National Cancer Institute) mice received intracerebral inoculations (IC) into the right hemisphere or IM into the left hindlimb with a Hamilton syringe and 30-gauge needle. Tissue samples were collected in gelatin-saline (phosphate-buffered saline, 0.3% gelatin) and stored at −80°C until used for viral titration. To determine virus lethality, at least three groups of mice (five to six mice per group) were inoculated by the IC or IM route with serial dilutions of each virus and monitored daily for signs of morbidity. Experiments were terminated at 21 days postinfection, and 50% lethal doses (LD_{50}) were calculated by the method of Reed and Muench (Reed and Muench, 1938).

Characterization or reassortants

L cell monolayers were infected with 10 PFU of virus stock per cell, and cytoplasmic extracts were prepared for polyacrylamide gel analysis (Tyler *et al.*, 1985). To resolve certain gene segments, 6 or 10% gels were run on long (30 cm) gel plates. To identify the parental origin of closely migrating gene segments, samples were double-loaded into wells with T3D or C9 dsRNA.

Determination of viral titer

Tissue samples were frozen and thawed three times and then sonicated for 30 s using a microtip probe to homogenize the tissue. L cell monolayers in six-well plates (10^6 cells per well) were inoculated in duplicate with serial 10-fold virus dilutions (Tyler *et al.*, 1985).

Statistical analysis

The effect of the derivation of individual reovirus gene segments was analyzed by nonparametric (Mann–Whitney) and parametric (*t* test and multiple regression analysis) statistical tests (Virgin *et al.*, 1997; Tyler *et al.*, 1996). Correlation was calculated by Spearmann (nonparametric) and regression (parametric) analysis. Statistical tests were performed using Stat-View software (Abacus Concepts, Berkley, CA).

ACKNOWLEDGMENTS

We thank our many colleagues, especially Dinah Bodkin for help in isolation of reassortant viruses, Herbert Virgin, James Hogle, Marie Chow, and Richard Sidman for helpful discussions, Constantine Daskalakis and Emilia Bagiella for help with statistics, William Lucas for critical reading of the manuscript, and Elaine Fremont for expert technical support. This work is dedicated to the memory of Bernie Fields. This research was supported by Grants P50 NS16998 and P01 NS35138 from the National Institutes of Health.

Note added in proof. Parker *et al. (J. Virol.* **76**: 4483–4496, 2002) and Broering *et al. (J. Virol.* **76**: 8285–8297; 2002) have recently shown that the T3D μ2 protein contributes to altered factory distribution in T3D infected cells. This suggests an additional μ2 function that could contribute to virus attenuation.

REFERENCES

Bissaillon, M., Bergeron, J., and Lemay, G. (1997). Characterization of the nucleoside triphosphate phosphohydrolase and helicase activities of reovirus lambda 1 protein. *J. Biol. Chem.* **272**, 18298.

Bodkin, D. K., and Fields, B. N. (1989). Growth and survival of reovirus in intestinal tissue: Role of the *L2* and S1 genes. *J. Virol.* **63**, 1188–1193.

Brentano, L., Noah, D. L., Brown, E. G., and Sherry, B. (1998). The reovirus protein mu2, encoded by the *M1* gene is an RNA-binding protein. *J. Virol.* **72**, 8354–8357.

Chappell, J. D., Barton, E. S., Smith, T. H., Baer, G. S., Duong, D. T., Nibert, M. L., and Dermody, T. S. (1997). Cleavage susceptibility of reovirus attachment protein sigma 1 during proteolytic disassembly of virions is determined by a sequence polymorphism in the sigma 1 neck. *J. Virol.* **72**, 8205–8213.

Flamand, A., Gagner, J.-P., Morrison, L. A., and Fields, B. N. (1991). Penetration of the nervous systems of suckling mice by mammalian reoviruses. *J. Virol.* **65**, 123–131

Furlong, D. B., Nibert, M. L., and Fields, B. N. (1988). Sigma 1 protein of mammalian reoviruses extends from the surface of viral particles. *J. Virol.* **62**, 246–256.

Haller, B. L., Barkon, M. L., Li, X. Y., Hu, W. M., Wetzel, J. D., Dermody, T. S., and Virgin, H. W. (1995). Brain- and intestine-specific variants of reovirus serotype 3 strain Dearing are selected during chronic infection of severe combined immunodeficient mice. *J. Virol.* **69**, 3933–3937.

Hrdy, D. B., Rubin, D. H., and Fields, B. N. (1982). Molecular basis of reovirus neurovirulence: Role of the *M2* gene in avirulence. *Proc. Natl. Acad. Sci. USA* **79**, 1298–1302.

Hrdy, D. B., Rosen, L., and Fields, B. N. (1979). Polymorphism of the migration of double-stranded RNA genome segments of reovirus isolates from humans, cattle, and mice. *J. Virol.* **31**, 104.

Izumi, K. M., and Stevens, J. G. (1990). Molecular and biological characterization of a herpes simplex virus type 1 (HSV-1) neuroinvasiveness gene. *J. Exp. Med.* **172**, 487–496.

Jayasuriya, A. K. (1991). Ph.D. thesis, Harvard University.

Kaye, K. M., Spriggs, D. R., Bassel-Duby, R., Fields, B. N., and Tyler, K. L. (1986). Genetic basis for altered pathogenesis of an immune-selected antigenic variant of reovirus type 3 Dearing. *J. Virol.* **59,** 90–97.

Keroack, M., and Fields, B. N. (1986). Viral shedding and transmission between hosts determined by reovirus *L2* gene. *Science* **232,** 1635–1638.

Mann, M. A., Knipe, D. M., Fischbach, G. D., and Fields, B. N. (2002). Type 3 Reovirus Neuroinvasion after Intramuscular Inoculation: Direct Invasion of Nerve Terminals and Age-Dependent Pathogenesis. *Virology* **303,** 222–231.

Matoba, Y., Colucci, W. S., Fields, B. N., and Smith, T. W. (1993). The reovirus *M1* gene determines the relative capacity of growth of reovirus in cultured bovine aortic endothelial cells. *J. Clin. Invest.* **92,** 2883–2888.

Matoba, Y., Sherry, B., Fields, B. N., and Smith, T. W. (1991). Identification of the viral genes responsible for growth of strains of reovirus in cultured mouse heart cells. *J. Clin. Invest.* **87,** 1628–1633.

McPhillips, T. H., and Ramig, R. F. (1984). Extragenic suppression of temperature-sensitive phenotype in reovirus: Mapping suppresser mutations. *Virology* **135,** 428–439.

Mims, C. (1987). "The Pathogenesis of Infectious Disease, 3rd ed." Academic Press, London/New York.

Morrison, L. A., Sidman, R. L., and Fields, B. N. (1991). Direct spread of reovirus from the intestinal lumen to the central nervous system through vagal autonomic nerve fibers. *Proc. Natl. Acad. Sci. USA* **88,** 3852–3856.

Nathanson, N., and Tyler, K. L. (1997). Entry, dissemination, shedding, and transmission of viruses. *In* "Viral Pathogenesis" (Nathanson *et al.*, Eds.), Lippincott-Raven Publishers, Philadelphia.

Nibert, M. L., and Schiff, L. A. (2001). Reoviruses and their replication. *In* "Fields Virology" (D. M. Knipe, and P. M. Howley, Eds.), 4th ed. Lippincott-William and Wilkins, Philadelphia.

Nibert, M. L., Margraf, R. L., and Coombs, K. M. (1996). Nonrandom segregation of parental alleles in reovirus reassortants. *J. Virol.* **70,** 7295–7300.

Nibert, M. L., Chappell, J. D., and Dermody, T. S. (1995). Infectious subvirion particles of reovirus type 3 Dearing exhibit a loss in infectivity and contain a cleaved sigma 1 protein. *J. Virol.* **69,** 5057–5067.

Noble, S., and Nibert, M. L. (1997). Characterization of an ATPase activity in reovirus cores and its genetic association with core-shell protein lambda 1. *J. Virol.* **71,** 2182–2191.

Reed, L. J., and Muench, H. (1938). A simple method of establishing fifty percent endpoints. *Am. J. Hyg.* **27,** 493.

Reinisch, K. M., Nibert, M. L., and Harrison, S. C. (2000). Structure of the reovirus core at 3.6 angstrom resolution. *Nature* **404,** 960–967.

Rubin, D. H., and Fields, B. N. (1980). Molecular basis of reovirus virulence: Role of the *M2* gene. *J. Exp. Med.* **152,** 853–868.

Sherry, B., and Blum, M. A. (1994). Multiple core proteins are determinants of reovirus-induced acute myocarditis. *J. Virol.* **68,** 8461–8465.

Tyler, K. L. (2001). Mamalian Reoviruses. *In* "Fields Virology" (B. N. Fields, D. M. Knipe, and P. M. Howley, Eds.), Lippincott-William and Wilkins, Philadelphia.

Tyler, K. L., Squier, M. K., Brown, A. L., Pike, B., Willis, D., Oberhaus, S. M., Dermody, T. S., and Cohen, J. J. (1996). Linkage between reovirus-induced apoptosis and inhibition of cellular DNA synthesis: Role of the S1 and *M2* genes. *J. Virol.* **70,** 7984–7991.

Tyler, K. L., Virgin, H. W., Bassel-Duby, R., and Fields, B. N. (1989). Antibody inhibits defined stages in the pathogenesis of reovirus serotype 3 infection of the central nervous system. *J. Exp. Med.* **170,** 887–900.

Tyler, K. L., McPhee, D. A., and Fields, B. N. (1986). Distinct pathways of viral spread in the host determined by reovirus S1 gene segment. *Science* **233,** 770–774.

Tyler, K. L., Bronson, R. T., Byers, K. B., and Fields, B. N. (1985). Molecular basis of viral neurotropism: Experimental reovirus infection. *Neurology* **35,** 88–92.

Virgin, H. W., Tyler, K. L., and Dermody, T. S. (1997). Reovirus *In* "Viral Pathogenesis" (Nathanson *et al.*, Eds.), Lippincott-Raven Publishers, Philadelphia.

Virgin, H. W., Mann, M. A., Fields, B. N., and Tyler, K. L. (1991). Monoclonal antibodies to reovirus reveal structure/function relationships between capsid proteins and genetics of susceptibility to antibody action. *J. Virol.* **65,** 6772–6781.

Weiner, H. L., Powers, M. L., and Fields, B. N. (1980). Absolute linkage of virulence and central nervous system tropism of reoviruses to viral hemagglutinin. *J. Infect. Dis.* **141,** 609–616.

Weiner, H. L., Drayna, D., Averill, D. R., Jr., and Fields, B. N. (1977). Molecular basis of reovirus virulence: Role of the S1 gene. *Proc. Natl. Acad. Sci. USA* **74,** 5744–5748.

ORIGINAL CONTRIBUTION

Progressive Multifocal Leukoencephalopathy and Apoptosis of Infected Oligodendrocytes in the Central Nervous System of Patients With and Without AIDS

Sarah M. Richardson-Burns, MS; B. K. Kleinschmidt-DeMasters, MD; Roberta L. DeBiasi, MD; Kenneth L. Tyler, MD

Context: Progressive multifocal leukoencephalopathy (PML) is a demyelinating disease of the central nervous system (CNS) caused by JC virus (JCV) that occurs in immunocompromised patients. Demyelination of the CNS is a consequence of virus-induced killing of oligodendrocytes, although the exact mechanism of cell death is unknown.

Objective: To examine archival autopsy and surgical pathologic specimens from 8 patients with PML, including 6 patients with human immunodeficiency virus (HIV)-associated PML and 2 patients with non-HIV–associated PML, for evidence of apoptosis.

Design: Apoptotic cells were identified by TUNEL (terminal deoxynucleotidyl transferase–mediated deoxyuridine triphosphate nick end in situ labeling) or immunohistochemical detection of activated caspase 3. The JCV-infected cells were identified by in situ hybridization for viral transcripts or immunohistochemical analysis for JCV T antigen.

Results: Apoptosis of JCV-infected oligodendrocyte apoptosis was a prominent feature in all cases of both HIV- and non–HIV-associated PML. There were no differences between number or distribution of apoptotic cells identified by TUNEL or immunohistochemical analysis for activated caspase 3. Bizarre astrocytes were occasionally positive for JCV but were not apoptotic. Neurons, astrocytes, macrophages, and oligodendrocytes remote from lesions were neither apoptotic nor JCV infected.

Conclusions: Our study demonstrates that apoptosis occurs in oligodendrocytes associated with demyelinated lesions of patients with both HIV-associated and non–HIV-associated PML. There were no differences in degree, location, or type of infected or apoptotic cells between patients with HIV-associated and non–HIV-associated PML. The extent of apoptosis did not correlate with the presence or intensity of host inflammatory response. Accumulation of viral particles in nuclei of infected cells made it difficult to identify morphologic changes in the nucleus typically associated with apoptosis.

Arch Neurol. 2002;59:1930-1936

From the Neuroscience Program (Ms Richardson-Burns and Dr Tyler) and Departments of Neurology (Drs Kleinschmidt-DeMasters, DeBiasi, and Tyler), Pathology (Dr Kleinschmidt-DeMasters), Pediatrics (Dr DeBiasi), Medicine (Dr Tyler), Immunology (Dr Tyler), and Microbiology (Dr Tyler), University of Colorado Health Sciences Center and Denver Veterans Affairs Medical Center (Drs DeBiasi and Tyler), Denver.

PROGRESSIVE MULTIFOCAL leukoencephalopathy (PML) is a fatal, demyelinating central nervous system (CNS) disease caused by JC virus (JCV), a human polyoma virus.[1-3] Seroepidemiologic studies indicate that approximately 80% of the US population has developed antibodies to JCV by adulthood. Initial infection with JCV is usually asymptomatic and is followed by viral latency. Clinically, symptomatic infection that results in PML is thought to be caused by immunosuppression-associated reactivation of latent virus either within the CNS or at extraneural sites with subsequent spread to the CNS.[1,4]

Progressive multifocal leukoencephalopathy is characterized by multiple foci of demyelination, located predominantly in the white matter or near the gray-white matter junction. The cardinal pathologic features of PML include enlarged hyperchromatic nuclei of oligodendroglia with viral inclusions, atypical enlarged bizarre astrocytes, and a variable degree of lymphocytic inflammatory response.[1,2,5-7] Clinically, PML often presents with motor weakness, speech disturbances, visual impairment, and cognitive abnormalities.

Progressive multifocal leukoencephalopathy occurs in individuals severely immunocompromised by infection with human immunodeficiency virus (HIV), lymphoproliferative or myeloproliferative diseases, hematologic malignancies, various solid tumors, or treatment with immunosuppressant medication.[1,2] In recent years, HIV infection has become the dominant underlying disease associated with PML, which develops in approxi-

Table 1. Summary of Patient Information*

Case No./ Sex/Age, y	Predisposing Factor	Autopsy (A) or Biopsy (B)	Duration†	Comments
1B/M/39	Chronic myelogenous leukemia, immunosuppressant drugs	B	1 mo	Autopsy was 7 mo after biopsy
1A		A	7 mo	Cord blood transplantation in February 1999; GVHD‡; biopsy for PML in July 2000
2/M/65	Large cell undifferentiated lung carcinoma	A	10 d	...
3/M/32	HIV positive	B	ND	Inflammatory PML
4/M/40	HIV positive for 13 y	A	3 mo	Undergoing HAART for 4 mo
5/M/35	HIV positive	A	ND	Inflammatory PML
6/F/23	HIV positive for 4 y	A	2 mo	Died of bronchopneumonia
7/M/27	HIV positive	A	5 mo	...
8/42/M	HIV positive	A	8 mo	...

*HIV indicates human immunodeficiency virus; ND, no data available; GVHD, graft-vs-host disease; PML, progressive multifocal leukoencephalopathy; and HAART, highly active antiretroviral therapy.
†Duration of illness after first clinical presentation with PML symptoms before biopsy or autopsy.
‡Patient developed GVHD while taking immunosuppressant medication.

mately 3% of patients with acquired immunodeficiency syndrome (AIDS).[2,8-10]

The demyelination associated with PML is secondary to death of JCV-infected oligodendroglia. The mechanism of JCV-induced oligodendrocyte cell death is unknown. It is also unclear whether only infected oligodendrocytes die or whether virus can also induce death in neighboring uninfected cells (the bystander effect).

Apoptosis is a distinct form of cell death in which affected cells undergo characteristic morphologic and biochemical changes, including cytoplasmic shrinkage, condensation and fragmentation of nuclear chromatin, membrane alterations, and changes in gene and protein expression.[11,12] Almost all forms of apoptosis are associated with sequential activation of cysteine-aspartyl proteases (caspases) by extracellular and/or intracellular stimuli. These proteases cleave numerous cellular substrates, leading to oligonucleosomal DNA fragmentation and the other morphologic hallmarks of apoptosis.[13,14]

Apoptosis has been implicated in glial loss in demyelinating diseases, including multiple sclerosis[15-18] and experimental allergic encephalomyelitis.[19] Apoptosis also occurs in virus-induced demyelinating diseases as exemplified by Theiler virus infection[20,21] and measles virus–associated subacute sclerosing panencephalitis.[22] Apoptosis of glia and neurons also occurs following infection with a variety of other neurotropic viruses.[23-30] Given the propensity for several neurotropic viruses to cause apoptosis, we attempted to determine whether PML was also associated with apoptosis. Knowing the pivotal role of oligodendrocyte damage in demyelinating disorders, we hypothesized that apoptosis might be the mechanism of oligodendrocyte death in PML.

METHODS

PATIENT INFORMATION

The autopsy, surgical pathologic specimens, and consultation files in the pathology department of the University of Colorado Health Sciences Center, Denver, were searched for autopsy and surgical pathologic cases of PML diagnosed during the past 20 years (**Table 1**). Cases were excluded based on (1) insufficient volume of tissue available for analysis (as was the case for many stereotactic biopsy specimens) or (2) the lack of availability of paraffin tissue blocks for preparation of freshly cut sections. Eight cases were identified that met clinical and pathologic criteria for PML, including typical clinical and neuroimaging findings and the presence of demyelination, inclusion-bearing oligodendrocytes, and bizarre astrocytes. In all cases, JCV transcript was detected in brain tissue by in situ hybridization (ISH). One of the patients (case 1) had both biopsy and autopsy tissue available for study. Cases included 2 patients with non–HIV-associated PML (cases 1-2) and 6 patients (cases 3-8) with HIV-associated PML. Only one of the AIDS patients (case 4) was receiving highly active antiretroviral therapy (HAART) at the time of diagnosis of PML. Two patients with HIV-associated PML (cases 3 and 5) had pathologic evidence of inflammatory PML characterized by the presence of significant perivascular lymphocytic inflammation.[7]

JCV IN SITU HYBRIDIZATION

Sections were deparaffinized as described for immunohistochemical analysis. Tissue was digested with the enzyme Pronase I (Ventana Medical Systems Inc, Tucson, Ariz) (20 minutes at 37°C), washed in diethylpyrocarbonate-treated water, and then incubated with 50 to 100 mL of JCV probe (Enzo Biochem Inc, Farmingdale, NY) (2 hours at 37°C) prepared according to the manufacturer's instructions. Slides were then washed in Tris-buffered saline (TBS), immersed in prewarmed stringency wash (Dako Corporation, Carpinteria, Calif) (30 minutes at 48°C), rewashed in TBS, and then incubated with Strept-avidin/AP (Dako) (10 minutes at 37°C). Slides were then washed in TBS, incubated with nitroblue tetrazolium/NCIP substrate solution (Novocastra; Vector Laboratories Inc, Burlingame, Calif) (30 minutes at 37°C), washed in deionized water and counterstained with nuclear fast red (Dako), dehydrated in graded ethanols followed by xylene, and then permanently mounted.

IMMUNOHISTOCHEMICAL ANALYSIS FOR ACTIVATED CASPASE 3 AND CELL-TYPE SPECIFIC MARKERS

Brain tissue sections were deparaffinized by baking for 5 minutes at 57°C, immersion in mixed xylenes, then rehydrated in graded alcohols. Tissue sections then underwent antigen retrieval (10 mM citrate buffer, 10 minutes at 90°C) followed by incubation with 3% water (4 minutes at 37°C) and blocking with 5% normal goat serum in phosphate-buffered saline (PBS). Immunocytochemical analysis was performed using a pri-

mary antibody specific for the activated form of caspase 3 (Cell Signaling Technology Inc, Beverly, Mass) diluted 1:25 in PBS containing 3% bovine serum albumin (BSA; Sigma-Aldrich Corporation, St Louis, Mo) (30 minutes at 37°C). Binding of primary antibody was detected using biotinylated secondary antibody followed by avidin-HRPO (Ventana Medical Systems Inc), using diaminobenzidine (DAB; Ventana Medical Systems Inc) as substrate. Immediately following the DAB reaction, sections were incubated with the second primary antibody against CD3 or glial fibrillary acid protein (GFAP) (Dako), both at a 1:100 dilution. Binding of second primary antibodies was detected using biotin-avidin-alkaline phosphatase secondary antibody and labeling substrate. Sections were counterstained with Gills 2 (1:9 dilution, Ventana Medical Systems Inc). All reactions were performed using the automated staining system (Ventana Medical Systems Inc).

TUNEL

A biotin-streptavidin–based TUNEL (terminal deoxynucleotidyl transferase–mediated deoxyuridine triphosphate nick end in situ labeling) kit optimized for neuronal tissues was used (NeuroTACS II; Trevigen Inc; Gaithersburg, Md). Deparaffinized brain tissue sections were permeabilized with Neuropore (Trevigen Inc) (30 minutes at room temperature), then samples were incubated at 37°C with a mixture of terminal deoxynucleotidyl transferase (TdT), deoxynucleotriphosphates conjugated to biotin, Mn^{2+}, and TdT reaction buffer for 1 hour. After stopping the TdT reaction and washing, the tissues were incubated 30 minutes at room temperature with streptavidin-conjugated horseradish peroxidase, washed, immersed in DAB diluted in PBS solution for 5 minutes at room temperature, then counterstained with blue counterstain (Trevigen Inc). The DAB-stained samples were dehydrated in a series of ascending ethanol concentrations followed by mixed xylenes, air-dried, permanently mounted, and stored at room temperature until imaging.

DUAL-LABEL FLUORESCENCE WITH TUNEL AND A SINGLE ANTIBODY

Tissue sections were permeabilized with Neuropore, a nonproteolytic permeabilization and blocking reagent (Trevigen Inc) for 30 minutes at room temperature then washed in TBS (140 mM sodium chloride, 20 mM Tris, pH 7.6), and nonspecific binding was blocked with 2% BSA (Sigma-Aldrich Corporation) diluted in Neuropore for 30 minutes at room temperature, then incubated (overnight at 4°C) with antibody against SV40 large T antigen (Oncogene Research Products, San Diego, Calif) diluted in 1% BSA containing Neuropore. The next day, TUNEL reactions were performed as described herein, except that after stopping the TdT reaction and washing, the samples were incubated with a mixture of streptavidin-Cy3 (Jackson Immunoresearch Laboratories Inc, West Grove, Pa) to detect TUNEL and secondary antibody (1:100) conjugated to fluorescein isothiocyanate (Jackson Immunoresearch) to detect the SV40 antibody. Finally, samples were incubated with 100 ng/mL of Hoechst 33342 (Molecular Probes Inc, Eugene, Ore) for 10 minutes at room temperature in the dark as counterstain, washed in PBS, mounted with anti-fade media, and stored in the dark at −20°C until imaging.

RESULTS

In each patient, we assessed the presence or absence of apoptosis in cells from brain regions affected by PML as identified by histologic criteria and from brain regions that were remote from demyelinating lesions and appeared histologically normal. The CNS cells infected with JCV were easily identified by ISH using a JCV riboprobe in all 8 patients (**Figure 1**A and B). Apoptotic cells were detected in areas of PML lesions in all 8 patients but not in brain regions remote from these lesions (data not shown). There were no differences between the number and the distribution of apoptotic cells identified by TUNEL or the presence of activated caspase 3. Accumulation of viral particles in the nuclei of infected cells made it impossible to identify morphologic changes in the nucleus typically associated with apoptosis, such as nuclear pyknosis or karyorrhexis. Staining results from all patients studied are summarized in **Table 2**.

In all 8 cases, most apoptotic cells were identified as oligodendrocytes by their morphologic structure, location, and absence of GFAP immunohistochemical staining. These cells were most abundant at the periphery, rather than in the center, of demyelinated lesions (Figure 1C and D). The number of JCV-infected oligodendrocytes corresponded to the number of apoptotic cells, suggesting that nearly all apoptotic cells were JCV infected and that infection with JCV induced apoptosis. Both HIV-associated and non–HIV-associated cases were otherwise similar in the distribution and cell-type specificity of infection and apoptosis.

In case 1, from which both biopsy and autopsy tissue was available, the biopsy tissue showed many oligodendrocytes containing inclusions on hematoxylin-eosin–stained sections, which were positive for JCV by ISH and often apoptotic (**Figure 2**A and B). In contrast, in sections prepared from tissues obtained at autopsy 7 months later, significantly fewer infected oligodendrocytes were present, and apoptotic cells were more rare. In the autopsy samples, numerous bizarre astrocytes were identified in the lesions and about half of these were positive for JCV by ISH but were not apoptotic (Figure 2C and D). Neurons, normal astrocytes, and macrophages were not found to be JCV infected by ISH or apoptotic in any of the 8 cases examined.

In an effort to better define the nature of the apoptotic cells in PML lesions, we performed dual-label immunohistochemical analysis with caspase 3 and GFAP. Bizarre atypical astrocytes, reactive astrocytes, and normal-appearing astrocytes were all GFAP positive, yet these cells were not apoptotic. Atypical bizarre astrocytes but not normal-appearing or reactive astrocytes were frequently found to be positive for JCV infection by ISH (Figure 2D).

We also performed co-labeling for apoptosis (caspase 3 or TUNEL) and JCV infection. Serial tissue sections (4 mm apart) were examined for JCV-infected cells using antibody to SV40 large T-antigen and apoptotic cells (TUNEL). Unfortunately, because of technical incompatibility between the required protocols, it was not possible to perform TUNEL or caspase 3 immunocytochemical analysis on sections in which JCV infection was identified by ISH. Using combined SV40 T-antigen and apoptosis staining, we found several examples of dual-positive (antigen and TUNEL) cells (**Figure 3**). In all cases in which we performed dual staining, most cells positive for JCV T antigen were also TUNEL positive, sug-

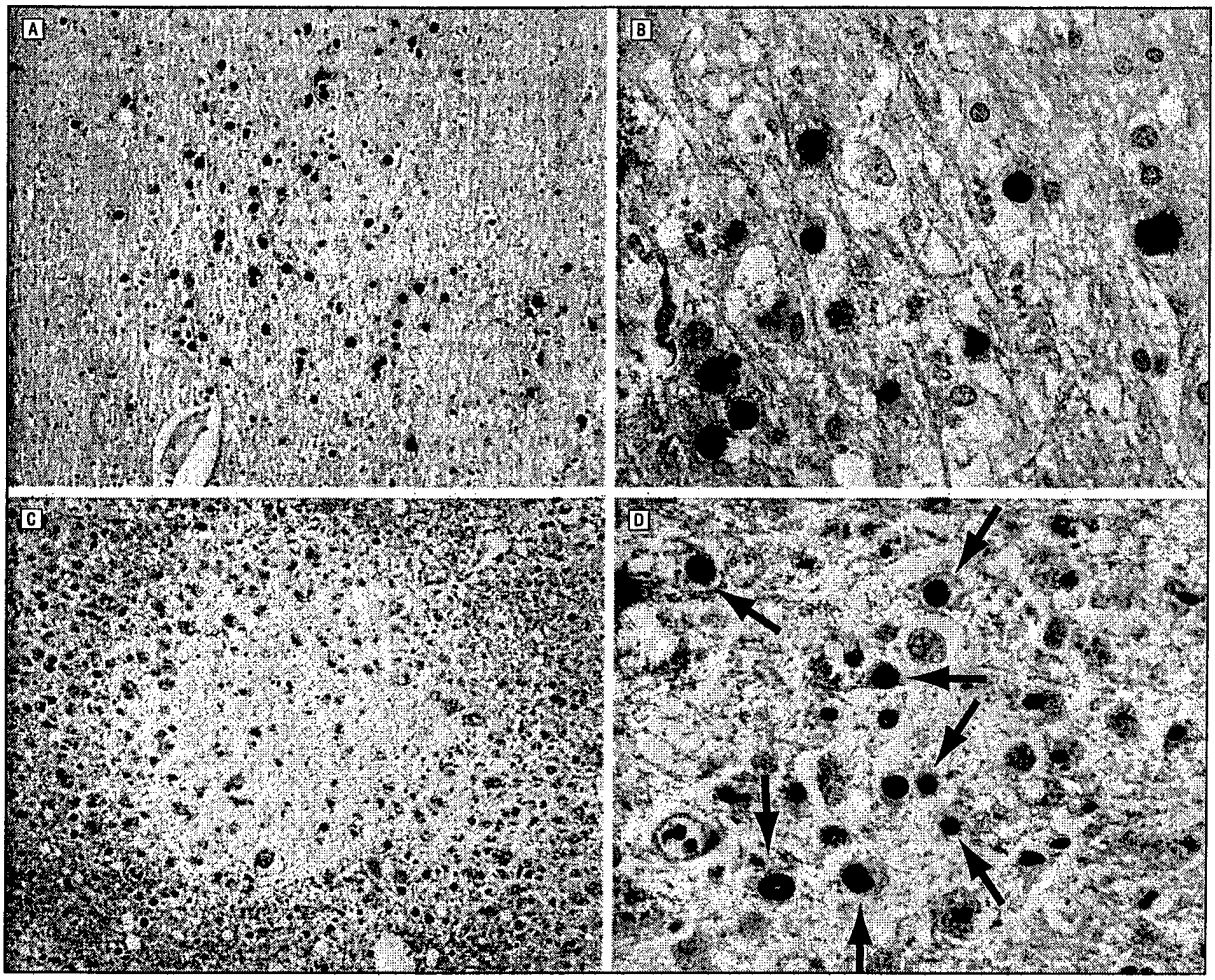

Figure 1. JC virus (JCV)-infected and apoptotic cells in progressive multifocal leukoencephalopathy (PML). Brain tissue sections from 2 patients with PML demonstrating numerous JCV-infected cells by in situ hybridization for JCV. Brain tissue cells that were JCV positive (dark blue) from case 5 (A) (original magnification ×100) and case 6 (B) (original magnification ×400). Tissue sections from 1 patient (D) (case 5) (original magnification ×400), demonstrating apoptotic oligodendrocytes (brown; arrows) detected by TUNEL (terminal deoxynucleotidyl transferase–mediated deoxyuridine triphosphate nick end in situ labeling), which are predominantly found at the periphery of lesions rather than in the demyelinated center where oligodendrocytes are absent (C) (original magnification ×100).

Table 2. Summary of Staining Results*

	JCV Infection			Apoptosis†				
	ISH			Oligodendrocytes		Astrocytes		
Case No.	Oligodendrocytes	Astrocytes	IHC	Lesional	Remote	Bizarre	Normal	Neurons
1A	+	+	+	+	–	+/–	–	–
1B	+	–	+	+	–	–	–	–
2	+	+	+	+	–	–	–	–
3	+	–	ND	+	–	–	–	–
4	+	+/–	+	+	–	–	–	–
5	+	–	+	+	–	+/–	–	–
6	+	+	+	+	–	–	–	–
7	+	+	+	+	–	–	–	–
8	+	–	+	+	–	–	–	–

*JCV indicates JC virus; ISH, in situ hybridization; IHC, immunohistochemical analysis; plus sign, positive; plus and minus sign, rare positive; minus sign, negative; and ND, not done.

†All cases showed apoptotic cells as identified by both the presence of the active fragment of caspase 3 and TUNEL (see Figure 1 footnote for expansion).

gesting that most productively infected cells were undergoing apoptosis. The rare examples of cells positive for T antigen and negative for TUNEL may represent a population of infected cells not yet undergoing apoptosis. The relative insensitivity of SV40 T-antigen staining compared with ISH (data not shown) for identifying JCV-

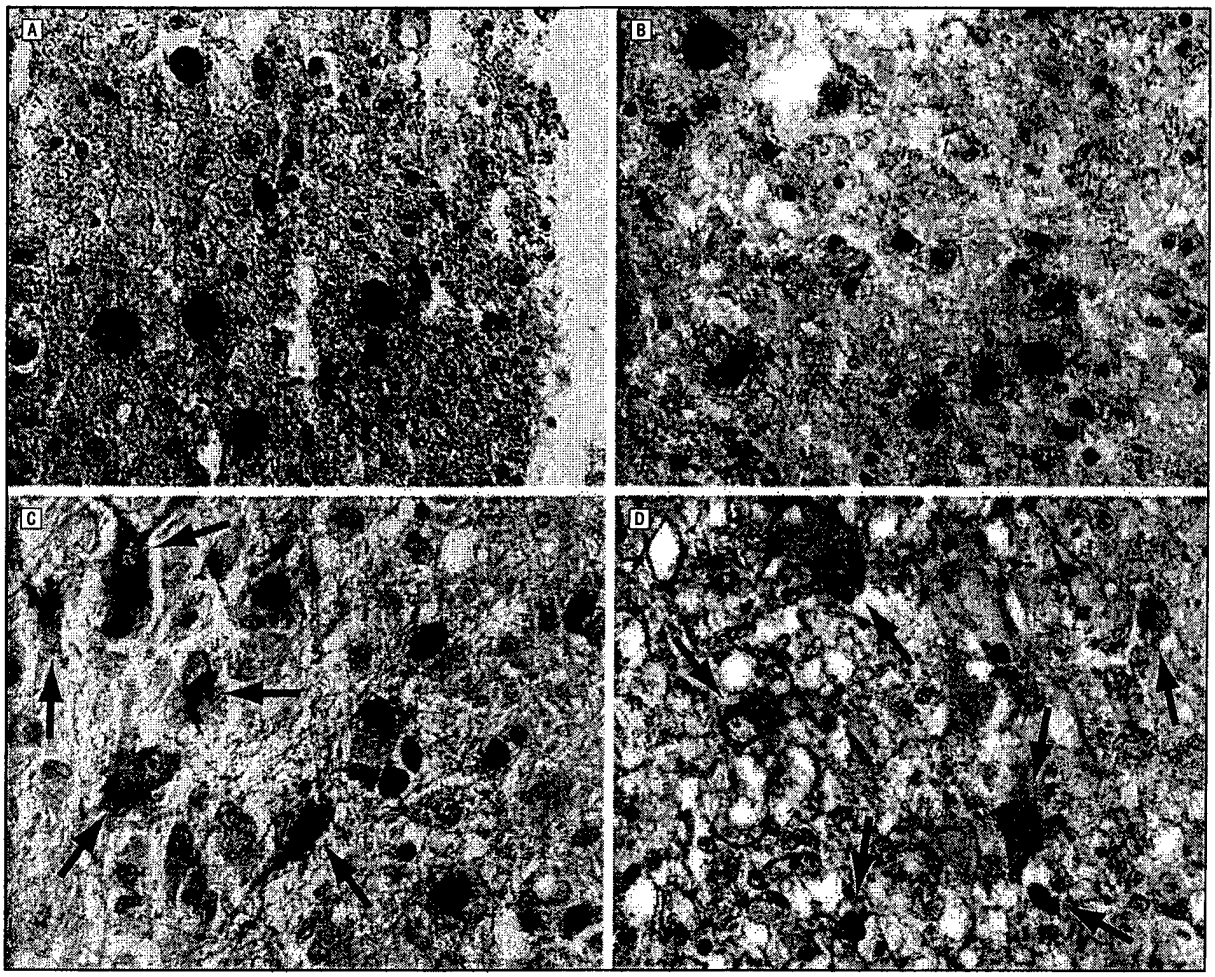

Figure 2. Oligodendrocytes containing viral inclusions were positive for JC virus (JCV) and apoptosis; in contrast, bizarre atypical astrocytes were occasionally JCV infected but were not apoptotic (original magnification ×400). Biopsy tissue sections from case 1, demonstrating oligodendrocytes positive for JCV transcripts (dark purple) (A) and apoptotic oligodendrocytes positive for activated caspase 3 (brown) (B). Autopsy tissue sections from case 1, demonstrating bizarre atypical astrocytes that were JCV infected (dark purple) (C). These bizarre atypical astrocytes were not apoptotic as demonstrated by dual-label immunohistochemical analysis showing no colocalization between glial fibrillary acid protein–positive (red; blue arrows) bizarre astrocytes and cells positive for activated caspase 3 (brown; black arrows) (D).

infected cells prevented accurate quantification of the percentage of infected cells that were also apoptotic and vice versa.

We next attempted to determine whether inflammatory cells were also undergoing apoptosis. We performed dual-label immunohistochemical analysis to detect CD3 and active caspase 3. The extent of inflammation was variable in AIDS and non-AIDS patients, although one AIDS patient (case 5) had a significant perivascular lymphocytic response consistent with the diagnosis of inflammatory PML.[7] Neither $CD3^+$ cells nor infiltrating macrophages were found to be JCV infected by ISH in any patient. Rare $CD3^+$ cells and $CD3^-$ lymphocyte-appearing cells (presumably B lymphocytes) were positive for activated caspase 3, indicating that apoptosis of these cells was occurring (data not shown). Apoptotic macrophages were not seen. There was no increase in the number of apoptotic cells in areas adjacent to lymphocytic collections, suggesting that the host immune response, regardless of its intensity, did not contribute significantly to apoptosis in other cells.

COMMENT

Our study demonstrates that apoptosis occurs in brain tissue of patients with both HIV-associated and non–HIV-associated PML. Apoptosis was limited almost exclusively to oligodendrocytes associated with demyelinated lesions. The number and distribution of apoptotic oligodendrocytes closely paralleled the number and distribution of infected oligodendrocytes as determined by JCV ISH, suggesting that apoptosis was the major mechanism responsible for cell death. Apoptosis as determined by TUNEL and immunohistochemical analysis for activated caspase 3 was rarely seen in the bizarre astrocytes present in PML lesions, even though these cells were JCV infected. Because only oligodendrocytes support productive JCV infection, this suggests that productive infection may be required for JCV-induced apoptosis.[31]

Apoptosis only occurred in cell types infected by JCV and was not seen in uninfected cells within PML lesions (eg, neurons) or in any cells in areas of the brain remote

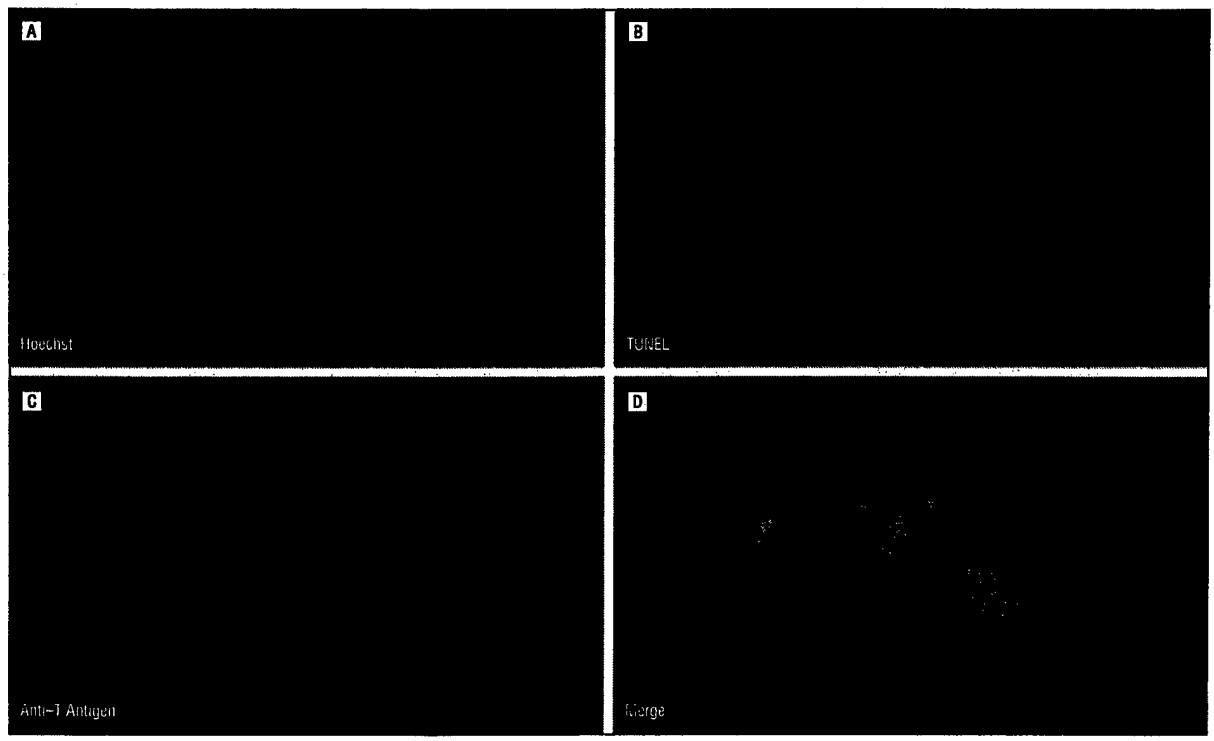

Figure 3. Apoptotic cells were also positive for viral T antigen (original magnification ×400). Dual-label immunohistochemical analysis and TUNEL (terminal deoxynucleotidyl transferase–mediated deoxyuridine triphosphate nick end in situ labeling) in a tissue section from case 7, demonstrating that infected cells (green; anti-SV40 large T antigen) are undergoing apoptosis (red; TUNEL). These double-labeled cells appear yellow in the merged image. Hoechst 33342 chromatin dye (blue) is the counterstain.

from demyelinative lesions. This indicates that apoptosis occurs as a direct consequence of viral infection and is not an indirect consequence of the severity of patient illness or other associated factors, such as hypoxia, hypotension, or ischemia. This is further supported by a previous study that indicated that JCV-infected oligodendrocytes overexpress p53 and Bax (a proapoptotic protein) and do not express Bcl-2 (an antiapoptotic protein).[32] Apoptosis also did not correlate with the degree of the host inflammatory response, although occasional infiltrating lymphocytes were found to be apoptotic.

Although our study clearly indicates that apoptosis is a major mechanism of oligodendrocyte death in PML, there are some potential limitations in our study. For example, we used biochemical rather than morphologic markers to identify apoptotic cells, because it was difficult to accurately evaluate nuclear pyknosis and karyorrhexis in JCV-infected cells due to the concomitant presence of potentially confounding virus-induced changes in the nucleus. In addition, the absence of specific markers for necrotic cell death comparable to those used to detect apoptosis meant that it was not possible to accurately quantify the relative contribution of apoptosis and necrosis to oligodendrocyte death. However, our finding that most cells positive for JCV T antigen are also undergoing apoptosis strongly suggests that it is apoptosis rather than necrosis that is the primary mechanism of oligodendrocyte cell death in JCV-infected cells in PML lesions.

We did not find significant differences in apoptosis between AIDS and non-AIDS patients or among patients with variable PML-associated inflammatory responses. Two patients with prolonged survival, including an AIDS patient who received HAART (case 4) and a non-AIDS patient (case 1), had increased numbers of infected atypical bizarre astrocytes and a reduced number of infected oligodendrocytes as determined by JCV ISH in autopsy tissue. The reduction in infected oligodendrocytes may be a consequence of HAART and/or prolonged survival with the disease.[33-35]

Oligodendrocyte death is the key initiating event responsible for the demyelination that is the cardinal pathologic feature of PML. We now show that JCV-infected oligodendrocytes die as a result of apoptosis. Elucidating the specific cellular pathways associated with JCV-induced oligodendrocyte apoptosis may reveal novel targets for therapy of this devastating disease. Most apoptotic signaling pathways involve activation of caspase cascades that originate with pathway-specific initiator caspases (eg, caspase 8 and 9), which converge on common downstream effector caspases (eg, caspase 3).[11,13,14,36] Effector caspases in turn act on cellular substrates to induce the morphologic changes in cellular membranes, cytoskeletal proteins, and chromatin that are the hallmarks of irreversible commitment to cell death. It is conceivable that if caspase activation could be inhibited at an early stage then some JCV-infected oligodendrocytes may be able to recover and survive. Support for the feasibility of this strategy comes from studies in which caspase inhibitors have been used successfully to protect neurons from apoptosis triggered by a variety of inciting stimuli, both in vivo and in vitro.[37-42]

Accepted for publication August 1, 2002.

Author contributions: *Study concept and design* (Ms Richardson-Burns and Drs Kleinschmidt-DeMasters, DeBiasi, and Tyler); *acquisition of data* (Ms Richardson-Burns); *analysis and interpretation of data* (Ms Richardson-Burns and Drs Kleinschmidt-DeMasters, DeBiasi, and Tyler); *drafting of the manuscript* (Ms Richardson-Burns and Drs DeBiasi and Tyler); *critical revision of the manuscript for important intellectual content* (Ms Richardson-Burns and Drs Kleinschmidt-DeMasters, DeBiasi, and Tyler); *statistical expertise* (Ms Richardson-Burns and Drs Kleinschmidt-DeMasters, DeBiasi, and Tyler); *obtained funding* (Dr Tyler); *administrative, technical, and material support* (Ms Richardson-Burns and Drs Kleinschmidt-DeMasters, DeBiasi, and Tyler); *study supervision* (Drs Kleinschmidt-DeMasters, DeBiasi, and Tyler).

This study was supported by grant DAMD 17-98-1-8614 from the US Army Medical Research and Material Command (Fort Detrick, Md), MERIT and REAP Awards from the Department of Veterans Affairs (Washington, DC), grant 1R01AG14071 from the National Institutes of Health (Bethesda, Md), and the Reuler-Lewin Family Professorship of Neurology (Denver, Colo).

We thank Traci D. Sachs, BA, for expert histologic assistance and Ron Bouchard, BA, for microscopy and digital imaging assistance.

Corresponding author and reprints: Kenneth L. Tyler, MD, Department of Neurology (B-182), University of Colorado Health Sciences Center, 4200 E Ninth Ave, Denver, CO 80262 (e-mail: ken.tyler@uchsc.edu).

REFERENCES

1. Brooks BR, Walker DL. Progressive multifocal leukoencephalopathy. *Neurol Clin.* 1984;2:299-313.
2. Berger JR, Major EO. Progressive multifocal leukoencephalopathy. *Semin Neurol.* 1999;19:193-200.
3. Berger JR, Concha M. Progressive multifocal leukoencephalopathy: the evolution of a disease once considered rare. *J Neurovirol.* 1995;1:5-18.
4. Berger JR, Kaszovitz B, Post MJ, Dickinson G. Progressive multifocal leukoencephalopathy associated with human immunodeficiency virus infection: a review of the literature with a report of sixteen cases. *Ann Intern Med.* 1987;107:78-87.
5. Weber F, Goldmann C, Kramer M, et al. Cellular and humoral immune response in progressive multifocal leukoencephalopathy. *Ann Neurol.* 2001;49:636-642.
6. Major EO, Amemiya K, Tornatore CS, Houff SA, Berger JR. Pathogenesis and molecular biology of progressive multifocal leukoencephalopathy, the JC virus-induced demyelinating disease of the human brain. *Clin Microbiol Rev.* 1992;5:49-73.
7. Hair LS, Nuovo G, Powers JM, Sisti MB, Britton CB, Miller JR. Progressive multifocal leukoencephalopathy in patients with human immunodeficiency virus. *Hum Pathol.* 1992;23:663-667.
8. Hou J, Major EO. Progressive multifocal leukoencephalopathy: JC virus induced demyelination in the immune compromised host. *J Neurovirol.* 2000;6(suppl 2):S98-S100.
9. Krupp LB, Lipton RB, Swerdlow ML, Leeds NE, Llena J. Progressive multifocal leukoencephalopathy: clinical and radiographic features. *Ann Neurol.* 1985;17:344-349.
10. Dworkin MS, Wan PC, Hanson DL, Jones JL. Progressive multifocal leukoencephalopathy: improved survival of human immunodeficiency virus-infected patients in the protease inhibitor era. *J Infect Dis.* 1999;180:621-625.
11. Reed JC. Mechanisms of apoptosis. *Am J Pathol.* 2000;157:1415-1430.
12. Hengartner MO. The biochemistry of apoptosis. *Nature.* 2000;407:770-776.
13. Earnshaw WC, Martins LM, Kaufmann SH. Mammalian caspases: structure, activation, substrates, and functions during apoptosis. *Annu Rev Biochem.* 1999;68:383-424.
14. Nunez G, Benedict MA, Hu Y, Inohara N. Caspases: the proteases of the apoptotic pathway. *Oncogene.* 1998;17:3237-3245.
15. Segal BM, Cross AH. Fas(t) track to apoptosis in MS: TNF receptors may suppress or potentiate CNS demyelination. *Neurology.* 2000;55:906-907.
16. Bonetti B, Stegagno C, Cannella B, Rizzuto N, Moretto G, Raine CS. Activation of NF-kappaB and c-jun transcription factors in multiple sclerosis lesions: implications for oligodendrocyte pathology. *Am J Pathol.* 1999;155:1433-1438.
17. Lucchinetti CF, Bruck W, Rodriguez M, Lassmann H. Distinct patterns of multiple sclerosis pathology indicates heterogeneity on pathogenesis. *Brain Pathol.* 1996;6:259-274.
18. Rodriguez M, Lucchinetti CF. Is apoptotic death of the oligodendrocyte a critical event in the pathogenesis of multiple sclerosis? *Neurology.* 1999;53:1615-1616.
19. Pender MP, Nguyen KB, McCombe PA, Kerr JF. Apoptosis in the nervous system in experimental allergic encephalomyelitis. *J Neurol Sci.* 1991;104:81-87.
20. Tsunoda I, Kurtz CI, Fujinami RS. Apoptosis in acute and chronic central nervous system disease induced by Theiler's murine encephalomyelitis virus. *Virology.* 1997;228:388-393.
21. Zheng L, Calenoff MA, Dal Canto MC. Astrocytes, not microglia, are the main cells responsible for viral persistence in Theiler's murine encephalomyelitis virus infection leading to demyelination. *J Neuroimmunol.* 2001;118:256-267.
22. Anlar B, Soylemezoglu F, Elibol B, et al. Apoptosis in brain biopsies of subacute sclerosing panencephalitis patients. *Neuropediatrics.* 1999;30:239-242.
23. Petito CK, Roberts B. Evidence of apoptotic cell death in HIV encephalitis. *Am J Pathol.* 1995;146:1121-1130.
24. Kaul M, Garden GA, Lipton SA. Pathways to neuronal injury and apoptosis in HIV-associated dementia. *Nature.* 2001;410:988-994.
25. Pekosz A, Phillips J, Pleasure D, Merry D, Gonzalez-Scarano F. Induction of apoptosis by La Crosse virus infection and role of neuronal differentiation and human bcl-2 expression in its prevention. *J Virol.* 1996;70:5329-5335.
26. Jackson AC, Rossiter JP. Apoptotic cell death is an important cause of neuronal injury in experimental Venezuelan equine encephalitis virus infection of mice. *Acta Neuropathol (Berl).* 1997;93:349-353.
27. Nava VE, Rosen A, Veliuona MA, Clem RJ, Levine B, Hardwick JM. Sindbis virus induces apoptosis through a caspase-dependent, CrmA-sensitive pathway. *J Virol.* 1998;72:452-459.
28. Oberhaus SM, Smith RL, Clayton GH, Dermody TS, Tyler KL. Reovirus infection and tissue injury in the mouse central nervous system are associated with apoptosis. *J Virol.* 1997;71:2100-2106.
29. Jackson AC, Rossiter JP. Apoptosis plays an important role in experimental rabies virus infection. *J Virol.* 1997;71:5603-5607.
30. Schobesberger M, Zurbriggen A, Summerfield A, Vandevelde M, Griot C. Oligodendroglial degeneration in distemper: apoptosis or necrosis? *Acta Neuropathol (Berl).* 1999;97:279-287.
31. Tretiakova A, Krynska B, Gordon J, Khalili K. Human neurotropic JC virus early protein deregulates glial cell cycle pathway and impairs cell differentiation. *J Neurosci Res.* 1999;55:588-599.
32. Yang B, Prayson RA. Expression of Bax, Bcl-2, and P53 in progressive multifocal leukoencephalopathy. *Mod Pathol.* 2000;13:1115-1120.
33. Clifford DB, Yiannoutsos C, Glicksman M, et al. HAART improves prognosis in HIV-associated progressive multifocal leukoencephalopathy. *Neurology.* 1999;52:623-625.
34. Cinque P, Pierotti C, Vigano MG, et al. The good and evil of HAART in HIV-related progressive multifocal leukoencephalopathy. *J Neurovirol.* 2001;7:358-363.
35. Antinori A, Ammassari A, Giancola ML, et al. Epidemiology and prognosis of AIDS-associated progressive multifocal leukoencephalopathy in the HAART era. *J Neurovirol.* 2001;7:323-328.
36. Thornberry NA, Lazebnik Y. Caspases: enemies within. *Science.* 1998;281:1312-1316.
37. Kondratyev A, Gale K. Intracerebral injection of caspase-3 inhibitor prevents neuronal apoptosis after kainic acid-evoked status epilepticus. *Brain Res Mol Brain Res.* 2000;75:216-224.
38. Ma J, Endres M, Moskowitz MA. Synergistic effects of caspase inhibitors and MK-801 in brain injury after transient focal cerebral ischaemia in mice. *Br J Pharmacol.* 1998;124:756-762.
39. Hara H, Friedlander RM, Gagliardini V, et al. Inhibition of interleukin 1beta converting enzyme family proteases reduces ischemic and excitotoxic neuronal damage. *Proc Natl Acad Sci U S A.* 1997;94:2007-2012.
40. Cheng Y, Deshmukh M, D'Costa A, et al. Caspase inhibitor affords neuroprotection with delayed administration in a rat model of neonatal hypoxic-ischemic brain injury. *J Clin Invest.* 1998;101:1992-1999.
41. Ray AM, Owen DE, Evans ML, Davis JB, Benham CD. Caspase inhibitors are functionally neuroprotective against oxygen glucose deprivation induced CA1 death in rat organotypic hippocampal slices. *Brain Res.* 2000;867:62-69.
42. Jiang D, Jha N, Boonplueang R, Andersen JK. Caspase 3 inhibition attenuates hydrogen peroxide-induced DNA fragmentation but not cell death in neuronal PC12 cells. *J Neurochem.* 2001;76:1745-1755.

Central Nervous System Apoptosis in Human Herpes Simplex Virus and Cytomegalovirus Encephalitis

Roberta L. DeBiasi,[1,2] B. K. Kleinschmidt-DeMasters,[2,3] Sarah Richardson-Burns,[7] and Kenneth L. Tyler[2,4,5,6]

Departments of [1]Pediatrics, [2]Neurology, [3]Pathology, [4]Microbiology, [5]Immunology, [6]Medicine, and [7]Neuroscience, University of Colorado Health Sciences Center, and the Denver Veterans Administration Hospital, Denver

Central nervous system (CNS) specimens from 10 immunocompetent patients with herpes simplex encephalitis (HSE) and 3 infants with congenital cytomegalovirus (CMV) encephalitis were analyzed to determine whether apoptosis is a feature of CNS injury in these patients. Apoptotic neurons and glia were detected in significant numbers in acute HSE and CMV encephalitis. Occurring predominantly in areas of productive viral infection, apoptosis appeared to result from direct viral injury to neurons and was not dependent on inflammatory T cell responses. In contrast to patients with acute cases, patients with late sequelae of HSE or CMV had no detectable virus and minimal neuronal or glial apoptosis, regardless of the degree of inflammation. This is the first demonstration of apoptotic neuronal death in humans with HSE. These results suggest that neuronal apoptosis is an important contributing factor to acute CNS injury and may serve as a novel therapeutic target in these patients.

Apoptosis is a distinct mechanism of cellular death which has been increasingly implicated in the pathogenesis of a wide variety of acute and chronic neurological diseases, including stroke, epilepsy, traumatic brain injury, and neurodegenerative diseases [1–3]. Apoptosis is also an important virus-induced mechanism of neuronal injury and death in infected neuronal cell cultures in vitro and in experimental models of viral central nervous system (CNS) in vivo infection [4, 5]. Among neurotropic viruses that have been shown to induce neuronal and/or glial apoptosis are arboviruses [6–13], bornaviruses [14], herpesviruses [15], lentiviruses [16, 17], paramyxoviruses [18–20], reoviruses [21], picornaviruses [22], rhabdoviruses [23–25], and togaviruses [26–32]. Despite the wealth of evidence supporting the importance of apoptotic cell death in experimental systems, its importance as a mechanism of cellular and tissue injury during human CNS viral infection remains poorly understood.

Received 9 May 2002; revised 1 August 2002; electronically published 11 November 2002.

Presented in part: 54th annual meeting of the American Academy of Neurology, April 2002, Denver, Colorado (abstract P04.003).

Human experimentation guidelines of the institutional review board of the University of Colorado Health Sciences Center were followed in the conduct of this study.

Financial support: Department of Veterans Affairs (Merit, Career Development and Research Enhancement Award Program grants to R.D.B. and K.L.T.); the US Army (Department of the Army Medical Research and Development 17-98-8614 to K.L.T. and B.K.D.); the National Institutes of Health (grant RO1 AG1407 to K.L.T.); the Infectious Diseases Society of America Ortho-McNeil Young Investigator Award (to R.D.B.); Reulen-Lewin Family Professorship in Neurology (to K.L.T.).

Reprints or correspondence: Dr. Kenneth L. Tyler, Dept. of Neurology (B-182), University of Colorado Health Sciences Center, 4200 E. 9th Ave., Denver, CO 80262 (ken.tyler@uchsc.edu).

The Journal of Infectious Diseases 2002;186:1547–57

0022-1899/2002/18611-0002$15.00

Studies of virus-induced apoptosis in the human CNS has largely been limited to evaluation of immunodeficient patients with human immunodeficiency virus (HIV)–associated neurological deficits [33–42]. To our knowledge, the only other viral infection in which apoptosis has been evaluated in human CNS tissues is in patients with subacute sclerosing panencephalitis (SSPE) following measles virus infection [43]. Although virus has been directly implicated in neuronal and/or glial apoptotic death in patients with HIV or SSPE, these findings are not clearly applicable to the more common situation of acute encephalitides affecting immunocompetent hosts, because, in both HIV-associated CNS disease and SSPE, it is difficult to separate the impact of an altered immune response from the direct effects of acute viral infection on neuronal and/or glial cells.

The focus or our study was to investigate whether apoptosis is an important mechanism of CNS damage in immunocompetent patients suffering from herpes simplex virus (HSV) encephalitis and infants with congenital cytomegalovisu (CMV) encephalitis, 2 of the most common causes of acute viral encephalitis in nonimmunocompromised hosts. Herpes simplex encephalitis (HSE) has classically been described as a necrotizing process; however, this designation antedated understanding of the distinction between necrotic and apoptotic cellular death. Significant advances in our understanding of the pathogenesis of this disease have occurred in the past decade, but, despite the availability of acyclovir therapy, clinical outcomes from HSE are still suboptimal, with 20% mortality and 40% prevalence of resultant neurologic deficits in affected patients [44]. Multiple investigators have confirmed the apoptosis-modulating effects (both pro- and antiapoptotic) of HSV infection and gene products in various cell lines in vitro [45–52], including neurons [53, 54]. Neuronal apoptosis has also been shown to

occur in HSV-infected animals [15, 55], but the role of apoptosis in HSV-induced CNS damage in humans remains unknown.

CMV infection is the most common congenital infection affecting humans, creating a risk of severe injury to the infected fetus [56]. Up to 10% of infants born to mothers with primary CMV infection are symptomatic at birth: 10% of symptomatic infants die, and 80% of survivors suffer severe neurological morbidity (9000 infants each year in the United States) [57, 58]. CMV encephalitis is also an important opportunistic infection in HIV-infected patients but is rarely recognized in immunocompetent adults and older children, whose immune systems are more developed than that of newborn infants [59]. Pathologically, encephalitis occurs in a periventricular pattern and may further cause polymicrogyria and hydrocephalus. Multiple investigators have identified both pro- and antiapoptotic effects of CMV infection and gene products in a variety of cell lines in vitro [60–67], which include neurons [68, 69]. The study of murine CMV infection in the developing mouse brain in vivo has revealed apoptosis in microglia/macrophages and uninfected cells to a greater degree than in infected cells [70], but a murine model of CMV retinitis has revealed significant apoptosis of both infected and uninfected cells [71]. A study of apoptosis in humans with CMV infection has been limited to HIV patients with CMV retinitis, in which apoptosis was found to contribute significantly to retinal cell loss [72]. There have been no attempts to determine the role of apoptosis in the CNS damage characteristic of infants suffering from congenital CMV CNS infection. This study is the first demonstration of CNS apoptosis in patients with acute HSE and congenital CMV infection.

Subjects, Materials, and Methods

Specimen Selection and Patient Description

Case subject. Archived autopsy and surgical biopsy CNS tissues were collected from case subjects with human HSV and CMV encephalitis in immunocompetent hosts from University of Colorado Health Sciences Center–affiliated hospitals. Case subjects were carefully chosen to include only those in which a definitive diagnosis of specific viral infection had been previously confirmed by culture, polymerase chain reaction (PCR), or detection of viral antigen in brain tissue. In some cases, supportive serologic studies or culture of virus from other sites were available. Only well-studied case subjects with definitive diagnoses were included for analysis in this study. Furthermore, only case subjects for which adequate amounts of tissue remained for serial sectioning, as described below, and with adequate preservation for immunohistochemical analysis were included.

The majority of acute HSV cases occurred in children and young adults with no known underlying disease or other predisposing factor. One case occurred in an individual being treated with combination drug therapy for atypical mycobacterial pulmonary infection. Although no specific immunologic deficit could be identified in this patient, the neuropathological features were similar to those reported in HSV-infected immunocompromised individuals. In these patients, it has been noted that there is a lack of inflammatory cell response and widespread pseudoischemic neuronal changes in association with large numbers of viral bearing cells [73]. We chose to include this case because it provided a rare opportunity to assess apoptosis in the absence of an inflammatory response.

The CMV cases analyzed were all congenital CMV infections, since immunocompetent adults are only rarely affected [59]. CMV infections in immunocompromised patients, including those with underlying HIV infection or malignancy, were specifically excluded.

In addition to selecting patients with acute HSV and CMV CNS infection, we also wished to analyze patients with neurologic sequelae occurring months to years after severe CNS herpetic infection, to assess the potential persistence of apoptotic injury. Three such patients with remote HSV infection were identified, with CNS abnormalities consisting of severe neuronal loss, gliosis, and cavitation in bilateral temporal lobes, as well as varying degrees of persistent lymphocytic inflammation. Two patients were identified with subacute and remote CMV infection (weeks to years following acquisition of virus), both of whom had severe gyral anomalies. Demographic and clinical information for these patients is summarized in table 1.

Exclusions. Cases in immunocompromised individuals were specifically excluded, including those in which the patient had 1 of the 3 most common immunocompromising conditions: congenital immunodeficiency, underlying malignancy, or HIV infection. We felt that it was particularly important to exclude HIV-infected patients with secondary herpetic infection, since it would be difficult to discern the specific contribution of each virus in the pathogenic process. Case subjects were also rejected because of inadequacy of tissue samples available for sequential sectioning or tissues with compromised integrity that precluded immunohistochemical analysis.

Control cases. Control cases, as described above, included patients in whom infection was clearly implicated by the above criteria but in whom infection was remote at the time biopsy/autopsy tissue was obtained. Additional control cases included assessment of baseline neuronal apoptosis in normal autopsy brain tissues (normal hippocampus) from patients at various ages of neurodevelopment (infancy to late adulthood). This was important for interpretation of the significance of occasional apoptotic neuronal/glial cells noted in some remotely-infected patients, as well as for determination of baseline age/developmental stage-specific neuronal/glial apoptosis levels in uninfected patients.

Immunohistochemical Evaluation

A protocol of serial sectioning was undertaken from each tissue block, so that mirror-image sections could be assessed for specific virus, presence of apoptosis, and presence of inflammatory T cells. Consecutive sections were cut (4 μm thick) from formalin-fixed, paraffin-embedded tissue blocks. When available, multiple sections (up to 5) from a given case patient were analyzed as a further experimental control, including areas both histologically involved and uninvolved in the infectious process. Sections were deparaffinized and rehydrated using standard methods and then evaluated

Table 1. Demographic and clinical summary of patients with herpes simplex virus (HSV) and cytomegalovirus (CMV) central nervous system infection.

Virus, disease stage, patient	Age, sex	Clinical summary
HSV		
Acute		
1	19 months, M	Seizures and coma (encephalitis)
2	8 years, M	Encephalitis
3	12 years, F	Fever, seizures 27 days after traumatic brain injury
4	17 years, M	Meningoencephalitis
5	19 years, M	Right temporal lobe mass and edema with near-herniation
6	66 years, M	Fever, altered mental status, focal and generalized seizures, focal neurologic findings after 10-year history of pulmonary atypical mycobacteria disease while receiving chronic medication regimen
7	72 years, F	Edematous right hemisphere after *Escherichia coli* sepsis
Remote		
8	25 years, F	Persistent seizure disorder and hemiparesis (HSE 12 years before)
9	68 years, F	Postherpetic neurologic deficits, language and memory deficits, confusion, gait disturbance (HSE 1 year before)
10	85 years, F	Postherpetic encephalitis dementia, aggressive behavior (HSE 3 years before)
CMV		
Acute		
11	25-week EGA fetus, M	Congenital CMV infection with oligohydramnios, fetal ascites, hydrocephalus, multiple intracranial hemorrhages first noted 1 week prior to TAB
Subacute		
12	23-week EGA fetus, F	Congenital CMV infection with oligohydramnios, fetal ascites, hepatomegaly with extramedullary hematopoesis, and polymicrogyria; high maternal CMV IgG with negative IgM, suggesting infection approximately 6–8 weeks prior to testing
Remote		
13	3 years, F	Previous congenital CMV infection with resultant hydrocephalus, left hemispheric atrophy, micropolygyria, profound retardation, deafness, blindness, spastic quadriplegia; symptomatic since 1 day of age

NOTE. EGA, estimated gestational age; HSE, herpes simplex encephalitis; TAB, therapeutic abortion.

by the following techniques by at least 2 independent observers in a blinded fashion.

Hematoxylin-eosin (HE) stain. A standard protocol was utilized for general histological definition, evidence of viral inclusion bodies (Cowdry A), inflammatory T cell infiltrate, and anoxic damage.

Virus-specific immunohistochemistry. We analyzed all sections for the presence and distribution of specific productive viral infection. After antigen retrieval (sections microwaved for 4 min in citrate buffer) and blockade of endogenous peroxidase activity (3% H_2O_2 for 4 min at 37°C), sections were incubated in either HSV-specific antibody which recognizes HSV-1 and -2 (B0114/B0116, DAKO; 1:800 dilution, 32 min at 37°C) or CMV-specific antibody (MAB-012D, BioMeda; prediluted, 32 min at 37° C). Sections were probed with avidin-horseradish peroxidase (Avidin-HRPO, Ventana Medical Systems). We visualized labeling by use of diaminobenzadine peroxidase substrate (Ventana) and counterstained using Gill's #2 (1:9 dilution for 4 min at 37°C). All reactions were performed on a Ventana Automated Staining System. Positive and negative control cases were included for all reactions.

Activated caspase-3/CD3 (pan–T-cell marker) immunohistochemistry (double labeling). To simultaneously identify inflammatory T cells within sections and determine whether these were a separate or identical population of cells showing evidence of apoptosis, we performed immunohistochemical colabeling on all sections using antibody directed against CD3, a pan–T-cell marker (A0452, DAKO), in conjunction with antibody directed against cleaved (activated) caspase-3 (Asp-175, Cell Signaling Technology). Caspase-3 is a cysteine protease that plays a central role in apoptosis. The presence of activated caspase-3 is a sensitive and specific marker of apoptosis. After antigen unmasking and blockade of endogenous peroxidase activity, sections were blocked and then incubated in cleaved caspase-3 antibody (1:25 dilution in blocking solution for 32 min at 37°C). Biotinylated universal antibody (Ventana) was used as secondary antiserum (8 min at 37°C). Sections were probed with avidin-HRPO (Ventana; 8 min at 37°C). We visualized activated caspase-3 labeling using diaminobenzadine peroxidase substrate (DAB; Ventana). Immediately after this step, sections were incubated with CD3 antibody (1:100 dilution; 32 min at 37°C). Biotinylated universal antibody (Ventana) was used as secondary antiserum (8 min at 37°C). We visualized labeling by CD3 antibody using the Enhanced Alkaline-phosphatase red kit (Ventana). Sections were counterstained with hematoxylin. All steps were performed on a Ventana Automated Staining System. Positive and negative control cases were used for all reactions.

TUNEL. We analyzed all sections for evidence of DNA fragmentation consistent with apoptotic cleavage by using in situ TUNEL (NeuroTacs II system; Trevigen). Terminal deoxynucleotidyl transferase (TdT) was utilized to incorporate biotinylated nucleotides at the sites of DNA breaks, which are characteristic of apoptosis. We made permeable sections with Proteinase K at a 1:400 dilution, diluted in a 50:50 mixture of PBS and Neuropore for 20 min at 37° C. Following the TdT-enzyme dependent step (1 h incubation at 37°C using coverslips and a humidified chamber), we treated sections with streptavidin-HRP for 20 minutes and visualized with DAB for 1–5 min. Blue counterstain was utilized to effectively visualize background cellular architecture. We performed a TdT-enzyme negative control case on all TUNEL runs to ensure that resultant brown staining was truly indicative of being TdT-dependent, rather than nonspecific background labeling.

Technical Issues/Control Cases

To ensure accurate interpretation of all immunohistochemical analyses described above, multiple negative controls were included in conjunction with all staining procedures for each evaluated case. Negative control sections were treated identically to sections for analysis within the same run, with the exception of the key enzyme or antibody required for specific immunoreactivity (i.e., anti-CD3 antibody, anti-cleaved caspase-3 antibody, TdT enzyme). As an additional negative control, uninvolved tissue sections from diseased patients (when available) were evaluated in conjunction with their respective involved tissue sections. All such controls were appropriately negative for viral antigen, activated caspase-3, and TUNEL.

Results

Apoptosis in HSE in association with productive viral infection. We evaluated 7 patients with acute HSE. Six (86%) of 7 had clear evidence of neuronal and glial apoptosis, as demonstrated by TUNEL and/or activated caspase-3 staining (table 2), with a high degree of congruity noted using both apoptosis detection methods. Apoptotic cells were unequivocally identified as neurons or glia by morphologic characteristics. Neurons made up a larger proportion of apoptotic cells, compared with glial cells. Apoptotic cells did not exhibit late morphologic features of apoptosis (nuclear condensation, margination, or pyknosis), suggesting apoptosis was detected at a relatively early stage at the time that tissues were obtained. Apoptotic cells were restricted predominantly to areas of productive viral infection and did not occur as a widespread, nonspecific process in histologically or virologically uninvolved areas within the same tissue section. Apoptotic neurons and glia were detected in acutely infected patients in regions of disrupted CNS tissue bearing HSV antigen, as measured by TUNEL (figure 1*A–C*) and/or activated caspase-3 (table 2). In contrast, evaluation of separate areas of anoxic tissue damage in these same patients showed no evidence of productive HSV infection or apoptotic damage, as measured by TUNEL (figure 1*D–F*) and active caspase-3 staining.

We also evaluated 3 patients with well-documented HSE infection occurring 1–12 years before biopsy or autopsy with chronic neurologic deficits, including dementia, aggressive behavior, language and memory deficits, gait disturbances, and seizure disorder with hemiparesis. Although all patients had histologically abnormal areas of CNS tissue evident by HE stain, none had evidence of ongoing productive viral infection with HSV (as demonstrated by negative HSV specific immunostain). In contrast to acutely infected patients, none of these 3 patients had significant apoptosis, as evidenced by TUNEL (figure 1*G–I*) or activated caspase-3 staining (table 2).

Apoptosis in congenital CMV CNS disease in association with productive viral infection. We analyzed tissues from a patient

Table 2. Results summary of patients with herpes simplex virus (HSV) and cytomegalovirus (CMV) central nervous system infection.

Virus, disease stage, patient	HE	Viral immunostain	CD3	Active caspase-3	TUNEL
HSV					
Acute					
1	Widespread cortical destruction	+++	+++	+++	+++
2	Cortical inflammation	++	++	+	++
3	Cortical microgliosis, inflammation	+	+	+	+
4	Massive cortical destruction	+++	++	−	−
5	Meninges inflamed; diffuse cortical neuronal death, edema, and necrosis beyond number of viral-infected cells; some Cowdry inclusions present	++	− (cortex) ++ (meninges)	++	Artifact (uninterpretable)
6	Cortical destruction, no inflammation	+++	−	+++	+++
7	Cortical microgliosis, inflammation	+	+	+	+
Remote					
8	Severe neuronal loss, multicystic cavitation, lymphocytes, microgliosis	−	+++	− (rare)	−
9	Severe neuronal loss, reactive astrocytosis, dramatic perivascular lymphocytic infiltrates	−	+++	− (rare)	−
10	Extensive neuronal necrosis and reactive astrocytosis	−	−	−	Artifact (uninterpretable)
CMV					
Acute					
11	Periventricular and intraparenchymal calcification; many multinucleated giant cells with Cowdry A inclusion bodies; focal micropolygyria of right hippocampus	+++ (periventricular)	+++	+++	++
Subacute					
12	Marked micropolygyria. Punctate necrosis with calcification throughout white matter; ependymitis; only rare CMV inclusions on multiple sections	− (except 2 cells)	−	−	−
Remote					
13	Polymicrogyria, ependymal destruction; no CMV inclusions	−	−	−	Artifact (uninterpretable)

NOTE. Scoring indicates relative quantitation of number of positively stained cells in histologically involved areas, ranging from no staining (−) to highest degree of staining (+++). HE, Hematoxylin-eosin stain.

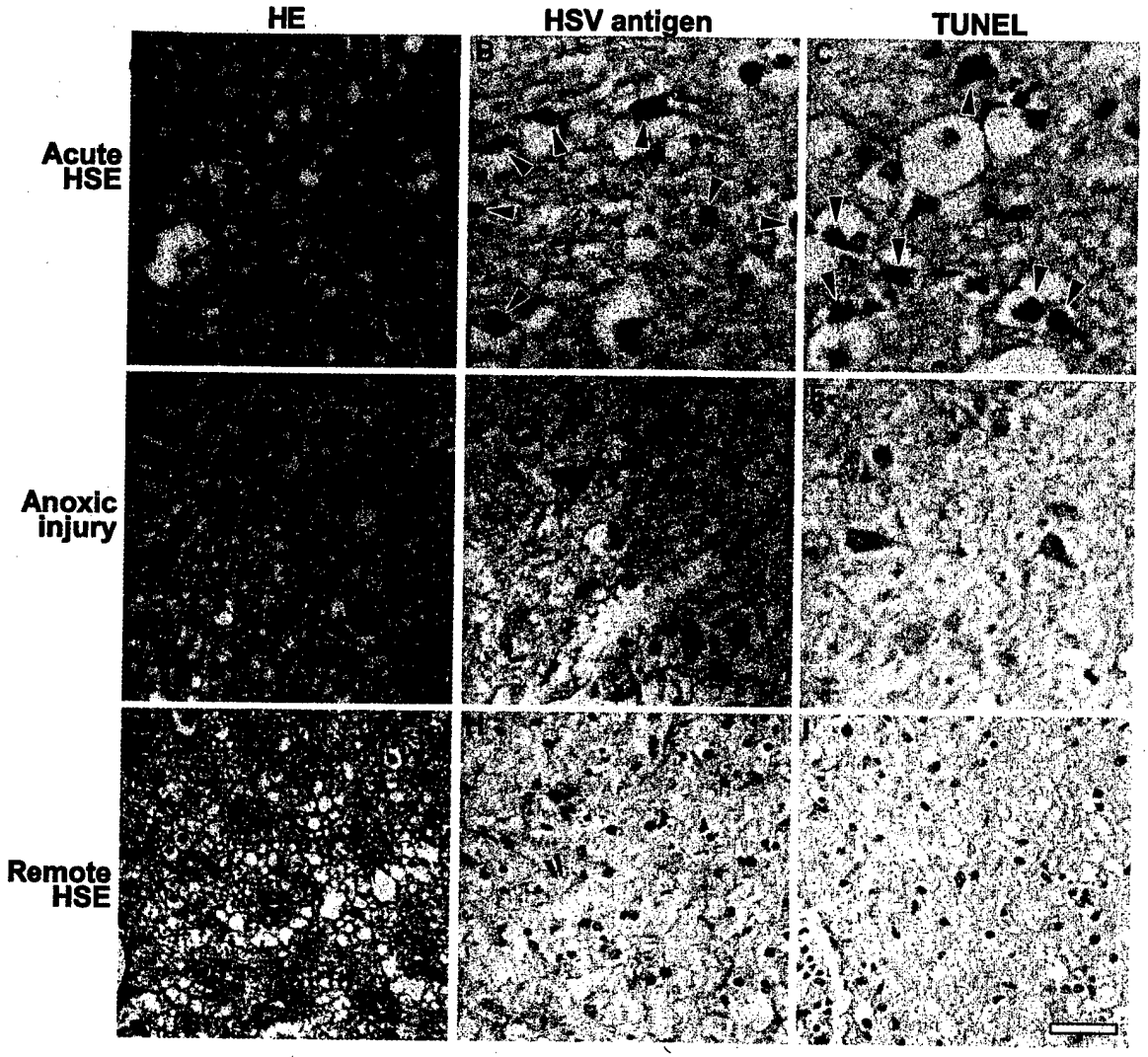

Figure 1. Apoptosis in acute herpes simplex virus (HSV) encephalitis (HSE). Sections of central nervous system (CNS) tissue from patient 1 with acute HSE *(A–F)* and patient 8 with remote HSE *(G–I)* are shown. CNS tissue from patient 1 with acute HSE demonstrates widespread cortical injury (hematoxyln-eosin stain [HE]; *A*), including many HSV-productively infected neurons (brown staining, *arrowheads*; *B*), and widespread neuronal/glial apoptosis (TUNEL; brown staining, *arrowheads*; *C*). In contrast, areas of adjacent cortical injury due to anoxia *(D)*, rather than productive viral infection *(E)*, have no evidence of apoptotic injury *(F)*. CNS tissue from patient 8 with chronic neurologic deficits resulting from HSE 12 years prior to death (remote) shows widespread cortical destruction *(G)*, without evidence of productive viral infection *(H)*, and no evidence of ongoing apoptosis *(I)*. Bar, 20 μm.

with recently-acquired congenital CMV disease and classic periventricular involvement. This patient had widespread Cowdry A inclusion bodies and multinucleated giant cells evident in the periventricular region on HE stain (figure 2*A*), in conjunction with large numbers of productively infected neurons (as measured by CMV-specific immunostain) in this region (figure 2*B*). There was nearly a 1:1 correlation between number of CMV-staining cells and apoptotic cells, as evidenced by both TUNEL (figure 2*C*) and activated caspase-3 techniques (table 2). Areas immediately adjacent to this periventricular concentrated distribution of CMV, as well as an area of focal polymicrogyria in the right hippocampus of this patient, were also evaluated and showed no evidence of histological, virologic, or apoptotic disruption.

We also evaluated 2 patients with severe neurologic sequelae of congenital CMV CNS infection, including marked micropolygyria, ependymitis, and diffuse white matter punctate necrosis/calcification. These sequelae were the result of infection occurring as recently as 6–8 weeks (subacute) but as long as 3 years (remote) after acquisition of CMV virus in utero. In contrast to the acutely-infected patient described above, we demonstrated minimal evidence of ongoing productive CMV in-

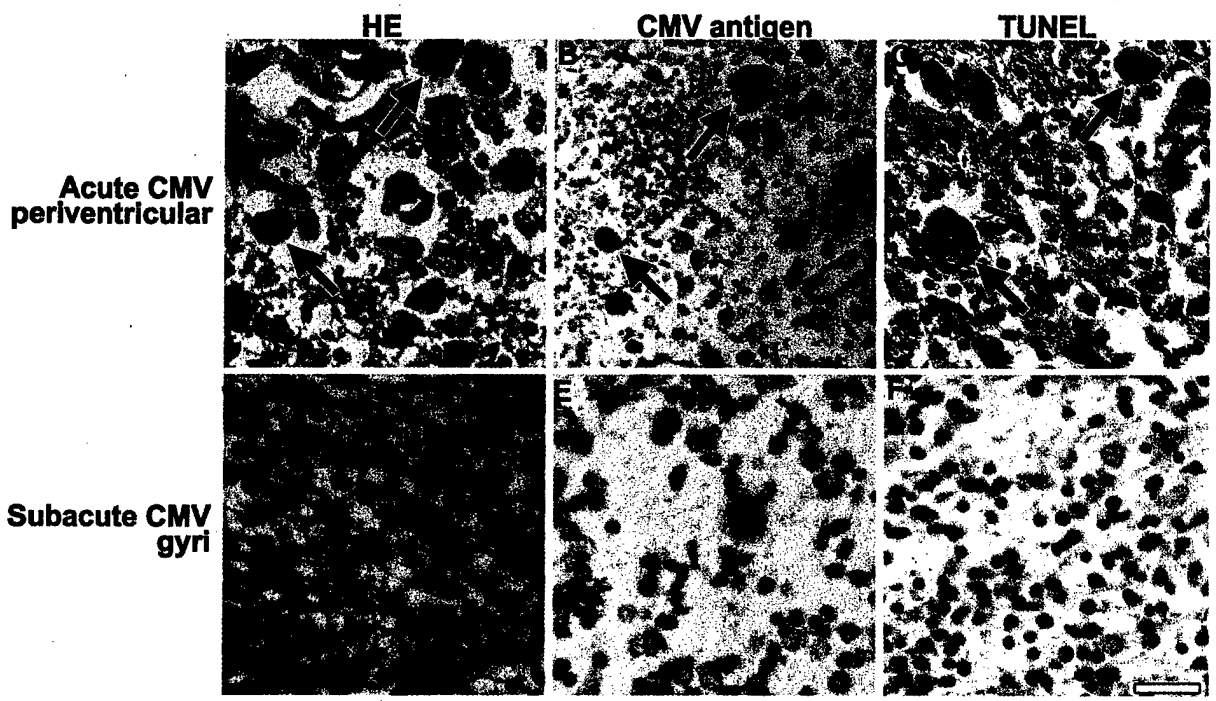

Figure 2. Apoptosis in congenital cytomegalovirus (CMV) central nervous system (CNS) infection. Sections of CNS tissue from patient 11 with acute periventricular CNS disease due to congenitally acquired CMV *(A–C)*, as well as patient 12 with subacute (6–8 weeks prior to analysis) congenitally acquired CMV *(D–F)*. CNS tissue from the acutely infected infant shows many multinucleated giant cells *(A)*, including cells with Cowdry A inclusion bodies *(arrows)*, productive CMV infection (dark brown staining, *arrows; B*), and evidence of apoptosis (TUNEL, dark brown staining, *arrows; C*). CNS tissue from the infant with subacute infection showed no periventricular multinucleated giant cells, productive viral infection or apoptosis. In an area of cortical polymicrogyria (hematoxyln-eosin stain [HE]; *D*) there was only one cell identified with productive CMV infection *(E)* and no evidence of apoptosis (TUNEL; *F*). Pale-brown staining seen is nonspecific and not different from that seen in uninfected control cases (data not shown). Bar, 20 μm.

fection, as evidenced by the absence of CMV inclusions bodies on HE stain, as well as rare (subacute) or absent (remote) CMV-specific immunostained cells in these patients. Neither case patient had significant apoptosis by either activated caspase-3 or TUNEL staining techniques (table 2 and figure 2*D–F* [subacute]). These results indicate that neuronal/glial apoptosis is associated with productive CMV viral infection acquired in utero and does not persist at timepoints remote from infection, even in patients with severe neurologic sequelae and gyral anomalies occurring weeks to years after acquisition of virus.

Apoptosis in HSV-infected neurons/glia. Having demonstrated apoptosis in CNS tissue of acute HSV- infected patients, we wished to further characterize whether apoptosis occurs in virus-infected neurons/glia or uninfected bystander cells. The majority of cells exhibiting evidence of apoptosis by activated caspase-3 staining were costained for HSV antigen, and these double-stained cells had morphological features identifying them as neuronal or glial in origin (figure 3*A*). Not all HSV-positive cells were apoptotic. Apoptotic cells were not seen outside areas of viral infection; however, not all apoptotic cells were antigen positive, suggesting that apoptosis occurs both as a direct consequence of viral infection and also through indirect bystander mechanisms in cells with close proximity to infected cells.

Apoptosis in CMV-infected neurons. Having demonstrated apoptosis in CNS tissue of a patient with acute CMV infection, we wished to further characterize whether apoptosis occurs in virus-infected neurons/glia or uninfected bystander cells. A large proportion of cells exhibiting evidence of apoptosis by activated caspase-3 staining were costained for CMV antigen, and these double-stained cells had morphological features unequivocally identifying them as of neuronal origin (figure 3*B*), often occurring in multinucleated giant cells bearing Cowdry A inclusions. In contrast to HSV infection (in which the number of virus-infected cells was substantially greater than apoptotic cells), the number of CMV-infected cells closely matched the number of apoptotic cells. This suggests that, in distinction to HSV infection, in which both direct and bystander apoptosis occur, in CMV infection, apoptosis results predominantly from direct viral injury to infected cells.

Neuronal apoptosis not dependent on inflammatory T cell responses to HSV or CMV infection. We wished to determine whether apoptosis resulted as a consequence of viral infection

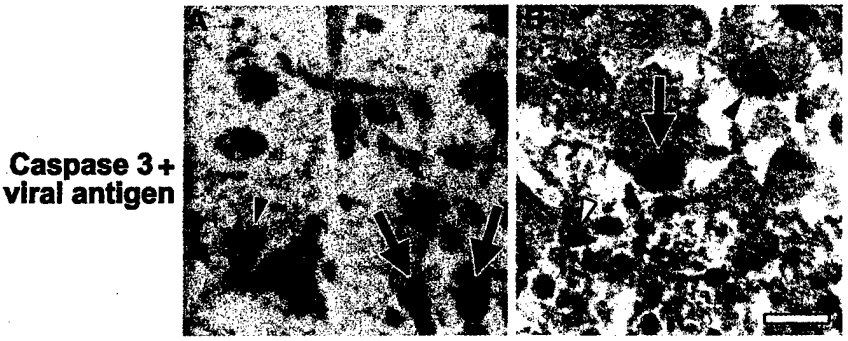

Figure 3. Costaining for apoptosis and productive viral infection. Sections of central nervous system (CNS) tissues from patient 1 with acute herpes simplex encephalitis (HSE; *A*) and patient 11 with acute cytomegalovirus (CMV) CNS infection *(B)* were costained for evidence of productive viral infection (HSV or CMV-specific antibody, indicated by red staining), as well as apoptosis (activated caspase-3 antibody, indicated by brown staining). In both acute HSV and acute CMV CNS infections, multiple neurons and glial cells were identified which were both infected with virus and undergoing apoptosis (colabeled cells are indicated by maroon staining, *large arrows*). Examples of cells with productive viral infection, but not undergoing apoptosis *(white arrowheads)*, as well as cells undergoing apoptosis without productive viral infection *(black arrowheads)* were also present in both CMV and HSV infection. Bar, 20 μm.

independent of the host immune response or alternatively, resulted from immune-mediated killing of virus-infected cells. We, therefore, examined the association between the degree of inflammatory response and the presence of apoptosis. Neuronal and glial apoptosis were noted in acutely infected patients, regardless of the degree of inflammatory T cell infiltrate (as measured by activated caspase-3 and CD3-labeling). The majority of acutely infected patients had significant inflammation as a component of their disease, but CD3-positive labeled cells represented a distinct population from apoptotic cells (as evidenced by lack of colabeling with activated caspase-3) (figure 4*A*). As a corollary observation, we still detected high levels of neuronal/glial apoptosis in an acutely infected patient who did not mount any inflammatory response to viral infection (table 2). Furthermore, despite the presence of extensive inflammatory cell infiltrates in 2 of 3 remotely infected patients (as evidenced by large numbers of CD3-positive staining cells), inflammatory T cells were not found to be apoptotic (no activated caspase-3 costaining) nor were adjacent neurons/glia (figure 4*C*). These results suggest that the inflammatory response and the apoptotic program are distinct (although possibly interacting) processes in HSV-infected patients.

CMV-infected infants had less T cell inflammatory response to infection, compared with HSV-infected patients, consistent with the fact that infants have relatively immature immune responses, compared with older children and adults. In spite of this less-robust inflammatory response, abundant neuronal/glial cell apoptosis was noted in the acute CMV-infected infant, as described earlier (figure 2). In areas where CD3-positive inflammatory cell infiltrates were detected, T cells represented a distinct population from cells exhibiting evidence of apoptosis, as measured by activated caspase-3 (figure 4*D*).

Taken together, results from the evaluation of tissues from all HSV and CMV-infected patients indicate that apoptosis occurs in neurons/glia of acutely infected patients, in close temporal and spatial association with productive viral infection, and is not dependent on secondary inflammatory T cell responses.

Absence of apoptosis in age-matched control subjects without CNS infection. To assess the degree of baseline apoptosis in CNS tissues as a function of age, we analyzed autopsy tissues (hippocampal sections) from uninfected patients who died from other causes. Tissue samples from 11 patients representing each decade of life from infancy to late adulthood were analyzed and showed minimal (infancy) or no (all other age groups) evidence of apoptosis, as measured by activated caspase-3 staining (data not shown). These results lend further support to the finding that the apoptosis that occurs in neurons/glia of HSV and CMV-infected patients is a pathologic process, distinct from normal developmental or age-related changes.

Discussion

Our study is the first demonstration of apoptotic neuronal death in patients with acute viral CNS infection, specifically in patients with HSE and congenital CMV infection. In addition to demonstrating neuronal/glial apoptosis in regions of the brain with acute productive viral infection, we demonstrate that apoptosis is not found in brains of patients with severe CNS injury and neurologic symptoms months to years after acute viral infection. In both CMV and HSV infection, the presence and degree of apoptosis did not correlate with the presence or magnitude of inflammatory response, indicating that apoptosis is a direct consequence of viral injury, rather than a secondary effect of virus-induced inflammatory responses. Our findings imply that apoptotic neuronal death is an important component

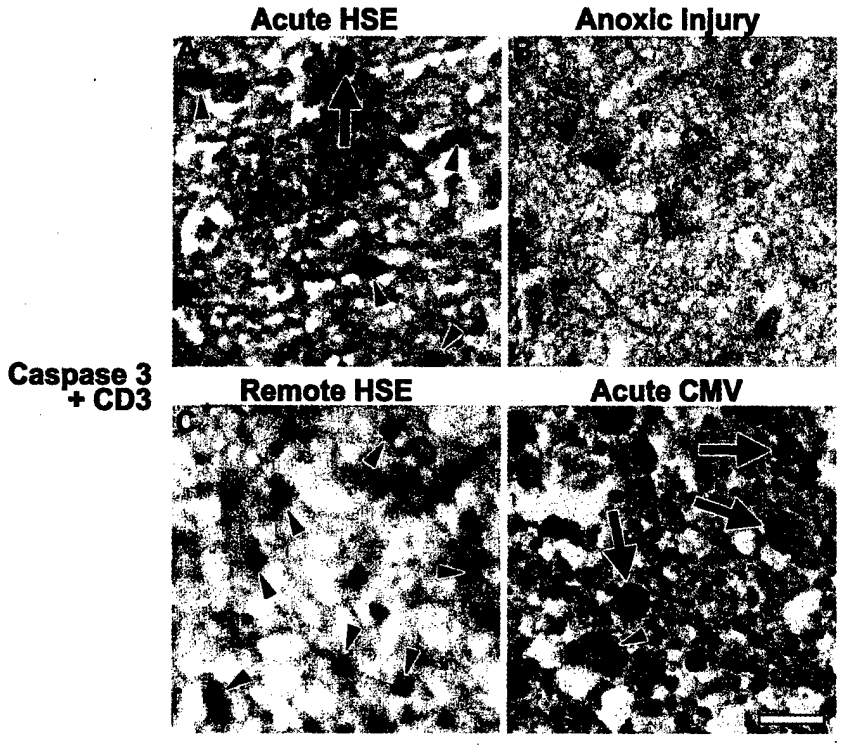

Figure 4. Costaining for apoptosis and CD3 T cell marker. Sections of central nervous system (CNS) tissues from patient 1 with acute herpes simplex encephalitis (HSE; *A* and *B*), patient 8 with remote HSE *(C)*, and patient 11 with acute cytomegalovirus (CMV) encephalitis *(D)* were costained for evidence of inflammatory cell infiltrate (CD3 antibody, indicated by red staining), as well as apoptosis (activated caspase-3 antibody, indicated by brown staining). In both the case of acute HSV *(A)* and acute CMV *(D)*, cells undergoing apoptosis *(large arrows)* were a distinct population from immune cells *(arrowheads)*, and no colabeled cells were detected. No apoptosis or immune cells were detected in a control area of anoxic cortical injury without productive viral infection (patient 1 with acute HSE; *B*). As a corollary, patient 8 with remote HSE (and no evidence of productive viral infection) had a robust immune cell response *(arrowheads; C)*, without evidence of apoptosis. Bar, 20 μm.

of CNS injury and destruction in the acute phase of infection of patients with viral CNS infection.

The correlation between the number of infected neurons and the degree of apoptotic neuronal death differed in HSV and congenital CMV infection. Although only one case of acute congenital CMV infection was available for analysis, CMV infection was associated with a nearly direct (1:1) correlation between the number of infected neurons and the number of apoptotic neurons, whereas tissues from patients with acute HSV infection showed many more infected nonapoptotic neurons than infected apoptotic neurons. There are several potential explanations for this difference in degree of observed apoptosis. First, HSV and CMV may differ in their capacity to induce apoptotic-signaling pathways in neuronal cells. Strain-specific differences in the capacity to induce apoptosis have been described in other viral models of neuronal apoptosis [74], and this may apply to different members of the herpesvirus family, as well. Alternatively, although we chose to analyze only immunocompetent hosts in this study, congenitally infected CMV patients are, to some degree, less immunocompetent at the time of their productive viral infection than older children and adults at the time of their acute HSV infections. Therefore, CMV-infected infants could be prone to higher degrees of direct virus-mediated apoptotic injury at the time of acute infection. Finally, the observed difference may be related to the relative tempo by which infection proceeds in HSV, compared with CMV-infected patients. The clinical presentation and histopathology associated with these 2 diseases are markedly different. In HSV infection, neurons/glia are rapidly infected, resulting in an overwhelming, lytic, hemorrhagic destructive process. It is rare to observe viral inclusion bodies and/or multinucleated giant cells in CNS tissues of patients with HSV infection. In contrast, neurons infected with CMV typically accumulate large amounts of virus prior to destruction, as reflected by easily observable Cowdry A viral inclusions within infected multinucleated giant cells. One potential consequences of this difference is that identification of infected cells on the basis of prominent cytomegaly in the case of CMV infection may greatly facilitate identification of infection and apoptosis in identical cells using sequential sections. Additionally, the accumulation

of large amounts of virus within an infected cell prior to cell lysis (as occurs in CMV) may in some manner potentiate the initiation of the apoptotic program.

Our study indicates that, in HSV and CMV infection, CNS apoptosis appears to result as a direct consequence of viral infection of neurons, rather than as a secondary consequence of virus-induced inflammatory T cell responses or in infiltrating T cells themselves. This is in contrast to experimental Murray Valley Encephalitis infection, in which inflammatory infiltrate includes apoptotic macrophages and lymphocytes [10]. Similarly, during experimental Semliki Forest Virus encephalitis, infiltrating leukocytes and neural precursor cells undergo apoptosis while productively infected neurons undergo necrosis [27]. However, apoptotic inflammatory cells may also secrete factors that induce apoptosis in neighboring cells, as seen in the case of HIV infection, in which infiltrating mononuclear phagocytes secrete a variety of factors that mediate neuronal apoptosis [75, 76]. Although apoptosis appears to be a direct effect of viral infection, rather than an indirect effect of proinflammatory cytokines, in HSE and congenital CMV CNS infection, it is possible that inflammatory responses provide an additional mechanism of tissue injury, and could interact in some way with virus-induced apoptotic signaling processes.

There are many plausible reasons why neuronal apoptosis likely has biological significance in viral infections of the human CNS. A complex network of intracellular signaling cascades is activated by apoptosis-inducing stimuli in neurons. In addition to the basic apoptosis-related biochemical and morphological changes seen in neuronal cells, apoptotic neurons also undergo alterations in neurotransmitter release, growth factor secretion, and cell-cell interactions. These changes can have deleterious effects on neighboring neurons during the primary insult, often resulting in a widening of the area of neuronal loss at timepoints directly following the initial insult [77].

This study suggests that apoptosis is an important mechanism of virus-induced neuronal and glial cell death in the CNS of humans with viral encephalitis. These results have importance not only for an improved understanding of the pathogenesis of human encephalitis but also for the potential development of novel therapeutic strategies. The importance of apoptotic death in virus-induced CNS disease has been underrecognized, due in part to the fact that classic histopathologic descriptions of encephalitis were made prior to the distinction between apoptotic and necrotic cellular death. We have demonstrated elsewhere the protective effect of apoptotic blockade in a murine model of viral myocarditis [78], and this study indicates that similar intervention may be may be useful as an adjunct to the treatment of patients with acute, but not remote, viral CNS infection. Identification of specific mechanisms underlying virus-induced injury in human viral encephalitis, including apoptosis, may lead to improved, novel and/or adjunctive strategies for the treatment of this devastating disease.

Acknowledgments

We thank Sarah Garza-Williams (The Children's Hospital, Denver) for her help in locating archived specimens and Traci Sachs (University of Colorado Health Sciences Center histology laboratory) for her technical help in preparation and immunohistochemical analysis of tissue sections.

References

1. Schulz JB, Weller M, Moskowitz MA. Caspases as treatment targets in stroke and neurodegenerative diseases. Ann Neurol **1999**;45:421–9.
2. Bredesen DE. Neural apoptosis. Ann Neurol **1995**;38:839–51.
3. Thompson CB. Apoptosis in the pathogenesis and treatment of disease. Science **1995**;267:1456–62.
4. Griffin DE, Hardwick JM. Perspective: virus infections and the death of neurons. Trends Microbiol **1999**;7:155–60.
5. Allsopp TE, Fazakerley JK. Altruistic cell suicide and the specialized case of the virus-infected nervous system. Trends Neurosci **2000**;23:284–90.
6. Despres P, Frenkiel MP, Ceccaldi PE, Duarte Dos SC, Deubel V. Apoptosis in the mouse central nervous system in response to infection with mouse-neurovirulent dengue viruses. J Virol **1998**;72:823–9.
7. Liao CL, Lin YL, Wang JJ, et al. Effect of enforced expression of human bcl-2 on Japanese encephalitis virus–induced apoptosis in cultured cells. J Virol **1997**;71:5963–71.
8. Liao CL, Lin YL, Wu BC, et al. Salicylates inhibit flavivirus replication independently of blocking nuclear factor kappa B activation. J Virol **2001**;75:7828–39.
9. Pekosz A, Phillips J, Pleasure D, Merry D, Gonzalez-Scarano F. Induction of apoptosis by La Crosse virus infection and role of neuronal differentiation and human bcl-2 expression in its prevention. J Virol **1996**;70:5329–35.
10. Matthews V, Robertson T, Kendrick T, Abdo M, Papadimitriou J, McMinn P. Morphological features of Murray Valley encephalitis virus infection in the central nervous system of Swiss mice. Int J Exp Pathol **2000**;81:31–40.
11. Schoneboom BA, Catlin KM, Marty AM, Grieder FB. Inflammation is a component of neurodegeneration in response to Venezuelan equine encephalitis virus infection in mice. J Neuroimmunol **2000**;109:132–46.
12. Jackson AC, Rossiter JP. Apoptotic cell death is an important cause of neuronal injury in experimental Venezuelan equine encephalitis virus infection of mice. Acta Neuropathol (Berl) **1997**;93:349–53.
13. Parquet MC, Kumatori A, Hasebe F, Morita K, Igarashi A. West Nile virus–induced bax-dependent apoptosis. FEBS Lett **2001**;500:17–24.
14. Weissenbock H, Hornig M, Hickey WF, Lipkin WI. Microglial activation and neuronal apoptosis in Bornavirus infected neonatal Lewis rats. Brain Pathol **2000**;10:260–72.
15. Geiger KD, Nash TC, Sawyer S, et al. Interferon-gamma protects against herpes simplex virus type 1–mediated neuronal death. Virology **1997**;238:189–97.
16. Adamson DC, Dawson TM, Zink MC, Clements JE, Dawson VL. Neurovirulent simian immunodeficiency virus infection induces neuronal, endothelial, and glial apoptosis. Mol Med **1996**;2:417–28.
17. Gendelman R, Orzech Y, Mashiah P, Birenbaum M, Gazit A, Yaniv A. Productive replication of caprine arthritis-encephalitis virus is associated with induction of apoptosis. J Gen Virol **1997**;78(Pt 4):801–5.
18. Manchester M, Eto DS, Oldstone MB. Characterization of the inflammatory response during acute measles encephalitis in NSE-CD46 transgenic mice. J Neuroimmunol **1999**;96:207–17.
19. Evlashev A, Moyse E, Valentin H, et al. Productive measles virus brain infection and apoptosis in CD46 transgenic mice. J Virol **2000**;74:1373–82.

20. Schneider-Schaulies S, ter MV. Pathogenic aspects of measles virus infections. Arch Virol Suppl **1999**;15:139–58.
21. Oberhaus SM, Smith RL, Clayton GH, Dermody TS, Tyler KL. Reovirus infection and tissue injury in the mouse central nervous system are associated with apoptosis. J Virol **1997**;71:2100–6.
22. Anderson R, Harting E, Frey MS, Leibowitz JL, Miranda RC. Theiler's murine encephalomyelitis virus induces rapid necrosis and delayed apoptosis in myelinated mouse cerebellar explant cultures. Brain Res **2000**;868:259–67.
23. Jackson AC. Apoptosis in experimental rabies in bax-deficient mice. Acta Neuropathol (Berl) **1999**;98:288–94.
24. Jackson AC, Park H. Experimental rabies virus infection of p75 neurotrophin receptor-deficient mice. Acta Neuropathol (Berl) **1999**;98:641–4.
25. Camelo S, Lafage M, Lafon M. Absence of the p55 Kd TNF-alpha receptor promotes survival in rabies virus acute encephalitis. J Neurovirol **2000**;6: 507–18.
26. Allsopp TE, Scallan MF, Williams A, Fazakerley JK. Virus infection induces neuronal apoptosis: a comparison with trophic factor withdrawal. Cell Death Differ **1998**;5:50–9.
27. Sammin DJ, Butler D, Atkins GJ, Sheahan BJ. Cell death mechanisms in the olfactory bulb of rats infected intranasally with Semliki forest virus. Neuropathol Appl Neurobiol **1999**;25:236–43.
28. Jan JT, Griffin DE. Induction of apoptosis by Sindbis virus occurs at cell entry and does not require virus replication. J Virol **1999**;73:10296–302.
29. Johnston C, Jiang W, Chu T, Levine B. Identification of genes involved in the host response to neurovirulent alphavirus infection. J Virol **2001**;75: 10431–45.
30. Griffin DE. A review of alphavirus replication in neurons. Neurosci Biobehav Rev **1998**;22:721–3.
31. Liang XH, Kleeman LK, Jiang HH, et al. Protection against fatal Sindbis virus encephalitis by beclin, a novel Bcl-2-interacting protein. J Virol **1998**; 72:8586–96.
32. Levine B, Goldman JE, Jiang HH, Griffin DE, Hardwick JM. Bcl-2 protects mice against fatal alphavirus encephalitis. Proc Natl Acad Sci USA **1996**; 93:4810–5.
33. Adle-Biassette H, Levy Y, Colombel M, et al. Neuronal apoptosis in HIV infection in adults. Neuropathol Appl Neurobiol **1995**;21:218–27.
34. Adle-Biassette H, Chretien F, Wingertsmann L, et al. Neuronal apoptosis does not correlate with dementia in HIV infection but is related to microglial activation and axonal damage. Neuropathol Appl Neurobiol **1999**;25:123–33.
35. Wiley CA, Achim CL, Hammond R, et al. Damage and repair of DNA in HIV encephalitis. J Neuropathol Exp Neurol **2000**;59:955–65.
36. Dollard SC, James HJ, Sharer LR, Epstein LG, Gelbard HA, Dewhurst S. Activation of nuclear factor kappa B in brains from children with HIV-1 encephalitis. Neuropathol Appl Neurobiol **1995**;21:518–28.
37. Gelbard HA, James HJ, Sharer LR, et al. Apoptotic neurons in brains from paediatric patients with HIV-1 encephalitis and progressive encephalopathy. Neuropathol Appl Neurobiol **1995**;21:208–17.
38. Petito CK, Roberts B. Evidence of apoptotic cell death in HIV encephalitis. Am J Pathol **1995**;146:1121–30.
39. James HJ, Sharer LR, Zhang Q, et al. Expression of caspase-3 in brains from paediatric patients with HIV-1 encephalitis. Neuropathol Appl Neurobiol **1999**;25:380–6.
40. Elovaara I, Sabri F, Gray F, Alafuzoff I, Chiodi F. Upregulated expression of Fas and Fas ligand in brain through the spectrum of HIV-1 infection. Acta Neuropathol (Berl) **1999**;98:355–62.
41. Kruman II, Nath A, Maragos WF, et al. Evidence that Par-4 participates in the pathogenesis of HIV encephalitis. Am J Pathol **1999**;155:39–46.
42. Krajewski S, James HJ, Ross J, et al. Expression of pro- and anti-apoptosis gene products in brains from paediatric patients with HIV-1 encephalitis. Neuropathol Appl Neurobiol **1997**;23:242–53.
43. McQuaid S, McMahon J, Herron B, Cosby SL. Apoptosis in measles virus–infected human central nervous system tissues. Neuropathol Appl Neurobiol **1997**;23:218–24.
44. Whitley RJ. Herpes simplex virus infections of the central nervous system. Encephalitis and neonatal herpes. Drugs **1991**;42:406–27.
45. Munger J, Roizman B. The US3 protein kinase of herpes simplex virus 1 mediates the posttranslational modification of BAD and prevents BAD-induced programmed cell death in the absence of other viral proteins. Proc Natl Acad Sci USA **2001**;98:10410–5.
46. Zhou G, Roizman B. The domains of glycoprotein D required to block apoptosis depend on whether glycoprotein D is present in the virions carrying herpes simplex virus 1 genome lacking the gene encoding the glycoprotein. J Virol **2001**;75:6166–72.
47. Aubert M, Blaho JA. Modulation of apoptosis during herpes simplex virus infection in human cells. Microbes Infect **2001**;3:859–66.
48. Irie H, Koyama H, Kubo H, et al. Herpes simplex virus hepatitis in macrophage-depleted mice: the role of massive, apoptotic cell death in pathogenesis. J Gen Virol **1998**;79(Pt 5):1225–31.
49. Zachos G, Koffa M, Preston CM, Clements JB, Conner J. Herpes simplex virus type 1 blocks the apoptotic host cell defense mechanisms that target Bcl-2 and manipulates activation of p38 mitogen- activated protein kinase to improve viral replication. J Virol **2001**;75:2710–28.
50. Galvan V, Roizman B. Herpes simplex virus 1 induces and blocks apoptosis at multiple steps during infection and protects cells from exogenous inducers in a cell- type-dependent manner. Proc Natl Acad Sci USA **1998**;95:3931–6.
51. Jerome KR, Fox R, Chen Z, Sears AE, Lee H, Corey L. Herpes simplex virus inhibits apoptosis through the action of two genes, Us5 and Us3. J Virol **1999**;73:8950–7.
52. Leopardi R, Van Sant C, Roizman B. The herpes simplex virus 1 protein kinase US3 is required for protection from apoptosis induced by the virus. Proc Natl Acad Sci USA **1997**;94:7891–6.
53. Thompson RL, Sawtell NM. HSV latency-associated transcript and neuronal apoptosis. Science **2000**;289:1651.
54. Perng GC, Jones C, Ciacci-Zanella J, et al. Virus-induced neuronal apoptosis blocked by the herpes simplex virus latency-associated transcript. Science **2000**;287:1500–3.
55. Ozaki N, Sugiura Y, Yamamoto M, Yokoya S, Wanaka A, Nishiyama Y. Apoptosis induced in the spinal cord and dorsal root ganglion by infection of herpes simplex virus type 2 in the mouse. Neurosci Lett **1997**;228:99–102.
56. Brown J, Abernathy MP. Cytomegalovirus infection. Semin Perinatol **1998**;22: 260–6.
57. Ahlfors K, Ivarsson SA, Harris S. Report on a long-term study of maternal and congenital cytomegalovirus infection in Sweden. Review of prospective studies available in the literature. Scand J Infect Dis **1999**;31:443–57.
58. Demmler GJ. Congenital cytomegalovirus infection. Semin Pediatr Neurol **1994**;1:36–42.
59. Arribas JR, Storch GA, Clifford DB, Tselis AC. Cytomegalovirus encephalitis. Ann Intern Med **1996**;125:577–87.
60. Skaletskaya A, Bartle LM, Chittenden T, McCormick AL, Mocarski ES, Goldmacher VS. A cytomegalovirus-encoded inhibitor of apoptosis that suppresses caspase-8 activation. Proc Natl Acad Sci USA **2001**;98:7829–34.
61. Goldmacher VS, Bartle LM, Skaletskaya A, et al. A cytomegalovirus-encoded mitochondria-localized inhibitor of apoptosis structurally unrelated to Bcl-2. Proc Natl Acad Sci USA **1999**;96:12536–41.
62. Wang J, Belcher JD, Marker PH, Wilcken DE, Vercellotti GM, Wang XL. Cytomegalovirus inhibits p53 nuclear localization signal function. J Mol Med **2001**;78:642–7.
63. Hayajneh WA, Colberg-Poley AM, Skaletskaya A, et al. The sequence and antiapoptotic functional domains of the human cytomegalovirus UL37 exon 1 immediate early protein are conserved in multiple primary strains. Virology **2001**;279:233–40.
64. Sindre H, Rollag H, Olafsen MK, Degre M, Hestdal K. Human cytomegalovirus induces apoptosis in the hematopoietic cell line MO7e. APMIS **2000**;108:223–30.
65. Lukac DM, Alwine JC. Effects of human cytomegalovirus major immediate-early proteins in controlling the cell cycle and inhibiting apoptosis: studies with ts13 cells. J Virol **1999**;73:2825–31.

66. Tanaka K, Zou JP, Takeda K, et al. Effects of human cytomegalovirus immediate-early proteins on p53-mediated apoptosis in coronary artery smooth muscle cells. Circulation **1999**;99:1656–9.
67. Zhu H, Shen Y, Shenk T. Human cytomegalovirus IE1 and IE2 proteins block apoptosis. J Virol **1995**;69:7960–70.
68. Cinatl J Jr, Cinatl J, Vogel JU, et al. Persistent human cytomegalovirus infection induces drug resistance and alteration of programmed cell death in human neuroblastoma cells. Cancer Res **1998**;58:367–72.
69. Lokensgard JR, Cheeran MC, Gekker G, Hu S, Chao CC, Peterson PK. Human cytomegalovirus replication and modulation of apoptosis in astrocytes. J Hum Virol **1999**;2:91–101.
70. Kosugi I, Shinmura Y, Li RY, et al. Murine cytomegalovirus induces apoptosis in non-infected cells of the developing mouse brain and blocks apoptosis in primary neuronal culture. Acta Neuropathol (Berl) **1998**;96:239–47.
71. Bigger JE, Tanigawa M, Zhang M, Atherton SS. Murine cytomegalovirus infection causes apoptosis of uninfected retinal cells. Invest Ophthalmol Vis Sci **2000**;41:2248–54.
72. Buggage RR, Chan CC, Matteson DM, Reed GF, Whitcup SM. Apoptosis in cytomegalovirus retinitis associated with AIDS. Curr Eye Res **2000**; 21:721–9.
73. Schiff D, Rosenblum MK. Herpes simplex encephalitis (HSE) and the immunocompromised: a clinical and autopsy study of HSE in the settings of cancer and human immunodeficiency virus–type 1 infection. Hum Pathol **1998**;29:215–22.
74. Tyler KL, Squier MK, Rodgers SE, et al. Differences in the capacity of reovirus strains to induce apoptosis are determined by the viral attachment protein sigma 1. J Virol **1995**;69:6972–9.
75. Tong N, Perry SW, Zhang Q, et al. Neuronal fractalkine expression in HIV-1 encephalitis: roles for macrophage recruitment and neuroprotection in the central nervous system. J Immunol **2000**;164:1333–9.
76. Kaul M, Garden GA, Lipton SA. Pathways to neuronal injury and apoptosis in HIV-associated dementia. Nature **2001**;410:988–94.
77. Raghupathi R, Graham DI, McIntosh TK. Apoptosis after traumatic brain injury. J Neurotrauma **2000**;17:927–38.
78. DeBiasi RL, Edelstein CL, Sherry B, Tyler KL. Calpain inhibition protects against virus-induced apoptotic myocardial injury. J Virol **2001**;75:351–61.

Quantitative CSF PCR in Epstein–Barr Virus Infections of the Central Nervous System

Adriana Weinberg, MD,[1,2] Shaobing Li, MD,[1] Megan Palmer, MD,[1] and Kenneth L. Tyler, MD[2–5]

Acute Epstein–Barr virus (EBV) infection of the central nervous system (CNS) is associated with meningoencephalitis and other neurological syndromes and with CNS lymphomas (CNSLs). Diagnosis is based on serological studies and more recently on detection of EBV DNA in cerebrospinal fluid (CSF) by polymerase chain reaction (PCR). We measured EBV DNA by quantitative PCR and EBV mRNA by RT-PCR in the CSF in patients with EBV-associated neurological disorders. EBV was identified as the cause of CNS infection in 28 patients: 14 with CNSL, 10 with encephalitis, and 4 with postinfectious neurological complications. CSF analysis showed that patients with CNSL had high EBV load (mean ± standard error of 4.8 ± 0.2 $\log_{10}$ DNA copies/ml) and low leukocyte counts (22 ± 7 cells/μl); encephalitis was characterized by high EBV load (4.2 ± 0.3 $\log_{10}$ DNA copies/ml) and high leukocyte counts (143 ± 62 cells/μl); and patients with postinfectious complications showed low EBV load (3.0 ± 0.2 $\log_{10}$ DNA copies/ml) with high leukocyte counts (88 ± 57 cells/μl). Lytic cycle EBV mRNA, a marker of viral replication, was identified in 10 CSF samples from patients with CNSL and encephalitis. These studies demonstrate the utility of quantitative CSF PCR and establish the presence of lytic cycle EBV mRNA in CSF of patients with EBV-associated neurological disease.

Ann Neurol 2002;52:543–548

Central nervous system (CNS) complications of Epstein–Barr virus (EBV) infection occur in 1 to 18% of patients with infectious mononucleosis and include encephalitis, meningitis, cerebellitis, polyradiculomyelitis, transverse myelitis, cranial and peripheral neuropathies, and psychiatric abnormalities.[1–7] EBV infections of the CNS can occur in the absence of infectious mononucleosis.[6] EBV has been associated with cranial and peripheral neuropathies, and serological evidence of active EBV infection has been reported in up to 29% of childhood cases of Guillain–Barré syndrome and 19% of childhood cases of facial palsy.[6,7] EBV-associated lymphomas represent another important cause of EBV-related CNS disease.[8–13] These disorders are particularly common in immunocompromised hosts including patients with acquired immune deficiency syndrome and transplant recipients.

Until recently, diagnosis of EBV-associated CNS disease depended predominantly on demonstration of the presence of antibodies in cerebrospinal fluid (CSF) and/or serum, because virus is only rarely isolated from CSF.[14–18] A role for EBV in the pathogenesis of CNS lymphomas (CNSLs) was established by demonstrating the presence of EBV genome and/or antigen in tumor cells using in situ hybridization or immunohistochemistry.[8] More recently, amplification of EBV DNA in the CSF by PCR has become an important method for diagnosis of EBV CNS infections and CNSL.[19–21]

In this study, we report the first use of quantitative EBV PCR and RT-PCR for a lytic cycle EBV mRNA in a large series of patients with EBV CNS infections.

Patients and Methods

Study Design and Definitions

CSF specimens containing EBV DNA detected by PCR were identified in the Diagnostic Virology Laboratory at the University of Colorado Health Sciences Center between October 1995 and March 2001. Clinical, laboratory, and follow-up information was obtained through a questionnaire submitted to the attending physician and/or neurology consultant, and from medical records review. Patients were grouped into the following diagnostic categories: (1) CNSL, defined by typical histopathology or by a typical radiographic exam and consistent clinical presentation in the absence of an alternate diagnosis; (2) encephalitis, defined by the presence of fever, altered mental status, and focal neurological signs or symptoms

From the Departments of [1]Pediatrics, [2]Medicine, [3]Microbiology and Immunology, and [4]Neurology, University of Colorado Health Sciences Center and [5]Denver Veterans Affairs Medical Center, Denver, CO.

Received Apr 16, 2002, and in revised form May 28. Accepted for publication May 29, 2002.

Address correspondence to Dr Weinberg, University of Colorado Health Sciences Center, Campus Box C227, Denver, CO 80262. E-mail: Adriana.Weinberg@uchsc.edu

indicative of parenchymal brain involvement, in the absence of other potential pathogenic agents; and (3) postinfectious complications, including cases of Guillain–Barré syndrome, acute demyelinating encephalitis, transverse myelitis, and polyradiculomyelitis, after acute EBV infection.

Qualitative Epstein–Barr Virus Polymerase Chain Reaction

Qualitative EBV PCR was performed as previously described[21,22] using duplicates of CSF aliquots stored at −70°C. Each assay included two negative water controls and two positive controls of EBV-producing B95-8 cell culture supernatant. The tests were considered valid if the controls yielded the expected results and if the replicates were concordant.

Quantitative Epstein–Barr Virus Polymerase Chain Reaction

Quantitative EBV PCR was performed using a competitive method adapted from a previously described assay.[23] The internal standard (IS) was synthesized by amplification of a 304bp fragment in the EBV region BMLF1 3501 to 3804, followed by deletion of an 81bp internal segment. The resultant 233bp IS was PCR-amplified and inserted in the vector PCR-Script SK+ (Stratagene, La Jolla, CA). *Escherichia coli* XL10-Gold Kan Ultracompetent cells (Stratagene) transformed with the IS-containing plasmid was grown in Luria–Bertani medium (Gibco BRL, Gaithersburg, MD) and selected with an ampicillin marker. The plasmid DNA was purified with a Qiagen tip 500 (Qiagen, Chatsworth, CA) and quantitated with a spectrophotometer (CECIL CE2401). The number of IS copies was confirmed by coamplification with known amounts of EBV B95-8 DNA quantitative standards (ABI, Columbia, MD). The PCR products were separated by agarose gel electrophoresis, stained with Vista Green, scanned with a Storm instrument (Molecular Dynamics, Sunnyvale, CA), and quantitated using ImageQuant software. Using 1,000 IS copies per reaction tube and dilutions of the quantitative standards, a linear relationship between input and measured DNA was identified between 1,000 to 1,000,000 copies of EBV DNA per milliliter of specimen. DNA, extracted from clinical specimens, was coamplified with 1,000 copies of IS per reaction tube, and quantitated by Storm. Positive and negative controls were run with each clinical specimen.

RNA Methods

EBV transcription of the early lytic cycle gene *BZLF1* was detected by RT-PCR as previously described.[24,25] CSF nucleic acids, purified with QIAamp viral RNA mini kit (Qiagen), were reverse transcribed and amplified using primers Z1 and Z2. Amplicon was detected by Southern blot using Z2B as a probe.

The BZLF1 target area was selected because the primers Z1 and Z2 anneal to exon 1 and exon 3, respectively. Therefore, RT-PCR typically generates two bands of 252 and 450kb molecular weight, corresponding to the cDNA and the genomic DNA, respectively. The presence of genomic DNA amplicon was used as an internal sensitivity control. The presence of both 450 and 252kb bands was interpreted as evidence of BZLF1 transcription. The presence of the 450kb band in the absence of the 252 one was interpreted as absence of BZLF1 transcription. The absence of both 450 and 252kb bands was interpreted as lack of homology between the primer pair and the clinical strains or insufficient nucleic acid template in the sample.

Statistical Analysis

Statistical analysis was performed using StatView 5.0.1 software (SAS Institute, Cary, NC).

Results

Description of the Patient Population

Of 528 CSF samples tested for EBV by PCR, 39 had positive results (7.4%). Eleven cases were excluded because other pathogenic agents in addition to EBV may have contributed to their illnesses. Demographic features of the 28 patients remaining in the study are shown in the Table. Twenty-two patients had primary or acquired immunocompromising conditions, including human immunodeficiency virus (HIV; n = 16), solid organ transplantation (n = 5), and common variable immunodeficiency (n = 1).

Central Nervous System Lymphoma

CNSL was diagnosed in 14 patients whose underlying disorders included advanced HIV infection (12) and transplantation (2). The presenting signs and symptoms included behavioral changes, seizures, aphasia, motor weakness, sensory abnormalities, and ataxia. Loss of developmental milestones was seen in children. Thirteen patients had computed tomography (CT) or magnetic resonance imaging studies of the CNS, which were abnormal in all but one case patient identifier ([PID] 10). PID 10 had a normal noncontrast CT accompanying aphasia and new-onset seizures. An magnetic resonance imaging was not performed. This patient had a lymph node biopsy, which showed non-Hodgkin lymphoma. Single-photon emission CT scans were positive in three cases and negative in one.

Histopathological diagnosis was made by brain biopsy in three patients. Three additional patients (PIDs 2, 10, and 13) had lymphoma diagnosed on biopsies from sites other than CNS, and one patient had both CNS and lymph node biopsy. Only the pediatric patients had EBV-specific serology performed at CNSL diagnosis: one consistent with acute infection and one with past infection.

Laboratory examination of the CSF (Fig) showed pleocytosis in 10 of 14 patients, erythrocytes in 6 cases, and elevated protein in all cases. Glucose concentration was normal in all but one patient who had 23 mg/dl of glucose in the CSF. The $\log_{10}$ EBV DNA copies per milliliter of CSF varied between 3.6 and 5.8 with a mean ± standard error (SE) of 4.8 ± 0.2.

Clinical management of CNSL patients varied (see

Table. Selected Clinical and Laboratory Characteristics of Patients with EBV-Associated Neurological Disorders

PID	Diagnosis	Gender	Age (yr)	Race	CSF EBV DNA (copies/ml)	CSF by the cycle mRNA	Underlying Conditions/ Treatment	EBV-Specific Therapy	Outcome
1	CNSL	M	26	H	4,100	nd	HIV/−	—	Fatal
2	CNSL[a]	M	32	H	10,000	nd	HIV/−	—	Fatal
3	CNSL[b]	M	37	W	15,000	nd	HIV/HAART	—	Fatal
4	CNSL[a]	M	56	H	25,540	+	HIV/HAART	ACV	Fatal
5	CNSL	M	38	W	28,000	+	HIV/ART	ACV	Fatal
6	CNSL	M	2	W	50,000	nd	Heart Tx/↓ IS	GCV	Fatal
7	CNSL[b]	M	33	W	50,000	nd	HIV/ART	ACV	Fatal
8	CNSL[b]	M	65	H	58,700	+	HIV/HAART	—	Stable
9	CNSL	M	45	H	92,000	nd	HIV/−	ACV	Fatal
10	CNSL[a,b]	M	48	W	115,000	+	HIV/HAART	—	Indeterminate[c]
11	CNSL	M	25	W	152,000	nd	HIV/HAART	ACV	Improved
12	CNSL	M	32	W	270,000	+	HIV/ART	ACV/GCV	Fatal
13	CNSL[a,b]	M	7	W	298,300	nd	Renal Tx/↓ IS	—	Improved
14	CNSL	M	38	W	605,000	nd	HIV/−	—	Fatal
15	Encephalitis	M	55	W	500	nd	NONE	ACV	Improved
16	Encephalitis	M	29	W	900	nd	HIV/HAART	—	Improved
17	Encephalitis	F	—	W	8,000	−	NONE	—	Improved
18	Encephalitis	M	47	W	8,900	nd	HIV/HAART	—	Improved
19	Encephalitis	M	71	W	17,900	−	Renal Tx/−	—	Improved
20	Encephalitis	M	43	W	29,000	+	HIV/HAART	ACV	Improved
21	Encephalitis	F	35	B	40,800	+	HIV/HAART	ACV	Improved
22	Encephalitis	M	19	W	64,400	+	Renal Tx/↓ IS	FOS	Improved
23	Encephalitis	M	18	W	77,000	+	NONE	ACV	Improved
24	Encephalitis	F	58	W	216,000	+	Renal Tx/↓ IS	ACV	Improved
25	ADEM	M	2	H	500	nd	NONE	ACV	Fatal
26	TRM	M	7	W	500	nd	NONE	—	Improved
27	PRM[d]	F	43	W	1,904	nd	CVID/IVIG	GCV	Improved
28	Guillain–Barré	M	55	W	2,000	nd	NONE	ACV	Stable

EBV = Epstein–Barr virus; CSF = cerebrospinal fluid; CNSL = central nervous system lymphoma; H = Hispanic; nd = not done; HIV = human immunodeficiency virus infection; W = white; HAART = highly active ART with three or more drugs including a protease inhibitor or nonnucleoside analog; ACV = acyclovir; Tx = transplantation; IS = immunosuppression; GCV = ganciclovir; ART = antiretroviral therapy with one or more nucleoside analogs; ADEM = acute demyelinating encephalitis; TRM = transverse myelitis; PRM = polyradiculomyelitis; CVID = combined variable immunodeficiency; IVIG = intravenous immunoglobulin.

[a]Patients with systemic lymphoma including the central nervous system.
[b]Patients treated with chemotherapy and/or radiation therapy.
[c]Outcome indeterminate because of insufficient follow-up (2 months).
[d]A detailed description of this case can be found in Majid and colleagues,[26] Case 4.

Table). Only 8 of the 12 HIV-infected patients received antiretroviral therapy. In addition, six received anti-EBV antivirals and five were treated with chemotherapy and/or radiotherapy. The clinical management of the two transplant recipients consisted of decreased immunosuppression and use of antivirals or chemotherapy. Clinical conditions improved or remained stable after 2 or more years of follow-up in two HIV-infected patients and one transplant recipient. There was no association between outcome and EBV viral load ($p = 0.37$, unpaired t test).

Epstein–Barr Virus Encephalitis

There were 10 patients with encephalitis (see Table). Seven had impaired immunity (four HIV infections and three transplantations). Signs and symptoms included fever, headache, seizures, aphasia, localized muscle weakness, and numbness or hyperesthesia. CT or magnetic resonance imaging were abnormal in all cases. Typical magnetic resonance findings included single or multiple areas of increased T_2 signal, often with gadolinium enhancement and associated edema in the cerebral hemispheres and cerebellum. One patient, a renal graft recipient (PID 22) who developed clinical and radiological abnormalities in the context of acute EBV infection by serological criteria underwent a brain biopsy, which showed areas of parenchymal and perivascular inflammation with polyclonal T-cell infiltrates, establishing the diagnosis of encephalitis.

The CSF (see Fig) leukocyte counts were elevated in all the patients with encephalitis and invariably showed a predominance of mononuclear cells. Reactive and atypical lymphocytes were each described in one patient. Erythrocytes were present in five cases. The CSF protein was elevated and glucose was normal in all cases. The EBV load in the CSF varied between 2.7

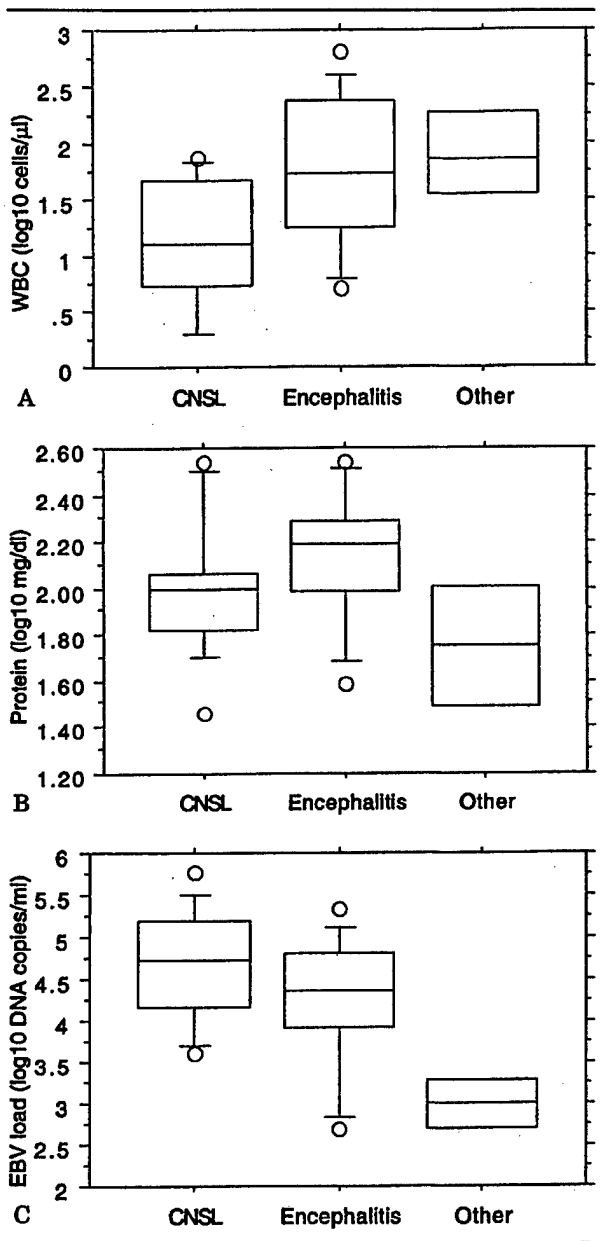

Fig. Cerebrospinal fluid analysis of patients with Epstein–Barr virus (EBV) infection of the central nervous system (CNS). Data were derived from 14 patients with CNS lymphoma (CNSL), 10 with encephalitis, and 4 with postinfectious complications (other). Leukocyte counts (A) were significantly different between CNSL and encephalitis patients ($p = 0.02$) but not for any other group comparisons ($p > 0.1$). Protein concentrations (B) were not statistically different among groups ($p > 0.1$). EBV load (C) was significantly lower in patients with postinfectious complications compared with encephalitis or CNSL ($p < 0.01$). The difference between CNSL and encephalitis did not quite reach statistical significance ($p = 0.07$). WBC = white blood cell (leukocyte)

and 5.3 $\log_{10}$ DNA copies per milliliter with mean ± SE of 4.2 ± 0.3 $\log_{10}$ copies per milliliter.

Six patients received EBV-specific antiviral therapy. The use of antivirals tended to be more common in patients with higher viral loads ($p = 0.09$, Mann–Whitney U test). This suggests an association between severity of disease and viral load, if we assume that the sicker patients were more likely to receive EBV-specific therapy. Among treated patients, signs of recovery began 2 to 7 days after initiating therapy. Two patients treated with anti-EBV antivirals, who had repeat measurements of EBV load in the CSF 7 and 14 days into therapy, respectively, showed greater than or equal to 1 $\log_{10}$ decreases of the viral load. Two HIV-infected patients with encephalitis had been receiving highly active antiretroviral therapy for 4 years when they developed EBV encephalitis and two started highly active antiretroviral therapy after the diagnosis of EBV infection. Management of immunosuppressive regimens in the three transplant recipients varied. All patients with EBV encephalitis improved clinically, regardless of underlying conditions, use of EBV-specific antiviral therapy, or EBV load.

Postinfectious Complications

Four patients experienced postinfectious complications, one each with Guillain–Barré syndrome, acute demyelinating encephalitis, polyradiculomyelitis, or transverse myelitis (see Table).

CSF examinations showed elevated leukocyte and protein in three cases each, erythrocyte and normal glucose in all cases. The EBV load varied between 2.7 and 3.3 $\log_{10}$ EBV DNA copies per milliliter (mean ± SE, 3 ± 0.2 $\log_{10}$ DNA copies/ml). PIDs 25 and 26 had serological evidence of acute EBV infection.

All patients received immunomodulators (corticosteroids or intravenous immunoglobulin). Three patients also received antivirals. PID 25 died of EBV-associated hemophagocytic syndrome soon after the diagnosis of acute demyelinating encephalitis was established. The other patients improved or remained stable.

Comparative Analysis of Cerebrospinal Fluid Findings in Patients with Epstein–Barr Virus–Associated Central Nervous System Infections

To identify correlations between CSF abnormalities and EBV-associated neurological disorders, the results of EBV quantitative PCR, leukocyte, and protein were compared among the three diagnostic categories. EBV load in the CSF was significantly higher in patients with CNSL and encephalitis versus postinfectious complications ($p < 0.01$). The difference in EBV load between patients with CNSL and encephalitis was not significant, although patients with CNSL had fewer CSF leukocyte ($p = 0.02$). Protein levels were statistically similar among all groups.

Regression analysis was used to determine correlations of EBV load in the CSF with leukocyte counts. There was a significant inverse correlation between

EBV load and leukocyte across all diagnostic categories ($p = 0.04$), which argues against the hypothesis that EBV in CSF resulted solely from latent viral DNA present in infiltrating lymphocytes. When patients with encephalitis were separately analyzed, the inverse correlation between EBV load and leukocyte almost reached significance ($p = 0.08$), suggesting that the inflammatory infiltrate might contribute to viral clearance.

Identification of mRNA Corresponding to a Lytic Cycle Gene in the Cerebrospinal Fluid

Twelve CSF samples were tested by RT-PCR for transcription of the lytic cycle gene *BZLF1* (Table). Ten samples, equally distributed between CNSL and encephalitis patients, which contained 4.5 to 5.8 $\log_{10}$ EBV DNA copies per milliliter, showed evidence of mRNA synthesis indicating active EBV replication in the CNS. In the remaining two samples, both DNA and RNA amplification failed, indicating decreased sequence homology between the primers the template and/or DNA copy number below the analytical sensitivity of the test.

Discussion

EBV PCR of the CSF established the association of neurological disorders with EBV in the absence of acute EBV infection. Most descriptions of the neurological complications of EBV are based on children with acute EBV infection.[1–7] In contrast, only 17% of our patients were children, despite the fact that users of the laboratory for EBV PCR include a similar number of adult and pediatric health care facilities. This preponderance of EBV CNS infections in adults, which differs from previous reports, could be partially ascribed to the high number of immunocompromised patients in our study. However, all three immunocompetent patients with EBV encephalitis were older than 18 years of age. Other investigators have also recently described isolated cases of EBV encephalomyelitis in adults with serological evidence of EBV reactivation.[26–29]

CSF analysis showed significant differences among diagnostic categories for EBV load and leukocytes. Patients with CNSL had high CSF EBV load in the presence of low leukocyte counts. Patients with encephalitis also had relatively high EBV load, but this was associated with higher CSF leukocytes than in patients with CNSL. Patients with postinfectious complications of EBV infection had a low EBV load associated with a relatively high CSF leukocyte count. These CSF patterns suggest the following pathogenic scenarios: rapid cellular and viral turnover with limited inflammatory response in CNSL, intense viral replication and vigorous inflammation associated with encephalitis, and low viral replication and vigorous inflammation associated with postinfectious complications.

Antivirals active against EBV were used in some patients, but their use did not affect the outcome of the disease. However, a selection bias favoring the use of antivirals in the sickest population might have occurred. This is suggested by the fact that, among patients with encephalitis, the use of acyclovir and ganciclovir was more common in individuals with high viral loads. This observation also might indicate an association between high CSF EBV load and severity of clinical manifestations, if we assume that physicians were more likely to treat sicker patients. Of note, the CSF EBV load decreased in the two encephalitis patients whose CSF was tested after 7 and 14 days of treatment, respectively, suggesting that the drugs inhibited the viral replication.

The presence of lytic cycle mRNA in the CSF in all 10 patients in whom this could be analyzed indicated that EBV was actively replicating in the CNS. This result is consistent with a lack of correlation between CSF EBV viral load and CSF leukocyte counts, which strongly suggests that the EBV DNA detected by PCR was from actively replicating virus and not just latent EBV DNA carried in inflammatory cells. Actively replicating EBV in the CNS may have resulted from either de novo infection or reactivation of latent virus. Because EBV does not become latent in neurons or other nonlymphoid cells, if CNS infection follows EBV reactivation, it is likely that this occurs at extraneural sites with subsequent spread of virus to CNS by infected lymphocytes.

It has been suggested previously that EBV encephalitis was a consequence of cytotoxic T-lymphocyte–mediated tissue destruction.[30] In this series, two patients with encephalitis had CSF atypical lymphocytes, consistent with cytotoxic T lymphocytes. Furthermore, EBV load decreased with higher leukocyte counts, suggesting a role of the inflammatory cells in viral clearance. These data taken collectively indicate that patients with severe EBV encephalitis might benefit from combined antiviral and T-cell immunosuppressive therapy.

This study was supported by grants from National Institute of Child Health and Human Development (N01-HD-3-3162) and National Institute of Health (U01A138858, A.W.) and by grants from the Department of Defense (DAMD 17-98-1-8614), Department of Veterans Affairs, and the Reuler-Lewin Family Professorship of Neurology (K.L.T.).

We thank Drs J. Anderson, A. Ansari, M. Barron, W. Burman, D. Cohn, S. Johnson, M. Landry, J. Nania, and W. Williams for referring the patient specimens and providing the clinical information, and Dr M. Levin for critical review of the manuscript.

References

1. Connelly KP, DeWitt LD. Neurologic complications of infectious mononucleosis. Pediatr Neurol 1994;10:181–184.

2. Cotton MF, Reiley T, Robinson CC, et al. Acute aqueductal stenosis in a patient with Epstein-Barr virus infectious mononucleosis. Pediatr Infect Dis J 1994;13:224–227.
3. Anderson MD, Kennedy CA, Lewis AW. Retrobulbar neuritis complicating acute Epstein-Barr virus infection. Clin Infect Dis 1994;18:799–801.
4. Tsutsumi H, Kamazaki H, Nakata S, et al. Sequential development of acute meningoencephalitis and transverse myelitis caused by Epstein-Barr virus during infectious mononucleosis. Pediatr Infect Dis J 1994;13:665–667.
5. Connolly M, Junker AK, Chan KW, et al. Cranial neuropathy, polyneurophathy and thrombocytopenia with Epstein-Barr virus infection. Dev Med Child Neurol 1994;36:1010–1015.
6. Grose C, Henle W, Henle G, et al. Primary Epstein-Barr virus infections in acute neurologic diseases. N Engl J Med 1975; 292:392–395.
7. Alpert G, Fleisher GR. Complications of infection with Epstein-Barr virus during childhood: a study of children admitted to the hospital. Pediatr Infect Dis J 1984;3:304–307.
8. Hochberg IH, Miller G, Schooley RT, et al. Central-nervous-system lymphoma related to Epstein-Barr virus. N Engl J Med 1983;309:745–748.
9. Cinque P, Brytting M, Vago L, et al. Epstein-Barr virus DNA in cerebrospinal fluid from patients with AIDS-related primary lymphoma of the central nervous system. Lancet 1993;342: 398–401.
10. Meerbach A, Gruhn B, Egerer R, et al. Semiquantitative PCR analysis of Epstein Barr virus DNA in clinical samples of patients with EBV-associated diseases. J Med Virol 2001;65:348–357.
11. Jones JL, Hanson DL, Dworkin MS, et al. Effect of antiretroviral therapy on recent trends in selected cancers among HIV-infected persons. J Acquir Immune Defic Syndr 1999; 21(suppl):11–17.
12. Buchbinder SP, Holmberg SD, Scheer S, et al. Combination antiretroviral therapy and incidence of AIDS-related malignancies. J Acquir Immune Defic Syndr 1999;21(suppl):23–25.
13. Palella FP Jr, Delaney KM, Moorman AC, et al. Declining morbidity and mortality among patients with advanced human immunodeficiency virus infection. New Engl J Med 1998;338: 853–860.
14. Halsted CC, Chang RS. Infectious mononucleosis and encephalitis: recovery of EB virus from spinal fluid. Exp Reason 1979;64:257–258.
15. Schiff JA, Schaefer JA, Robinson JE. Epstein-Barr virus in cerebrospinal fluid during infectious mononucleosis encephalitis. Yale J Biol Med 1982;55:59–63
16. Joncas JH, Chicoine L, Thivierge R, et al. Epstein-Barr virus antibodies in the cerebrospinal fluid: a case of infectious mononucleosis with encephalitis. Am J Dis Child 1974;127: 282–285.
17. Bray PF, Culp KW, McFarlin DE, et al. Demyelinating disease after neurologically complicated primary Epstein-Barr virus infection. Neurology 1992;42: 278–282.
18. Paskavitz JF, Anderson CA, Filley CM, et al. Acute arcuate fiber demyelinating encephalopathy following Epstein-Barr virus infection. Ann Neurol 1995;38:127–131.
19. Cinque, P, Vago L, Dahl H, et al. Polymerase chain reaction on cerebrospinal fluid for diagnosis of virus-associated opportunistic diseases of the central nervous system in HIV-infected patients. AIDS 1996;10:951–958.
20. D'Arminio Monforte A, Cinque P, Vago L, et al. A comparison of brain biopsy and CSF-PCR in the diagnosis of CNS lesions in AIDS patients. J Neurol 1997;244:35–39.
21. Pedneault L, Katz BZ, Miller G. Detection of Epstein-Barr virus in the brain by the polymerase chain reaction. Ann Neurol 1992;32:184–192.
22. Weinberg A, Spiers D, Cai GY, et al. Evaluation of a commercial polymerase chain reaction kit for the diagnosis of CMV infection of the central nervous system. J Clin Microbiol 1998; 11:3382–3384.
23. Weinberg A, Hodges TN, Li S, et al. A comparison of polymerase chain reaction, antigenemia and rapid blood culture for the detection and prevention of cytomegalovirus disease after lung transplantation. J Clin Microbiol 2000;38:768.
24. Zhang JX, Chen HL, Zong YS, et al. Epstein-Barr virus expression within keratinizing nasopharyngeal carcinoma. J Med Virol 1998;55:227–233.
25. Chen HL, Lung ML, Chan KH, et al. Tissue distribution of Epstein-Barr virus genotypes. J Virol 1996;70:7301–7305.
26. Majid A, Galetta SL, Sweeney CJ, et al. Epstein-Barr virus myeloradiculitis and encephalomyeloradiculitis. Brain 2002;125: 159–165.
27. Imai S, Usui N, Sugiura M, et al. Epstein-Barr virus genomic sequences and specific antibodies in cerebrospinal fluid in children with neurologic complications of acute and reactivated EBV infections. J Med Virol 1993;40:278–284.
28. Bray PF, Culp KW, McFarlin DE, et al. Demyelinating disease after neurologically complicated primary Epstein-Barr virus infection. Neurology 1992;42:278–282.
29. Tselis, A, Duman R, Storch GA, et al. Epstein-Barr virus encephalomyelitis diagnosed by polymerase chain reaction: detection of the genome in the CSF. Neurology 1997;48: 1351–1355.
30. Lehrnbecher T, Chittka B, Nanan R, et al. Activated T lymphocytes in the cerebrospinal fluid of a patient with Epstein-Barr virus-associated meningoencephalitis. Pediatr Infect Dis J 1996;15:631–632.

Journal of NeuroVirology, 8: 365–380, 2002
 ISSN 1355-0284/02 $12.00+.00
DOI: 10.1080/13550280290100806

Reovirus-induced neuronal apoptosis is mediated by caspase 3 and is associated with the activation of death receptors

Sarah M Richardson-Burns,[1] Douglas J Kominsky,[2] and Kenneth L Tyler[1,2,3,4]

[1]Neuroscience Program, Departments of [2]Neurology, [3]Medicine, [3]Immunology, and [3]Microbiology, University of Colorado Health Sciences Center, Denver, Colorado, USA; and [4]Denver Veteran's Affairs Medical Center, Denver, Colorado, USA

Reovirus infection of the central nervous system (CNS) is an important experimental system for understanding the pathogenesis of neurotropic viral infection. Infection of neonatal mice with T3 reoviruses causes lethal encephalitis in which injury results from virus-induced apoptosis. We now show that this apoptosis *in vivo* is associated with activation of caspase 3, and use neuroblastoma and primary neuronal cultures to identify the cellular pathways involved. Reovirus-induced apoptosis in neuronal cultures is initiated by activation of the tumor necrosis factor (TNF) receptor superfamily death receptors and is inhibited by treatment with soluble death receptors (DRs). The DR-associated initiator caspase, caspase 8, is activated following infection, this activation is inhibited by a cell-permeable peptide inhibitor (IETD-CHO). In contrast to our previous findings in non-neuronal cell lines, reovirus-induced neuronal apoptosis is not accompanied by significant release of cytochrome *c* from the mitochondria or with caspase 9 activation following infection. This suggests that in neuronal cells, unlike their non-neuronal counterparts, the mitochondria-mediated apoptotic pathway associated with cytochrome *c* release and caspase 9 activation does not play a significant role in augmenting reovirus-induced apoptosis. Consistent with these results, peptide caspase inhibitors show a hierarchy of efficacy in inhibiting reovirus-induced apoptosis, with inhibitors of caspase 3 > caspase 8 >>> caspase 9. These studies provide a comprehensive profile of the pattern of virus-induced apoptotic pathway activation in neuronal culture. *Journal of NeuroVirology* (2002) **8**, 365–380.

Keywords: apoptosis; caspases; CNS; neuroblastoma; neuronal cultures; virus

Viruses cause disease by injuring or killing discrete populations of cells in host organs. Cell loss or damage is particularly detrimental in tissues with limited ability to regenerate, such as the mature central nervous system (CNS). In cell culture, many neurotropic viruses have the capacity to kill target cells, including neurons, by inducing apoptosis. A small group of viruses, including human immunodeficiency virus (HIV) (Petito *et al*, 1999), Dengue (Despres *et al*, 1996), Sindbis (Nava *et al*, 1998; Jan and Griffin, 1999), Theiler's (Jelachich and Lipton, 2001), rabies (Jackson and Rossiter, 1997a), and reovirus (Oberhaus *et al*, 1997), have been shown to induce apoptosis in experimental or natural models

Address correspondence to Kenneth L Tyler, Department of Neurology (B-182), University of Colorado Health Sciences Center, 4200 E. 9th Avenue, Denver, CO 80262, USA. E-mail: ken.tyler@uchsc.edu

The authors would like to thank Ron Bouchard for help with microscopy, Penny Clarke for advice about apoptosis assays, and Suzanne Meintzer for help with viral plaque assays. The University of Colorado Cancer Center provided flow cytometry equipment and facilities. This work was supported by Public Health Service grant 1R01AG14071 from the National Institute of Aging, Merit and REAP grants from the Department of Veterans Affairs, and a U.S. Army Medical Research Acquisition Activity grant (DAMD 17-98-1-8614). Dr. Tyler is also supported by the Reuler-Lewin Family Professorship of Neurology.

Received 13 May 2002; revised 21 May 2002; accepted 24 May 2002.

of encephalitis *in vivo*. Despite the importance of apoptosis as a mechanism of virus-induced cell death, little is known about the nature of apoptotic signaling pathways activated during neurotropic viral infection. Identifying mechanisms of virus-induced apoptosis is critical not only to understanding the pathogenesis of CNS viral infections but may also be relevant to neurodegenerative and other neurological diseases in which apoptosis contributes to neuronal loss (Allsopp and Fazakerley, 2000; Honig and Rosenberg, 2000; Mattson, 2000; Raghupathi *et al*, 2000; Yuan and Yankner, 2000).

Apoptosis is a distinct form of cell death in which affected cells undergo characteristic morphological and biochemical changes, including cytoplasmic shrinkage, condensation and fragmentation of nuclear chromatin, membrane alterations, and changes in gene and protein expression (Reed, 2000; Hengartner, 2000). Most forms of apoptosis are associated with sequential activation of cysteine-aspartyl proteases (caspases) by extracellular and/or intracellular stimuli, ultimately causing cleavage of cellular substrates, including laminins, poly-ADP-ribose polymerase (PARP), and DNA (Nunez *et al*, 1998; Earnshaw *et al*, 1999). Caspase activation has been implicated in neuronal apoptosis induced by diverse stimuli, including potassium deprivation (D'Mello *et al*, 2000), N-methyl-D-aspartate (NMDA) excitotoxicity (Ma *et al*, 1998; Budd and Lipton, 1999), and ischemic insults (Chien *et al*, 2000; Rentsch *et al*, 2001; Velier *et al*, 1999).

Experimental infection with mammalian reoviruses has provided a classic model for studying the pathogenesis of viral infection *in vivo* and virus-cell interactions *in vitro* (Tyler, 2001). Reoviruses induce apoptosis in a variety of cells in culture, including fibroblasts, kidney cells, cardiac myocytes, and cells derived from a variety of human cancers. Our laboratory has shown that reovirus-induced apoptosis of undifferentiated epithelial and cancer cells is initiated by death receptor (DR) activation and involves sequential activation of caspase cascades, starting with the DR-associated initiator caspase, caspase 8 (Clarke *et al*, 2000, 2001). Caspase 8 activation leads to the cleavage of the Bcl-2 family protein Bid, which translocates to the mitochondrion where it facilitates release of apoptosis-inducing factors including cytochrome *c* (Kominsky, 2002). Once in the cytoplasm, cytochrome *c* forms part of the apoptosome complex that leads to the activation of caspase 9 (Li *et al*, 1997). Caspases 8 and 9 contribute to the activation of effector caspases, notably caspase 3, which act on cellular substrates, resulting in the morphological hallmarks of apoptosis.

Although reovirus can induce apoptosis in neurons *in vivo* (Oberhaus *et al*, 1997), studies of the cellular pathways involved in reovirus-induced apoptosis have been limited to non-neuronal cell lines. We now show that reovirus-induced apoptosis in neurons *in vivo* involves activation of the effector caspase, caspase 3, and use both neuroblastoma-derived cell lines and primary cultures of terminally differentiated neurons to investigate cellular pathways leading to this activation.

Results

Reovirus-induced apoptosis in the neonatal mouse brain is associated with caspase 3 activation

We have previously shown that type 3 reovirus strain Dearing (T3D)-induced encephalitis in neonatal mice is associated with apoptosis in the CNS (Oberhaus *et al*, 1997). To better understand the mechanisms by which this occurs, we looked for activation of caspase 3, a key effector caspase that is activated in many forms of apoptosis. Activated caspase 3 was detected by immunohistochemistry in mouse brain tissue at day 7 post infection and correlated with distribution of viral antigen and Terminal deoxynucleotidyl transferase (TdT)-mediated dUTP Nick-End Labeling (TUNEL) staining on serial tissue sections. We found that activated caspase 3 staining colocalized to regions of mouse brain also containing viral antigen and apoptotic cells (TUNEL positive), including the cingulate cortex, hippocampus, and thalamus (Figure 1). Having shown that reovirus-induced neuronal apoptosis involved caspase activation *in vivo*, we next used neuronal cultures to investigate the cellular pathways involved *in vitro*.

Reovirus induces apoptosis in mouse neuroblastoma-derived cells and mouse primary cortical cultures

Major morphological features of apoptosis include modification of the plasma membrane, compaction and margination of nuclear chromatin, and oligonucleosomal DNA fragmentation. We looked for evidence of these apoptotic features in reovirus-infected mouse neuroblastoma-derived cell line NB41a3 (NB4) and in primary mouse cortical cultures derived from embryonic (E20) mice (MCC). Translocation of phosphatidylserine (PS) from the inner to the outer leaflet of the plasma membrane is an early morphological feature of apoptosis that can be detected by annexin V staining (Martin *et al*, 1995). We detected PS translocation (annexin V labeling) in T3D-infected NB4 as early as 6 h following infection. By 10 h post infection, there was a significant ($P < .001$) increase in annexin V labeling in T3D-infected cells (53% ± 3%) as compared to mock (15% ± 1%) (Figure 2A). Propidium iodide (PI), which can only enter cells with compromised plasma membranes, was used as a second label in the annexin V assay, staining late apoptotic cells (also annexin V positive) and necrotic cells (only PI positive). Cells were treated with 30% ethanol for 1 h prior to the annexin V assay to generate necrotic cells as a negative control. In contrast to virus-infected cells, these necrotic (only PI-positive) cells did not show annexin V labeling (5% ± 1%).

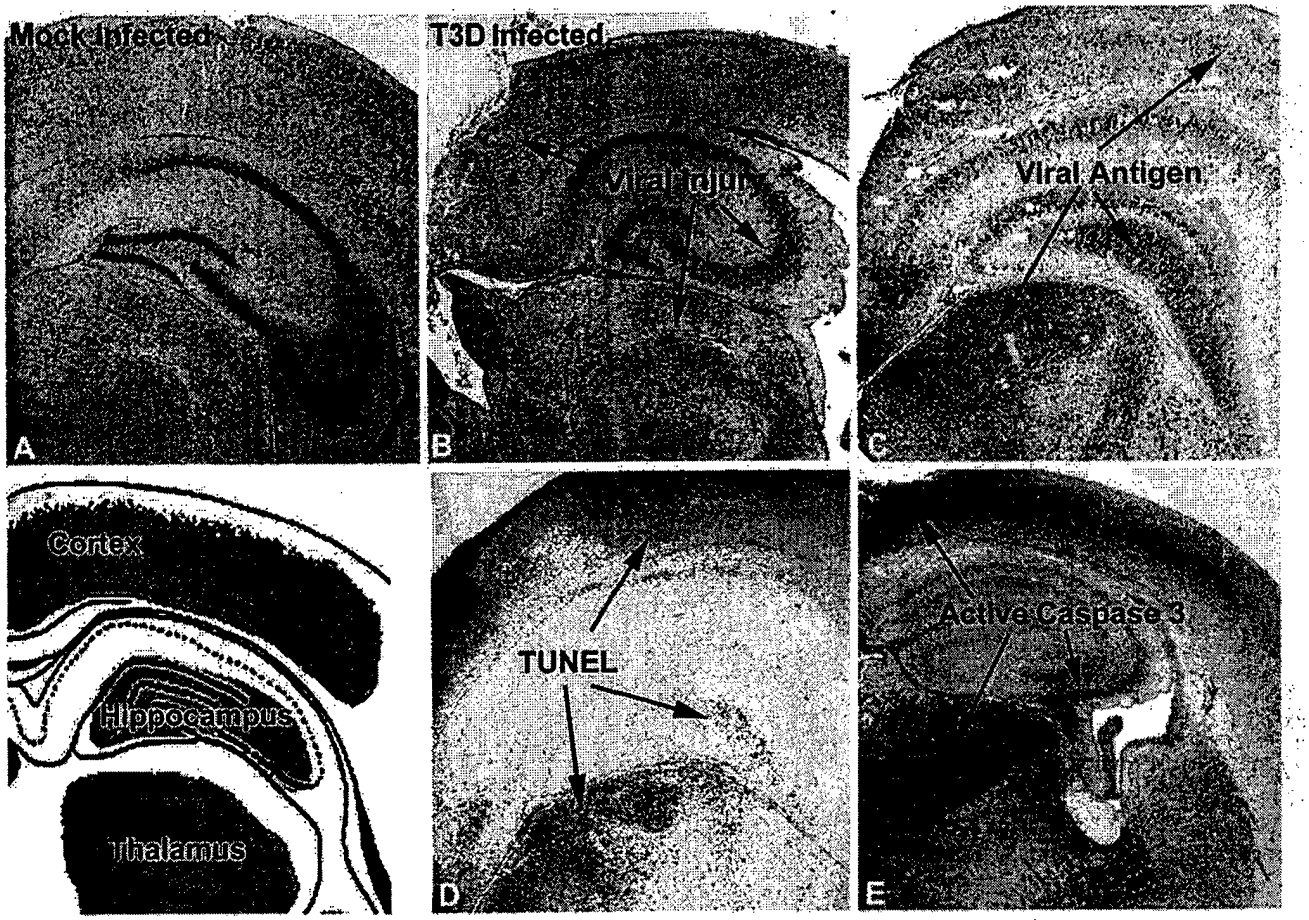

Figure 1 Coronal sections of neonatal mouse brain 7 days after intracranial inoculation of 10,000 PFU of strain T3D reovirus or mock inoculation (eight mice per treatment group). Hematoxylin and eosin–stained tissue reveals marked destruction of brain tissue in the T3D infected brain (**B**) as compared to the uninfected brain (**A**). Using immunohistochemistry, serial sections of T3D-infected brain tissue were stained for viral antigen (**C**), TUNEL/apoptosis marker (**D**), and active caspase 3 (**E**). Staining for viral antigen, TUNEL, and active caspase 3 was undetectable in the mock-infected brains (data not shown).

These results were confirmed by finding changes in nuclear structure characteristic of apoptosis, including chromatin condensation and margination in cells stained by the fluorescent nuclear dye, Hoechst 33342 (Figure 2**B**). Proapoptotic signal transduction leads to activation of a caspase-activated endonuclease that cleaves DNA at internucleosomal points (located at ~180-bp intervals) and exposes 3′ OH ends normally bound by nuclear proteins. These two features of apoptosis were detected by DNA ladder assay and TUNEL (Gavrieli *et al*, 1992), respectively. Apoptotic DNA fragmentation detected by DNA ladder assay was present in T3D-infected NB4 and MCC (Figure 2**C**). There was significantly greater levels of free 3′ OH ends detected by TUNEL in T3D-infected NB4 and MCC as compared to mock infected cells at 48 h post infection (Figure 2**D**). As an additional control, we also infected the neuronal cultures with type 1 reovirus strain Lang (T1L), a reovirus strain that induces significantly less apoptosis than T3D in non-neuronal cell cultures (Tyler *et al*, 1995). The percentage of TUNEL-positive cells in T1L-infected neuronal cultures was similar to that in mock-infected cultures (see Figure 2**D**).

Reovirus-induced neuronal apoptosis requires viral binding at host cell receptors

In order to insure that apoptosis seen in reovirus-infected neuronal cultures occurred as a direct consequence of viral binding, we tested whether a monoclonal antibody (9BG5, hereafter "anti-T3D") specific for the T3D $\sigma 1$ viral attachment protein would inhibit virus-induced apoptosis. Anti-T3D has been shown to protect neonatal mice from T3D-induced neuronal injury (Virgin *et al*, 1988; Tyler *et al*, 1989), and inhibits apoptosis in non-neuronal cultures *in vitro* (Tyler *et al*, 1995; Oberhaus *et al*, 1997). T3D inoculum was preincubated (1 h) with either anti-T3D or an isotype-matched control antibody specific for the T1L $\sigma 1$ protein (5C6) (Virgin *et al*, 1988; Tyler *et al*, 1989) prior to infection of neuronal cultures. Nuclear morphology assays and TUNEL were performed at 48 h post infection to

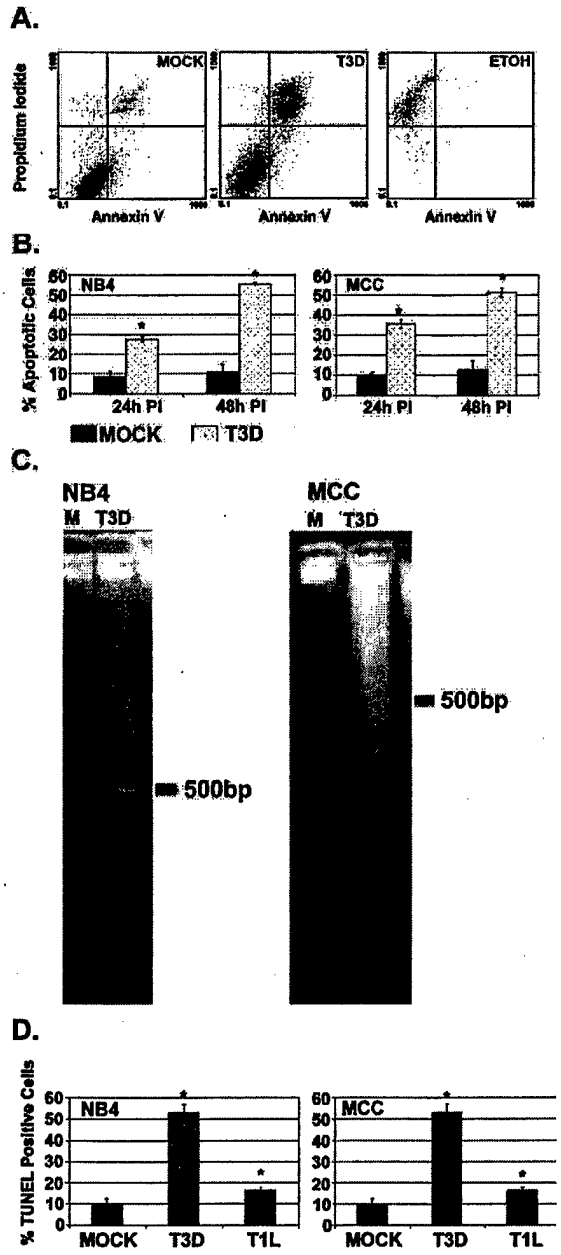

Figure 2 (A) Scatter plots representing flow cytometric analysis of mock (M)-infected, T3D-infected, and ethanol (ETOH)-treated mouse NB41a3 neuroblastoma cells (NB4), stained with annexin V–FITC and propidium iodide at 10 h post infection generated following flow cytometry. Annexin V–FITC fluorescence intensity is on the *x* axis (FL1 channel) and propidium iodide fluorescence is on the *y* axis (FL3 channel). (B) Percent apoptosis in M- and T3D-infected NB4 and mouse primary cortical cultures (MCC) at 24 and 48 h post infection. Data are presented as mean ± standard error of three to four experiments with 300 cells counted per condition per experiment, $^*P < .001$ for M versus T3D at both 24 and 48 h post infection by Tukey-Kramer multiple-comparison test. PI = post infection. (C) By 48 h PI, T3D infection–induced oligonucleosomal DNA fragmentation ("ladders") in NB4 and MCC. (D) The percentage of TUNEL-positive NB4 and MCC following M infection, T3D infection, and T1L infection. Data are presented as mean ± standard error of six experiments with 300 cells counted per condition per experiment, $^*P < .001$ for M versus T3D and T3D versus T1L by Tukey-Kramer multiple-comparison test.

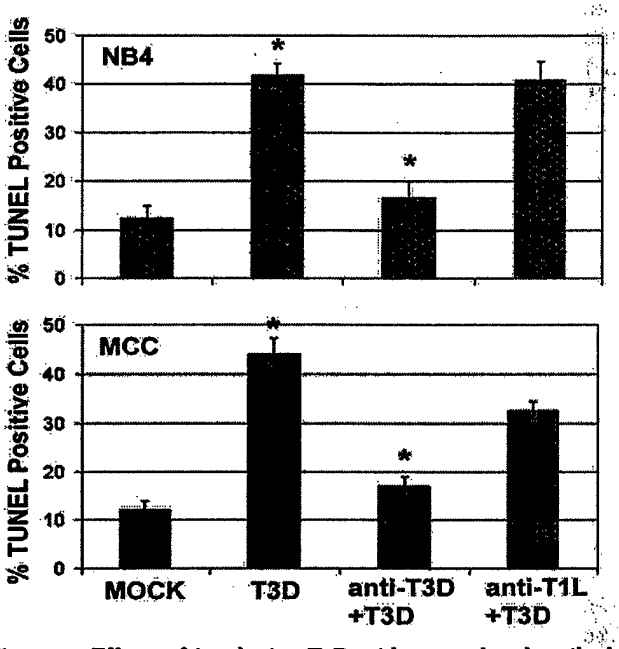

Figure 3 Effects of incubating T3D with monoclonal antibody (anti-T3D) specific for the T3D viral attachment protein or with an isotype-matched control antibody (anti-T1L) specific for the T1L viral attachment protein prior to infection of mouse neuroblastoma cells (NB4) and mouse primary cortical cultures (MCC). These are compared with T3D- and mock-infected NB4 and MCC. Data are percentage TUNEL-positive cells in each treatment. Data are presented as mean ± standard error of three experiments with 300 cells counted per condition per experiment, $^*P < .001$ for anti-T3D + T3D versus anti-T1L + T3D and anti-T3D + T3D versus T3D by Tukey-Kramer multiple-comparison test.

determine percentage of apoptotic cells present in each sample. Treatment of T3D with anti-T3D but not with control anti-T1L significantly inhibited reovirus-induced apoptosis in both types of neuronal culture (Figure 3).

Reovirus induces both direct and bystander apoptosis

Reovirus encephalitis is associated with both direct and "bystander" apoptosis as indicated by many cells in T3D-infected mouse cortex dual labeled for reovirus antigen and apoptosis and fewer cells positive for apoptosis marker alone (Oberhaus *et al*, 1997) (Figure 4A). In order to determine if both these mechanisms of apoptosis also occurred in neuronal cultures, we performed dual labeling by immunocytochemistry and TUNEL to determine whether cells infected with T3D were also undergoing apoptosis. We found that although the great majority of cells were undergoing apoptosis, there was a subset of apoptotic cells that were uninfected (antigen negative) but located in proximity to virus-infected cells. Thus, although most apoptotic cells in reovirus-infected neuronal cultures were virus-infected, some cells appeared to be undergoing "bystander" apoptosis (Table 1; Figure 4B, C).

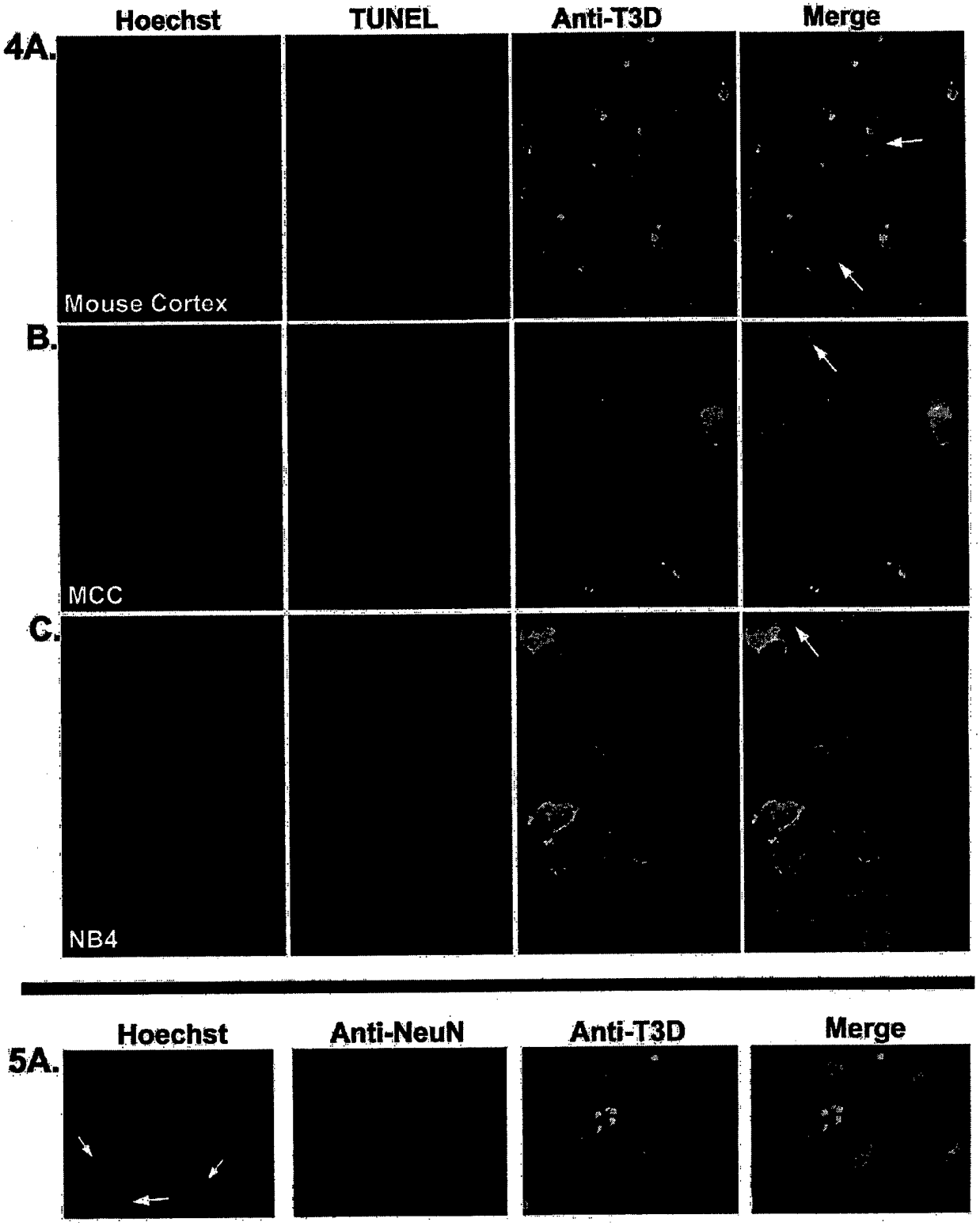

Figure 4–5A

Figure 4 (A) A coronal section of T3D-infected neonatal mouse cortex was triple labeled with Hoechst 33342 (nuclear dye), TUNEL-Cy3 (apoptosis marker), and immunohistochemistry for viral antigen–FITC (anti-T3D) to determine whether cells positive for viral antigen were also undergoing apoptosis. Colocalization of viral antigen and apoptosis was also detected in (B) mouse primary cortical cultures (MCC) and (C) mouse neuroblastoma cells (NB4) by triple labeling with Hoechst 33342, TUNEL-Cy3, and anti-T3D–FITC. Apoptotic cells that are not T3D-infected may be undergoing "bystander" apoptosis (indicated by white arrows). **Figure 5(A)** T3D infected mouse primary cortical cultures (MCC) were triple labeled with Hoechst 33342, immunocytochemistry for neuron nuclear protein-Cy3 (anti-NeuN), and immunocytochemistry for viral antigen-FITC (anti-T3D) to determine if the T3D infected cells were neurons. The primary cortical cultures are heterogeneous with approximately 70% neurons and 30% glia. Neurons (Cy3-red) are positive for NeuN and T3D (FITC-green). The large nuclei (Hoechst-blue) of glia are neither NeuN positive nor T3D positive (indicated by white arrows).

Table 1 Percentage distribution of apoptotic (TUNEL +) and infected (antigen +) cells in neuronal cultures

	Antigen + *TUNEL+*	*Antigen +* *TUNEL −*	*Antigen −* *TUNEL +*	*Antigen −* *TUNEL −*
NB4*				
24 h PI**	7% (± 2%)	52% (± 2%)	11% (± 1%)	31% (± 3%)
48 h PI	33% (± 2%)	38% (± 3%)	13% (± 2%)	16% (± 3%)
MCC***				
24 h PI	6% (± 1%)	36% (± 4%)	11% (± 2%)	47% (± 4%)
48 h PI	38% (± 2%)	26% (± 3%)	12% (± 3%)	25% (± 3%)

*NB4 = NB41a3; mouse neuroblastoma cell line.
**PI = post infection.
***MCC = mouse primary cortical cultures.

T3 reovirus grows in mouse neuroblastoma-derived cell lines and mouse primary cortical cultures and infects neurons in mixed primary cortical cultures

To determine if T3D infects neurons *in vitro* as seen *in vivo*, we used dual lable immunocytocchemistry to detect neurons (anti-neuron nuclear protein; NeuN) and reovirus infected cells (anti-T3D) in mixed (70% neurons, 30% glia) primary cortical cultures. Reovirus antigen was only detectable in cells that were also expressing neuron nuclear protein, indicating that following infection of mouse cortical cultures *in vitro*, T3D infection is restricted to neurons (Figure 5A). Although we have previously shown that reovirus-induced apoptosis in non-neuronal cells does not require viral replication, and that differences in the capacity of reovirus strains to induce apoptosis is not correlated with their replication efficiency in target cells (Rodgers *et al*, 1997; Tyler *et al*, 1995), we wished to determine whether this was true in neuronal cultures. We assessed viral yield by plaque assay following infection with T3D in NB4 and MCC. T3D grows in both types of neuronal culture. T1L grows to a significantly lower titer in NB4 as compared to T3D infected cells and does not grow in MCC (Figure 5B).

Reovirus-induced apoptosis in neuronal cultures is mediated by caspase 3 and caspase inhibition protects neurons from apoptosis

Many proapoptotic signaling pathways involve activation of caspase cascades that originate with pathway-specific initiator caspases (e.g., caspases 8 and 9) and converge on common downstream effector caspases (e.g., caspase 3). Having shown that caspase 3 was activated in the brains of T3D-infected neonatal mice, we wished to determine whether it was also activated in T3D-infected neuronal cultures. We first looked for caspase 3 activation in NB4 using a fluorogenic caspase substrate assay. Cell lysate was mixed with DEVD-AFC, a fluorogenic substrate that binds active caspase 3, allowing its

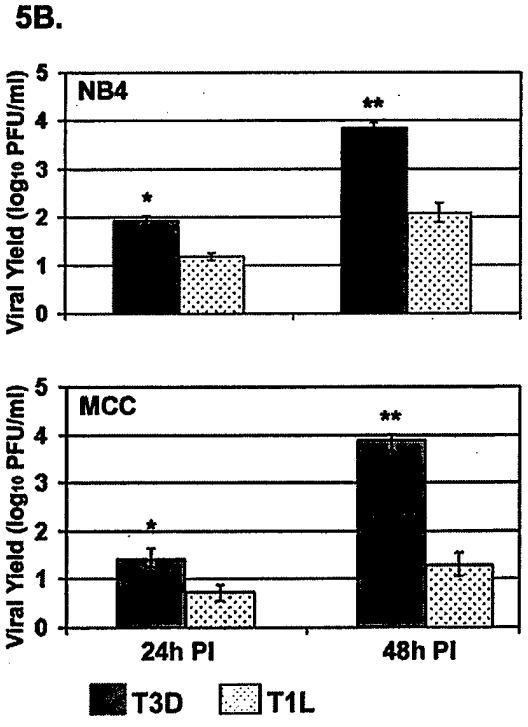

Figure 5 (B) One step growth curves were performed for both T3D and T1L in mouse neuroblastoma cells (NB4) and mouse primary cortical cultures (MCC). The data are represented as mean viral yield (log10 PFU/ml) ± standard error obtained at the designated timepoint after an initial exposure to viral inoculum at time 0 (*$P < 0.01$ and **$P < 0.001$ by Tukey-Kramer multiple comparisons test).

detection by fluoremetry. We detected significantly greater levels of active caspase 3 in T3D-infected NB4 as compared with mock-infected cells by 24 h post infection (Figure 6A). We next performed immunocytochemistry to detect the active caspase 3 fragment in T3D-infected NB4 and MCC at 24 h post infection. In both types of neuronal culture, T3D infection significantly increased the number of cells positive for active caspase 3 as compared to mock-infected cells (Figure 6B). Lastly, we wished to understand whether inhibition of caspase 3 activity could protect neuronal cultures from T3D-induced apoptosis. NB4 and MCC were treated with the cell-permeable caspase 3 inhibitor, DEVD-FMK, for 1 h prior to infection with T3D and throughout the infection. At 48 h post infection, TUNEL or apoptotic morphology assay was performed. We found that caspase 3 inhibition protected NB4 and MCC from T3D-induced neuronal apoptosis (Figure 6C).

Reovirus-induced apoptosis in neuronal cultures is associated with activation of caspase 8 and death receptors of the TNF receptor superfamily

Having established that reovirus-induced apoptosis was associated with activation of the downstream effector caspase, caspase 3, we next wished to determine which upstream caspases were involved in initiating this process. Having previously shown that caspase 8 activation is an early event in reovirus-induced apoptosis in non-neuronal cells, we looked for the presence of caspase 8 activation that preceded caspase 3 activation in NB4 (Clarke *et al*, 2001). Using a cell-free fluorogenic substrate assay for detecting active caspase 8, we found that caspase 8 was active in T3D-infected NB4 by 20 h post infection (Figure 7A). We also performed Western blot analysis to detect antibody of caspase 8 in whole cell lysates from infected NB4. This showed the presence of caspase 8 cleavage products, indicative of caspase 8 activation at ~20 h post infection (Figure 7B). Furthermore, we used immunocytochemistry to detect active caspase 8 in T3D-infected MCC at 20 h post infection (Figure 7B).

Having shown that caspase 8 was activated in reovirus-infected neuronal cultures, we wished to determine whether inhibition of this activity could protect neuronal cultures from reovirus-induced apoptosis. We pretreated NB4 and MCC with the cell-permeable caspase 8 inhibitor IETD-CHO (IETD) or the caspase 9 inhibitor Z-LEHD-FMK (LEHD) 1 h prior to and during T3D infection, then assayed apoptosis by TUNEL staining at 48 h post infection. In T3D-infected NB4 and MCC (MCC data not shown), inhibition of caspase 8 activity, but not inhibition of caspase 9 activity, significantly decreased the percentage of TUNEL-positive NB4 (Figure 7D). We next assayed cells treated with IETD to determine whether inhibition of caspase 8 activation was associated with inhibition of effector caspase activation. IETD did not

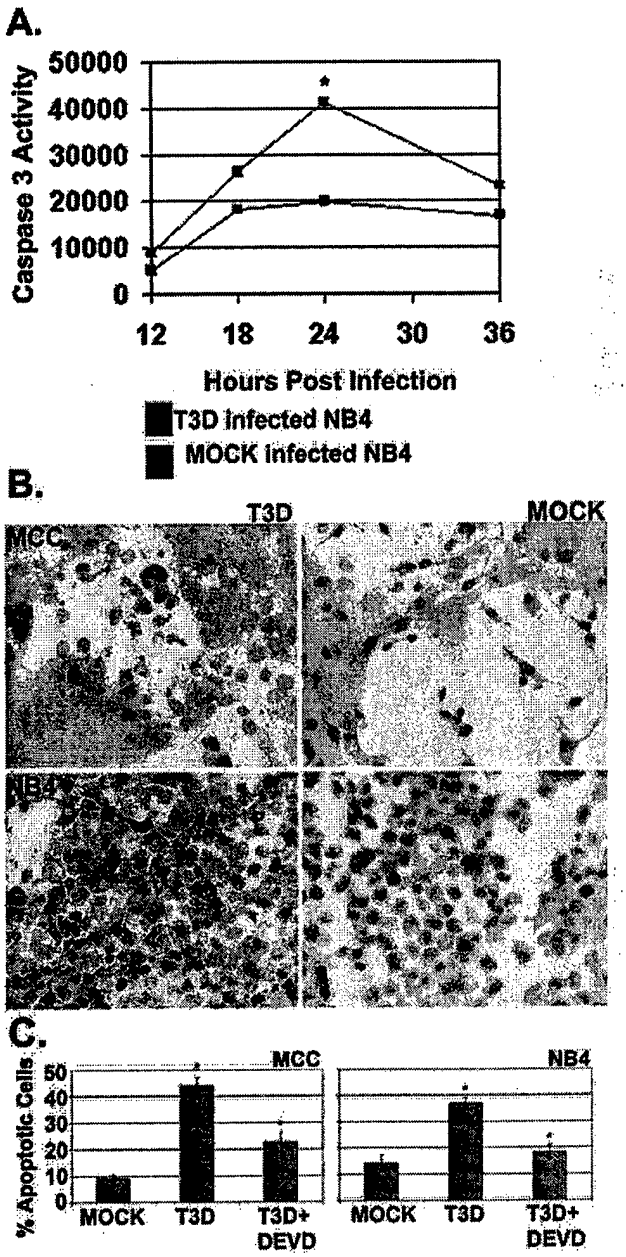

Figure 6 (A) Caspase 3 activity is increased in T3D-infected mouse neuroblastoma cells (NB4) as compared to mock infected cells at 24 h post infection. Data are raw fluorescent values obtained at 405 nm excitation and 500 nm emission. Data are mean raw fluorescence ± SEM (*$P < .01$ by Tukey-Kramer multiple-comparison test). (B) Immunocytochemistry was performed on mouse primary cortical cultures (MCC) and NB4 at 24 h post infection (PI) to detect the presence of active caspase 3 (anti–active caspase 3). Active caspase 3 is detectable in T3D-infected neuronal cultures but not in mock infected neuronal cultures. Cells were counterstained with Blue Counterstain. (C) The effect of inhibition by specific cell-permeable peptide inhibitor of caspase 3, DEVD-CHO (DEVD) on T3D-induced apoptosis in NB4 and MCC. Data are percentage of TUNEL-positive cells in NB4 or percentage apoptotic cells in MCC cells in each treatment. Data are presented as mean ± standard error of six experiments with 300 cells counted per condition per experiment, *$P < .001$ for M versus T3D and T3D versus T3D-DEVD by Tukey-Kramer multiple-comparison test.

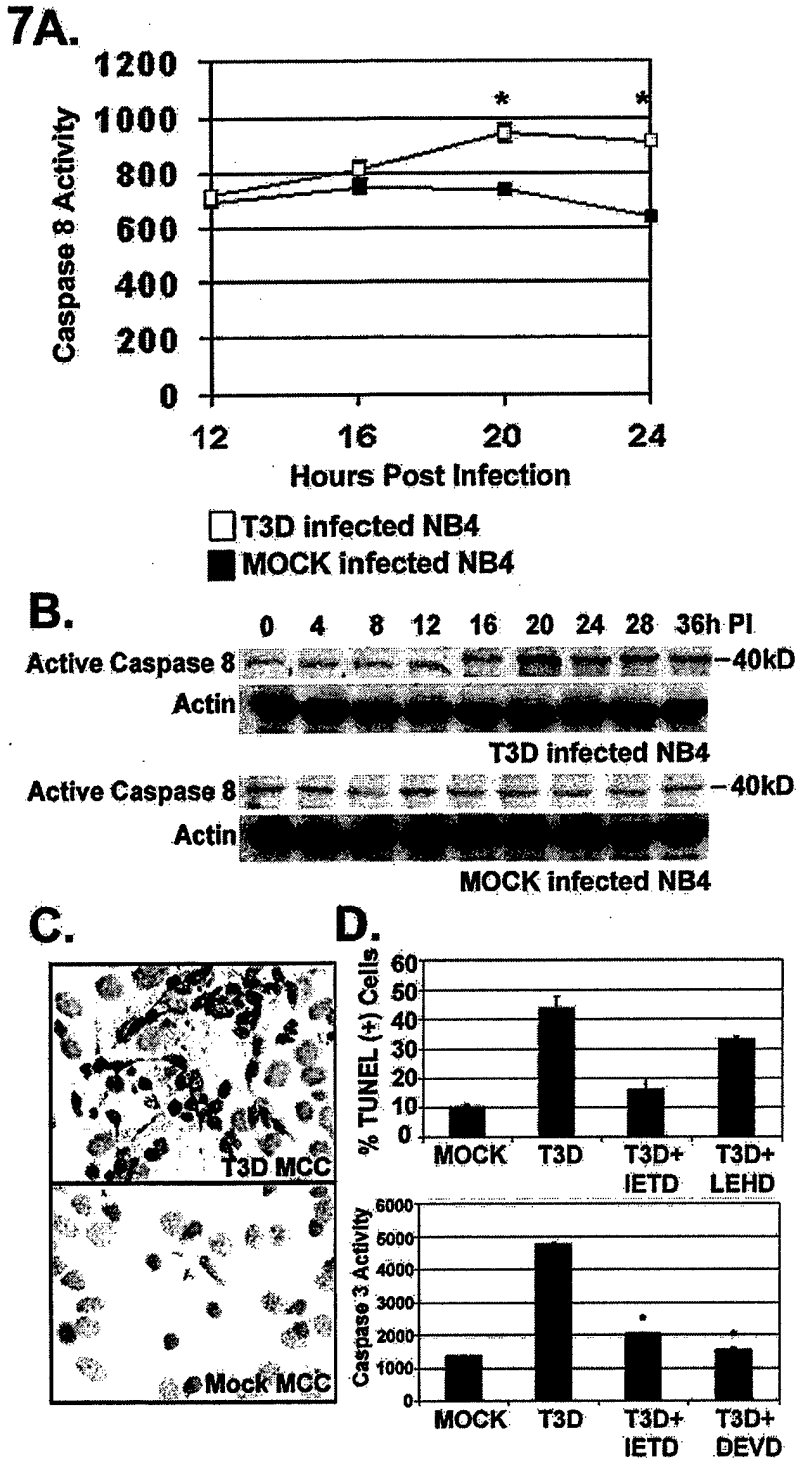

Figure 7 (A) Caspase 8 activity is increased in T3D-infected mouse neuroblastoma cells (NB4) as compared to mock-infected cells at 20 and 24 h post infection. Data are raw fluorescent values obtained at 405 nm excitation and 500 nm emission. Data are mean fluorescence ± SEM (* $P < .01$ by Tukey-Kramer multiple-comparison test). (B) Active caspase 8 (40-kDa cleavage fragment of pro-caspase 8) is increased in T3D-infected NB4 as compared to mock infected NB4 by 20 h post infection (PI) as detected by Western blot analysis. Protein loading was normalized by Western blot detection of actin levels. (C) Active caspase 8 is detectable in T3D-infected mouse primary cortical cultures (MCC) at 20 h PI by immunocytochemistry. (D) The effect of inhibition by specific cell-permeable peptide inhibitors of caspase 8, IETD-CHO (IETD) and caspase 9, Z-LEHD-FMK (LEHD), on T3D-induced apoptosis in NB4. Data are percentage of TUNEL-positive cells in each treatment at 48 h PI. Data are presented as mean ± standard error of six experiments with 300 cells counted per condition per experiment, * $P < .001$ T3D versus T3D + IETD by Tukey-Kramer multiple-comparison test. At 24 h PI, caspase 3 activity was decreased in T3D-infected NB4 treated with either the caspase 8 inhibitor, IETD-CHO (IETD), or the caspase 3 inhibitor, DEVD-CHO (DEVD), as compared to untreated T3D-infected NB4. Data are raw fluorescent values obtained at 405 nm excitation and 500 nm emission. Data are mean raw fluorescence ± SEM (* $P < .01$ for T3D versus T3D + IETD, T3D versus DEVD by Tukey-Kramer multiple-comparison test).

directly inhibit caspase 3 activity at the concentrations tested (data not shown). Caspase 3 activity was measured in reovirus-infected IETD-treated cultures by fluorogenic substrate assay. We found that caspase 3 activity was significantly decreased by treatment of T3D-infected NB4 with IETD, suggesting that in T3D-induced neuronal apoptosis, caspase 3 activity was at least in part mediated by active caspase 8 (Figure 7D).

Caspase 8 is a DR-associated initiator caspase. The presence of active caspase 8 in T3D-infected neuronal cultures, and the inhibition of reovirus-induced apoptosis by caspase 8 inhibitor, suggested that reovirus-induced neuronal apoptosis was mediated by activation of DRs. Tumor necrosis factor (TNF) receptor superfamily DRs are transmembrane proteins activated by death-inducing ligands, including TNFα, TNF-related apoptosis-inducing ligand (TRAIL), and Fas ligand (FasL) (Ashkenazi and Dixit, 1998). To test whether reovirus activates DR signaling in neuronal cultures, we treated T3D-infected NB4 and MCC with several different soluble recombinant death receptors (Fc:DR5/TRAIL-R2, Fc:TNFR-1, Fc:CD95/FASR), and assayed apoptosis by TUNEL staining at 48 h post infection. In T3D-infected NB4, we found that treatment with either Fc:DR5/TRAIL-R2 or Fc:TNFR-1 significantly decreased the percentage of TUNEL-positive cells. Treatment of T3D-infected NB4 with Fc:CD95/FASR had no effect on T3D-induced apoptosis (Table 2). In T3D-infected MCC, we found that treatment with either Fc:TNFR-1 or Fc:CD95/FASR significantly decreased the percentage of TUNEL-positive cells. Treatment of T3D-infected MCC with Fc:DR5/TRAIL-R2 had no effect on T3D-induced apoptosis (see Table 2). These results indicate that DRs play a key role in reovirus-induced neuronal apoptosis.

Mitochondria-associated proapoptotic signaling mediated by cytochrome c and caspase 9 is not a major factor in reovirus-induced apoptosis in neuronal cultures

We have recently shown that reovirus-induced DR-initiated apoptosis of HEK293 cells is amplified by mitochondria-associated apoptotic signaling, as indicated by robust release of cytochrome *c* from the mitochondria and activation of caspase 9 (Kominsky, 2002). We wanted to understand whether there was similar involvement of the mitochondria in reovirus-induced apoptosis in neuronal cultures. Using Western blot analysis of cell lysates from T3D-infected NB4 separated into cytoplasmic and membrane/mitochondrial fractions, we did not find evidence of significant release of cytochrome *c* in the cytoplasm (Figure 8A). Cytosolic cytochrome *c* participates in the apoptosome-mediated activation of caspase 9 (Li *et al*, 1997). Small amounts of active caspase 9 were detectable by Western blot in reovirus-infected NB4, but only at late times (28 to 36 h) post infection, well after the peak of caspase 3 activation (Figure 8B). In T3D-infected MCC, there was no increase in cytosolic cytochrome *c* and active caspase 9 was not detected (data not shown). In contrast to the effects seen with caspase 3 inhibitor (see Figure 6C), treatment of T3D-infected NB4 with caspase 9 inhibitor (Z-LEHD-FMK) did not inhibit T3D-induced apoptosis (see Figure 7D). Taken together, these data suggest that mitochondria-mediated apoptosis associated with release of cytochrome *c* from the mitochondria and activation of caspase 9 does not significantly contribute to reovirus-induced neuronal apoptosis.

Table 2 Percent inhibition of T3D-induced apoptosis in neuronal cultures by soluble death receptors

Fc:Receptor	*Fc:DR5*	*Fc:TNFR*	*Fc:FASR*
NB4*	23% (± 4%)	22% (± 4%)	1% (± 5%)
	$P < .001$	$P < .01$	NS**
MCC***	4% (± 4%)	25% (± 6%)	49% (± 6%)
	NS	$P < .05$	$P < .001$

*NB4 = NB41a3; mouse neuroblastoma cell line.
**NS = not significant.
***MCC = mouse primary cortical cultures.

Discussion

In this paper, we show that T3 reovirus-induced neuronal apoptosis in the neonatal mouse CNS involves activation of caspase 3, a key effector downstream of many proapoptotic signaling molecules. Active caspase 3 staining was found in brain regions with reovirus-induced tissue injury and colocalized with reovirus antigen and TUNEL (apoptosis marker). To further elucidate the signal transduction mechanisms by which reovirus induces apoptosis in neurons, we investigated reovirus-induced neuronal apoptosis *in vitro* using neuron-derived cell lines and primary cultures of terminally differentiated neurons.

T3D kills and also grows in mouse neuroblastoma-derived cell line NB41a3 (NB4) and mouse primary cortical cultures derived from embryonic (E20) mice (MCC). Using a variety of different assays, we show that T3D-induced neuronal cell death results from apoptosis as demonstrated by changes in the location of plasma membrane PS as detected by annexin V staining, nuclear condensation and/or margination as shown by nuclear dye assays, and apoptosis-specific DNA fragmentation as seen using TUNEL and DNA laddering. We also found that caspase 3 is activated in reovirus-infected neuronal cultures, paralleling results seen in the CNS following infection *in vivo*.

Having shown that caspase 3 was activated in reovirus-infected neuronal cultures, we wished to determine the upstream events in this process. We found that caspase 8, a DR-associated initiator caspase, is activated in both NB4 and MCC cultures as early as 18 h following T3D infection.

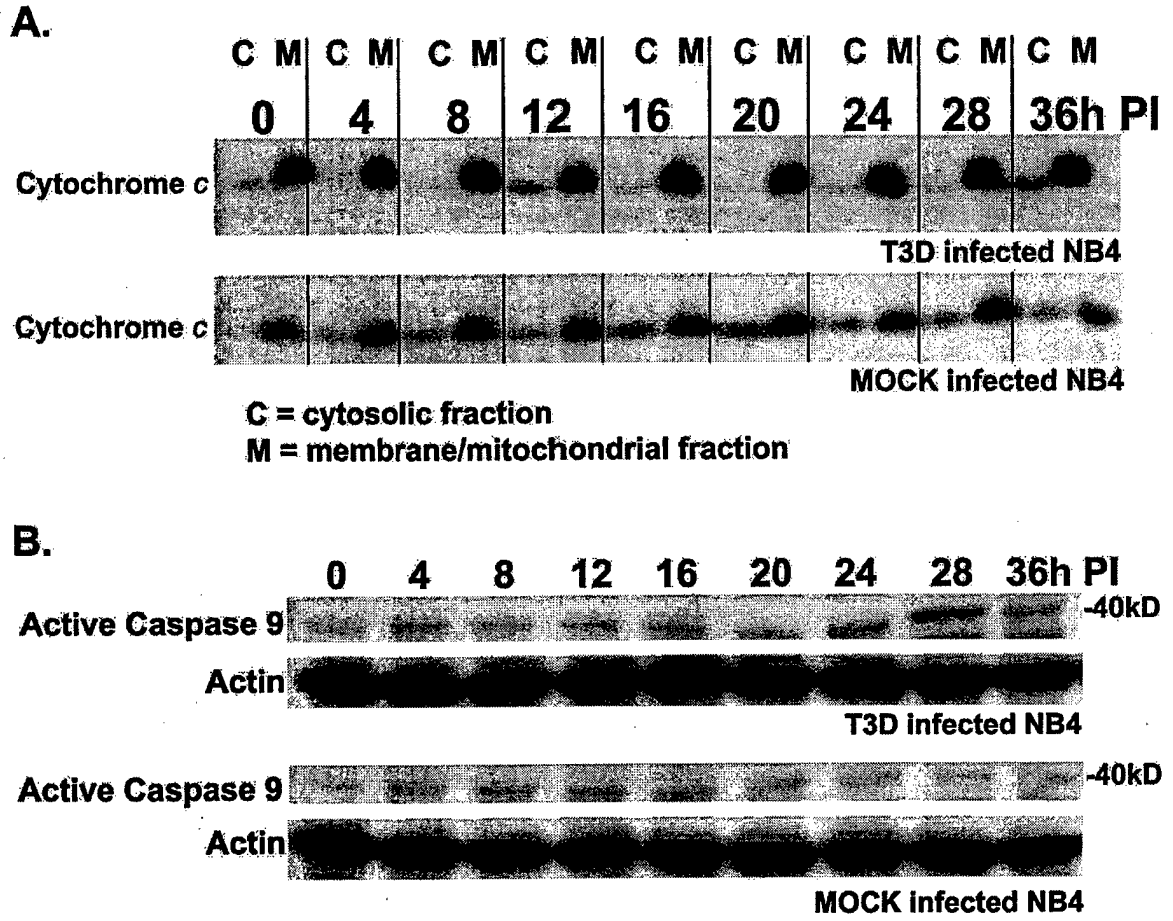

Figure 8 (A) Significant levels of cytosolic cytochrome *c* are not detected in T3D-infected mouse neuroblastoma cells (NB4) nor in mock-infected cells by Western blot analysis. (B) There is no difference in levels of active caspase 9 (40-kDa cleavage fragment of pro-caspase 9) between T3D-infected and mock-infected NB4 at time points preceeding caspase 3 activation (approximately 24 h post infection) as detected by Western blot analysis. Protein loading was normalized by Western blot detection of actin levels. PI = post infection.

Caspase 8 is activated by stimulation of the TNF receptor superfamily DRs following binding of death-inducing ligands such as TNFα, TRAIL, and FasL (Ashkenazi and Dixit, 1998). Caspase 8 activation has been implicated in apoptosis induced by viruses including HIV (Patel *et al*, 2000), Epstein-Barr virus (Tepper and Seldin, 1999), and Sendai virus (Bitzer *et al*, 1999). Recent studies from our laboratory indicate that in epithelial cell lines, and in certain human breast and lung cancer cell lines, reovirus stimulates TRAIL release from infected cells, activating DR4/DR5 (TRAILR1/TRAILR2) signaling pathways, leading to caspase 8–dependent apoptosis (Clarke *et al*, 2000, 2001). Reovirus-induced release of death ligands such as TRAIL may be a possible mechanism of induction of "bystander" apoptosis, which has been seen in the CNS following reovirus infection (Oberhaus *et al*, 1997), and also occurs in T3D-infected neuronal cultures (see Figure 4).

The expression of DRs and their role in apoptosis have been extensively studied in both epithelial and cells in the immune system (Dorr *et al*, 2002; Pettersen, 2000; Gupta, 2000; Strater and Moller, 2000), but less is understood about the role of DRs in neuronal apoptosis. Similarly, the role of DRs in virus-induced apoptosis remains poorly understood. CNS-specific changes in the expression or activity of CD95/FASR and TNF receptors and/or their corresponding death-inducing ligands have been implicated in neuronal apoptosis *in vitro* (McGuire *et al*, 2001), as well as in a variety of models of both viral and nonviral apoptosis *in vivo* (Tan *et al*, 2001; Rosenbaum *et al*, 2000; Sporer *et al*, 2000; Jelachich and Lipton, 2001). We now show that inhibition of reovirus-induced apoptosis in neuronal cultures is achieved using Fc-coupled soluble forms of TNF receptor superfamily DRs, specifically Fc:DR4/DR5 (TRAIL-R1/TRAIL-R2), Fc:FASR (CD95), or Fc:TNFR1. These results differ from those

in non-neuronal cells in which only Fc:DR4/DR5 significantly inhibited reovirus-induced apoptosis (Clarke *et al*, 2000), and suggest that the pathways of DR activation induced by a common stimulus, in this case viral infection, may differ between different populations of cells in specific target organs.

Sequential activation of caspases occurs in most forms of apoptosis, including during reovirus-induced apoptosis. Therefore, it is conceivable that if caspase activation could be inhibited early or at various stages in the apoptotic signal cascade, then dying cells may be able to recover and survive. Caspase inhibitors have been used successfully to protect neurons from apoptosis both *in vivo* and *in vitro* following several types of apoptotic stimuli (Kondratyev and Gale, 2000; Ma *et al*, 1998; Hara *et al*, 1997; Ray *et al*, 2000; Jiang *et al*, 2001; Jan *et al*, 2000). Here we demonstrate that cell-permeable peptide caspase inhibitors show a hierarchy of efficacy in their capacity to inhibit reovirus-induced neuronal apoptosis, with caspase 3 and caspase 8 inhibitors being significantly more than caspase 9 inhibitor (see Figure 7**D**). We have previously shown that inhibition of apoptosis can limit reovirus-induced myocardial injury *in vivo* (DeBiasi *et al*, 1999, 2001). It will be important to see whether caspase inhibition, which effectively inhibits reovirus-induced neuronal death *in vitro*, can also prevent reovirus-induced CNS injury *in vivo*.

Activation of the mitochondrial apoptotic pathway plays an integral role in augmenting DR-initiated signaling in reovirus-induced apoptosis of HEK293 cells. In these cells, apoptosis is associated with Bid cleavage, robust release of cytochrome *c* into the cytoplasm, and strong caspase 9 activation (Kominsky, 2002). In contrast to these findings, we did not detect increased levels of cytochrome *c* in the cytoplasm of reovirus-infected neurons, nor was there significant activation of the mitochondrion-associated initiator caspase, caspase 9. These results suggest that, in contrast to reovirus infected non-neuronal cells, mitochondria-associated apoptotic signaling mediated by cytochrome *c* and caspase 9 does not significantly contribute to reovirus-induced neuronal apoptosis.

These studies provide a profile of the activation of apoptotic signaling pathways in neuronal cells following viral infection, and indicate that these pathways may differ in important features from those in non-neuronal cells. It is increasingly evident that apoptosis is a factor in acute and chronic neurological diseases, including stroke, epilepsy, traumatic brain injury, and neurodegenerative diseases. Many neurotropic viral infections, including those caused by HIV (Patel *et al*, 2000; Ohagen *et al*, 1999; Kaul *et al*, 2001; Gray *et al*, 2000), La Crosse virus (Pekosz *et al*, 1996), Sindbis virus (Nava *et al*, 1998; Jan *et al*, 2000; Lewis *et al*, 1996), Dengue virus (Despres *et al*, 1996), Venezuelan equine encephalitis virus (Jackson and Rossiter, 1997b; Jackson *et al*, 1991), Rabies virus (Jackson and Rossiter, 1997a), herpes simplex virus (Thompson and Sawtell, 2000), and poliovirus (Lopez-Guerrero *et al*, 2000; Girard *et al*, 1999), are associated with apoptosis, suggesting that this form of cell death is likely to be a common feature of many CNS infections. This suggests that strategies designed to inhibit apoptosis may provide a novel approach for the treatment of virus-induced CNS diseases.

Materials and methods

Tissue culture

Neuroblastoma-derived cell line The mouse neuroblastoma-derived cell line, NB41a3 (ATCC CCL-147) was obtained from the American Type Culture Collection (ATCC, Rockville, MD) and maintained in minimal essential media supplemented with 2 mM glutamine, 50 U/ml of penicillin and streptomycin (P/S), 1 mM nonessential amino acids, and 10% heat-inactivated fetal bovine serum (FBS; GibcoBRL, Gaithersburg, MD). Cells were plated at densities of 2×10^5 cells per milliliter in tissue culture–treated 6-well, 12-well, or 96-well plates (Costar, Acton, MA), or polystyrene 8-well chamber slides (Lab-Tek II, Nunc/Nalgene International, Fisher Scientific, Pittsburgh, PA) and maintained at 37°C in 5% CO_2.

Primary cultures Primary cortical cultures were prepared from embryonic day 20 (E20) Swiss-Webster mice. Pregnant mice were euthanized by isofluorane inhalation followed by cervical dislocation. Fetuses were removed from the uterus, separated, and immediately submerged in ice cold sterile Hanks buffer (without calcium chloride, magnesium chloride, magnesium sulfate, and phenol red; GibcoBRL). Fetuses were decapitated with sterile scissors, and brains were removed and immediately submerged in fresh ice-cold sterile Hanks buffer. The frontal cortex was dissected, the meninges were removed, and the cortical tissue was washed three times in fresh ice-cold Hanks buffer, then dissociated with a 1-ml pipette tip. The percentage of viable cells was quantified by trypan blue staining using a hemocytometer.

Cells were plated at densities of 10^5 cells per milliliter in poly-D-lysine (PDL)-coated 6-well polystyrene plates or 8-well glass chamber slides (BioCoat, BD Biosciences, San Jose, CA) and maintained in Neurobasal media supplemented with 2 mM Glutamax, 50 U/ml P/S, 100 μM glucose, and 10% heat-inactivated FBS (GibcoBRL) at 37°C in 5% CO_2. At 24 h following plating, the serum-containing medium was replaced by serum-free medium containing the nonserum nutritional supplement B27 (Gibco BRL) to limit non-neuronal cell proliferation. Half the medium was replaced every 3 to 4 days, and cells were allowed to mature for 10 to 14 days before use in experiments.

Viral infections

Cells For most apoptosis and signal transduction assays, subconfluent cell monolayers were infected with plaque-purified second passage laboratory stocks of T3D or T1L at a MOI of 100 PFU per cell. This multiplicity of infection (MOI) was selected to generate a synchronized infection of all susceptible cells in the culture. For infections, the cell culture medium was aspirated and replaced with viral stock diluted in a minimal volume of cold gelatin saline, then incubated at 37°C for 1 h, with rocking every 15 min. Following the 1-h infection, fresh medium was added to the cells, which continued to be maintained at 37°C with 5% CO_2.

Mice Postnatal day 2 mice were infected with either T3D (10^5 PFU) or mock-infected with an equivalent volume of diluent medium via intracerebral (IC) injection. Injections were made using a 29-gauge needle in a 10-μl volume. Animals were sacrificed 7 days after infection.

Histology

For histopathological and immunohistochemical staining, eight whole mouse brains per treatment group (e.g., mock-infected, T3D-infected) were fixed by immersion in 10% buffered formalin for 24 to 30 h at room temperature (RT), then cut in half along the mid-coronal line for sectioning. Fixed tissues were transferred to 70% ethanol, paraffin-embedded, and sectioned at 4 μm thickness. For each animal, a coronal section that showed cingulate gyrus, hippocampus, and thalamus was stained with hematoxylin and eosin for studies of the extent of virus-induced pathology. Paraffin-embedded sections were baked at 57°C for 5 min to enhance antigen retrieval, then deparaffinized by immersion in mixed xylenes, followed by rehydration in a series of descending ethanol concentrations followed by phosphate-buffered saline.

Viral growth assays

Viral growth in neuronal cell cultures was assayed by determining viral titer at 0, 24, or 48 h following reovirus infection at a MOI of 10. This MOI resulted in more distinct one-step growth curves but essentially similar peak titers to that seen with MOI 100 (data not shown). At the indicated times, infected neuronal cells were lysed via three freeze (−70°C)–thaw (37°C) cycles, followed by manual disruption with a 1-ml pipette tip. Viral titer in cell lysates was determined by plaque assay on monolayers of L929 mouse fibroblasts, as previously described (Tyler *et al*, 1985).

Apoptosis assays

Flow cytometric analysis For the annexin V–PI assay (Flow-TACS, Trevigen, Gaithersburg, MD), 6 wells per treatment group of 5×10^5 cells were gently harvested with a 1:1 mixture of trypsin-versene (0.25%, GibcoBRL) and Accumax (Innovative Cell Technologies, San Diego, CA), then resuspended and washed in PBS. Once in suspension, cells were incubated with 1.5 μg annexin V–fluorescein isothiocyanate (FITC) in 100 μl binding buffer for 15 min in the dark at RT. PI (0.25 μg in 400 μl binding buffer) was added, then cells were analyzed by flow cytometry (Coulter Epics; Beckman Coulter, Fullerton, CA). Annexin V–FITC was measured by the FL1 channel (*x*-axis), and PI was measured by the FL3 channel (*y*-axis).

Nuclear morphology assays Apoptotic cells were identified by evaluating nuclear morphology at various times following reovirus infection by staining fixed cells with the fluorescent nuclear DNA intercalating dye, Hoechst 33342 (Molecular Probes, Eugene, OR). Apoptotic nuclei were identified by the presence of condensed and/or marginized chromatin. Cells were grown and infected in chamber slides, fixed at 24 or 48 h following infection with 3.7% formaldehyde/PBS for 20 min at RT, then incubated with Hoechst 33342 (1 μg/ml PBS) in the dark for 15 min at RT. The slides were mounted with an antifade mounting media (4 mg phenylenediamine in 1 ml PBS and 3 ml glycerol or Anti-Fade Kit from Molecular Probes). Apoptotic cells were quantified and imaged by fluorescence microscopy at 200× magnification (Zeiss Axioplan 2 Digital Microscope with Cooke SensiCam 12 bit Camera). For each condition, percentage of apoptotic cells was determined by counting 300 hundred cells in at least three individual samples.

Apoptotic DNA ladder assays We evaluated the fragmentation patterns of DNA isolated from control and reovirus-infected cells using the method described by Gong *et al* (1994). Briefly, 1×10^6 neuronal cells were harvested 48 h after infection with 0.25% trypsin/versene (GibcoBRL) for 5 min at RT, then resuspended in 1 ml Hanks buffer, fixed with 10 ml cold 70% ethanol, and placed at −20°C overnight. The next day, the ethanol was removed, DNA was extracted with a sodium phosphate-citrate buffer (92 parts 0.2 M Na_2HPO_4, 8 parts 0.1 M citric acid, pH 7.8), vacuum-dried, then incubated with 0.25% Nonidet-P 40, RNase A (3 μg) and proteinase K (3 μg) at 37°C for 30 min. Extracted DNA was separated by electrophoresis in a 2% TBE (25 mM tris-borate, 0.5 mM EDTA)/agarose gel containing 10 μg ethidium bromide at 22 V for 18 h. DNA ladder pattern was visualized by ultraviolet (UV) illumination. A 100-base pair (bp) DNA molecular weight marker with high intensity bands at 600 bp, 1.5 kilobases (kb), and 2.0 kb (GibcoBRL) was used to estimate molecular weight of DNA fragments.

TUNEL A biotin/streptavidin-based TUNEL kit optimized for neuronal tissues and cells was used

(NeuroTACS II; Trevigen, Gaithersburg, MD). At 48 h following reovirus infection, cells grown in chamber slides were fixed with 3.7% formaldehyde/PBS for 10 min, post-fixed in methanol for 20 min, then permeabilized in Neuropore (Trevigen) for 30 min at RT under hydrophobic coverslips. For each condition, percentage of TUNEL-positive cells was determined by counting 300 hundred cells in at least three individual samples.

Brain tissue sections underwent antigen retrieval, deparaffinization, and rehydration, then were permeabilized with Neuropore for 30 min at 37°C under hydrophobic coverslips. The remainder of the TUNEL assay for both neuronal cells and brain tissue sections was performed in accordance with the manufacturer's guidelines.

Inhibitor assays Nuclear morphology assays and TUNEL were used to determine whether treatment of T3D-infected neuronal cultures with anti-reovirus sigma 1 antibodies (anti-T3D sigma 1, 9BG5; anti-T1L sigma 1, 5C6) from (Virgin *et al*, 1988), cell-permeable caspase inhibitors, or soluble recombinant DRs could block T3D-induced apoptosis. Caspase inhibitors used include DEVD-CHO, IETD-CHO, and Z-LEHD-FMK (Calbiochem, San Diego, CA). Neuronal cultures were incubated at 37°C with 25 μM caspase inhibitor for 1 h prior to infection and throughout infection. The cytopathic effect induced by vehicle (DMSO) alone was minimal (data not shown). Soluble DRs used include Fc:DR5 (TRAILR2), Fc:CD95(FAS), and Fc:TNFR1 (Alexis Corporation, San Diego, CA). Neuronal cultures were incubated at 37°C with 1 to 5 μg/ml soluble receptor for 1 h prior to infection and throughout infection. For assays using Fc:receptors, neuronal cultures were infected by T3D at MOI 50.

Caspase 3 and 8 activation assays Caspase 3 or caspase 8 activity in reovirus-infected and control neuroblastoma cells was detected via ApoAlert Caspase 3 and 8 Activity Fluorometric Assays per manufacturer's guidelines (Clontech, Palo Alto, CA). Samples were transferred to 96-well enzyme-linked immunosorbent assay (ELISA) plates for detection of fluorescent activity with a fluoremeter (Cytofluor Series 4000; PerSeptive Biosystems) set at 400 nm excitation filter and 505 nm emission filter.

Immunocytochemistry and immunohistochemistry

Single antibody In preparation for immunoassays, neuronal cell cultures were grown and infected in 8-well chamber slides, fixed at various times following virus infection with 3.7% formaldehyde/PBS for 1 h at RT, and permeabilized with Neuropore for 30 min at RT. Brain tissue underwent deparaffinization, rehydration, and permeabilization in Neuropore for 30 min at RT. Samples were washed in Tris-buffered saline (TBS; 140 mM NaCl, 20 mM Tris, pH 7.6), nonspecific binding was blocked with 5% normal goat serum in TBS (NGS; Vector Laboratories, Burlingame, CA), then samples were incubated (overnight at 4°C) with primary antibody (1:50 to 1:100) diluted in 3% bovine serum albumin (BSA; Sigma-Aldrich, St. Louis, MO) in TBS/0.1% Tween (TBST). Samples were next washed in TBST and incubated in blocking buffer with the appropriate secondary antibody conjugated to horseradish peroxidase (HRP) (Amersham, Piscataway, NJ) or FITC (Jackson Immunoresearch Laboratories, West Groue, PA) for 1 h at 37°C. Samples were washed with TBST and either exposed to diaminobenzidine (DAB) for HRP-conjugated secondary antibody then permanently mounted, or immediately mounted with antifade medium if the secondary antibody was conjugated to FITC. Mounted samples were stored as described for TUNEL. Primary antibodies used for immunocytochemistry include rabbit polyclonal anti–active caspase 3, mouse monoclonal anti–active caspase 8, and rabbit polyclonal anti–active caspase 9 (Cell Signaling Technology, Beverly, MA), rabbit polyclonal anti–active caspase 8, mouse monoclonal anti–cytochrome *c* (Santa Cruz Biotechnology, Santa Cruz, CA), mouse monoclonal anti-NeuN (Chemicon, Temecula, CA), and rabbit polyclonal reovirus antisera (Tyler *et al*, 1985).

Double antibody labeling The protocol described for fluorescent single antibody labeling was used with the addition of another incubation (usually 2 h at 37°C) for the second primary antibody following the incubation and washes for the first primary antibody. The secondary antibodies were conjugated to different fluorophores with differing spectra, such as FITC and Cy3. The secondary antibodies were mixed together, diluted in 3% BSA/TBST, and incubated for 1 h at 37°C. Samples were then washed in TBST, incubated with Hoechst 33342 (100 ng/ml)/PBS for 10 min at RT in the dark as counterstain, mounted with antifade medium, and stored in the dark at −20°C until imaging.

Double label (antibody + TUNEL) For both neuronal cells and brain tissue sections, binding of the primary antibody for the immunoassay was performed prior to TUNEL staining by diluting the primary antibody (1:100) in Neuropore and incubating for 1 h at 37°C or overnight at 4°C under hydrophobic coverslips. The TdT reaction was performed as described for TUNEL. A mixture of strep-Cy3 (Jackson Immunoresearch Laboratories) to detect TUNEL and secondary antibody (1:100) conjugated to FITC to detect the primary antibody. Samples were washed and mounted as described for double-antibody labeling.

Western blots

Cell lysates Whole-cell lysates, mitochondrial/membrane lysates, and cytosolic/mitochondria-free lysates were prepared from neuronal cell cultures

by growing and infecting the cells in 6-well plates. At various times following viral infection, cells were harvested by incubation with 0.25% trypsin/versene (GibcoBRL), washed in PBS, and resuspended in the appropriate lysis buffer. Two wells of a 6-well plate were used for whole cell lysates. The cell pellet was resuspended in 150 μl of whole cell lysis buffer (1% Nonidet P40, 0.15 M NaCl, 5 mM EDTA, 0.01 M Tris pH 8.0, 1 M PMSF, 0.02 mg/ml leupeptin, 0.02 mg/ml trypsin inhibitor), briefly sonicated with a microtip probe, then mixed with 150 μl of Laemmli buffer (4% sodium dodecyl sulfate, 20% glycerol, 10% beta-mercaptoethanol, 0.004% bromophenol blue, 0.125 M Tris-HCl, pH 6.8). The remaining 4 wells of the 6-well plate was used for preparation of both mitochondrial/membrane lysates and cytosolic/mitochondria-free lysates. The cell pellet was resuspended in 300 μl of mitochrondria-free extraction lysis buffer (220 mM mannitol, 68 mM sucrose, 50 mM PIPES-KOH, pH 7.4, 50 mM KCl, 5 mM EGTA, 2 mM $MgCl_2$, 1 mM DTT; protease inhibitor cocktail, Boehringer Mannheim, Indianapolis, ID), incubated on ice for 30 min allowing mitochondria to swell, homogenized in a 2-ml glass dounce-homogenizer with 40 strokes, then centrifuged at 14,000 × *g* for 15 min at 4°C to remove mitochondria and cell membranes. The supernatant was transferred to a fresh microfuge tube and 300 μl of Laemmli buffer was added. The mitochondria/membrane pellet was resuspended in 150 μl whole cell lysis buffer, briefly sonicated with a microtip probe, and mixed with 150 μl Laemmli buffer. All lysates were stored at −20°C until use.

Gels and immunoblots Lysates were boiled for 7 min and electrophoresed (Hoefer Pharmacia Biotech, San Francisco, CA) in 10% or 15% glycine/polyacrylamide gels or 10% or 15% Tricine/polyacrylamide gels (for small proteins and peptides) at constant voltage of 60 V through the stacking gel and 150 V through the resolving gel. Proteins were electroblotted onto Hybond-C nitrocellulose membranes (Amersham) and immunoblotting was performed as described (Poggioli *et al*, 2000). Primary antibodies used for immunoblots include anti-actin (Calbiochem), anti–caspase 9 (Cell Signaling Technology, Beverly, MA), and anti–cytochrome *c* and anti–caspase 8 (BD-Pharmingen, La Jolla, CA).

References

Allsopp TE, Fazakerley JK (2000). Altruistic cell suicide and the specialized case of the virus-infected nervous system. *Trends Neurosci* **23**: 284–290.

Ashkenazi A, Dixit VM (1998). Death receptors: Signaling and modulation. *Science* **281**: 1305–1308.

Bitzer M, Prinz F, Bauer M, Spiegel M, Neubert WJ, Gregor M, Schulze-Osthoff K, Lauer U (1999). Sendai virus infection induces apoptosis through activation of caspase-8 (FLICE) and caspase-3 (CPP32). *J Virol* **73**: 702–708.

Budd SL, Lipton SA (1999). Signaling events in NMDA receptor-induced apoptosis in cerebrocortical cultures. *Ann N Y Acad Sci* **893**: 261–264.

Chien CT, Hsu SM, Chen CF, Lee PH, Lai MK (2000). Prolonged ischemia potentiates apoptosis formation during reperfusion by increase of caspase 3 activity and free radical generation. *Transplant Proc* **32**: 2065–2066.

Clarke P, Meintzer SM, Gibson S, Widmann C, Garrington TP, Johnson GL, Tyler KL (2000). Reovirus-induced apoptosis is mediated by TRAIL. *J Virol* **74**: 8135–8139.

Clarke P, Meintzer SM, Spalding AC, Johnson GL, Tyler KL (2001). Caspase 8-dependent sensitization of cancer cells to TRAIL-induced apoptosis following reovirus-infection. *Oncogene* **20**: 6910–6919.

DeBiasi RL, Edelstein CL, Sherry B, Tyler KL (2001). Calpain inhibition protects against virus-induced apoptotic myocardial injury. *J Virol* **75**: 351–361.

DeBiasi RL, Squier MK, Pike B, Wynes M, Dermody TS, Cohen JJ, Tyler KL (1999). Reovirus-induced apoptosis is preceded by increased cellular calpain activity and is blocked by calpain inhibitors. *J Virol* **73**: 695–701.

D'Mello SR, Kuan CY, Flavell RA, Rakic P (2000). Caspase-3 is required for apoptosis-associated DNA fragmentation but not for cell death in neurons deprived of potassium. *J Neurosci Res* **59**: 24–31.

Despres P, Flamand M, Ceccaldi PE, Deubel V (1996). Human isolates of dengue type 1 virus induce apoptosis in mouse neuroblastoma cells. *J Virol* **70**: 4090–4096.

Dorr J, Bechmann I, Waiczies S, Aktas O, Walczak H, Krammer PH, Nitsch R, Zipp F (2002). Lack of tumor necrosis factor-related apoptosis-inducing ligand but presence of its receptors in the human brain. *J Neurosci* **22**: RC209.

Earnshaw WC, Martins LM, Kaufmann SH (1999). Mammalian caspases: Structure, activation, substrates, and functions during apoptosis. *Annu Rev Biochem* **68**: 383–424.

Gavrieli Y, Sherman Y, Ben Sasson SA (1992). Identification of programmed cell death in situ via specific labeling of nuclear DNA fragmentation. *J Cell Biol* **119**: 493–501.

Girard S, Couderc T, Destombes J, Thiesson D, Delpeyroux F, Blondel B (1999). Poliovirus induces apoptosis in the mouse central nervous system. *J Virol* **73**: 6066–6072.

Gong J, Traganos F, Darzynkiewicz Z (1994). A selective procedure for DNA extraction from apoptotic cells applicable for gel electrophoresis and flow cytometry. *Anal Biochem* **218**: 314–319.

Gray F, Adle-Biassette H, Brion F, Ereau T, Le MI, Levy V, Corcket G (2000). Neuronal apoptosis in human immunodeficiency virus infection. *J Neurovirol* **6(Suppl 1)**: S38–S43.

Gupta S (2000). Molecular steps of cell suicide: An insight into immune senescence. *J Clin Immunol* **20**: 229–239.

Hara H, Friedlander RM, Gagliardini V, Ayata C, Fink K, Huang Z, Shimizu-Sasamata M, Yuan J, Moskowitz MA (1997). Inhibition of interleukin 1beta converting enzyme family proteases reduces ischemic and excitotoxic neuronal damage. *Proc Natl Acad Sci USA* **94**: 2007–2012.

Hengartner MO (2000). The biochemistry of apoptosis. *Nature* **407**: 770–776.

Honig LS, Rosenberg RN (2000). Apoptosis and neurologic disease. *Am J Med* **108**: 317–330.

Jackson AC, Rossiter JP (1997a). Apoptosis plays an important role in experimental rabies virus infection. *J Virol* **71**: 5603–5607.

Jackson AC, Rossiter JP (1997b). Apoptotic cell death is an important cause of neuronal injury in experimental Venezuelan equine encephalitis virus infection of mice. *Acta Neuropathol (Berl)* **93**: 349–353.

Jackson AC, SenGupta SK, Smith JF (1991). Pathogenesis of Venezuelan equine encephalitis virus infection in mice and hamsters. *Vet Pathol* **28**: 410–418.

Jan JT, Chatterjee S, Griffin DE (2000). Sindbis virus entry into cells triggers apoptosis by activating sphingomyelinase, leading to the release of ceramide. *J Virol* **74**: 6425–6432.

Jan JT, Griffin DE (1999). Induction of apoptosis by Sindbis virus occurs at cell entry and does not require virus replication. *J Virol* **73**: 10296–10302.

Jelachich ML, Lipton HL (2001). Theiler's murine encephalomyelitis virus induces apoptosis in gamma interferon-activated M1 differentiated myelomonocytic cells through a mechanism involving tumor necrosis factor alpha (TNF-alpha) and TNF-alpha-related apoptosis-inducing ligand. *J Virol* **75**: 5930–5938.

Jiang D, Jha N, Boonplueang R, Andersen JK (2001). Caspase 3 inhibition attenuates hydrogen peroxide-induced DNA fragmentation but not cell death in neuronal PC12 cells. *J Neurochem* **76**: 1745–1755.

Kaul M, Garden GA, Lipton SA (2001). Pathways to neuronal injury and apoptosis in HIV-associated dementia. *Nature* **410**: 988–994.

Kominsky DJ, Bickel RJ, Tyler KL (2002). Reovirus-induced apoptosis requires both death receptor and mitochondria-mediated caspase-dependent pathways of cell death. *Cell Death Differ* **9**: 926–933.

Kondratyev A, Gale K (2000). Intracerebral injection of caspase-3 inhibitor prevents neuronal apoptosis after kainic acid-evoked status epilepticus. *Brain Res Mol Brain Res* **75**: 216–224.

Lewis J, Wesselingh SL, Griffin DE, Hardwick JM (1996). Alphavirus-induced apoptosis in mouse brains correlates with neurovirulence. *J Virol* **70**: 1828–1835.

Li P, Nijhawan D, Budihardjo I, Srinivasula SM, Ahmad M, Alnemri ES, Wang X (1997). Cytochrome *c* and dATP-dependent formation of Apaf-1/caspase-9 complex initiates an apoptotic protease cascade. *Cell* **91**: 479–489.

Lopez-Guerrero JA, Alonso M, Martin-Belmonte F, Carrasco L (2000). Poliovirus induces apoptosis in the human U937 promonocytic cell line. *Virology* **272**: 250–256.

Ma J, Endres M, Moskowitz MA (1998). Synergistic effects of caspase inhibitors and MK-801 in brain injury after transient focal cerebral ischaemia in mice. *Br J Pharmacol* **124**: 756–762.

Martin SJ, Reutelingsperger CP, McGahon AJ, Rader JA, van Schie RC, LaFace DM, Green DR (1995). Early redistribution of plasma membrane phosphatidylserine is a general feature of apoptosis regardless of the initiating stimulus: Inhibition by overexpression of Bcl-2 and Abl. *J Exp Med* **182**: 1545–1556.

Mattson MP (2000). Apoptosis in neurodegenerative disorders. *Nat Rev Mol Cell Biol* **1**: 120–129.

McGuire SO, Ling ZD, Lipton JW, Sortwell CE, Collier TJ, Carvey PM (2001). Tumor necrosis factor alpha is toxic to embryonic mesencephalic dopamine neurons. *Exp Neurol* **169**: 219–230.

Nava VE, Rosen A, Veliuona MA, Clem RJ, Levine B, Hardwick JM (1998). Sindbis virus induces apoptosis through a caspase-dependent, CrmA-sensitive pathway. *J Virol* **72**: 452–459.

Nunez G, Benedict MA, Hu Y, Inohara N (1998). Caspases: The proteases of the apoptotic pathway. *Oncogene* **17**: 3237–3245.

Oberhaus SM, Smith RL, Clayton GH, Dermody TS, Tyler KL (1997). Reovirus infection and tissue injury in the mouse central nervous system are associated with apoptosis. *J Virol* **71**: 2100–2106.

Ohagen A, Ghosh S, He J, Huang K, Chen Y, Yuan M, Osathanondh R, Gartner S, Shi B, Shaw G, Gabuzda D (1999). Apoptosis induced by infection of primary brain cultures with diverse human immunodeficiency virus type 1 isolates: Evidence for a role of the envelope. *J Virol* **73**: 897–906.

Patel CA, Mukhtar M, Pomerantz RJ (2000). Human immunodeficiency virus type 1 Vpr induces apoptosis in human neuronal cells. *J Virol* **74**: 9717–9726.

Pekosz A, Phillips J, Pleasure D, Merry D, Gonzalez-Scarano F (1996). Induction of apoptosis by La Crosse virus infection and role of neuronal differentiation and human bcl-2 expression in its prevention. *J Virol* **70**: 5329–5335.

Petito CK, Kerza-Kwiatecki AP, Gendelman HE, McCarthy M, Nath A, Podack ER, Shapshak P, Wiley CA (1999). Review: Neuronal injury in HIV infection. *J NeuroVirol* **5**: 327–341.

Pettersen RD (2000). CD47 and death signaling in the immune system. *Apoptosis* **5**: 299–306.

Poggioli GJ, Keefer C, Connolly JL, Dermody TS, Tyler KL (2000). Reovirus-induced G(2)/M cell cycle arrest requires sigma1s and occurs in the absence of apoptosis. *J Virol* **74**: 9562–9570.

Raghupathi R, Graham DI, McIntosh TK (2000). Apoptosis after traumatic brain injury. *J Neurotrauma* **17**: 927–938.

Ray AM, Owen DE, Evans ML, Davis JB, Benham CD (2000). Caspase inhibitors are functionally neuroprotective against oxygen glucose deprivation induced CA1 death in rat organotypic hippocampal slices. *Brain Res* **867**: 62–69.

Reed JC (2000). Mechanisms of apoptosis. *Am J Pathol* **157**: 1415–1430.

Rentsch M, Beham A, Iesalnieks I, Mirwald T, Anthuber M, Jauch KW (2001). Impact of prolonged cold ischemia and reperfusion on apoptosis, activation of caspase 3, and expression of bax after liver transplantation in the rat. *Transplant Proc* **33**: 850–851.

Rodgers SE, Barton ES, Oberhaus SM, Pike B, Gibson CA, Tyler KL, Dermody TS (1997). Reovirus-induced apoptosis of MDCK cells is not linked to viral yield and is blocked by Bcl-2. *J Virol* **71**: 2540–2546.

Rosenbaum DM, Gupta G, D'Amore J, Singh M, Weidenheim K, Zhang H, Kessler JA (2000). Fas (CD95/APO-1) plays a role in the pathophysiology of focal cerebral ischemia. *J Neurosci Res* **61**: 686–692.

Sporer B, Koedel U, Goebel FD, Pfister HW (2000). Increased levels of soluble Fas receptor and Fas ligand in

the cerebrospinal fluid of HIV-infected patients. *AIDS Res Hum Retroviruses* **16:** 221–226.

Strater J, Moller P (2000). Expression and function of death receptors and their natural ligands in the intestine. *Ann N Y Acad Sci* **915:** 162–170.

Tan Z, Levid J, Schreiber SS (2001). Increased expression of Fas (CD95/APO-1) in adult rat brain after kainate-induced seizures. *Neuroreport* **12:** 1979–1982.

Tepper CG, Seldin MF (1999). Modulation of caspase-8 and FLICE-inhibitory protein expression as a potential mechanism of Epstein-Barr virus tumorigenesis in Burkitt's lymphoma. *Blood* **94:** 1727–1737.

Thompson RL, Sawtell NM (2000). HSV latency-associated transcript and neuronal apoptosis. *Science* **289:** 1651.

Tyler KL (2001). *Fileds virology: mammalian reoviruses*, 4th ed. Knipe DM, Howley PM (eds). Lippincott-Williams & Wilkins: Philadelphia, PA.

Tyler KL, Bronson RT, Byers KB, Fields B (1985). Molecular basis of viral neurotropism: experimental reovirus infection. *Neurology* **35:** 88–92.

Tyler KL, Squier MK, Rodgers SE, Schneider BE, Oberhaus SM, Grdina TA, Cohen JJ, Dermody TS (1995). Differences in the capacity of reovirus strains to induce apoptosis are determined by the viral attachment protein sigma 1. *J Virol* **69:** 6972–6979.

Tyler KL, Virgin HW, Bassel-Duby R, Fields BN (1989). Antibody inhibits defined stages in the pathogenesis of reovirus serotype 3 infection of the central nervous system. *J Exp Med* **170:** 887–900.

Velier JJ, Ellison JA, Kikly KK, Spera PA, Barone FC, Feuerstein GZ (1999). Caspase-8 and caspase-3 are expressed by different populations of cortical neurons undergoing delayed cell death after focal stroke in the rat. *J Neurosci* **19:** 5932–5941.

Virgin HW, Bassel-Duby R, Fields BN, Tyler KL (1988). Antibody protects against lethal infection with the neurally spreading reovirus type 3 (Dearing). *J Virol* **62:** 4594–4604.

Yuan J, Yankner BA (2000). Apoptosis in the nervous system. *Nature* **407:** 802–809.

JOURNAL OF VIROLOGY, Nov. 2002, p. 11414–11424 Vol. 76, No. 22
0022-538X/02/$04.00+0 DOI: 10.1128/JVI.76.22.11414–11424.2002

Reovirus-Induced Apoptosis Requires Mitochondrial Release of Smac/DIABLO and Involves Reduction of Cellular Inhibitor of Apoptosis Protein Levels

Douglas J. Kominsky,[1] Ryan J. Bickel,[1] and Kenneth L. Tyler[1,2,3]*

Departments of Neurology[1] and Medicine, Microbiology, and Immunology,[2] University of Colorado Health Science Center, and Denver Veteran's Affairs Medical Center,[3] Denver, Colorado 80262

Received 6 May 2002/Accepted 6 August 2002

Many viruses belonging to diverse viral families with differing structure and replication strategies induce apoptosis both in cultured cells in vitro and in tissues in vivo. Despite this fact, little is known about the specific cellular apoptotic pathways induced during viral infection. We have previously shown that reovirus-induced apoptosis of HEK cells is initiated by death receptor activation but requires augmentation by mitochondrial apoptotic pathways for its maximal expression. We now show that reovirus infection of HEK cells is associated with selective cytosolic release of the mitochondrial proapoptotic factors cytochrome *c* and Smac/DIABLO, but not the release of apoptosis-inducing factor. Release of these factors is not associated with loss of mitochondrial transmembrane potential and is blocked by overexpression of Bcl-2. Stable expression of caspase-9b, a dominant-negative form of caspase-9, blocks reovirus-induced caspase-9 activation but fails to significantly reduce activation of the key effector caspase, caspase-3. Smac/DIABLO enhances apoptosis through its action on cellular inhibitor of apoptosis proteins (IAPs). Reovirus infection is associated with selective down-regulation of cellular IAPs, including c-IAP1, XIAP, and survivin, effects that are blocked by Bcl-2 expression, establishing the dependence of IAP down-regulation on mitochondrial events. Taken together, these results are consistent with a model in which Smac/DIABLO-mediated inhibition of IAPs, rather than cytochrome *c*-mediated activation of caspase-9, is the key event responsible for mitochondrial augmentation of reovirus-induced apoptosis. These studies provide the first evidence for the association of Smac/DIABLO with virus-induced apoptosis.

The apoptotic pathways leading to cell death can be generally divided into two nonexclusive signaling cascades involving death receptors (extrinsic pathways) or mitochondria (intrinsic pathway) (2, 37). Induction of apoptosis through the death receptor pathway is initiated by the binding of ligand to the receptor, causing oligomerization of the receptor. This induces the formation of the death-induced signaling complex, leading to the activation of the initiator caspase, caspase-8 (2). Caspase-8 can then activate downstream effector caspases. Apoptosis via the mitochondrial pathway involves specific signals that allow the release of proapoptotic molecules from the inner-membrane space, including cytochrome *c* (28), second mitochondrion-derived activator of caspase (Smac/DIABLO) (11, 55), apoptosis-inducing factor (AIF) (50), and endonuclease G (26). Cytosolic cytochrome *c*, Apaf-1, and procaspase-9 form a complex termed the apoptosome (63). Formation of the apoptosome leads to the activation of caspase-9 and subsequent effector caspase activation. Relocalization of Smac/DIABLO to the cytoplasm promotes caspase activation through inhibition of the inhibitor of apoptosis (IAP) protein family (11, 55).

IAP proteins are negative regulators of apoptosis that inhibit caspase activity. IAP family members are characterized by the presence of one or more baculoviral IAP repeat domains (9). Six human IAP family members have been identified: NAIP, c-IAP1, c-IAP2, XIAP, survivin, and BRUCE (1, 12, 15, 27, 39). Four of these proteins—c-IAP1, c-IAP2, XIAP, and survivin—have been shown to directly interact with caspase-3, caspase-7, and caspase-9 and, at least in the cases of c-IAP1, c-IAP2, and XIAP, inhibit caspase activity (10, 41, 51). Additionally, reduction of c-IAP2 and XIAP protein levels is associated with apoptosis (25). The proapoptotic mitochondrial protein Smac/DIABLO has been shown to directly interact with XIAP eliminating XIAP's ability to bind to and inhibit caspases and thereby promoting apoptosis (14).

The Bcl-2 protein family is of central importance in the regulation of the mitochondrial apoptotic pathway. Members of this family may be either antiapoptotic (e.g., Bcl-2 and Bcl-xl) or proapoptotic (e.g., Bid, Bax, and Bak). Bcl-2 appears to play a role in the maintenance of mitochondrial integrity and inhibits mitochondrial release of proapoptotic factors. Conversely, Bid, Bax, and Bak appear to facilitate the release of these factors (22).

Activation of the death receptor and mitochondrion-associated death pathways are not mutually exclusive, and these pathways may interact (cross talk) at many levels. One important link between these two pathways appears to involve the caspase-8-dependent cleavage of Bid. Truncated Bid translocates to the mitochondrion, where it facilitates release of mitochondrial proteins, presumably by inducing the homo-oligomerization of Bax or Bak (58). This process may result in alteration of the mitochondrial permeability transition pore and loss of mitochondrial membrane potential ($\Delta\Psi_m$). How-

* Corresponding author. Mailing address: Department of Neurology (B-182), University of Colorado Health Science Center, 4200 E. 9th Ave., Denver, CO 80262. Phone: (303) 393-2874. Fax: (303) 393-4686. E-mail: Ken.Tyler@uchsc.edu.

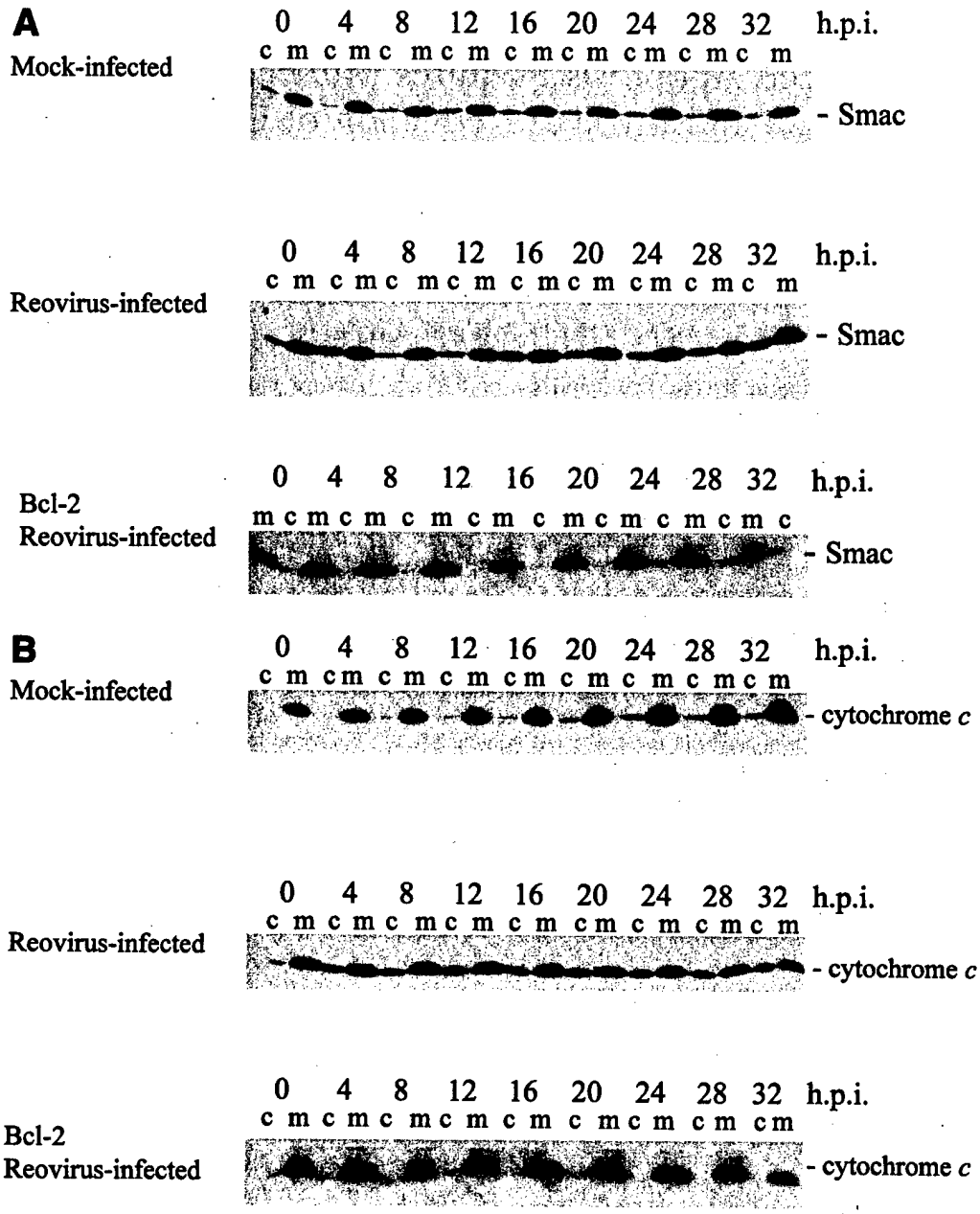

FIG. 1. Smac/DIABLO and cytochrome *c* are present in the cytosol of reovirus-infected cells. HEK 293 lysates were prepared at the indicated time points from mock-infected cells, reovirus-infected cells, or Bcl-2-overexpressing reovirus-infected cells and resolved using SDS-PAGE. Western blot analysis was performed using anti-Smac antibodies (A) and anti-cytochrome *c* antibodies (B). The Western is representative of two separate experiments. Lanes c, cytoplasmic fraction; lanes m, mitochondrial fraction. h.p.i., hours postinfection.

ever, recent evidence has shown that Bid-dependent release of mitochondrial proteins can occur without perturbing mitochondrial structure and function (20, 57).

Mammalian reoviruses are nonenveloped double-stranded RNA viruses that replicate exclusively in the cytoplasm. Reoviruses have been shown to induce apoptosis both in cultured cells in vitro (33, 38, 54) and in specific tissues, including the heart and brain, in vivo (6, 34). Apoptosis is an important mechanism of reovirus-induced tissue injury in vivo, and inhibition of apoptosis dramatically reduces the severity of disease (6).

Reovirus-induced apoptosis has been shown to involve death receptor 4 (DR4), death receptor 5 (DR5), and their cognate ligand, tumor necrosis factor-related apoptosis-inducing ligand (TRAIL). Inhibition of the TRAIL/death receptor interaction with anti-TRAIL antibodies or soluble forms of DR4/DR5 inhibits cell death (5). Recently we have shown that reovirus-induced apoptosis also requires activation of the mitochondrial apoptotic pathway (21). In reovirus-infected HEK cells, there is a caspase-8-dependent cleavage of Bid leading to the subsequent release of cytochrome *c* and activation of caspase-9 and the effector caspase, caspase-3. Caspase-3 activation is inhib-

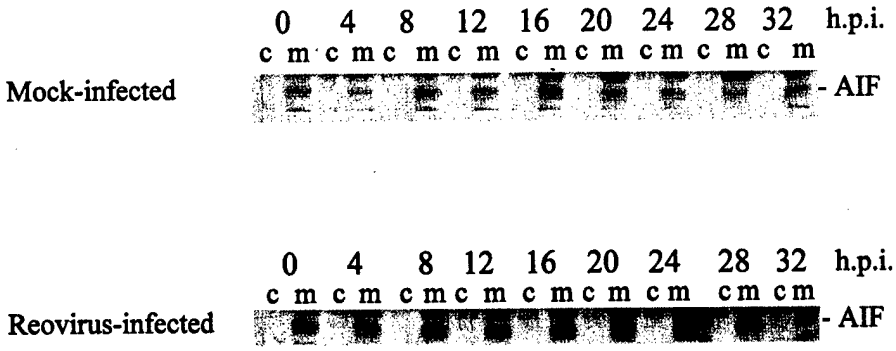

FIG. 2. Reovirus infection does not induce the mitochondrial release of AIF. HEK 293 lysates were prepared at the indicated time points from mock-infected and reovirus-infected cells and resolved using SDS-PAGE. Blots were probed with anti-AIF antibodies and are representative of three separate experiments. Lanes c, cytoplasmic fraction; lanes m, mitochondrial fraction. h.p.i., hours postinfection.

ited in cells overexpressing a dominant-negative form of the adaptor protein FADD (FADD-DN) and in cells overexpressing Bcl-2, consistent with the importance of both extrinsic and intrinsic pathways in reovirus-induced apoptosis (21).

In this study we set out to better characterize the mitochondrion-dependent apoptotic processes induced following reovirus infection. Release of the mitochondrial proteins Smac/DIABLO and AIF were examined. Additionally, the fate of a number of IAP protein family members was determined. We find that Smac/DIABLO is released into the cytosol of infected HEK 293 cells, while AIF remained sequestered in the mitochondria. The release of cytochrome *c* and Smac/DIABLO occur without disturbing the mitochondrial membrane potential. Additionally, by utilizing a dominant-negative isoform of caspase-9, we find that while the mitochondrial pathway is required for caspase-3 activation, caspase-9 is dispensable for this process. Finally, we find that a specific subset of IAP proteins are down-regulated following reovirus infection. These results suggest that activation of Smac/DIABLO-dependent rather that caspase-9-dependent pathways represents the key mitochondrial event during reovirus-induced apoptosis and provide the first evidence for involvement of Smac/DIABLO in virus-induced apoptosis.

MATERIALS AND METHODS

Reagents. Anti-cytochrome *c* (7H8.2C12) (1:1,000), anti-poly(ADP-ribose) polymerase (anti-PARP) (C2-10) (1:2,000), and anti-XIAP/hILP (1:500) antibodies were purchased from Pharmingen (San Diego, Calif.). Anti-caspase-9 (1:1,000) antibodies were purchased from Cell Signaling Technology (Beverly, Mass.). Anti-AIF, anti-c-IAP1, anti-c-IAP2, and antisurvivin antibodies were from Santa Cruz Biotechnology (Santa Cruz, Calif.). Antiactin antibodies (JLA20) (1:5,000) and anti-Smac/DIABLO (1:1,000) were from Calbiochem (Darmstadt, Germany). Anti-human cytochrome *c* oxidase (subunit II) antibodies (12C4-F12) (1:1,000) and the mitochondrial potential sensor JC-1 were from Molecular Probes (Eugene, Oreg.). Valinomycin was obtained from Sigma (St. Louis, Mo.). Anti-Fas antibody (CH-11) was from Upstate Biotechnology (Lake Placid, N.Y.). An ApoAlert caspase-3 fluorometric assay kit was purchased from Clontech (Palo Alto, Calif.).

Cells, virus, and DNA constructs. HEK 293 cells (ATCC CRL1573) were grown in Dulbecco's modified Eagle's medium supplemented with of penicillin and streptomycin (100 U/ml each) and containing 10% fetal bovine serum. Jurkat cells were a gift of John Cohen and were grown in RPMI supplemented with penicillin and streptomycin (100 U/ml each) and containing 10% fetal bovine serum. HEK 293 cells stably overexpressing Bcl-2 were provided by Gary Johnson. The cell line was constructed by cloning full-length Bcl-2 into the pLXSN vector and transfecting cells via retroviral transduction. The dominant-negative caspase-9b construct was a gift of Emad Alnemri and has been previously described (47). The caspase-9b construct was transfected into HEK 293 cells using Lipofectamine (Gibco, Grand Island, N.Y.). Reovirus (type 3 Abney) is a laboratory stock, which has been plaque purified and passaged (twice) in L929 cells (ATCC CCL1) to generate working stocks (53). All experiments were performed using a multiplicity of infection of 100. High multiplicities of infection were chosen to ensure synchronized infection of all susceptible cells and to maximize the apoptotic stimulus.

Mitochondrial membrane potential measurement. HEK 293 cells were seeded in six-well plates at 10^6 cells per well in a volume of 2 ml and then infected with reovirus for the indicated time periods. Control cells were treated with valinomycin at a final concentration of 100 nM for 10 min at 37°C. Cells were harvested and washed two times with phosphate-buffered saline (PBS). Cells were resuspended in 1 ml of PBS containing JC-1 (10 μg/ml) and incubated for 30 min at 37°C. Cells were washed two times in PBS and resuspended in 1 ml of PBS. Finally, cells were analyzed using a Coulter Epics XL flow cytometer (Beckman-Coulter, Hialeah, Fla.).

Western blot analysis. Reovirus-infected cells were harvested at the indicated times, pelleted by centrifugation, washed with ice-cold phosphate-buffered saline, and lysed by sonication in 150 μl of lysis buffer (1% NP-40, 0.15 M NaCl, 5.0 mM EDTA, 0.01 M Tris [pH 8.0], 1.0 mM phenylmethylsulfonyl fluoride, leupeptin [0.02 mg/ml], trypsin inhibitor [0.02 mg/ml]). Lysates were cleared by centrifugation (20,000 × *g*, 2 min), mixed 1:1 with sodium dodecyl sulfate (SDS) sample buffer, boiled for 5 min, and stored at −70°C. Mitochondrion-free extracts were prepared as previously described (21) in buffer containing 220 mM mannitol, 68 mM sucrose, 50 mM PIPES-KOH (pH 7.4), 50 mM KCl, 5 mM EGTA, 2 mM $MgCl_2$, 1 mM dithiothreitol, and protease inhibitors (complete cocktail; Boehringer Mannheim, Indianapolis, Ind.). Proteins were separated by SDS-polyacrylamide gel electrophoresis (SDS-PAGE) and transferred to Hybond-C Extra nitrocellulose membrane (Amersham, Little Chalfont, Buckinghamshire, England) for immunoblotting. Blots were then probed with the specified antibodies at the dilutions described above. Proteins were visualized using the ECL detection system (Amersham).

Caspase-3 activation assays. Caspase-3 activation assays were performed using a kit obtained from Clontech. Experiments were performed using 10^6 cells/time point. Cells were centrifuged at 200 × *g*, supernatants were removed, and the cell pellets were frozen at −70°C until cells were collected at all the time points. Assays were performed as previously described (21) in 96-well plates and analyzed using a fluorescent plate reader (CytoFluor 4000; PerSeptive Biosystems, Framingham, Mass.). Results of all experiments are reported as means ± standard errors of the means.

RESULTS

Smac/DIABLO is released from the mitochondria following reovirus infection. Several proteins possessing proapoptotic functions are localized to the mitochondria. These include cytochrome *c* (28), Smac/DIABLO (11, 55), AIF (50), and endonuclease G (26). Additionally, it has been reported that stores of the procaspase forms of several caspases are present

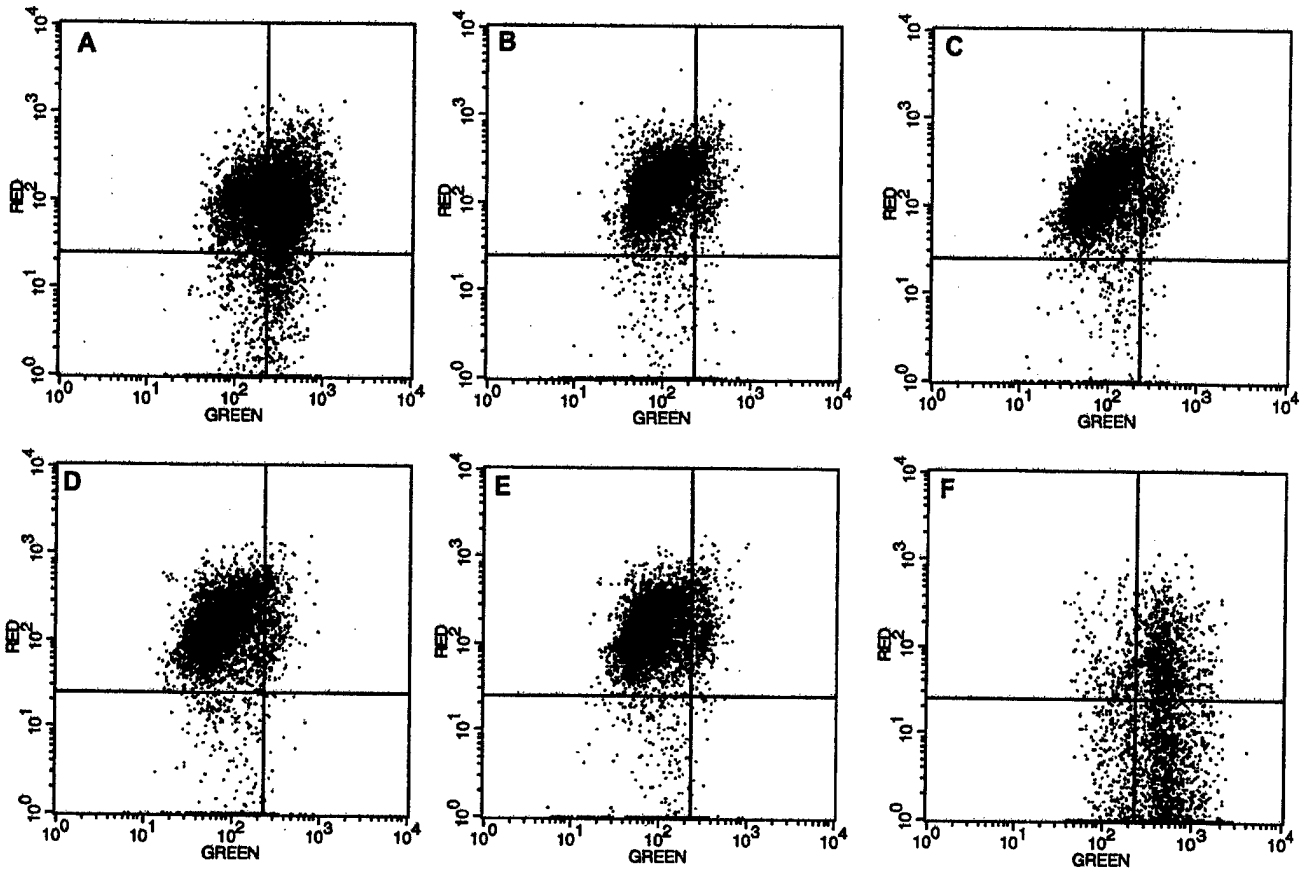

FIG. 3. Mitochondrial $\Delta\Psi_m$ is not altered in reovirus-infected cells. HEK 293 cells were mock-infected (A) or infected with reovirus for 0 h (B), 6 h (C), 12 h (D), or 24 h (E). Control cells were treated with valinomycin (panel F). Cells were incubated with the membrane potential-sensitive dye JC-1 and analyzed using flow cytometry. Red fluorescence indicates mitochondria with intact $\Delta\Psi_m$ and green fluorescence indicates loss of $\Delta\Psi_m$. Results are representative of three separate experiments.

in mitochondria (23, 29, 30, 36, 49). We have previously reported that cytochrome *c* is released from the mitochondria of reovirus-infected cells, leading to the activation of caspase-9 (21). We wished to determine whether additional mitochondrial molecules were also involved in reovirus-induced apoptosis. We began by examining the distribution of Smac/DIABLO following reovirus infection. Mitochondrion-free lysates were prepared from both mock- and reovirus-infected cells at the indicated time points and analyzed by Western blot for the presence of cytosolic Smac/DIABLO (Fig. 1A). Blots were also probed with anti-cytochrome *c* antibodies and the full time course of cytochrome *c* release is also shown (Fig. 1B). Antisera directed against the mitochondrial integral membrane protein cytochrome *c* oxidase (subunit II) were employed to ensure the samples were free of mitochondrial contamination (data not shown). Smac/DIABLO is released into the cytoplasm of reovirus-infected cells (Fig. 1A) and Smac/DIABLO and cytochrome *c* are detected in the cytoplasm of infected cells beginning at 4 h postinfection (Fig. 1). The Smac/DIABLO band detected at 0 h postinfection represents background levels as similar amounts of protein are also detected in mock-infected extracts (Fig. 1). Additionally, the release of both proteins is blocked in cells overexpressing Bcl-2 (Fig. 1). Interestingly, the release of Smac/DIABLO appears to exhibit a biphasic pattern which we have previously described for other events following reovirus infection, including caspase-8 activation, Bid cleavage, and caspase-3 activation (21). The early phase of Smac/DIABLO release was detectable at 4 h postinfection and then diminished. A second phase of Smac/DIABLO release was detectable at ~16 h postinfection and was sustained over the remainder of the time course (Fig. 1A).

AIF is not released from the mitochondria of reovirus-infected cells. AIF is a mitochondrial protein that can translocate to the nucleus, leading to nuclear apoptosis (50). The relocalization of AIF to the nucleus induces a caspase-independent apoptotic pathway (19). It has been shown that AIF is released from the mitochondria of cells following human immunodeficiency virus (HIV) infection (13) and herpes simplex virus type 1 (HSV-1) infection (61). We examined AIF localization in reovirus-infected cells using mitochondrion-free lysates. As shown in Fig. 2, AIF is not detected in the cytoplasm following reovirus infection. We also prepared nuclear extracts from both mock- and reovirus-infected cells to ensure that AIF had not translocated the nucleus. We could not detect nuclearly localized AIF following reovirus infection (data not shown). These experiments demonstrate that the mitochondrial proapoptotic proteins Smac/DIABLO and cytochrome *c*, but not AIF, are released in reovirus-infected cells.

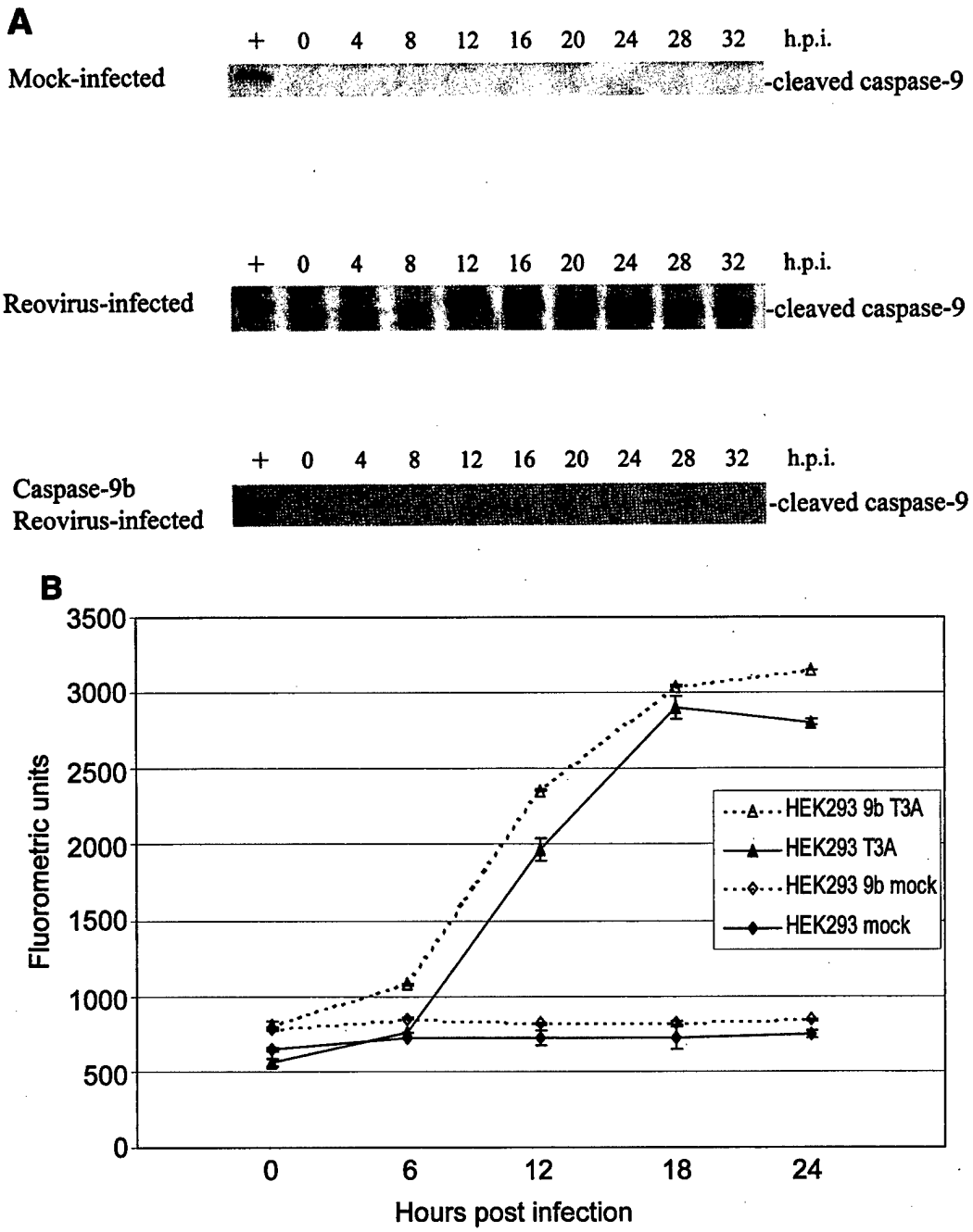

FIG. 4. Inhibition of caspase-9 activation does not prevent effector caspase activation. Western blot analysis was performed using HEK 293 lysates harvested at the indicated time points from mock-infected and reovirus-infected cells and probed with anti-caspase-9 antibodies (A) or anti-PARP antibodies (C). Control lanes represent Jurkat cell lysates untreated (−) or treated (+) with activating anti-Fas antibody and harvested at 8 h posttreatment. Each Western blot is representative of two separate experiments. (B) Fluorogenic substrate assays were performed in triplicate. Error bars represent standard error of the mean. Fluorescence is expressed as arbitrary units. h.p.i., hours postinfection.

Mitochondrial membrane potential is maintained following reovirus infection. We have shown that reovirus infection results in the caspase-8-dependent cleavage of the proapoptotic protein Bid (21). It has been reported that Bid-dependent cytochrome *c* release can occur in the absence of mitochondrial membrane potential ($\Delta\Psi_m$) loss (20, 57). Previous studies suggested that reovirus infection did not alter $\Delta\Psi_m$ in monkey kidney CV-1 cells (46). In light of our data indicating the release of both cytochrome *c* and Smac/DIABLO from the mitochondria of infected cells, we wanted to determine the state of the $\Delta\Psi_m$ following infection of HEK 293 cells using the $\Delta\Psi_m$-sensitive dye JC-1. Using JC-1, high $\Delta\Psi_m$ is indicated by red fluorescence and low $\Delta\Psi_m$ is indicated by green fluorescence. As shown in Fig. 3, no $\Delta\Psi_m$ reduction is detected over

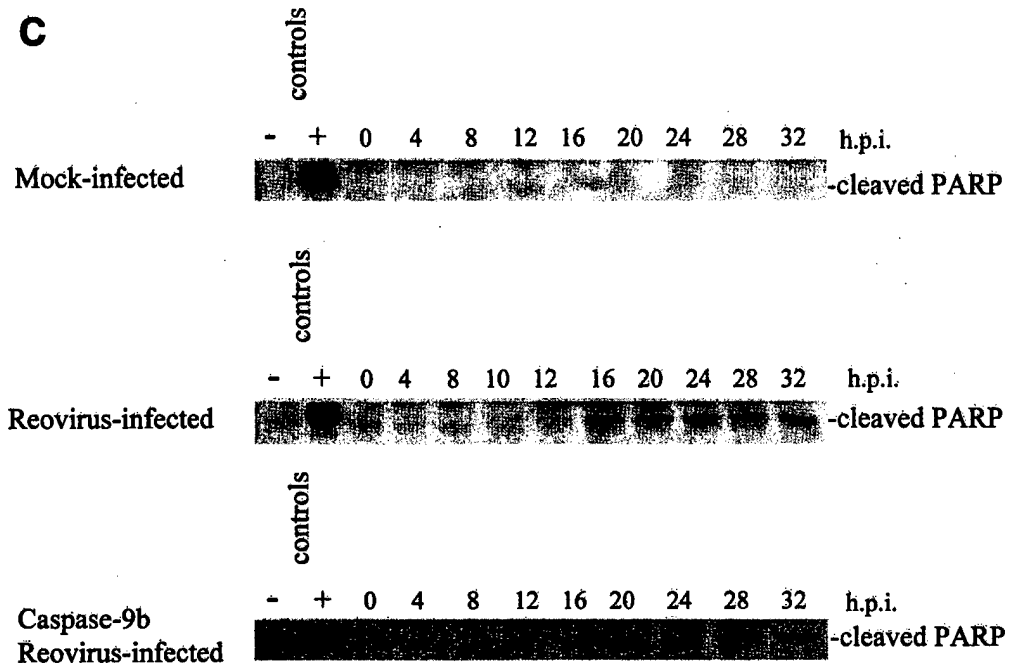

FIG. 4—*Continued.*

the reovirus infection time course (Fig. 3B to E) compared to mock-infected cells (Fig. 3A). As a control cells were treated with the apoptosis-inducing agent valinomycin, a K^+ ionophore that induces loss of $\Delta\Psi_m$ (Fig. 3F) to show the shift in red to green fluorescence that accompanies $\Delta\Psi_m$ perturbation.

Caspase-9 activation is dispensable for effector caspase activation following reovirus infection. Having shown that both cytochrome *c* and Smac/DIABLO are released from the mitochondria of reovirus-infected cells, we wanted to determine the importance of the contribution of these proteins to reovirus-induced apoptosis. Cells were transfected with a dominant-negative form of caspase-9, caspase-9b (47). Unlike Bcl-2 overexpression, which blocks all mitochondrially mediated events, caspase-9b only interferes with the cytochrome *c*-dependent process of caspase-9 activation. Expression of the caspase-9b isoform was confirmed by Western blotting (data not shown). As shown in Fig. 4A, caspase-9b expression prevents the activation of endogenous caspase-9, as evidenced by the failure to detect the 37-kDa fragment of active caspase-9. We next infected cells expressing caspase-9b and utilized a caspase-3 fluorogenic substrate assay to measure the activity of caspase-3. We found that inhibition of caspase-9 activation did not prevent reovirus-induced activation of caspase-3 (Fig. 4B). This result was confirmed by examining the cleavage of the endogenous caspase-3 substrate PARP. As shown in Fig. 4C, the 85-kDa cleavage fragment of PARP is detected in both reovirus-infected cells and reovirus-infected, caspase-9b-expressing cells. These results in conjunction with our previous studies establishing the importance of the mitochondrial pathway in reovirus-induced apoptosis indicated that cytochrome *c*-dependent caspase-9 activation was not required for apoptosis following reovirus infection.

XIAP is cleaved in reovirus-infected cells. Having shown that Smac/DIABLO was released from mitochondria in reovirus-infected cells, we next wished to determine whether this was associated with alterations in cellular levels of IAPs. XIAP is a ubiquitously expressed protein (27) that is cleaved following induction of apoptosis (8, 18). Therefore, using Western blot analysis we looked for the presence of cleaved XIAP following reovirus infection. As shown in Fig. 5, the ~30-kDa XIAP cleavage fragment is detected at 12 h postinfection and persists over the time course of the infection. This fragment is not detected in mock-infected or in reovirus-infected cells overexpressing Bcl-2 (Fig. 5), indicating that activation of the mitochondrial apoptotic pathway is required for XIAP cleavage.

c-IAP1 and survivin are down-regulated in reovirus-infected cells. We next examined the cellular levels of several other IAP family members following reovirus infection. Survivin, like XIAP, has been shown to inhibit apoptosis. We used Western blot analysis to examine survivin protein levels following reovirus infection. Survivin protein levels were found to dramatically decrease in reovirus-infected cells beginning at ~12 h postinfection (Fig. 6). This reduction was not seen in mock-infected cells and was strongly inhibited in reovirus-infected, Bcl-2-overexpressing cells (Fig. 6). We also examined levels of two other IAPs, c-IAP1 and c-IAP2. Both c-IAP1 and c-IAP2 have been shown to directly inhibit caspases (40). As shown in Fig. 7, c-IAP1 protein levels are reduced over the time course following reovirus infection, while c-IAP1 levels remain unchanged in both mock-infected and reovirus-infected cells overexpressing Bcl-2. The reduction of c-IAP1 protein levels appears to begin at ~16 h postinfection (Fig. 7), which correlates well with the second phase of Smac/DIABLO release

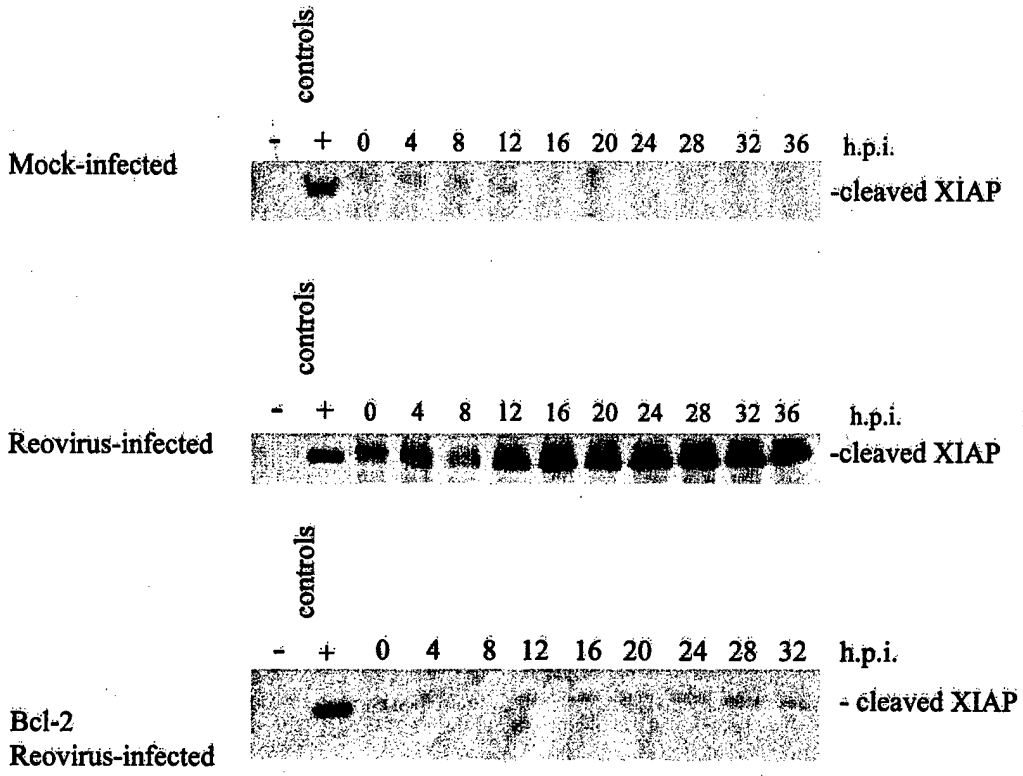

FIG. 5. Reovirus infection leads to the cleavage of XIAP. Western blot analysis was performed using HEK 293 lysates harvested at the indicated time points from mock-infected, reovirus-infected, and Bcl-2-overexpressing reovirus-infected cells and probed with anti-XIAP antibodies. Control lanes represent Jurkat cell lysates untreated (−) or treated (+) with activating anti-Fas antibody and harvested at 8 h posttreatment. The Western blot is representative of three separate experiments. h.p.i., hours postinfection.

from the mitochondria (Fig. 1A). c-IAP2 levels remain relatively unchanged in both mock-infected and reovirus-infected cells (Fig. 8), indicating that c-IAP2 does not play a role in reovirus-induced apoptosis. These results indicate that reovirus infection is associated with selective reduction in cellular levels of specific IAPs.

DISCUSSION

Several viruses have been found to induce apoptosis in infected cells (40). Apoptosis also plays an important role in virus-induced tissue injury in vivo. However, the exact cellular pathways involved in virus-induced apoptosis are still incompletely understood. To this end a number of studies have been undertaken to elucidate the apoptotic pathways induced by viral infection both in vivo and in vitro.

Several studies have demonstrated that infection by a diverse group of viruses may induce apoptosis, at least in part, through a death-receptor-dependent mechanism. These include HIV (31, 59), measles virus (44, 56), influenza A virus (32), Sindbis virus (24), and hepatitis C virus (62) infections. The mitochondrion-dependent apoptotic pathway has also been shown to play a central role in virus-induced apoptosis. A number of viruses have been found to cause relocalization of proapoptotic mitochondrial proteins through both direct and indirect interactions. Among these are HIV (13, 16, 17), influenza A virus (4), HSV-1 (61), HSV-8 (45), hepatitis B virus (52), and West Nile virus (35). These data suggest that depending on the specific viruses and cells studied, both death receptor and mitochondrial pathways can contribute to virus-induced apoptosis.

There is considerable cross talk between death-receptor and mitochondrial apoptotic pathways. For example, death-receptor-dependent activation of caspase-8 leads to cleavage of Bid, resulting in the release of mitochondrial proapoptotic proteins, including cytochrome *c* and Smac/DIABLO, into the cytoplasm. Indeed, it has been suggested that cells can be grouped based upon the degree of mitochondrial involvement in death-receptor-mediated apoptosis (42, 43). The cytochrome *c*-dependent activation of caspase-9 has been thought to be of central importance in this process. However, several recent reports suggest that Smac/DIABLO release rather than caspase-9 activation may be the critical mitochondrial event in both TRAIL-induced (7, 60) and FasL-induced apoptosis (48).

Reovirus-induced apoptosis requires engagement of cellular receptors, including junction adhesion molecule and sialic acid residues (3), and has been shown to involve the DR4/DR5/TRAIL death receptor apoptotic pathway (5). We have shown recently that, in reovirus-infected HEK cells, although apoptosis is initiated by death receptor activation, its full expression requires the participation of mitochondrial apoptotic pathways (21). We have also previously shown that reovirus infection is associated with mitochondrial release of cytochrome *c* and subsequent activation of caspase-9 (21). Additionally, we dem-

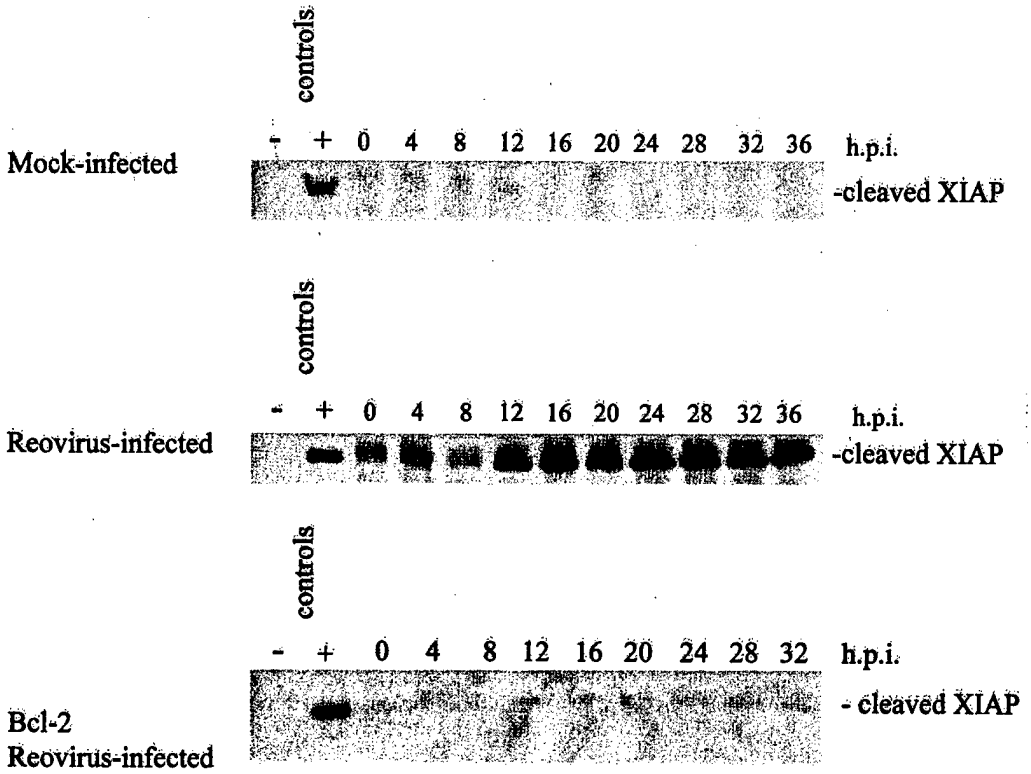

FIG. 5. Reovirus infection leads to the cleavage of XIAP. Western blot analysis was performed using HEK 293 lysates harvested at the indicated time points from mock-infected, reovirus-infected, and Bcl-2-overexpressing reovirus-infected cells and probed with anti-XIAP antibodies. Control lanes represent Jurkat cell lysates untreated (−) or treated (+) with activating anti-Fas antibody and harvested at 8 h posttreatment. The Western blot is representative of three separate experiments. h.p.i., hours postinfection.

from the mitochondria (Fig. 1A). c-IAP2 levels remain relatively unchanged in both mock-infected and reovirus-infected cells (Fig. 8), indicating that c-IAP2 does not play a role in reovirus-induced apoptosis. These results indicate that reovirus infection is associated with selective reduction in cellular levels of specific IAPs.

DISCUSSION

Several viruses have been found to induce apoptosis in infected cells (40). Apoptosis also plays an important role in virus-induced tissue injury in vivo. However, the exact cellular pathways involved in virus-induced apoptosis are still incompletely understood. To this end a number of studies have been undertaken to elucidate the apoptotic pathways induced by viral infection both in vivo and in vitro.

Several studies have demonstrated that infection by a diverse group of viruses may induce apoptosis, at least in part, through a death-receptor-dependent mechanism. These include HIV (31, 59), measles virus (44, 56), influenza A virus (32), Sindbis virus (24), and hepatitis C virus (62) infections. The mitochondrion-dependent apoptotic pathway has also been shown to play a central role in virus-induced apoptosis. A number of viruses have been found to cause relocalization of proapoptotic mitochondrial proteins through both direct and indirect interactions. Among these are HIV (13, 16, 17), influenza A virus (4), HSV-1 (61), HSV-8 (45), hepatitis B virus (52), and West Nile virus (35). These data suggest that depending on the specific viruses and cells studied, both death receptor and mitochondrial pathways can contribute to virus-induced apoptosis.

There is considerable cross talk between death-receptor and mitochondrial apoptotic pathways. For example, death-receptor-dependent activation of caspase-8 leads to cleavage of Bid, resulting in the release of mitochondrial proapoptotic proteins, including cytochrome *c* and Smac/DIABLO, into the cytoplasm. Indeed, it has been suggested that cells can be grouped based upon the degree of mitochondrial involvement in death-receptor-mediated apoptosis (42, 43). The cytochrome *c*-dependent activation of caspase-9 has been thought to be of central importance in this process. However, several recent reports suggest that Smac/DIABLO release rather than caspase-9 activation may be the critical mitochondrial event in both TRAIL-induced (7, 60) and FasL-induced apoptosis (48).

Reovirus-induced apoptosis requires engagement of cellular receptors, including junction adhesion molecule and sialic acid residues (3), and has been shown to involve the DR4/DR5/TRAIL death receptor apoptotic pathway (5). We have shown recently that, in reovirus-infected HEK cells, although apoptosis is initiated by death receptor activation, its full expression requires the participation of mitochondrial apoptotic pathways (21). We have also previously shown that reovirus infection is associated with mitochondrial release of cytochrome *c* and subsequent activation of caspase-9 (21). Additionally, we dem-

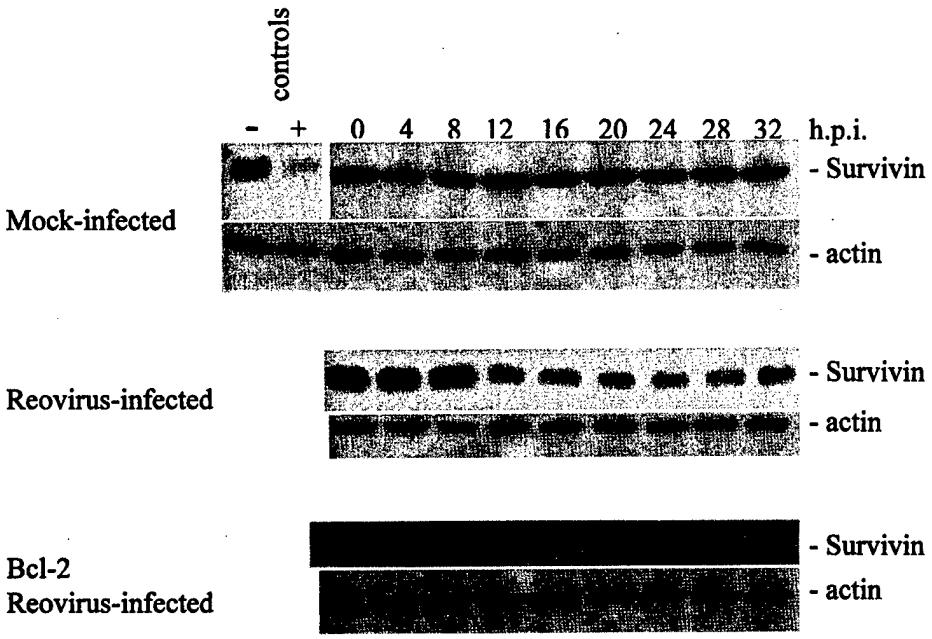

FIG. 6. Cellular levels of survivin are reduced following reovirus infection. Western blot analysis was performed using HEK 293 lysates harvested at the indicated time points from mock-infected, reovirus-infected, and Bcl-2-overexpressing reovirus-infected cells and probed with antisurvivin antibodies and antiactin to demonstrate equal protein loading. Control lanes represent Jurkat cell lysates untreated (−) or treated (+) with activating anti-Fas antibody and harvested at 8 h posttreatment. The Western blot is representative of two separate experiments. h.p.i., hours postinfection.

onstrated that the activation of caspase-8 and caspase-3 and the cleavage of Bid occur in a biphasic manner (21). We have postulated that the early phase of caspase activation and Bid truncation are necessary to activate the mitochondrial apoptotic pathway, which leads to the second, more intense phase of caspase activation and apoptosis (21). We now show that in addition to cytochrome *c*, Smac/DIABLO is also released from mitochondria of infected cells and that the release of Smac/

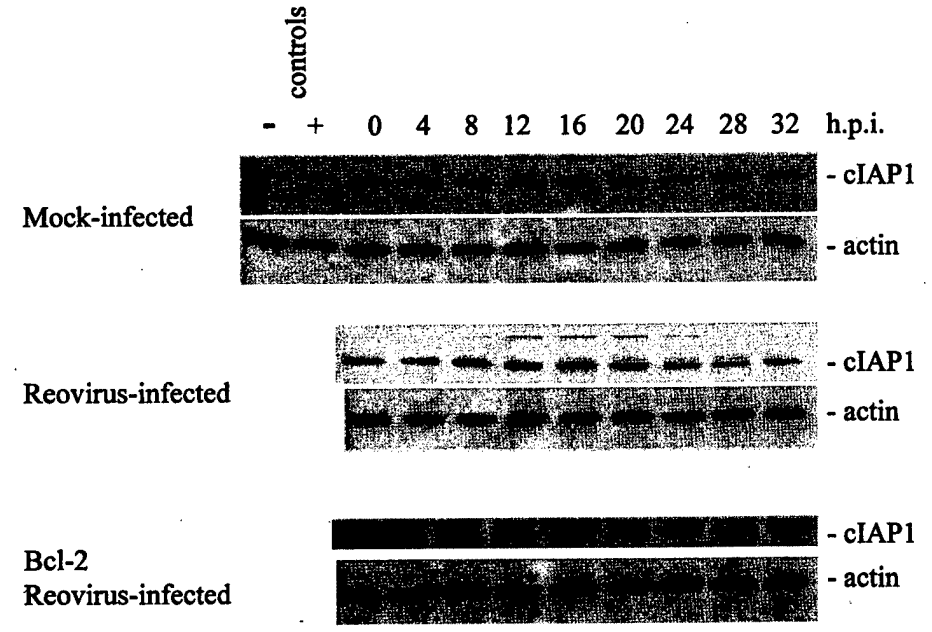

FIG. 7. Reovirus infection induces a reduction in c-IAP1 protein level. Western blot analysis was performed using HEK 293 lysates harvested at the indicated time points from mock-infected, reovirus-infected, and Bcl-2-overexpressing reovirus-infected cells and probed with anti-c-IAP1 antibodies and antiactin to demonstrate equal protein loading. Control lanes represent Jurkat cell lysates untreated (−) or treated (+) with activating anti-Fas antibody and harvested at 8 h posttreatment. The Western blot is representative of two separate experiments. h.p.i., hours postinfection.

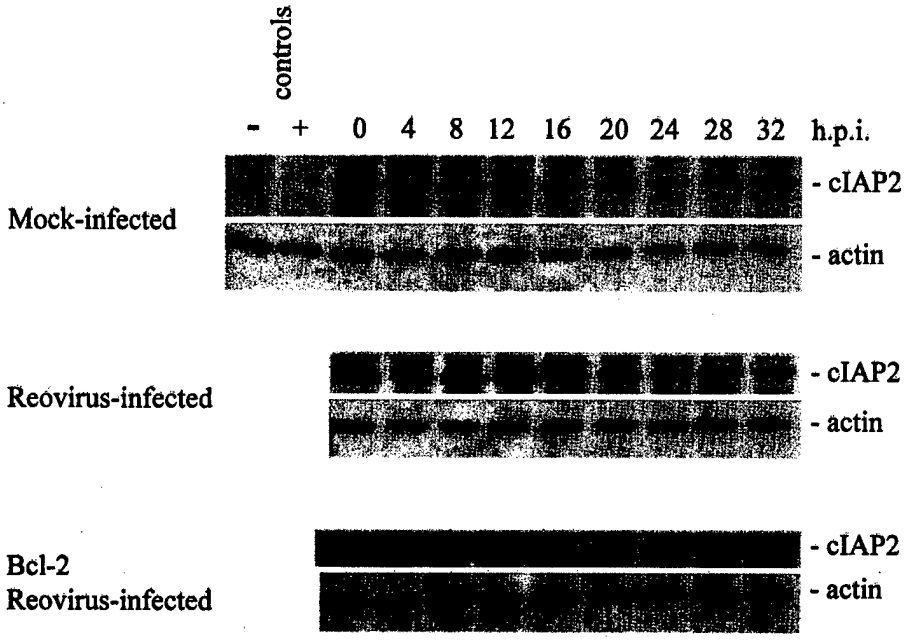

FIG. 8. Cellular c-IAP2 protein levels are unaffected following reovirus infection. Western blot analysis was performed using HEK 293 lysates harvested at the indicated time points from mock-infected, reovirus-infected, and Bcl-2-overexpressing reovirus-infected cells and probed with anti-c-IAP2 antibodies and antiactin to demonstrate equal protein loading. Control lanes represent Jurkat cell lysates untreated (−) or treated (+) with activating anti-Fas antibody and harvested at 8 h posttreatment. The Western blot is representative of two separate experiments. h.p.i., hours postinfection.

DIABLO occurs in a biphasic manner. Another mitochondrial protein, AIF, remains sequestered, indicating that reovirus-induced release of mitochondrial proapoptotic proteins is a selective process and is not indiscriminately associated with the release of all mitochondrial proapoptotic factors. This selective release is consistent with previous results (46) and our present studies indicating that reovirus infection does not alter mitochondrial $\Delta\Psi_m$ in infected cells and that mitochondrial ultrastructure is not significantly disrupted in the early stages of reovirus infection (K. L. Tyler, unpublished data).

We had previously demonstrated that overexpression of Bcl-2 was capable of preventing effector caspase activation following reovirus infection, indicating that mitochondrial apoptotic pathways were involved in reovirus-induced apoptosis in many cell types (21, 38). Having shown that reovirus infection induces the release of both Smac/DIABLO and cytochrome *c*, we next wanted to determine if we could elucidate the relative contribution of these proteins to reovirus-induced apoptosis. We utilized a dominant-negative caspase-9 construct (caspase-9b) to specifically inhibit endogenous caspase-9 activation following reovirus infection. We found that inhibition of caspase-9 activation did not significantly alter activation of the effector caspase, caspase-3. These data indicate that cytochrome *c* release and subsequent caspase-9 activation were not the critical mitochondrial event in reovirus-induced apoptosis.

Having shown that Smac/DIABLO was also released from mitochondria in reovirus-infected cells, we wished to determine whether this was associated with alterations of IAPs known to interact with Smac/DIABLO. We therefore examined the cellular levels of several IAP proteins following reovirus infection. We find that XIAP is cleaved following reovirus infection, beginning at ~12 h postinfection. This cleavage is blocked in Bcl-2-overexpressing cells. Additionally, we show that survivin and c-IAP1 protein levels are reduced following reovirus infection, with the reduction first being appreciable at ~12 h postinfection. Both of these events are inhibited in Bcl-2-overexpressing cells, indicating that they require activation of mitochondrial apoptotic pathways. Cellular levels of c-IAP2 were unaffected following reovirus infection, indicating that the effects of reovirus infection on IAPs are selective.

In this work we provide further evidence for the importance of the mitochondrial apoptotic pathway, and specifically for the release of Smac/DIABLO, in reovirus-induced apoptosis. Additionally, we elucidate the intracellular mechanisms of this process by showing that removal or down-regulation of certain IAP proteins appears to be an important part of cell death. Unfortunately, specific inhibitors of Smac/DIABLO release or function are not currently available, and therefore the necessity of Smac/DIABLO release cannot be directly assessed at this time. However, we believe that our data strongly implicate the release of Smac/DIABLO as the required mitochondrial event for reovirus-induced apoptosis. A possible model for the events involved in reovirus-induced apoptosis is shown in Fig. 9. Following caspase-8 activation, the proapoptotic protein Bid is cleaved. Truncated Bid either directly or indirectly induces the release of the mitochondrial proteins cytochrome *c* and Smac/DIABLO. Cytosolic cytochrome *c* induces the activation of caspase-9, and Smac/DIABLO interferes with the ability of XIAP, survivin, and c-IAP1 to prevent caspase activation. While caspase-9 may play a role in amplifying effector caspase activation, this appears to be unnecessary for reovirus-induced apoptosis. These studies provide the first direct evidence for

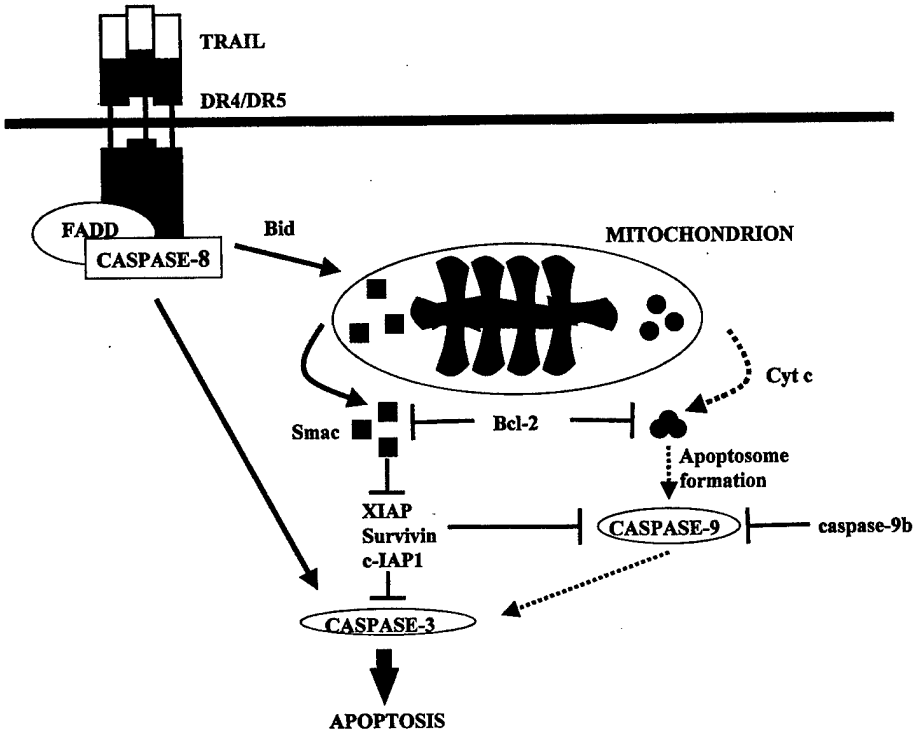

FIG. 9. Model of cellular pathways involved in reovirus-induced apoptosis in HEK cells. Reovirus infection leads to the activation of caspase-8 and cleavage of the proapoptotic molecule Bid. These events promote the release of Smac/DIABLO and cytochrome *c* from the mitochondria of infected cells. The release of these proteins can be prevented by the overexpression of Bcl-2. Cytosolic Smac/DIABLO inhibits the antiapoptotic effect exerted by XIAP, survivin, and c-IAP1, leading to the sustained activation of both initiator caspases and the effector caspase, caspase-3. While caspase-9 is activated and undoubtedly participates in reovirus-induced apoptosis, its activation appears to be dispensable for this process.

the association of Smac/DIABLO with virus-induced apoptosis.

ACKNOWLEDGMENTS

This work was supported by a U.S. Army Medical Research and Material Command grant (DAMD179818614), merit and REAP grants from the Department of Veterans Affairs, and Public Health Service grant 1RO1AG14071 from the National Institute of Aging. K. L. Tyler is supported by the Reuler-Lewin Family Professorship of Neurology. D. J. Kominsky was supported by NIH training grant T32NS07321.

We acknowledge the UCHSC Cancer Center Media Core for supplying tissue culture medium.

REFERENCES

1. **Ambrosini, G., C. Adida, and D. C. Altieri.** 1997. A novel anti-apoptosis gene, survivin, expressed in cancer and lymphoma. Nat. Med. **3**:917–921.
2. **Ashkenazi, A., and V. M. Dixit.** 1998. Death receptors: signaling and modulation. Science **281**:1305–1308.
3. **Barton, E. S., J. C. Forrest, J. L. Connolly, J. D. Chappell, Y. Liu, F. J. Schnell, A. Nusrat, C. A. Parkos, and T. S. Dermody.** 2001. Junction adhesion molecule is a receptor for reovirus. Cell **104**:441–451.
4. **Chen, W., P. A. Calvo, D. Malide, J. Gibbs, U. Schubert, I. Bacik, S. Basta, R. O'Neill, J. Schickli, P. Palese, P. Henklein, J. R. Bennink, and J. W. Yewdell.** 2001. A novel influenza A virus mitochondrial protein that induces cell death. Nat. Med. **7**:1306–1312.
5. **Clarke, P., S. M. Meintzer, S. Gibson, C. Widmann, T. P. Garrington, G. L. Johnson, and K. L. Tyler.** 2000. Reovirus-induced apoptosis is mediated by TRAIL. J. Virol. **74**:8135–8139.
6. **DeBiasi, R. L. C. L. Edelstein B. Sherry, and K. L. Tyler.** 2001. Calpain inhibition protects against virus-induced apoptotic myocardial injury. J. Virol **75**:351–361.
7. **Deng, Y., Y. Lin, and X. Wu.** 2002. TRAIL-induced apoptosis requires Bax-dependent mitochondrial release of Smac/DIABLO. Genes Dev. **16**:33–45.
8. **Deveraux, Q. L., E. Leo, H. R. Stennicke, K. Welsh, G. S. Salvesen, and J. C. Reed.** 1999. Cleavage of human inhibitor of apoptosis protein XIAP results in fragments with distinct specificities for caspases. EMBO J. **18**:5242–5251.
9. **Deveraux, Q. L., and J. C. Reed.** 1999. IAP family proteins—suppressors of apoptosis. Genes Dev. **13**:239–252.
10. **Deveraux, Q. L., R. Takahashi, G. S. Salvesen, and J. C. Reed.** 1997. X-linked IAP is a direct inhibitor of cell-death proteases. Nature **388**:300–304.
11. **Du, C., M. Fang, Y. Li, L. Li, and X. Wang.** 2000. Smac, a mitochondrial protein that promotes cytochrome c-dependent caspase activation by eliminating IAP inhibition. Cell **102**:33–42.
12. **Duckett, C. S., F. Li, Y. Wang, K. J. Tomaselli, C. B. Thompson, and R. C. Armstrong.** 1998. Human IAP-like protein regulates programmed cell death downstream of Bcl-x_L and cytochrome *c*. Mol. Cell. Biol. **18**:608–615.
13. **Ferri, K. F., E. Jacotot, J. Blanco, J. A. Este, N. Zamzami, S. A. Susin, Z. Xie, G. Brothers, J. C. Reed, J. M. Penninger, and G. Kroemer.** 2000. Apoptosis control in syncytia induced by the HIV type 1-envelope glycoprotein complex: role of mitochondria and caspases. J. Exp. Med. **192**:1081–1092.
14. **Goyal, L.** 2001. Cell death inhibition: keeping caspases in check. Cell **104**: 805–808.
15. **Hauser, H. P., M. Bardroff, G. Pyrowolakis, and S. Jentsch.** 1998. A giant ubiquitin-conjugating enzyme related to IAP apoptosis inhibitors. J. Cell Biol. **141**:1415–1422.
16. **Jacotot, E., K. F. Ferri, C. El Hamel, C. Brenner, S. Druillennec, J. Hoebeke, P. Rustin, D. Metivier, C. Lenoir, M. Geuskens, H. L. Vieira, M. Loeffler, A. S. Belzacq, J. P. Briand, N. Zamzami, L. Edelman, Z. H. Xie, J. C. Reed, B. P. Roques, and G. Kroemer.** 2001. Control of mitochondrial membrane permeabilization by adenine nucleotide translocator interacting with HIV-1 viral protein rR and Bcl-2. J. Exp. Med. **193**:509–519.
17. **Jacotot, E., L. Ravagnan, M. Loeffler, K. F. Ferri, H. L. Vieira, N. Zamzami, P. Costantini, S. Druillennec, J. Hoebeke, J. P. Briand, T. Irinopoulou, E. Daugas, S. A. Susin, D. Cointe, Z. H. Xie, J. C. Reed, B. P. Roques, and G. Kroemer.** 2000. The HIV-1 viral protein R induces apoptosis via a direct effect on the mitochondrial permeability transition pore. J. Exp. Med. **191**: 33–46.
18. **Johnson, D. E., B. R. Gastman, E. Wieckowski, G. Q. Wang, A. Amoscato, S. M. Delach, and H. Rabinowich.** 2000. Inhibitor of apoptosis protein hILP

undergoes caspase-mediated cleavage during T lymphocyte apoptosis. Cancer Res. **60**:1818–1823.
19. **Joza, N., S. A. Susin, E. Daugas, W. L. Stanford, S. K. Cho, C. Y. Li, T. Sasaki, A. J. Elia, H. Y. Cheng, L. Ravagnan, K. F. Ferri, N. Zamzami, A. Wakeham, R. Hakem, H. Yoshida, Y. Y. Kong, T. W. Mak, J. C. Zuniga-Pflucker, G. Kroemer, and J. M. Penninger.** 2001. Essential role of the mitochondrial apoptosis-inducing factor in programmed cell death. Nature **410**:549–554.
20. **Kim, T. H., Y. Zhao, M. J. Barber, D. K. Kuharsky, and X. M. Yin.** 2000. Bid-induced cytochrome c release is mediated by a pathway independent of mitochondrial permeability transition pore and Bax. J. Biol. Chem. **275**: 39474–39481.
21. **Kominsky, D. J., R. J. Bickel, and K. L. Tyler.** 2002. Reovirus-induced apoptosis requires both death receptor- and mitochondrial-mediated caspase-dependent pathways of cell death. Cell Death Differ. **9**:926–933.
22. **Korsmeyer, S. J., M. C. Wei, M. Saito, S. Weiler, K. J. Oh, and P. H. Schlesinger.** 2000. Pro-apoptotic cascade activates BID, which oligomerizes BAK or BAX into pores that result in the release of cytochrome c. Cell Death Differ. **7**:1166–1173.
23. **Krajewski, S., M. Krajewska, L. M. Ellerby, K. Welsh, Z. Xie, Q. L. Deveraux, G. S. Salvesen, D. E. Bredesen, R. E. Rosenthal, G. Fiskum, and J. C. Reed.** 1999. Release of caspase-9 from mitochondria during neuronal apoptosis and cerebral ischemia. Proc. Natl. Acad. Sci. USA **96**:5752–5757.
24. **Li, H., H. Zhu, C. J. Xu, and J. Yuan.** 1998. Cleavage of BID by caspase 8 mediates the mitochondrial damage in the Fas pathway of apoptosis. Cell **94**:491–501.
25. **Li, J., J. M. Kim, P. Liston, M. Li, T. Miyazaki, A. E. Mackenzie, R. G. Korneluk, and B. K. Tsang.** 1998. Expression of inhibitor of apoptosis proteins (IAPs) in rat granulosa cells during ovarian follicular development and atresia. Endocrinology **139**:1321–1328.
26. **Li, L. Y., X. Luo, and X. Wang.** 2001. Endonuclease G is an apoptotic DNase when released from mitochondria. Nature **412**:95–99.
27. **Liston, P., N. Roy, K. Tamai, C. Lefebvre, S. Baird, G. Cherton-Horvat, R. Farahani, M. McLean, J. E. Ikeda, A. MacKenzie, and R. G. Korneluk.** 1996. Suppression of apoptosis in mammalian cells by NAIP and a related family of IAP genes. Nature **379**:349–353.
28. **Liu, X., C. N. Kim, J. Yang, R. Jemmerson, and X. Wang.** 1996. Induction of apoptotic program in cell-free extracts: requirement for dATP and cytochrome c. Cell **86**:147–157.
29. **Mancini, M., C. E. Machamer, S. Roy, D. W. Nicholson, N. A. Thornberry, L. A. Casciola-Rosen, and A. Rosen.** 2000. Caspase-2 is localized at the Golgi complex and cleaves golgin-160 during apoptosis. J. Cell Biol. **149**:603–612.
30. **Mancini, M., D. W. Nicholson, S. Roy, N. A. Thornberry, E. P. Peterson, L. A. Casciola-Rosen, and A. Rosen.** 1998. The caspase-3 precursor has a cytosolic and mitochondrial distribution: implications for apoptotic signaling. J. Cell Biol. **140**:1485–1495.
31. **Miura, Y., N. Misawa, N. Maeda, Y. Inagaki, Y. Tanaka, M. Ito, N. Kayagaki, N. Yamamoto, H. Yagita, H. Mizusawa, and Y. Koyanagi.** 2001. Critical contribution of tumor necrosis factor-related apoptosis-inducing ligand (TRAIL) to apoptosis of human CD4+ T cells in HIV-1-infected hu-PBL-NOD-SCID mice. J. Exp. Med. **193**:651–660.
32. **Nichols, J. E., J. A. Niles, and N. J. Roberts, Jr.** 2001. Human lymphocyte apoptosis after exposure to influenza A virus. J. Virol. **75**:5921–5929.
33. **Oberhaus, S. M., T. S. Dermody, and K. L. Tyler.** 1998. Apoptosis and the cytopathic effects of reovirus. Curr. Top. Microbiol. Immunol. **233**:23–49.
34. **Oberhaus, S. M., R. L. Smith, G. H. Clayton, T. S. Dermody, and K. L. Tyler.** 1997. Reovirus infection and tissue injury in the mouse central nervous system are associated with apoptosis. J. Virol. **71**:2100–2106.
35. **Parquet, M. C., A. Kumatori, F. Hasebe, K. Morita, and A. Igarashi.** 2001. West Nile virus-induced bax-dependent apoptosis. FEBS Lett. **500**:17–24.
36. **Qin, Z. H., Y. Wang, K. K. Kikly, E. Sapp, K. B. Kegel, N. Aronin, and M. DiFiglia.** 2001. Pro-caspase-8 is predominantly localized in mitochondria and released into cytoplasm upon apoptotic stimulation. J. Biol. Chem. **276**: 8079–8086.
37. **Reed, J. C.** 1998. Bcl-2 family proteins. Oncogene **17**:3225–3236.
38. **Rodgers, S. E., E. S. Barton, S. M. Oberhaus, B. Pike, C. A. Gibson, K. L. Tyler, and T. S. Dermody.** 1997. Reovirus-induced apoptosis of MDCK cells is not linked to viral yield and is blocked by Bcl-2. J. Virol. **71**:2540–2546.
39. **Rothe, M., M. G. Pan, W. J. Henzel, T. M. Ayres, and D. V. Goeddel.** 1995. The TNFR2-TRAF signaling complex contains two novel proteins related to baculoviral inhibitor of apoptosis proteins. Cell **83**:1243–1252.
40. **Roulston, A., R. C. Marcellus, and P. E. Branton.** 1999. Viruses and apoptosis. Annu. Rev. Microbiol. **53**:577–628.
41. **Roy, N., Q. L. Deveraux, R. Takahashi, G. S. Salvesen, and J. C. Reed.** 1997. The c-IAP-1 and c-IAP-2 proteins are direct inhibitors of specific caspases. EMBO J. **16**:6914–6925.
42. **Scaffidi, C., S. Fulda, A. Srinivasan, C. Friesen, F. Li, K. J. Tomaselli, K. M. Debatin, P. H. Krammer, and M. E. Peter.** 1998. Two CD95 (APO-1/Fas) signaling pathways. EMBO J. **17**:1675–1687.
43. **Scaffidi, C., I. Schmitz, J. Zha, S. J. Korsmeyer, P. H. Krammer, and M. E. Peter.** 1999. Differential modulation of apoptosis sensitivity in CD95 type I and type II cells. J. Biol. Chem. **274**:22532–22538.
44. **Servet-Delprat, C., P. O. Vidalain, O. Azocar, F. Le Deist, A. Fischer, and C. Rabourdin-Combe.** 2000. Consequences of Fas-mediated human dendritic cell apoptosis induced by measles virus. J. Virol. **74**:4387–4393.
45. **Sharp, T. V., H. W. Wang, A. Koumi, D. Hollyman, Y. Endo, H. Ye, M. Q. Du, and C. Boshoff.** 2002. K15 protein of Kaposi's sarcoma-associated herpesvirus is latently expressed and binds to HAX-1, a protein with antiapoptotic function. J. Virol. **76**:802–816.
46. **Sharpe, A. H., L. B. Chen, and B. N. Fields.** 1982. The interaction of mammalian reoviruses with the cytoskeleton of monkey kidney CV-1 cells. Virology **120**:399–411.
47. **Srinivasula, S. M., M. Ahmad, Y. Guo, Y. Zhan, Y. Lazebnik, T. Fernandes-Alnemri, and E. S. Alnemri.** 1999. Identification of an endogenous dominant-negative short isoform of caspase-9 that can regulate apoptosis. Cancer Res. **59**:999–1002.
48. **Sun, X. M., S. B. Bratton, M. Butterworth, M. MacFarlane, and G. M. Cohen.** 2002. Bcl-2 and Bcl-xL inhibit CD95-mediated apoptosis by preventing mitochondrial release of Smac/DIABLO and subsequent inactivation of X-linked inhibitor-of-apoptosis protein. J. Biol. Chem. **277**:11345–11351.
49. **Susin, S. A., H. K. Lorenzo, N. Zamzami, I. Marzo, C. Brenner, N. Larochette, M. C. Prevost, P. M. Alzari, and G. Kroemer.** 1999. Mitochondrial release of caspase-2 and -9 during the apoptotic process. J. Exp. Med. **189**:381–394.
50. **Susin, S. A., H. K. Lorenzo, N. Zamzami, I. Marzo, B. E. Snow, G. M. Brothers, J. Mangion, E. Jacotot, P. Costantini, M. Loeffler, N. Larochette, D. R. Goodlett, R. Aebersold, D. P. Siderovski, J. M. Penninger, and G. Kroemer.** 1999. Molecular characterization of mitochondrial apoptosis-inducing factor. Nature **397**:441–446.
51. **Tamm, I., Y. Wang, E. Sausville, D. A. Scudiero, N. Vigna, T. Oltersdorf, and J. C. Reed.** 1998. IAP-family protein survivin inhibits caspase activity and apoptosis induced by Fas (CD95), Bax, caspases, and anticancer drugs. Cancer Res. **58**:5315–5320.
52. **Terradillos, O., C. A. de La, T. Pollicino, C. Neuveut, D. Sitterlin, H. Lecoeur, M. L. Gougeon, A. Kahn, and M. A. Buendia.** 2002. The hepatitis B virus X protein abrogates Bcl-2-mediated protection against Fas apoptosis in the liver. Oncogene **21**:377–386.
53. **Tyler, K. L., M. K. Squier, A. L. Brown, B. Pike, D. Willis, S. M. Oberhaus, T. S. Dermody, and J. J. Cohen.** 1996. Linkage between reovirus-induced apoptosis and inhibition of cellular DNA synthesis: role of the S1 and M2 genes. J. Virol. **70**:7984–7991.
54. **Tyler, K. L., M. K. Squier, S. E. Rodgers, B. E. Schneider, S. M. Oberhaus, T. A. Grdina, J. J. Cohen, and T. S. Dermody.** 1995. Differences in the capacity of reovirus strains to induce apoptosis are determined by the viral attachment protein sigma 1. J. Virol. **69**:6972–6979.
55. **Verhagen, A. M., P. G. Ekert, M. Pakusch, J. Silke, L. M. Connolly, G. E. Reid, R. L. Moritz, R. J. Simpson, and D. L. Vaux.** 2000. Identification of DIABLO, a mammalian protein that promotes apoptosis by binding to and antagonizing IAP proteins. Cell **102**:43–53.
56. **Vidalain, P. O., O. Azocar, B. Lamouille, A. Astier, C. Rabourdin-Combe, and C. Servet-Delprat.** 2000. Measles virus induces functional TRAIL production by human dendritic cells. J. Virol. **74**:556–559.
57. **von Ahsen, O., C. Renken, G. Perkins, R. M. Kluck, E. Bossy-Wetzel, and D. D. Newmeyer.** 2000. Preservation of mitochondrial structure and function after Bid- or Bax-mediated cytochrome c release. J. Cell Biol. **150**:1027–1036.
58. **Wei, M. C., W. X. Zong, E. H. Cheng, T. Lindsten, V. Panoutsakopoulou, A. J. Ross, K. A. Roth, G. R. MacGregor, C. B. Thompson, and S. J. Korsmeyer.** 2001. Proapoptotic BAX and BAK: a requisite gateway to mitochondrial dysfunction and death. Science **292**:727–730.
59. **Zhang, M., X. Li, X. Pang, L. Ding, O. Wood, K. Clouse, I. Hewlett, and A. I. Dayton.** 2001. Identification of a potential HIV-induced source of bystander-mediated apoptosis in T cells: upregulation of trail in primary human macrophages by HIV-1 tat. J. Biomed. Sci. **8**:290–296.
60. **Zhang, X. D., X. Y. Zhang, C. P. Gray, T. Nguyen, and P. Hersey.** 2001. Tumor necrosis factor-related apoptosis-inducing ligand-induced apoptosis of human melanoma is regulated by smac/DIABLO release from mitochondria. Cancer Res. **61**:7339–7348.
61. **Zhou, G., and B. Roizman.** 2000. Wild-type herpes simplex virus 1 blocks programmed cell death and release of cytochrome *c* but not the translocation of mitochondrial apoptosis-inducing factor to the nuclei of human embryonic lung fibroblasts. J. Virol. **74**:9048–9053.
62. **Zhu, N., C. F. Ware, and M. M. Lai.** 2001. Hepatitis C virus core protein enhances FADD-mediated apoptosis and suppresses TRADD signaling of tumor necrosis factor receptor. Virology **283**:178–187.
63. **Zou, H., Y. Li, X. Liu, and X. Wang.** 1999. An APAF-1.cytochrome c multimeric complex is a functional apoptosome that activates procaspase-9. J. Biol. Chem. **274**:11549–11556.

Cell Death and Differentiation (2002) 9, 926–933

www.nature.com/cdd

Reovirus-induced apoptosis requires both death receptor- and mitochondrial-mediated caspase-dependent pathways of cell death

DJ Kominsky[1], RJ Bickel[1], and KL Tyler[*,1,2,3]

[1] Department of Neurology, University of Colorado Health Science Center, Denver, Colorado 80262, USA
[2] Department of Medicine, Microbiology, and Immunology, University of Colorado Health Science Center, Denver, Colorado 80262, USA
[3] Denver Veteran's Affairs Medical Center, Denver, Colorado 80220, USA
* Corresponding author: KL Tyler, Department of Neurology (B-182), University of Colorado Health Science Center, 4200 E. 9th Avenue, Denver, CO 80262, USA. Tel: (303) 393-2874; Fax: (303) 393-4686; E-mail: Ken.Tyler@uchsc.edu.

Received 17.10.01; revised 14.1.02; accepted 6.2.02
Edited by CJ Thiele

Abstract

Apoptosis plays an important role in the pathogenesis of many viral infections. Despite this fact, the apoptotic pathways triggered during viral infections are incompletely understood. We now provide the first detailed characterization of the pattern of caspase activation following infection with a cytoplasmically replicating RNA virus. Reovirus infection of HEK293 cells results in the activation of caspase-8 followed by cleavage of the pro-apoptotic protein Bid. This initiates the activation of the mitochondrial apoptotic pathway leading to release of cytochrome *c* and activation of caspase-9. Combined activation of death receptor and mitochondrial pathways results in downstream activation of effector caspases including caspase-3 and caspase-7 and cleavage of cellular substrates including PARP. Apoptosis is initiated by death receptor pathways but requires mitochondrial amplification producing a biphasic pattern of caspase-8, Bid, and caspase-3 activation.
Cell Death and Differentiation (2002) **9**, 926–933. doi:10.1038/sj.cdd.4401045

Keywords: apoptosis; reovirus; caspase; death receptor; mitochondria

Abbreviations: JAM, junction adhesion molecule; TNF, tumor necrosis factor; TRAIL, TNF-related apoptosis-inducing ligand; DR, death receptor; DISC, death-inducing signaling complex; FADD, Fas-associated death domain; DEVD-AFC, Asp-Glu-Val-Asp-7-amino-4-methyl coumarin; PARP, poly(ADP-ribose) polymerase; Ac-YVAD-CHO, Ac-Tyr-Val-Ala-Asp-CHO; Ac-DEVD-CHO, Ac-Asp-Glu-Val-Asp-CHO; Ac-IETD-CHO, Ac-Ile-Asp-Thr-Glu-CHO

Introduction

Apoptosis is a particular type of cell death that is characterized by distinctive changes in cellular morphology, including cell shrinkage, zeiosis, nuclear condensation, chromatin margination and subsequent degradation that are associated with inter-nucleosomal DNA fragmentation. Apoptosis may be initiated by a wide variety of cellular insults, including death receptor stimulation, γ-radiation, and cytotoxic compounds. Induction or inhibition of apoptosis is an important feature of many types of viral infection, both *in vitro* and *in vivo*. Despite this fact, the mechanisms of virus-induced apoptosis remain largely unknown. This is particularly true for RNA viruses, the majority of which have cytoplasmic intracellular sites of replication and do not require nuclear integrity for successful propogation.

Mammalian reoviruses are non-enveloped double-stranded RNA viruses whose replication occurs exclusively in the cytoplasm. Reoviruses induce apoptosis in a wide variety of cultured cells *in vitro*.[1–3] Apoptosis also plays a critical role during reovirus infection *in vivo*, and is the mechanism of virus-induced tissue injury in key target organs, including the central nervous system and heart.[1,4,5] Inhibition of apoptosis dramatically reduces the extent of reovirus-induced tissue injury *in vivo*.[5]

It has been shown recently that reovirus-induced apoptosis requires interaction with its cell surface receptors including junction adhesion molecule (JAM).[6] Apoptosis involves the tumor necrosis factor (TNF) superfamily of cell surface death receptors, specifically DR4, DR5 and their ligand, TNF-related apoptosis-inducing ligand (TRAIL),[7] and is inhibited by anti-TRAIL antibodies or soluble forms of DR4 or DR5 which inhibit interaction of TRAIL with functional cell surface DR4 and DR5.[7] The contribution of mitochondrial apoptotic pathways to this process has been unknown, as has the exact nature of the caspase cascades activated and their inter-relationship.

Apoptosis induced by activation of cell surface death receptors ('extrinsic pathway') involves the formation of a death-induced signaling complex (DISC) that recruits and activates caspase-8.[8] Activated caspase-8 can, in turn, activate downstream effector caspases including caspases-3 and -7. Mitochondria play a central role in an 'intrinsic' pathway of apoptosis. In this pathway, apoptotic stimuli enhance mitochondrial membrane permeability and permit the translocation of cytochrome *c* and other pro-apoptotic molecules from the mitochondria into the cytosol.[9–12] A cytosolic complex including cytochrome *c* and Apaf-1 (apoptosome) activates caspase-9.[13] Activated caspase-9, like activated caspase-8, can activate additional downstream effector caspases including caspase-3. The intrinsic and extrinsic pathways are linked by Bid, a pro-apoptotic

Bcl-2 family member. Caspase-8-dependent cleavage of Bid allows this protein to translocate to the mitochondrion, where it directly or indirectly facilitates cytochrome *c* release.[14–18] The importance of the mitochondrial apoptotic pathway in augmenting death-receptor initiated apoptosis can be assessed by studying the pattern of caspase activation and the effects of Bcl-2 expression. Death receptor-initiated, mitochondrial-dependent apoptosis is generally associated with early low level activation of caspase-8 and is inhibitable by Bcl-2.[19,20] Conversely, mitochondrial-independent, death receptor-initiated apoptosis is associated with more robust caspase-8 activation and is not inhibited by Bcl-2 expression.[19,20]

In this paper we provide the first comprehensive characterization of the pattern of caspase activation following infection with a cytoplasmically replicating RNA virus. We show that reovirus infection results in the activation of death receptor- and mitochondrial-associated initiator caspases, caspase-8 and caspase-9. Activation of these initiator caspases is followed by activation of the effector caspases caspase-3 and caspase-7. Caspase-8-dependent cleavage of the Bid provides a linkage between the death receptor and mitochondrial pathways of apoptosis following reovirus infection. Inhibition of caspase-8 activation prevents the cleavage of Bid, and the subsequent activation of the mitochondrial pathway. Both the mitochondrial and death receptor-initiated pathways are essential for reovirus-induced apoptosis as inhibition of death receptor pathways by over-expression of dominant negative FADD (FADD-DN) or of mitochondrial pathways by over-expression of Bcl-2 prevents reovirus-induced effector caspase activation. Consistent with this model, cell permeable inhibitors of both group II caspases (caspase-2, -3, and -7) and group III caspases (caspase-6, -8, and -9) but not of group I caspases (caspase-1, -4, and -5) inhibit reovirus-induced caspase-3 activation. These studies provide not only a comprehensive profile of caspase activation following virus infection, but also the first demonstration that both death receptor and mitochondrial pathways can play an essential role in virus-induced apoptosis.

Results

Caspase-8 is activated following reovirus infection

Apoptosis initiated via TNF receptor superfamily cell death receptors involves the adaptor molecule FADD and subsequent activation of caspases, starting with the initiator caspase, caspase-8.[21] We therefore wanted to examine whether reovirus infection induced the activation of caspase-8. As shown in Figure 1a, reovirus infection induces the activation of caspase-8 as evidenced by the disappearance of the full-length proenzyme (seen as a 55/54 kD doublet). The reduction in caspase-8 immunoreactivity appeared to be biphasic. A first phase of activation was detectable as early as 8 h post-infection. A second, more intense phase of activation began at 22 h post-infection and continued through $\geqslant$34 h (Figure 1a,b). No cellular morphological changes were observed correlating with the early phase of caspase-8 activation.

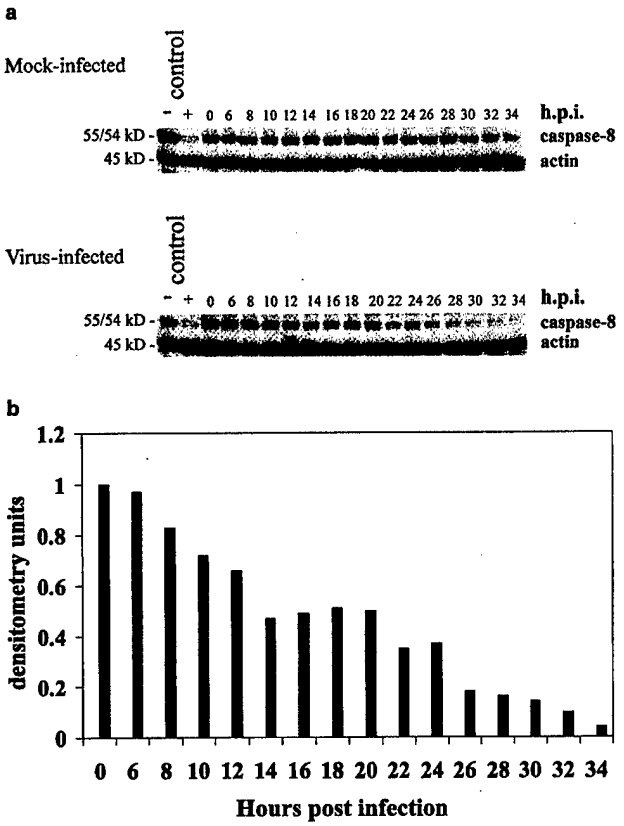

Figure 1 Reovirus infection induces the activation of caspase-8. HEK 293 lysates were prepared at the indicated times points from mock-infected or reovirus-infected cells and probed with anti-caspase-8 antibodies and anti-actin antibodies (**a**). Control lanes represent Jurkat cell lysates untreated (−) or treated (+) with activating anti-Fas antibody and harvested at 8 h post treatment. The Western is representative of two separate experiments. The graph displays densitometric analysis of the virus-infected Western blot analysis (**b**). Values are expressed as arbitrary densitometric units

Reovirus infection is associated with release of mitochondrial cytochrome *c* and activation of caspase-9

Reovirus-induced activation of caspase-8 revealed a biphasic pattern. This suggested that apoptosis signals initiated through the death receptor pathway might be amplified by other apoptotic pathways. We therefore looked for evidence that reovirus infection activated mitochondrial-associated apoptotic signaling pathways. We first wished to determine whether reovirus infection was associated with release of cytochrome *c* and activation of caspase-9. Mitochondria-free lysates were prepared from both mock- and reovirus-infected cells at the indicated time points and analyzed by Western blot for the presence of cytosolic cytochrome *c* (Figure 2). Blots were probed with antisera directed against the mitochondrial integral membrane protein cytochrome *c* oxidase (subunit II) to detect potential mitochondrial contamination of the samples. Cytosolic cytochrome *c* is detected in reovirus-infected cells at ~10 h post-infection (Figure 2a). In order to determine whether cytochrome *c* release was dependent on death receptor-initiated signaling, we also examined the

cellular localization of mitochondrial cytochrome *c* following reovirus infection in FADD-DN expressing cells. As shown in Figure 2b, cytochrome *c* is found at only trace levels in the cytoplasm of reovirus-infected FADD-DN expressing cells. These results indicate that caspase-8 activation occurs upstream of, and is required for, the release of cytochrome *c*. We next wished to determine whether caspase-9 was activated. Activation of caspase-9 involves the cleavage of the 46 kD pro-enzyme into a 37 kD active fragment. Activated caspase-9 was first detectable in reovirus-infected cells at 10 h post-infection (Figure 3), and was not detected in mock-infected cells. Activation increased steadily from 10 to 18 h and then persisted for $\geqslant$32 h.

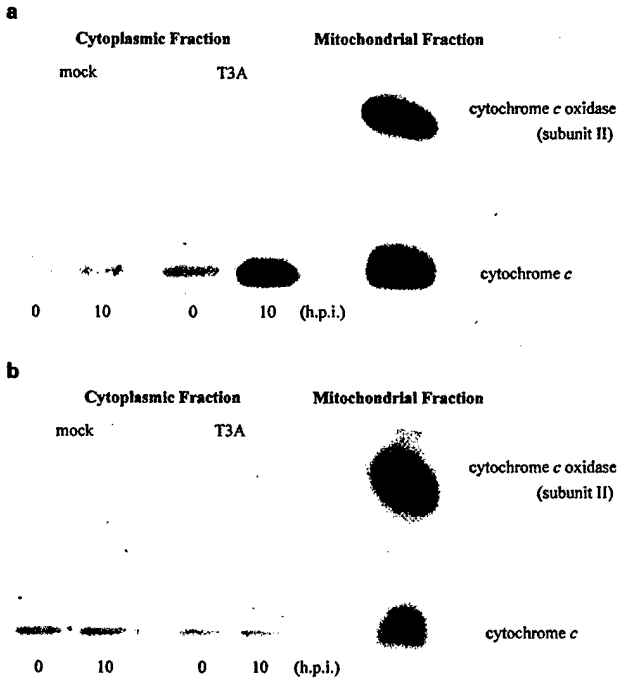

Figure 2 Cytochrome *c* is present in the cytosol of reovirus infected cells. HEK 293 cell lysates (**a**) and FADD-DN expressing HEK 293 cells lysates (**b**) were prepared at the indicated time points as described (see Materials and Methods) and resolved using SDS–PAGE. Western blot analysis was performed using anti-cytochrome *c* antibodies and anti-cytochrome *c* oxidase (subunit II) and are representative of three separate experiments

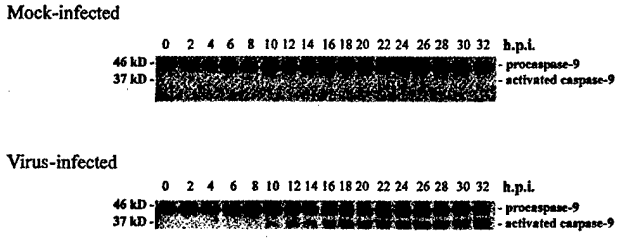

Figure 3 Caspase-9 is activated in reovirus-infected cells. HEK 293 cell lysates were prepared from mock-infected or reovirus-infected cells at the indicated time points and resolved by SDS–PAGE. Western blot analysis was performed using anti-caspase-9 antibodies and the blot is representative of three separate experiments

Bid is cleaved following reovirus infection

Bid is a pro-apoptotic member of the Bcl-2 protein family. Activation of both Fas receptor by Fas and DR4/DR5 by TRAIL can induce caspase-8 dependent cleavage of Bid.[15,17,18] Cleaved Bid can facilitate the release of cytochrome *c* from the mitochondrion and lead to subsequent apoptosome-mediated activation of caspase-9.[16] We wished to determine whether Bid was cleaved following reovirus infection, and if this cleavage depended on caspase-8 activation. Western blot analysis revealed that full-length Bid levels remain relatively unchanged in mock-infected cells (Figure 4a). However, following reovirus infection there was a biphasic pattern of Bid cleavage, analogous to that seen with caspase-8 (Figure 4a). Loss of the full length immunoreactive Bid was first detected as early as 10 h post-infection. A second phase of Bid cleavage began at 26 h post-infection and continued through $\geqslant$40 h (Figure 4a,b). In order to determine whether Bid cleavage was dependent on caspase-8 activation, we examined levels of immunoreactive Bid in cells in which caspase-8 activation was blocked by stable expression of DN-FADD. FADD-DN expression completely inhibited reovirus-induced Bid cleavage, indicating that Bid cleavage is caspase-8 dependent (Figure 4c).

Reovirus infection is associated with activation of caspase-3 and caspase-7

Effector caspases, including caspases-3, -6 and -7, form part of the final common pathway for death receptor and mitochondrial apoptotic pathways. Having shown that reovirus infection resulted in activation of both death receptor and mitochondrion-associated initiator caspases we next wished to determine which effector caspases were activated. Caspase-3 activation was evaluated by Western blot, using an antibody specific for the activated form of the enzyme. Activation of caspase-3 is associated with the appearance of specific cleavage product at ~20 kD representing the large subunit of active caspase-3. As shown in Figure 5a, this fragment appears beginning at ~8 h post-infection in reovirus infected cells, but not in the mock infected controls. There is a biphasic activation profile, with the initial activation phase beginning at 8 h post-infection and a second, more intense activation phase beginning at 24 h post-infection (Figure 5a). A similar pattern of caspase activation was seen in fluorogenic substrate assays using a caspase-3 specific substrate (DEVD-AFC) (see Figure 6c). An initial phase of activation at 6–12 h was followed by a rapid activation peak 12–18 h. Activated caspase-3 cleaves a variety of cellular substrates to induce the morphological hallmarks of apoptosis. We therefore examined the cleavage of PARP. PARP is cleaved by caspase-3 from the full-length 116 kD protein to an 85 kD inactive fragment. As shown in Figure 5b, PARP cleavage exceeding that seen in mock-infected cells was first detectable at 14 h post-infection and persisted until $\geqslant$20 h post-infection. These experiments established that reovirus infection results in activation of the effector caspase, caspase-3 and is associated with cleavage of cellular substrates of caspase-3.

Other effector caspases may also be activated downstream of caspase-8 and caspase-9. Therefore, we

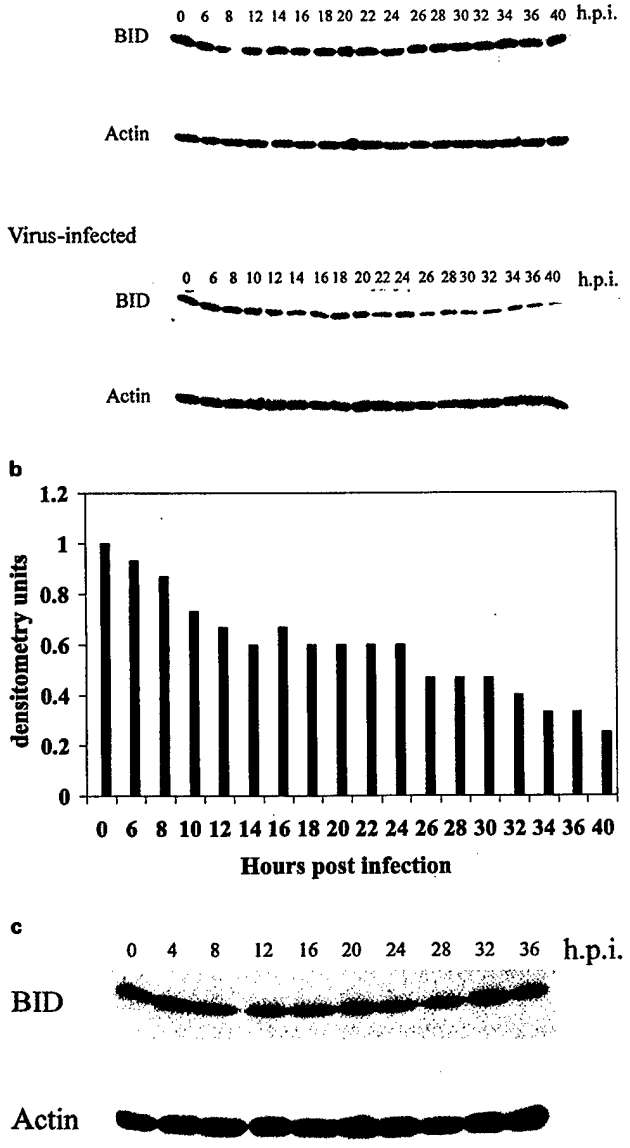

Figure 4 Reovirus infection leads to cleavage of full-length Bid. Lysates were prepared at the indicated time points from mock-infected or reovirus-infected HEK 293 cells (**a**) and reovirus infected FADD-DN expressing HEK 293 cells (**c**) and probed with anti-Bid antibodies and anti-actin antibodies. Each Western blot is representative of two separate experiments. The graph displays densitometric analysis of the virus-infected Western blot analysis (**b**). Values are expressed as arbitrary densitometric units

examined the activation state of two other effector caspases, caspase-6 and caspase-7. We found no evidence by immunoblot of caspase-6 activation in reovirus-infected cells (data not shown). Caspase-7 is activated in infected cells as evidenced by the detection of the 20 kD large subunit of active caspase-7 (Figure 5C). However, caspase-7 activation appears to occur later than activation of caspase-3, and the amount of activation appears less.

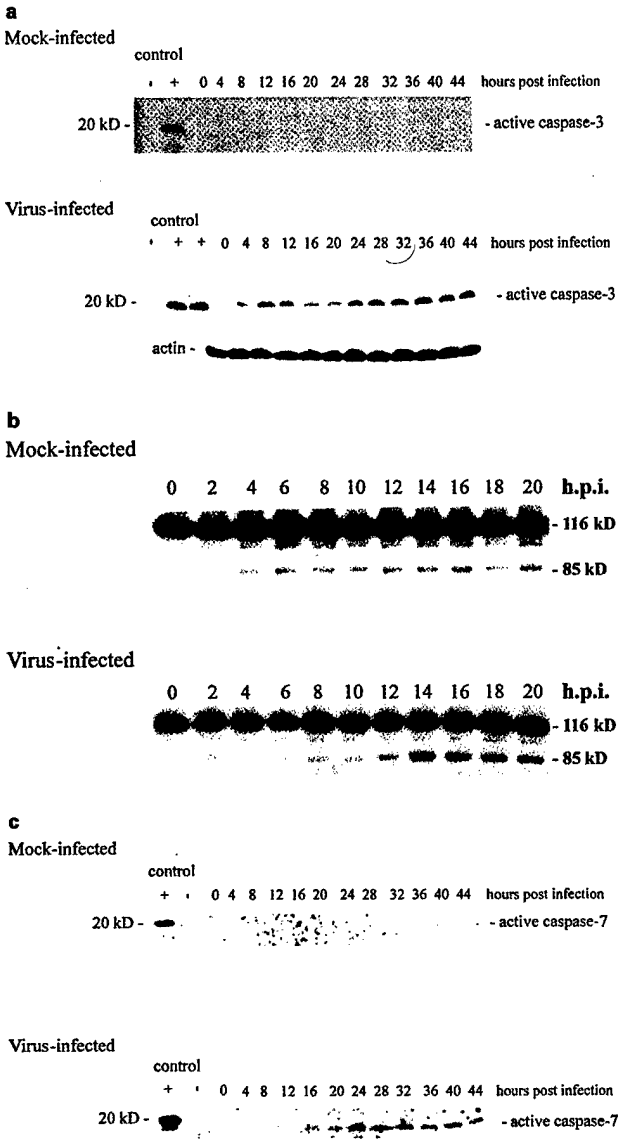

Figure 5 Reovirus infection leads to activation of caspase-3. Western blot analysis was performed using HEK 293 lysates harvested at the indicated time points from mock-infected and reovirus-infected cells and probed with anti-caspase-3 antibodies (**a**), anti-PARP antibodies (**b**), or anti-caspase-7 antibodies (**c**). Control lanes represent Jurkat cell lysates untreated (–) or treated (+) with activating anti-Fas antibody and harvested at 8 h post treatment. Each Western is representative of two separate experiments

In order to determine whether activation of effector caspases was completely dependent on the initial activation of death-receptor mediated pathways, we examined effector caspase activation in cells stably expressing DN-FADD. As shown in Figure 6a, the activation of both caspase-3 and caspase-7 is blocked in cells stably expressing DN-FADD. Caspase-3 activity, as measured in a fluorogenic substrate assay, is almost completely inhibited in these cells (Figure 6c). This suggests that activation of death-receptor initiated apoptotic signaling pathways is required for reovirus-induced effector caspase activation and apoptosis.

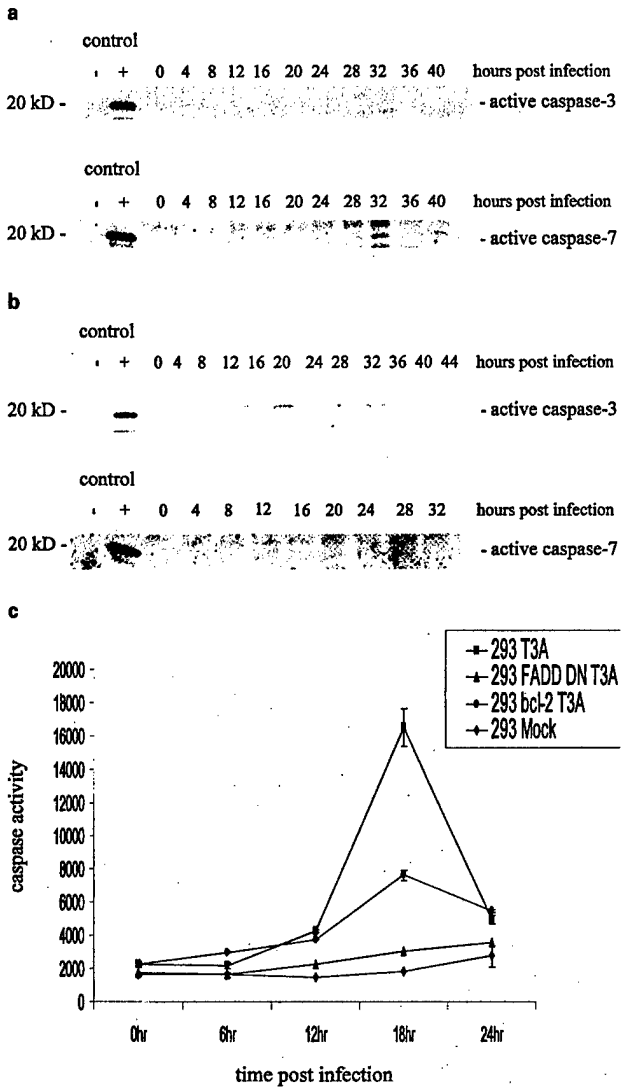

Figure 6 Effector caspase activation in inhibited in FADD-DN and Bcl-2 over-expressing cells. Western blot analysis was performed using cell lysates prepared from reovirus-infected FADD-DN over-expressing cells (**a**) or Bcl-2 overexpressing cells (**b**) at the indicated time points and probed with anti-caspase-3 antibodies and anti-caspase-7 antibodies. Control lanes represent Jurkat cell lysates untreated (−) or treated (+) with activating anti-Fas antibody and harvested at 8 h post treatment. Western blots are representative of two separate experiments. Fluorogenic substrate assays (**c**) were performed in triplicate. Error bars represent standard error of the mean. Fluorescence is expressed as arbitrary units

Bcl-2 overexpression inhibits effector caspase activation following reovirus infection

Experiments with FADD-DN indicated that death-receptor pathways were necessary for reovirus-induced apoptosis. Activation of both caspase-8 and Bid showed a biphasic pattern with an early activation phase at 8–10 h followed by a later activation phase. Reovirus-induced initiation of mitochondrial apoptotic pathways occurred downstream of caspase-8 activation, began slightly later following infection, and was not biphasic. This suggested that mitochondrial apoptotic pathways might play a central role in amplifying death receptor-initiated signaling. The capacity of Bcl-2 to inhibit apoptosis has been used as evidence suggesting an essential role for mitochondrial apoptotic pathways.[19,20] We wished to determine whether Bcl-2 over-expression in HEK cells inhibited caspase activation. Caspase activation was examined using both Western blot analysis and fluorogenic substrate assays. As shown in Figure 6b, activation of both caspase-3 and caspase-7 is inhibited in cells over-expressing Bcl-2. The late phase of caspase-8 activation was also inhibited in these cells although the low level early phase of caspase-8 activation was preserved (data not shown). Caspase-3 activity, as measured in a fluorogenic substrate assay, is also significantly reduced in these cells (Figure 6c). However, the pattern of inhibition differs from that seen in cells stably expressing DN-FADD. In Bcl-2 expressing cells there is some residual caspase-3 activation suggesting that death receptor-mediated apoptotic pathways can induce low levels of effector caspase activation, but full induction requires augmentation by mitochondrial apoptotic pathways. This low level of caspase-3 activation in Bcl-2 overexpressing cells was not reflected in cellular morphology.

Effects of synthetic caspase peptide inhibitors on caspase-3 activation

Caspases can be categorized into three major groups based on their pattern of substrate specificity.[22,23] Group I includes caspase-1, -4, and 5; group II includes caspase-2, -3, and 7; group III includes caspase-6, -8 and -9. Cell permeable, reversible, peptide caspase inhibitors have been developed based on these caspase substrate profiles.[22,23] We tested the capacity of three reversible cell permeable caspase inhibitors with specificity for group I (Ac-YVAD-CHO), group II (Ac-DEVD-CHO), and group III (Ac-IETD-CHO) caspases to inhibit reovirus-induced caspase-3 activation at 18 h post-infection. As shown in Figure 7, the group II inhibitor Ac-DEVD-CHO completely inhibited reovirus-induced caspase-3 activity at a concentration of 10 μM. The group I inhibitor (Ac-YVAD-CHO) had no effect on caspase-3 activation, consistent with a lack of involvement of caspases-1, -4 or -5 in reovirus-induced apoptosis. The group III inhibitor Ac-IETD-CHO achieved maximal inhibition of reovirus-induced caspase-3 activation at a concentration of 5 μM. However, the maximum degree of inhibition (65%) was not as high as that seen with the group II inhibitor. These data suggest that while the activation of group III caspases, including caspase-8 and -9, is critically important to reovirus-induced apoptosis that other as yet unidentified caspases may also contribute to caspase-3 activation. However, the fact that expression of DN-FADD was as effective as treatment with the group II inhibitor Ac-DEVD-CHO in blocking caspase-3 activation, suggests that the apical caspases that contribute to caspase-3 activation all depend on an initial death-receptor initiated caspase activation signal.

Discussion

Understanding the mechanisms of virus-induced apoptosis is crucial to understanding how viruses injure target tissues and

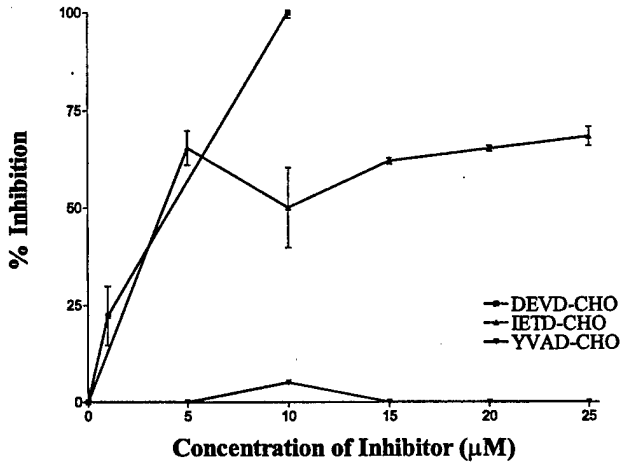

Figure 7 Synthetic peptide inhibition of DEVD-specific caspase activation. HEK 293 cells were pretreated with the synthetic peptide inhibitors at the concentrations shown for 1 h prior to reovirus infection (M.O.I. 100). Fluorogenic substrate assays were performed at 18 h post infection. Values are expressed as per cent inhibition where untreated reovirus-infected cells represent 0% inhibition and mock-infected cells represent 100% inhibition

induce disease. The exact pathways leading to virus-induced apoptosis are still incompletely understood. Since caspases play a central role in virtually all known apoptotic signaling pathways, it is not surprising that they have been implicated in virus-induced apoptosis. Pancaspase peptide inhibitors have been shown to inhibit apoptosis induced by viruses as diverse as Sindbis,[24,25] HIV-1,[26,27] Herpes simplex virus type 1,[28] influenza,[29] Sendai,[30] and TGEV.[31]

The events that initiate caspase activation in virus-infected cells are still incompletely understood. Activation of caspase-8 plays an important role in apoptosis induced by HIV-1,[26] influenza,[29] Sendai,[30] and Sindbis,[24] suggesting that death-receptor initiated processes may be important in apoptosis induced by these viruses.

Many forms of virus-induced apoptosis are inhibited by anti-apoptotic members of the Bcl-2 family.[32–35] One of the most thoroughly investigated mechanisms for the anti-apoptotic actions of Bcl-2 involves its inhibition of the release of cytochrome *c* from mitochondria.[36,37] Abnormalities of mitochondrial transmembrane potential and release of cytochrome *c* have been described following infection with HIV,[38] TGEV,[31] chicken anemia virus,[39] and herpes simplex virus.[28] These studies suggest that both mitochondrial and death-receptor mediated pathways may play an important role in virus-induced apoptosis.

Reovirus-induced apoptosis involves the DR4/DR5/TRAIL system of cell surface death receptors.[7] In this study we found that caspase-8 was activated within 8 h of reovirus infection. The activation of caspase-8 occurs in two distinct phases, consistent with a model in which initial death-receptor mediated activation of caspase-8 is subsequently augmented by activation of caspase-9 or other caspases (discussed below). Following activation, caspase-8 cleaves Bid, a pro-apoptotic Bcl-2 family protein. Cleaved Bid provides an essential link between reovirus-induced death-receptor mediated caspase-8 activation and activation of mitochondrial pathways. Inhibition of caspase-8 activation by over-expression of DN-FADD prevented Bid cleavage, suggesting that reovirus infection also activated the mitochondrial apoptotic pathway. Cytochrome *c* was found to be present in the cytoplasm of infected cells at ~10 h post infection. Additionally, cytochrome *c* release was blocked in FADD-DN expressing cells suggesting that this event requires caspase-8. We also found that caspase-9 is activated at ~12 h post infection.

Having shown that reovirus infection was associated with activation of both death-receptor and mitochondrial-associated initiator caspases, we next wished to determine which effector caspases were subsequently activated. Here we show that the effector caspase, caspase-3 is activated beginning at ~8 h post infection and peaking at ~18 h post infection. Additionally, caspase-7 was activated in reovirus-infected cells, although this event occurs later than caspase-3 activation. Another effector caspase, caspase-6, was not activated in reovirus-infected cells.

There is evidence that although mitochondrial cytochrome *c* release and caspase-9 activation occur downstream of death receptor stimulation, that these events are not necessarily required for all forms of death-receptor initiated apoptosis.[19,20] Therefore we examined the effects of Bcl-2 overexpression on effector caspase activation following reovirus infection. Bcl-2 overexpression inhibits the activation of both caspase-3 and caspase-7, as well as the second phase of caspase-8 activation. This data is consistent with earlier studies suggesting that reovirus-induced apoptosis could be inhibited in MDCK cells over-expressing Bcl-2.[2] This provides conclusive evidence of the importance of the mitochondrial apoptotic pathway in reovirus-induced cell death.

Caspases can be broadly grouped into three categories based on their pattern of substrate specificity.[22,23] A group II caspase inhibitor completely blocked reovirus-induced caspase-3 activity at low concentrations. This result is consistent with the known activation of caspases-3 and -7 in reovirus infection. A group I caspase inhibitor had no effect, even at high concentrations. This suggested that caspases-1, -4 and -5 do not play a significant role in reovirus-induced apoptosis. A group III caspase inhibitor significantly reduced caspase-3 activity, but its effect was only partial when compared to the group II inhibitor. This result was consistent with our observation that caspase-8 and -9 were involved in reovirus-induced caspase-3 activation. The lack of complete inhibition of caspase-3 activation by the group III inhibitor suggests that additional, as yet unidentified, caspases may also contribute to reovirus-induced caspase-3 activation. However, the complete inhibition of caspase-3 activation seen in cells expressing DN-FADD suggests that death receptor activation is the key initiating event in all reovirus-induced caspase activation cascades that ultimately contribute to effector caspase activation.

Our data provides the first comprehensive model of the events leading to apoptosis when cells are infected with a non-enveloped RNA virus whose replication cycle occurs entirely within the cytoplasm (Figure 8). Apoptosis is initiated through cell surface death receptors leading to

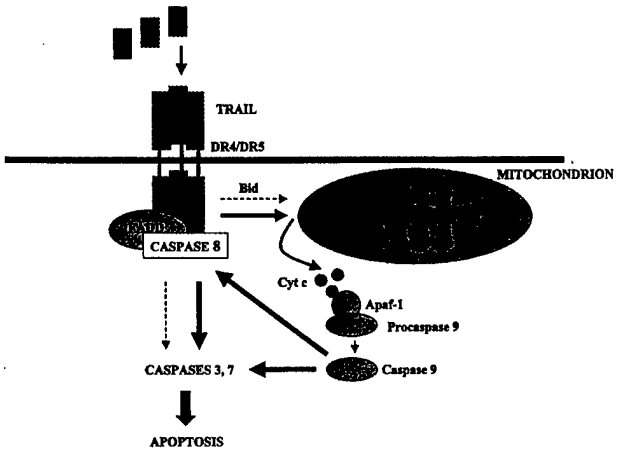

Figure 8 Schematic representation of reovirus-induced apoptosis pathways. Reovirus infection promotes release of cell-associated TRAIL and DR4/DR5-dependent apoptosis. An early phase of caspase-8 activation leads to cleavage of Bid and low level activation of caspase-3 (dashed arrows). This is followed by a second phase of caspase activation in which release of cytochrome *c* activates caspase-9 inducing further caspase-8 activation (solid arrows). Caspase-8 and caspase-9 contribute to effector caspase activation

the activation of caspase-8. Caspase-8 activation is essential for virus-induced apoptosis, and inhibition of this activation in cells stably expressing DN-FADD completely inhibits reovirus-induced effector caspase activation. Caspase-8 activation results in cleavage of Bid and activation of mitochondrial apoptotic pathways. Activation of caspase-8 in the absence of augmentation from the mitochondrial pathway, as occurs in cells stably expressing Bcl-2, results in only low levels of effector caspase activation. These results are consistent with the biphasic pattern of activation of caspase-8, Bid, and caspase-3. Early activation of caspase-8 and Bid induces the mitochondrial pathway which in turn amplifies caspase-8 and Bid activation allowing full expression of apoptosis.

Materials and Methods

Reagents

Anti-cytochrome *c* (7H8.2C12) (1:1000), anti-PARP (C2-10) (1:2000), anti-caspase-6 (B93-4) (1:1000), anti-caspase-8 (B9-2) (1:2000), and anti-caspase-9 (1:1000) antibodies were purchased from Pharmingen (San Diego, CA, USA). Anti-caspase-3 (1:1000) and anti-caspase-7 (1:1000) were purchased from Cell Signaling Technology (Beverly, MA, USA). Anti-Bid antibodies (1:1000) were from Trevigen (Gaithersburg, MD, USA). Anti-actin antibodies (JLA20) (1:5000) were from Calbiochem (Darmstadt, Germany). Anti-human cytochrome *c* oxidase (subunit II) antibodies (12C4-F12) (1:1000) were from Molecular Probes (Eugene, OR, USA). Anti-Fas antibody (CH-11) was from Upstate Biotechnology (Lake Placid, NY, USA). Caspase synthetic peptide inhibitors used were caspase-3 Inhibitor I (cell permeable), caspase-8 Inhibitor I (cell permeable), and caspase-1 Inhibitor I (cell permeable) (Calbiochem, Darmstadt, Germany). ApoAlert caspase-3 fluorometric assay kit was purchased from Clontech (Palo Alto, CA, USA).

Cells, virus, and DNA constructs

HEK293 cells (ATCC CRL1573) were grown in Dulbecco's modified Eagle's medium (DMEM) supplemented with 100 U/ml each of penicillin and streptomycin and containing 10% fetal bovine serum. Jurkat cells were a gift of Dr. John Cohen and were grown in RPMI supplemented with 100 U/ml each of penicillin and streptomycin and containing 10% fetal bovine serum. FADD-DN cells were a gift of Dr. Gary Johnson and express amino acids 80–208 of the FADD cDNA (with the addition of an AU1 epitope tag at the N-terminus) from the CMV promoter of pcDNA3 (Invitrogen, Carlsbad, CA, USA). HEK 293 cells stably over-expressing Bcl-2 were provided by Dr. Gary Johnson. The cell line was constructed by cloning full-length Bcl-2 into the pLXSN vector and transfecting cells via retroviral transduction. Reovirus (Type 3 Abney, T3A) is a laboratory stock, which has been plaque purified and passaged (twice) in L929 cells (ATCC CCL1) to generate working stocks.[40] All experiments were performed using an M.O.I. of 100. High M.O.I.s were chosen to insure synchronized infection of all susceptible cells, and to maximize the apoptotic stimulus.

Western blot analysis

Reovirus-infected cells were harvested at the indicated times, pelleted by centrifugation, washed with ice-cold phosphate-buffered saline, and lysed by sonication in 150 μl of lysis buffer (1% NP40, 0.15 M NaCl, 5.0 mM EDTA, 0.01 M Tris (pH 8.0), 1.0 mM PMSF, 0.02 mg/ml leupeptin, 0.02 mg/ml trypsin inhibitor). Lysates were cleared by centrifugation (20 000 × *g*, 2 min), mixed 1:1 with SDS sample buffer, boiled for 5 min, and stored at −70°C. To prepare mitochondrial-free extracts, cells were pelleted, washed twice in ice-cold PBS, and incubated on ice for 30 min in buffer containing 220 mM mannitol, 68 mM sucrose, 50 mM PIPES-KOH (pH 7.4), 50 mM KCl, 5 mM EGTA, 2 mM $MgCl_2$, 1 mM DTT, and protease inhibitors (complete cocktail, Boehringer Mannheim, Indianapolis, IN, USA). Cells were lysed using 40 strokes in a Dounce homogenizer (B pestle). Lysates were centrifuged at 14 000 × *g* for 15 min at 4°C to remove debris. Supernatants and mitochondrial pellets were prepared for electrophoresis as above. Proteins were separated by SDS–PAGE electrophoresis and transferred to Hybond-c extra nitrocellulose membrane (Amersham, Buckinghamshire, UK) for immunobloting. Blots were then probed with the specified antibodies at the dilutions described above. Proteins were visualized using the ECL detection system (Amersham, Buckinghamshire, UK). Densitometric analysis was performed using a FluorS Multilmager system and Quantity One software (Bio-Rad, Hercules, CA, USA).

Caspase-3 activation assays

Caspase-3 activation assays were performed using a kit obtained from Clontech (Palo Alto, CA, USA). Experiments were performed using 1×10^6 cells/time point. Cells were centrifuged at 200 × *g*, supernatants were removed, and the cell pellets were frozen at −70°C until all the time points were collected. Assays were performed in 96-well plates and analyzed using a fluorescent plate reader (CytoFluor 4000, PerSeptive Biosystems, Framingham, MA, USA). Cleavage of DEVD-AFC, a synthetic caspase-3 substrate, was used to determine caspase-3 activation. Cleavage after the second Asp residue produces free AFC. The amount of fluorescence detected is directly proportional to amount of caspase-3 activity. Because all of the fluorogenic substrate assay experiments were performed at the same time, both the mock and reovirus-induced caspase-3 activation profiles are the same in all of these experiments and are included in each figure to facilitate comparisons. Results of all experiments are reported as means ± S.E.M.

Acknowledgements

This work was supported by Public Health Service grant 1RO1AG14071 from the National Institute of Aging, Merit and REAP grants from the Department of Veterans Affairs, and a US Army Medical Research and Material Command grant (DAMD179818614). Tissue culture media was obtained from the UCHSC Cancer Center Media Core.

References

1. Oberhaus SM, Dermody TS and Tyler KL (1998) Apoptosis and the cytopathic effects of reovirus. Curr. Top. Microbiol. Immunol. 233: 23–49
2. Rodgers SE, Barton ES, Oberhaus SM, Pike B, Gibson CA, Tyler KL and Dermody TS (1997) Reovirus-induced apoptosis of MDCK cells is not linked to viral yield and is blocked by Bcl-2. J. Virol. 71: 2540–2546
3. Tyler KL, Squier MK, Rodgers SE, Schneider BE, Oberhaus SM, Grdina TA, Cohen JJ and Dermody TS (1995) Differences in the capacity of reovirus strains to induce apoptosis are determined by the viral attachment protein sigma 1. J. Virol. 69: 6972–6979
4. Oberhaus SM, Smith RL, Clayton GH, Dermody TS and Tyler KL (1997) Reovirus infection and tissue injury in the mouse central nervous system are associated with apoptosis. J. Virol. 71: 2100–2106
5. DeBiasi RL, Edelstein CL, Sherry and Tyler KL (2001) Calpain inhibition protects against virus-induced apoptotic myocardial injury. J. Virol. 75: 351–361
6. Barton ES, Forrest JC, Connolly JL, Chappell JD, Liu Y, Schnell FJ, Nusrat A, Parkos CA and Dermody TS (2001) Junction adhesion molecule is a receptor for reovirus. Cell 104: 441–451
7. Clarke P, Meintzer SM, Gibson S, Widmann C, Garrington TP, Johnson GL and Tyler KL (2000) Reovirus-induced apoptosis is mediated by TRAIL. J. Virol. 74: 8135–8139
8. Ashkenazi A and Dixit VM (1998) Death receptors: signaling and modulation. Science 281: 1305–1308
9. Li P, Nijhawan D, Budihardjo I, Srinivasula SM, Ahmad M, Alnemri ES and Wang X (1997) Cytochrome c and dATP-dependent formation of Apaf-1/caspase-9 complex initiates an apoptotic protease cascade. Cell 91: 479–489
10. Verhagen AM, Ekert PG, Pakusch M, Silke J, Connolly LM, Reid GE, Moritz RL, Simpson RJ and Vaux DL (2000) Identification of DIABLO, a mammalian protein that promotes apoptosis by binding to and antagonizing IAP proteins. Cell 102: 43–53
11. Du C, Fang M, Li Y, Li L and Wang X (2000) Smac, a mitochondrial protein that promotes cytochrome c-dependent caspase activation by eliminating IAP inhibition. Cell 102: 33–42
12. Joza N, Susin SA, Daugas E, Stanford WL, Cho SK, Li CY, Sasaki T, Elia AJ, Cheng Hy, Ravagnan L, Ferri KF, Zamzami N, Wakeham A, Hakem R, Yoshida H, Kong YY, MakTW, Zuniga-Pflucker JC, Kroemer G and Penninger JM (2001) Essential role of the mitochondrial apoptosis-inducing factor in programmed cell death. Nature 410: 549–554
13. Zou H, Li Y, Liu X and Wang X (1999) An APAF-1-cytochrome c multimeric complex is a functional apoptosome that activates procaspase-9. J. Biol. Chem. 274: 11549–11556
14. Gross A, Yin XM, Wang K, Wei MC, Jockel J, Milliman C, Erdjument-Bromage H, Tempst P and Korsmeyer SJ (1999) Caspase cleaved BID targets mitochondria and is required for cytochrome c release, while BCL-XL prevents this release but not tumor necrosis factor-R1/Fas death. J. Biol. Chem. 274: 1156–1163
15. Li H, Zhu H, Xu CJ and Yuan J (1998) Cleavage of BID by caspase 8 mediates the mitochondrial damage in the Fas pathway of apoptosis. Cell 94: 491–501
16. Luo X, Budihardjo I, Zou H, Slaughter C and Wang X (1998) Bid, a Bcl2 interacting protein, mediates cytochrome c release from mitochondria in response to activation of cell surface death receptors. Cell 94: 481–490
17. Yamada H, Tada-Oikawa S, Uchida A and Kawanishi S (1999) TRAIL causes cleavage of bid by caspase-8 and loss of mitochondrial membrane potential resulting in apoptosis in BJAB cells. Biochem. Biophys. Res. Commun. 265: 130–133
18. Yin XM, Wang K, Gross A, Zhao Y, Zinkel S, Klocke B, Roth KA and Korsmeyer SJ (1999) Bid-deficient mice are resistant to Fas-induced hepatocellular apoptosis. Nature 400: 886–891
19. Scaffidi C, Schmitz I, Zha J, Korsmeyer SJ, Krammer PH and Peter ME (1999) Differential modulation of apoptosis sensitivity in CD95 type I and type II cells. J. Biol. Chem. 274: 22532–22538
20. Scaffidi C, Fulda S, Srinivasan A, Friesen C, Li F, Tomaselli K,J Debatin KM, Krammer PH and Peter ME (1998) Two CD95 (APO-1/Fas) signaling pathways. EMBO J. 17: 1675–1687
21. Hu S, Vincenz C, Ni J, Gentz R and Dixit VM (1997) I-FLICE, a novel inhibitor of tumor necrosis factor receptor-1- and CD- 95-induced apoptosis. J. Biol. Chem. 272: 17255–17257
22. Thornberry NA, Rano TA, Peterson EP, Rasper DM, Timkey T, Garcia-Calvo M, Houtzager VM, Nordstrom PA, Roy S, Vaillancourt JP, Chapman KT and Nicholson DW (1997) A combinatorial approach defines specificities of members of the caspase family and granzyme B. Functional relationships established for key mediators of apoptosis. J. Biol. Chem. 272: 17907–17911
23. Talanian RV, Quinlan C, Trautz S, Hackett MC, Mankovich JA, Banach D, Ghayur T, Brady KD and Wong WW (1997) Substrate specificities of caspase family proteases. J. Biol. Chem. 272: 9677–9682
24. Nava VE, Rosen A, Veliuona MA, Clem RJ, Levine B and Hardwick JM (1998) Sindbis virus induces apoptosis through a caspase-dependent, CrmA- sensitive pathway. J. Virol. 72: 452–459
25. Jan JT, Chatterjee S and Griffin DE (2000) Sindbis virus entry into cells triggers apoptosis by activating sphingomyelinase, leading to the release of ceramide. J. Virol. 74: 6425–6432
26. Stewart SA, Poon B, Song JY and Chen IS (2000) Human immunodeficiency virus type 1 vpr induces apoptosis through caspase activation. J. Virol. 74: 3105–3111
27. Biard-Piechaczyk M, Robert-Hebmann V, Richard V, Roland J, Hipskind RA and Devaux C (2000) Caspase-dependent apoptosis of cells expressing the chemokine receptor CXCR4 is induced by cell membrane-associated human immunodeficiency virus type 1 envelope glycoprotein (gp120). Virology 268: 329–344
28. Galvan V, Brandimarti R, Munger J and Roizman B (2000) Bcl-2 blocks a caspase-dependent pathway of apoptosis activated by herpes simplex virus 1 infection in HEp-2 cells. J. Virol. 74: 1931–1938
29. Takizawa T, Tatematsu C, Ohashi K and Nakanishi Y (1999) Recruitment of apoptotic cysteine proteases (caspases) in influenza virus-induced cell death. Microbiol. Immunol. 43: 245–252
30. Bitzer M, Prinz F, Bauer M, Spiegel M, Neubert WJ, Gregor M, Schulze-Osthoff K and Lauer U (1999) Sendai virus infection induces apoptosis through activation of caspase- 8 (FLICE) and caspase-3 (CPP32). J. Virol. 73: 702—708
31. Eleouet JF, Chilmonczyk S, Besnardeau L and Laude H (1998) Transmissible gastroenteritis coronavirus induces programmed cell death in infected cells through a caspase-dependent pathway. J. Virol. 72: 4918–4924
32. O'Brien V (1998) Viruses and apoptosis. J. Gen. Virol. 79: 1833–1845
33. Razvi ES, Welsh RM (1995) Apoptosis in viral infections. Adv. Virus Res. 45: 1–60
34. Teodoro JG and Branton PE (1997) Regulation of apoptosis by viral gene products. J. Virol. 71: 1739–1746
35. Shen Y and Shenk TE (1995) Viruses and apoptosis. Curr. Opin. Genet. Dev. 5: 105–111
36. Adams JM and Cory S (1998) The Bcl-2 protein family: arbiters of cell survival. Science 281: 1322–1326
37. Reed JC (1998) Bcl-2 family proteins. Oncogene 17: 3225–3236
38. Ferri KF, Jacotot E, Blanco J, Este JA, Zamzami N, Susin SA, Xie Z, Brothers G, Reed JC, Penninger JM and Kroemer G (2000) Apoptosis control in syncytia induced by the HIV type 1-envelope glycoprotein complex: role of mitochondria and caspases. J. Exp. Med. 192: 1081–1092
39. Danen-van Oorschot AA, Der Eb AJ and Noteborn MH (2000) The chicken anemia virus-derived protein apoptin requires activation of caspases for induction of apoptosis in human tumor cells. J. Virol. 74: 7072–7078
40. Tyler KL, Squier MK, Brown AL, Pike B, Willis D, Oberhaus SM, Dermody TS and Cohen JJ (1996) Linkage between reovirus-induced apoptosis and inhibition of cellular DNA synthesis: role of the S1 and M2 genes. J. Virol. 70: 7984–7991

ELSEVIER

Journal of Clinical Virology 25 (2002) S5–S11

JOURNAL OF CLINICAL VIROLOGY

www.elsevier.com/locate/jcv

Use of PCR for the diagnosis of herpesvirus infections of the central nervous system

Roberta L. DeBiasi [a,b,*], B.K. Kleinschmidt-DeMasters [b,c], Adriana Weinberg [a,f,g], Kenneth L. Tyler [b,d,e,f]

[a] *Department of Pediatrics, University of Colorado Health Sciences Center, 4200 East Ninth Avenue, Denver, CO 80262, USA*
[b] *Department of Neurology, University of Colorado Health Sciences Center and The Denver Veterans Administration Hospital, 4200 East Ninth Avenue, Denver, CO 80262, USA*
[c] *Department of Pathology, University of Colorado Health Sciences Center, 4200 East Ninth Avenue, Denver, CO 80262, USA*
[d] *Department of Microbiology, University of Colorado Health Sciences Center, 4200 East Ninth Avenue, Denver, CO 80262, USA*
[e] *Department of Immunology, University of Colorado Health Sciences Center, 4200 East Ninth Avenue, Denver, CO 80262, USA*
[f] *Department of Medicine, University of Colorado Health Sciences Center, 4200 East Ninth Avenue, Denver, CO 80262, USA*
[g] *The Clinical Virology Laboratory, University of Colorado Health Sciences Center, 4200 East Ninth Avenue, Denver, CO 80262, USA*

Abstract

Polymerase chain reaction (PCR) analysis of cerebrospinal fluid (CSF) has revolutionized the diagnosis of nervous system viral infections, particularly those caused by human herpesviruses (HHV). The PCR technique allows the detection of minute quantities of DNA or RNA in body fluids and tissues. Both fresh-frozen and formalin-fixed tissues may be utilized for PCR assays, with the latter making archival studies possible. CSF PCR has now replaced brain biopsy as the gold standard for the diagnosis of herpes simplex virus (HSV) encephalitis. PCR analysis of both CSF and nervous system tissues has also broadened our understanding of the spectrum of disease caused by HSV-1 and -2, cytomegalovirus (CMV), Epstein–Barr virus (EBV), varicella zoster virus (VZV) and HHV-6. PCR results obtained from tissue specimens must be interpreted cautiously, since this highly sensitive technique may detect portions of viral genomic material that may be present even in the absence of active viral infection. Tissue PCR results in particular must be corroborated with clinical and neuropathologic evidence of central nervous system (CNS) infection. In several neurological diseases, negative PCR results have provided evidence against a role for herpesviruses as the causative agents. This review summarizes the role of CSF PCR in the diagnosis and therapeutic management of herpesvirus infections of the nervous system, particularly those caused by HSV and VZV.

Keywords: Polymerase chain reaction; Viral infections; Nervous system; Cerebrospinal fluid; Herpes simplex virus; Varicella zoster virus; Cytomegalovirus; Epstein–Barr virus

* Corresponding author. Tel.: +1-303-393-4684; fax: +1-303-393-5271
E-mail address: roberta.debiasi@uchsc.edu (R.L. DeBiasi).

1386-6532/02/$ - see front matter
PII: S1386-6532(02)00028-8

1. Polymerase chain reaction (PCR): background and technical issues

PCR can be applied to the diagnosis of any disease in which nucleic acid (e.g. DNA, RNA) or their expression as messenger RNA (mRNA) plays a role. PCR techniques allow the in vitro synthesis of millions of copies of a specific gene segment of interest, allowing the rapid detection of as few as one to 10 copies of the target DNA from the original sample. The widespread availability of an in-house test in most hospitals, or ready access to a reference laboratory has led to the incorporation of PCR testing on cerebrospinal fluid (CSF) and body fluids into medical practice in the United States and other developed countries.

In infectious diseases, PCR is ideally suited for identifying fastidious organisms that may be difficult or impossible to culture (DeBiasi and Tyler, 1999). The technique can be performed rapidly and inexpensively, with a turnaround time of 24 h or less rather than the standard minimum of 1–28 days required for viral culture. Unlike the traditional culture methods that may yield negative results after patient receives even small doses of antiviral drugs, CSF PCR retains its sensitivity after short courses of antiviral therapy or passive immunization. This allows the prompt initiation of empiric therapy when a patient first presents with suspected meningitis or encephalitis, without potentially compromising definitive diagnostic tests. PCR is also preferable to serological testing, which often requires 2–4 weeks after acute infection for the development of a diagnostic rise in antibody titers, and is of limited value for viruses with high basal seroprevalence rates. In contrast to serologic testing, CSF PCR yields positive results during acute infection, when the amount of replicating virus is maximal. Finally, CSF PCR is substantially less invasive than brain biopsy, which was previously the gold standard for the diagnosis of many central nervous system (CNS) herpesvirus infections.

The exquisite sensitivity of PCR is both its greatest virtue and greatest potential limitation. A positive CSF PCR result indicates the presence of viral nucleic acid and is, in general, a marker of recent or ongoing active CNS viral infection by that particular pathogen, especially in an immunocompetent individual (Tyler, 1994). False-positive CSF PCR results, in which a positive result does not indicate active CSF infection, can occur due to inadvertent contamination of specimens or failure to properly confirm the specificity of the amplified product. It is theoretically possible that positive CSF PCR results in patients with systemic disease and traumatic lumbar punctures or breakdown of the blood–brain barrier may reflect their systemic infection rather than CNS disease, although data on this point are lacking.

Replicating virus and viral DNA do not persist indefinitely, so that the CSF PCR test becomes negative over time, especially in immunocompetent patients (Haanpaa et al., 1998). While most CSF testing in the clinical setting of suspected meningitis or meningoencephalomyelitis is performed within 1–2 days following the onset of neurological symptoms, positive test results can persist for 2–4 weeks after the onset of clinical disease depending on the virus and the treatment initiated (Weber et al., 1996). False-negative tests can occur if PCR inhibitors are present in CSF. However, modest CSF xanthochromia, high protein levels, or high white blood cell counts do not generally have a negative impact on CSF PCR testing.

CSF PCR testing may be performed on fresh or frozen samples. Refrigeration for a few hours or even days does not appear to significantly reduce the yield of the test (Weinberg, personal communication). However, viral DNA is relatively more stable than RNA in archived samples. The exquisite sensitivity of the technique allows the use of small volumes of CSF for analysis (i.e. 30 μl), although laboratories generally request at least 0.5 ml.

Quantitative PCR by several techniques is increasingly being applied to clinical samples. One technique involves the use of internal oligonucleotides—labeled at one end with a fluorescent dye and at the other end with a quencher dye—along with the PCR primers during amplification. Fluorescence emitted during PCR is measured and directly correlated to the number of copies of the target nucleic acid in the original sample. Several

studies have suggested that nucleic acid copy number ("viral load") may be a marker for the severity of disease or may help predict the outcome, although it remains to be determined whether this is true for all herpesvirus infections (Domingues et al., 1998).

2. Our clinical virology laboratory's experience

The UCHSC clinical virology laboratory performs CSF PCR for herpesviruses (herpes simplex virus, HSV; Epstein–Barr virus, EBV; cytomegalovirus, CMV; and varicella zoster virus, VZV) three times a week, which makes clinically useful data rapidly available for the management of patients with presumed diagnoses of herpesvirus encephalitis, and reduces unnecessary therapeutic interventions. Upon receipt of CSF specimens are stored at −70 °C in 30 μl aliquots. DNA is extracted from each aliquot with InstaGene purification matrix (Boehringer Mannheim, Mannheim, Germany). Amplification is carried out in 50 μl mixtures containing 20 μl of extracted DNA, 1.25 U of PfuI (Stratagene LaJolla, California, USA), 100 μM of each four deoxynucleoside triphosphates, and 1 μM of each primer in PfuI buffer (Stratagene). Samples are amplified in duplicate for 45 cycles. Amplified DNAs are separated according to molecular weight using agarose gel electrophoresis and transferred to nylon membranes. The identity of the DNA bands is confirmed by hybridization with a digoxigenin-labeled probe (Boehringer Mannheim), followed by an anti-digoxigenin antibody conjugated to alkaline phosphatase and CSPD® chemiluminescent substrate (Tropix, Bedford, MA, USA). Each assay includes a negative water control and two positive sensitivity controls. Tests are considered valid if controls yield the expected results and if patient replicates agree.

Our HSV PCR detects ≥ 2 genomic equivalents per reaction. Upon review of 2214 CSF specimens received at our institution for HSV PCR analysis between 1997 and 2001, 79 specimens (3.6%) yielded positive results. The prevalence of other herpesviruses based on the review of all herpesvirus PCRs performed at our institution is as follows: EBV 7.4% (39/528 samples between 1995 and 2001), VZV 3.9% (22/569 samples between 1998 and 2002), and CMV 2.3% (11/483 samples between 1999 and 2002).

3. Use of PCR for the diagnosis of specific CNS herpesvirus infections

CSF PCR testing has played a critical role in establishing the frequency and distribution of herpesvirus infections in immunocompetent populations. Detection of HSV-1, HSV-2, CMV, and VZV DNA correlates strongly with specific clinical syndromes of encephalitis/myelitis and meningitis. Occasional immunocompetent or immunocompromised patients have more than one herpesvirus detected in CSF by PCR, and EBV has been the most frequent agent associated with a dual positive result. In a large series of 662 patients, mostly immunocompetent, detection of human herpesviruses (HHV)-6 and EBV by CSF PCR did not correlate clinically in several individuals with the presence of a CNS infection known to be caused by that virus (Studahl et al., 2000). Similarly, in a large study of immunocompromised (HIV-infected) individuals, conducted to assess the diagnostic reliability of CSF PCR by comparison with biopsy or autopsy diagnoses, the most frequent false-positive herpesvirus detected was HHV-6 (Cinque et al., 1996). Additional large studies are necessary to determine the extent of false-positive PCR results for herpesviruses, especially with regard to HHV-6 and EBV in immunocompromised hosts.

3.1. HSV

3.1.1. HSV-1

Despite the high prevalence of seropositivity to HSV in the general population and the fact that the virus becomes latent in dorsal root ganglia of most humans, HSV DNA is not detected in CSF of HSV-seropositive individuals who are neurologically normal or who have other types of non-HSV CNS infections (Tyler, 1994). The sensitivity and specificity of CSF PCR exceeds 95% for HSV encephalitis (Lakeman and Whitley, 1995), and as

a result, CSF PCR has replaced brain biopsy as the diagnostic test of choice for HSV encephalitis. The high sensitivity and specificity of CSF PCR means that in patients with a low pre-test probability of HSV encephalitis an appropriately performed negative test essentially excludes the diagnosis. Conversely, in patients with a high pre-test probability of HSV encephalitis, a negative test, although dramatically decreasing the likelihood of HSV encephalitis, does not entirely exclude it. A positive CSF PCR for HSV in the appropriate clinical setting is initially diagnostic of HSV encephalitis (Tebas et al., 1998) The use of HSV CSF PCR has also led to the identification of mild or atypical forms of encephalitis that were formerly attributed to other viruses, often in the absence of brain biopsy (Domingues et al., 1997) and that may account for 17% of total cases of HSV encephalitis (Fodor et al., 1998). CSF PCR has established the diagnosis and role of HSV-1 in brainstem encephalitis (Tyler et al., 1995), myelitis (Studahl et al., 2000), multifocal or diffuse encephalitis without temporal lobe involvement in children (Schlesinger et al., 1995a), and neonatal encephalitis. In children, symptoms of HSV encephalitis may recur after antiviral therapy. These "relapses" have been attributed both to residual active infection and post-infectious immune-mediated processes. CSF PCR may help distinguish between these possibilities (Ito et al., 2000). Quantitative CSF PCR in cases of pediatric HSV encephalitis is currently being studied as a method for monitoring response to antiviral drugs (Ando et al., 1993).

3.1.2. HSV-2

CSF PCR has helped clinicians to recognize that HSV-2 may cause aseptic meningitis even in the absence of genital herpetic lesions (Schlesinger et al., 1995b), and established HSV-2 as the most common cause of benign recurrent lymphocytic meningitis, including many cases previously diagnosed as Mollaret's meningitis (Tedder et al., 1994). CSF viral cultures are typically negative during recurrent episodes of HSV-2 meningitis. However, CSF PCR is positive in patients with recurrent episodes of HSV-2 meningitis. CSF PCR has illustrated that immunocompetent adults may develop HSV-2-induced meningoencephalitis and meningitis (Studahl et al., 2000), as well as rare cases of HSV-2 brainstem encephalitis and recurrent thoracic myelitis.

3.2. VZV

CSF PCR for VZV has considerably broadened the understanding of the neurologic complications due to VZV infection. VZV infection can involve virtually every part of the central and peripheral nervous system (Kleinschmidt-DeMasters and Gilden, 2001). The combination of serological studies and CSF PCR for VZV has been particularly helpful in identifying cases of VZV CNS infections without associated rash (*sine herpete*) (Bergstrom, 1996). Since the virus can only rarely be cultured from CSF, the diagnosis of meningitis or meningoencephalitis previously depended on the presence of a characteristic vesicular erythematous rash before, during, or after CNS infection, and VZV-mediated neurologic diseases were under-recognized. CSF PCR for VZV has shown that aseptic meningitis and brainstem encephalitis due to this virus may occur in immunocompetent hosts (Haanpaa et al., 1998; Studahl et al., 2000). In HIV-infected patients, CSF PCR for VZV DNA may have utility in monitoring therapeutic response and in predicting the outcome of VZV meningoencephalitis. For example, in a series of 516 HIV-infected patients, PCR became negative in patients treated with antivirals whose clinical conditions improved, but remained positive despite appropriate therapy in several patients who subsequently died (Cinque et al., 1997). In addition, patients with detectable CSF VZV DNA, which was considered an indicator of subclinical reactivation of VZV antecedent to clinical disease, who were treated with antiviral agents, had improved outcome. Monitoring of CSF PCR allowed for the effective use of prophylactic therapy in this patient population.

PCR on both CSF and fluid from auricular vesicles has confirmed that VZV causes Ramsay Hunt syndrome, the second most common cause of seventh nerve facial paralysis after Bell's palsy (Murakami et al., 1998). Ramsay Hunt syndrome can be difficult to recognize since the rash is

hidden in the ear or mouth, and the rash may be delayed, particularly in pediatric patients. PCR on endoneurial fluids and posterior auricular muscle samples collected during decompressive facial nerve surgery for Bell's palsy identified HSV-1 DNA in 79% of patients and confirmed that neither EBV or VZV is an important cause of idiopathic Bell's palsy. A subsequent study using PCR identified a subset of patients with acute peripheral facial palsy that has zoster *sine herpete* (Furuta et al., 2000). VZV was responsible for a significant percentage of the total number of cases of facial palsy (29%), and an even higher percentage of reactivations (88%) in HSV-seronegative patients. Hence, PCR has verified a role for herpesviruses in both of the common causes of facial nerve paralysis and has distinguished which virus is causative in clinically confusing cases.

PCR testing on fresh, frozen, or archival-fixed and paraffin-embedded CNS tissues has allowed the detection of VZV nucleic acid, even from small or imperfectly preserved specimens. Tissue PCR of cerebral arteries has established a direct role for VZV in cases of large-vessel and small-vessel vasculopathy (Melanson et al., 1996). In a patient with waxing and waning VZV vasculitis, the detection of VZV DNA by PCR led to the discovery that VZV antigen was also present, indicating a productive infection in blood vessels as the cause of the disease. Brain tissues may be positive for VZV DNA by PCR even when the virus is no longer detectable by other methods, such as light microscopy for viral inclusions, immunohistochemistry, or in situ hybridization.

3.3. EBV

CSF PCR testing has been found to be nearly 100% sensitive as a tumor marker for EBV-related CNS lymphoma, and has changed the way in which clinicians diagnose CNS lymphoma in immunocompromised individuals (Landgren et al., 1994). In a study of AIDS patients with CNS mass lesions, a positive EBV CSF PCR correctly identified all 17 CNS lymphoma cases and was positive in only one of 68 AIDS patients with non-CNS lymphoma mass lesions (Cinque et al., 1996). CSF PCR for EBV is also positive during the acute phase of the illness in children with infectious mononucleosis and neurological complications such as transverse myelitis, meningoencephalitis, and aseptic meningitis (Weber et al., 1996). CSF PCR is not positive in EBV-seropositive individuals in the absence of CNS infection. However, positive EBV PCR may be seen in patients with evidence of other viral or non-viral CNS infection, raising the possibility that these infections may trigger viral reactivation. Studies are currently in progress to determine whether quantitative PCR will be useful for distinguishing different types of EBV CNS infections or for identifying the causative agent in cases in which there is evidence for dual infection with EBV and another pathogen (Weinberg et al., in press).

3.4. CMV

CSF PCR is a useful technique for detecting CMV CNS infections in immunodeficient hosts, with a reported sensitivity of 82% and specificity of 99% in AIDS patients (Cinque et al., 1995). The clinical utility of the test in the setting of congenital CMV infection is being investigated, particularly with respect to correlating neurologic outcome with CSF viral load (Whitley, personal communication). CMV viral load has also been monitored in peripheral blood leukocytes as a method to predict which immunosuppressed patients might develop end-organ disease.

3.5. HHV-6, HHV-7 and HHV-8

CSF PCR testing has corroborated the role of HHV-6 in febrile seizures, meningitis, encephalitis, and encephalopathy in immunocompetent and immunocompromised individuals (Yoshikawa and Asano, 2000). HHV-6 genome has been demonstrated in CSF from up to 57% of children younger than 1 year of age who have febrile seizures and has also been seen in children with recurrent febrile convulsions. The role of HHV-7 in neurological disease is unclear, although the detection of HHV-7 DNA in CSF and serum of children with exanthem subitum and encephalopathy has been reported (Torigoe et al., 1996). Encephalitis in immunocompromised individuals

associated with HHV-8 has been described, but this awaits additional confirmation. HHV-8 DNA has been detected in primary CNS lymphomas in some studies but not others. In the study in which HHV-8 was detected, the virus was surmised to play an indirect role in the development of primary CNS lymphoma, and was thought be present in the adjacent non-neoplastic lymphocytes but not the lymphoma cells (Corboy et al., 1998).

4. Use of tissue PCR to exclude herpesvirus as etiologic agents of nervous system disease

Given the protean manifestations of herpesvirus-mediated infections of the central and peripheral nervous system, efforts have been made to detect these viruses by PCR on tissues from several disease entities characterized by arteritis and/or inflammation. PCR testing of various tissue specimens has made it unlikely that VZV plays an etiologic role in giant cell arteritis and has provided no evidence that VZV, CMV, EBV, or HSV play a role in childhood multifocal encephalomalacia. Negative PCR results have also made it unlikely that HSV plays a causative role in Meniere's disease. A survey of a variety of peripheral nerve diseases, including inflammatory peripheral neuropathies, revealed no HSV DNA by PCR in peripheral nerves, making it unlikely that HSV plays a significant role in these disorders (Kleinschmidt-DeMasters et al., 2001).

The significance of the detection of HSV in CNS tissues is uncertain. HSV viral genome was first detected in human brain tissue using nucleic acid hybridization techniques in 1979 and 1981. Since then, PCR has confirmed the presence of HSV DNA in brainstem, olfactory bulbs and limbic areas of individuals without CNS disease (Baringer and Pisani, 1994). Since HSV has never been isolated by culture from normal human brain tissue, the presence of the viral genome, as detected by PCR, is of uncertain significance. Further studies are needed to determine whether the entire viral genome is present, and if so, if this represents latent virus or virus potentially capable of reactivation. Positive PCR results may instead represent the presence of random viral sequences or fragments of virus in neurons or other CNS cells. Tissue PCR remains a research technique that requires further study prior to its potential use as a clinical diagnostic method.

Acknowledgements

Research support has been provided by the Reuler–Lewin Family Professorship of Neurology and the US Army (Medical Research Grant DAMD 17-98-1-8614). We thank Erich Schmidt for his assistance in compiling data from the UCHSC Clinical Virology Laboratory databases.

References

Ando Y, Kimura H, Miwata H, Kudo T, Shibata M, Morishima T. Quantitative analysis of herpes simplex virus DNA in cerebrospinal fluid of children with herpes simplex encephalitis. J Med Virol 1993;41:170–3.

Baringer JR, Pisani P. Herpes simplex virus genomes in human nervous system tissue analyzed by polymerase chain reaction. Ann Neurol 1994;36:823–9.

Bergstrom T. Polymerase chain reaction for diagnosis of varicella zoster virus central nervous system infections without skin manifestations. Scand J Infect Dis Suppl 1996;100:41–5.

Cinque P, Baldanti F, Vago L, Terreni MR, Lillo F, Furione M, Castagna A, Monforte AD, Lazzarin A, Linde A. Ganciclovir therapy for cytomegalovirus (CMV) infection of the central nervous system in AIDS patients: monitoring by CMV DNA detection in cerebrospinal fluid. J Infect Dis 1995;171:1603–6.

Cinque P, Bossolasco S, Vago L, Fornara C, Lipari S, Racca S, Lazzarin A, Linde A. Varicella-zoster virus (VZV) DNA in cerebrospinal fluid of patients infected with human immunodeficiency virus: VZV disease of the central nervous system or subclinical reactivation of VZV infection? Clin Infect Dis 1997;25:634–9.

Cinque P, Vago L, Dahl H, Brytting M, Terreni MR, Fornara C, Racca S, Castagna A, Monforte AD, Wahren B, Lazzarin A, Linde A. Polymerase chain reaction on cerebrospinal fluid for diagnosis of virus-associated opportunistic diseases of the central nervous system in HIV-infected patients. AIDS 1996;10:951–8.

Corboy JR, Garl PJ, Kleinschmidt-DeMasters BK. Human herpesvirus 8 DNA in CNS lymphomas from patients with and without AIDS. Neurology 1998;50:335–40.

DeBiasi RL, Tyler KL. Polymerase chain reaction in the diagnosis and management of central nervous system infections. Arch Neurol 1999;56:1215–9.

Domingues RB, Lakeman FD, Mayo MS, Whitley RJ. Application of competitive PCR to cerebrospinal fluid samples from patients with herpes simplex encephalitis. J Clin Microbiol 1998;36:2229–34.

Domingues RB, Tsanaclis AM, Pannuti CS, Mayo MS, Lakeman FD. Evaluation of the range of clinical presentations of herpes simplex encephalitis by using polymerase chain reaction assay of cerebrospinal fluid samples. Clin Infect Dis 1997;25:86–91.

Fodor PA, Levin MJ, Weinberg A, Sandberg E, Sylman J, Tyler KL. Atypical herpes simplex virus encephalitis diagnosed by PCR amplification of viral DNA from CSF. Neurology 1998;51:554–9.

Furuta Y, Ohtani F, Kawabata H, Fukuda S, Bergstrom T. High prevalence of varicella-zoster virus reactivation in herpes simplex virus-seronegative patients with acute peripheral facial palsy. Clin Infect Dis 2000;30:529–33.

Haanpaa M, Dastidar P, Weinberg A, Levin M, Miettinen A, Lapinlampi A, Laippala P, Nurmikko T. CSF and MRI findings in patients with acute herpes zoster. Neurology 1998;51:1405–11.

Ito Y, Kimura H, Yabuta Y, Ando Y, Murakami T, Shiomi M, Morishima T. Exacerbation of herpes simplex encephalitis after successful treatment with acyclovir. Clin Infect Dis 2000;30:185–7.

Kleinschmidt-DeMasters BK, Gilden DH. Varicella-zoster virus infections of the nervous system: clinical and pathologic correlates. Arch Pathol Lab Med 2001;125:770–80.

Kleinschmidt-DeMasters BK, DeBiasi RL, Tyler KL. Polymerase chain reaction as a diagnostic adjunct in herpesvirus infections of the nervous system. Brain Pathol 2001;11:452–64.

Lakeman FD, Whitley RJ. Diagnosis of herpes simplex encephalitis: application of polymerase chain reaction to cerebrospinal fluid from brain-biopsied patients and correlation with disease. National Institute of Allergy and Infectious Diseases Collaborative Antiviral Study Group. J Infect Dis 1995;171:857–63.

Landgren M, Kyllerman M, Bergstrom T, Dotevall L, Ljungstrom L, Ricksten A. Diagnosis of Epstein–Barr virus-induced central nervous system infections by DNA amplification from cerebrospinal fluid. Ann Neurol 1994;35:631–5.

Melanson M, Chalk C, Georgevich L, Fett K, Lapierre Y, Duong H, Richardson J, Marineau C, Rouleau GA. Varicella-zoster virus DNA in CSF and arteries in delayed contralateral hemiplegia: evidence for viral invasion of cerebral arteries. Neurology 1996;47:569–70.

Murakami S, Nakashiro Y, Mizobuchi M, Hato N, Honda N, Gyo K. Varicella-zoster virus distribution in Ramsay Hunt syndrome revealed by polymerase chain reaction. Acta Otolaryngol 1998;118:145–9.

Schlesinger Y, Buller RS, Brunstrom JE, Moran CJ, Storch GA. Expanded spectrum of herpes simplex encephalitis in childhood. J Pediatr 1995a;126:234–41.

Schlesinger Y, Tebas P, Gaudreault-Keener M, Buller RS, Storch GA. Herpes simplex virus type 2 meningitis in the absence of genital lesions: improved recognition with use of the polymerase chain reaction. Clin Infect Dis 1995b;20:842–8.

Studahl M, Hagberg L, Rekabdar E, Bergstrom T. Herpesvirus DNA detection in cerebral spinal fluid: differences in clinical presentation between alpha-, beta-, and gamma-herpesviruses. Scand J Infect Dis 2000;32:237–48.

Tebas P, Nease RF, Storch GA. Use of the polymerase chain reaction in the diagnosis of herpes simplex encephalitis: A decision analysis model. Am. J. Med. 1998;105:287–95.

Tedder DG, Ashley R, Tyler KL, Levin MJ. Herpes simplex virus infection as a cause of benign recurrent lymphocytic meningitis. Ann Intern Med 1994;121:334–8.

Torigoe S, Koide W, Yamada M, Miyashiro E, Tanaka-Taya K, Yamanishi K. Human herpesvirus 7 infection associated with central nervous system manifestations. J Pediatr 1996;129:301–5.

Tyler KL. Polymerase chain reaction and the diagnosis of viral central nervous system diseases. Ann Neurol 1994;36:809–11.

Tyler KL, Tedder DG, Yamamoto LJ, Klapper JA, Ashley R, Lichtenstein KA, Levin MJ. Recurrent brainstem encephalitis associated with herpes simplex virus type 1 DNA in cerebrospinal fluid. Neurology 1995;45:2246–50.

Weber T, Frye S, Bodemer M, Otto M, Luke W. Clinical implications of nucleic acid amplification methods for the diagnosis of viral infections of the nervous system. J Neurovirol 1996;2:175–90.

Weinberg A, Li S, Palmer M, Tyler KL. Use of quantitative CSF PCR in the analysis of Epstein–Barr virus infection of the central nervous system. Ann. Neurol. (in press).

Yoshikawa T, Asano Y. Central nervous system complications in human herpesvirus-6 infection. Brain Dev 2000;22:307–14.

AMERICAN SOCIETY FOR VIROLOGY

22nd Annual Meeting

UNIVERSITY OF CALIFORNIA, DAVIS
DAVIS, CALIFORNIA

July 12 - 16, 2003

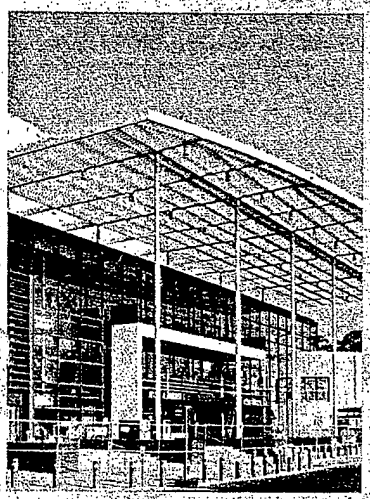

SCIENTIFIC PROGRAM AND ABSTRACTS

W13-5

BCL-2 FAMILY PROTEINS BID AND BIM PLAY A KEY ROLE IN REGULATING THE REOVIRUS-INDUCED MITOCHONDRIAL PATHWAY OF APOPTOSIS IN PRIMARY NEURONAL CULTURES.

Sarah Richardson-Burns, Kenneth L. Tyler. Depts. of Neuroscience, Neurology, Medicine, Microbiology Immunology University of Colorado Health Sciences Center, Denver, CO.

We have previously shown that reovirus 3 (T3D)-induced tissue injury in the mouse CNS results from apoptosis, and that the essential features of this system are replicated in primary mouse neuronal cultures (MCC). We now show that Bid and Bim, two members of the BH3-only domain containing pro-apoptotic Bcl-2 family, play a critical role in T3D-induced neuronal apoptosis. MCC were generated from P0 Swiss-Webster mice and infected with T3D. We have previously shown that neuronal apoptosis involves cell surface death receptors (DR) and activation of the DR-associated caspase 8. By 18 h post-infection (pi) we detected cleavage of Bid and appearance of its caspase 8-associated cleavage product truncated Bid in immunoblots. We also detected a substantial increase in cellular levels of Bim. Bim is regulated through the JNK cascade, through both increased expression, and phosphorylation. JNK is activated in reovirus-infected MCC, as evidenced by the appearance of the phosphorylated (active) form of the JNK-dependent transcription factor c-JUN. Inhibition of either caspase 8 activation (with IETD), or JNK activation with pharmacologic inhibitors or by adenovirus-mediated transfection of DN-c-JUN, inhibited reovirus-induced apoptosis in MCC. Both Bid and Bim act by facilitating release of pro-apoptotic proteins from the mitochondrial intermembrane space into the cytosol. We detected significant release of Smac, but not of cytochrome c or AIF, in immunoblots of subcellular fractions of reovirus-infected MCC. Smac induces apoptosis by inhibiting cellular inhibitor of apoptosis proteins (IAPs). We found significant degradation of several IAPs including XIAP and survivin in T3D infected MCC. These data suggest that the BH3-only Bcl-2 family proteins Bid and Bim play a critical role in the regulation of the mitochondrial apoptotic pathway in reovirus-infected primary neuronal cultures.

W13-8

TWO DISTINCT PHASES OF VIRUS-INDUCED NF-KAPPAB-REGULATION ENHANCE TRAIL-INDUCED APOPTOSIS IN INFECTED CELLS

Penny Clarke, Suzanne M. Meintzer, and Kenneth L. Tyler. Department of Neurology, University of Colorado Health Sciences Center, Denver, Colorado 80262

Viruses often utilize cellular transcription factors to promote viral growth and influence cell fate. We have previously shown that nuclear factor - kappaB (NF-κB) is activated following reovirus infection and that this activation is required for virus-induced apoptosis. We now identify a second phase of reovirus-induced NF-κB regulation. We show that at later times post infection NF-κB activation is blocked in reovirus-infected cells. This results in the termination of virus-induced NF-κB activity and the inhibition of tumor necrosis factor (TNF) alpha and etoposide-induced NF-κB activation in infected cells. Reovirus-induced inhibition of NF-κB activation occurs by a mechanism that prevents degradation of IκBα, the cytoplasmic inhibitor of NF-κB. This effect requires viral replication, and is blocked in the presence of the viral RNA synthesis inhibitor ribavirin. In many epithelial cell lines, reovirus-induced apoptosis is mediated by TNF related apoptosis inducing ligand (TRAIL). We show that ribavirin inhibits reovirus-induced apoptosis in TRAIL-resistant HEK293 cells and prevents the ability of reovirus infection to sensitize TRAIL-resistant cells to TRAIL-induced apoptosis. Further, TRAIL-induced apoptosis is enhanced in HEK293 cells expressing IκBδN2, an IκB super-repressor that blocks NF-κB activation. These results indicate that the ability of reovirus to inhibit NF-κB activation sensitizes HEK293 cells to TRAIL and facilitates virus-induced apoptosis in TRAIL-resistant cells. Our studies show that reovirus infection results in a bimodal alteration in NF-κB regulation

W42-10

REOVIRUS NON-STRUCTURAL PROTEIN SIGMA 1 SMALL IS A NOVEL NUCLEOCYTOPLASMIC SHUTTLING PROTEIN

Cristen C. Hoyt [1], George J. Poggioli [3], and Kenneth L. Tyler [1,2,3,4]
Department of Immunology[1], Departments of Medicine [2], Microbiology [3], and Neurology [4] at University of Colorado Health Sciences Center and Denver Veterans Affairs Medical Center, Denver, Colorado 80220.

The reovirus non-structural protein sigma 1 small plays a key role in virus-induced perturbation of cell cycle regulation in infected cells. Despite this fact, little is known about how this protein interacts with host cells during either natural infection or *in vitro* transfection. Previous immunocytochemical and immunoprecipitation studies suggested that sigma 1 small (σ 1s) could be detected in both the cytoplasm and nucleus of infected cells. Examination of the σ 1s amino acid sequence revealed the presence of a putative nuclear localization signal (NLS) (^{14}RRSRRRLK^{21}). In order to determine whether σ 1s contained a functional NLS we created a fusion protein containing green fluorescent protein-σ 1s-pyruvate kinase (GFP-σ 1s-PK) and transfected this into L929 cells. GFP-σ 1s-PK was present in the nucleus as well as the cytoplasm. A control fusion protein lacking σ 1s (GFP-PK) was exclusively retained in the cytoplasm. Deletion of the putative NLS from the GFP-σ 1s-PK fusion protein abrogated nuclear localization. The pattern of cellular fluorescence seen following transfection with GFP-σ 1s-PK suggested that σ 1s might also contain a nuclear export signal (NES). A putative NES was identified in the σ 1s amino acid sequence (^{75}LSMDLIRVLP^{84}). Deletion of this putative NES did not prevent nuclear localization of the fusion protein, but did abrogate its subsequent export to the cytoplasm. Similar results were seen when cells transfected with GFP-σ 1s-PK were treated with leptomycin B, an inhibitor of CRM-1 mediated nuclear export. Our studies demonstrate that σ 1s functions as a nucleocytoplasmic shuttling protein containing discrete nuclear export and nuclear localization signals, and utilizes a CRM-1 dependent nuclear export pathway. This is the first demonstration of a shuttle protein in the family reoviridae.

International Society of Neurovirology
5th mtg. Baltimore, MD. Sept 3-6, 2003

Identification and manipulation of neuronal apoptotic signaling pathways in reovirus-infected neuronal cell cultures and in a murine model of viral encephalitis.

Sarah Richardson-Burns, Ph.D.
Neuroscience program. University of Colorado Health Sciences Center, Denver, CO

Ronald Bouchard, B.A. Research Service. Denver VA Medical Center, Denver, CO

Kenneth L. Tyler, M.D.*
Department of Neurology, Microbiology, Immunology and Medicine. University of Colorado Health Sciences Center & Neurology Service Denver VA Medical Center, Denver, CO

*Presenting author.
Telephone: 303-322-4916
FAX: 303-393-4686
Email: Ken.Tyler@UCHSC.edu
Mail: Neurology (127), Denver VAMC, 1055 Clermont Street, Denver, CO 80220

Support: VA MERIT & Research Enhancement and Enrichment Program (REAP) Grants and U.S. Army Medical Research & Material Command Grant DAMD17-98-1-8614, and the Reuler-Lewin Family Professorship of Neurology (all KLT).

The cellular mechanisms underlying virus-induced cell death in the central nervous system (CNS) are poorly understood. Reovirus infection is a classic experimental model system for studying viral encephalitis and virus-induced neuronal death. Neurotropic reoviruses infect neurons and cause lethal encephalitis in neonatal mice. Neuronal cell death is due to apoptosis, a form of programmed cell death characterized by distinct biochemical and morphologic changes that are executed by apoptosis-specific proteases (caspases). Following intracerebral infection of neonatal mice with reovirus T3 Dearing (T3D), neuronal cell death was shown to be due to apoptosis as established by criteria including: (1) the presence of characteristic histopathologic changes in neurons, (2) positive TUNEL staining, and (3) demonstration of the presence of activated caspase 3 in infected cells. In order to better understand the cellular basis for reovirus-induced neuronal apoptosis we investigated this process in primary neuronal cortical and hippocampal cultures in which reovirus infection replicated the essential features seen in mice. These studies have provided a comprehensive picture of virus-induced apoptotic signaling in neurons. T3D induces apoptosis in neurons by triggering death receptor (DR)-mediated apoptosis, involving the Fas/FasL system as well as other TNFR superfamily death receptors. DR-initiated apoptotic signaling required amplification by activation of mitochondrial death signaling for maximal activation of effector caspases exemplified by caspase 3. Crosstalk between DR and mitochondrial apoptotic pathways was associated with DR activation-induced caspase 8-mediated cleavage of the pro-apoptotic Bcl-2 family protein Bid. Cleaved Bid translocated to the mitochondria along with Bax and Bim, two other pro-apoptotic Bcl-2 family proteins. Convergence of

cleaved Bid, Bax, and Bim at the mitochondria resulted in release of the apoptogenic protein Smac/DIABLO from the mitochondria into the cytosol. Cytosolic Smac blocks inhibitor of apoptosis (IAP) family proteins relieving IAP-mediated negative regulation of caspases. As would be predicted from these results, T3D-induced neuronal apoptosis in vitro can be inhibited by blocking activation of DRs, specific caspases including caspase 8 and caspase 3, over-expression of anti-apoptotic proteins including Bcl-2, and by inhibition of JNK/c-Jun signaling. Having identified the mechanisms of reovirus-induced neuronal apoptosis in vitro we next sought to determine whether these pathways were also active in a mouse model of encephalitis, and whether manipulation of apoptotic signaling pathways would modify the pathogenesis of reovirus-induced apoptosis. The caspase inhibitors ZVAD-FMK and OPH-QVD, and the neuroprotective tetracycline derivative minocycline, inhibit T3D-induced apoptosis and injury in the CNS of infected mice and prolong survival. These studies suggest that drugs or other agents designed to inhibit virus-induced neuronal apoptosis may have potential as therapeutic agents for treating viral CNS infections.